Mathematical Problems in Engineering

Resource-Constrained Signal Processing in Sensor Networks

Guest Editors: Shuli Sun, Wendong Xiao, and Kung Yao

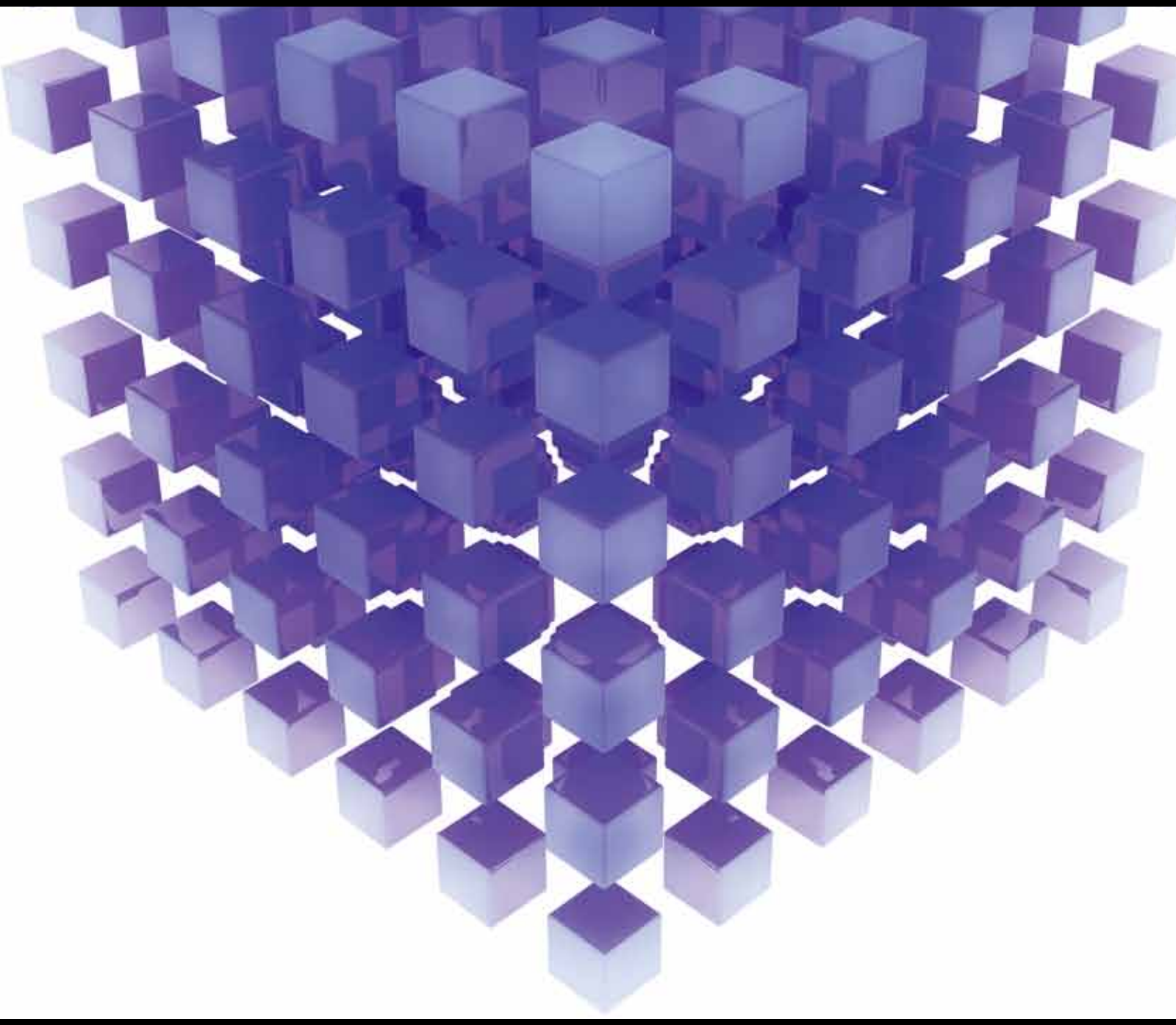

Resource-Constrained Signal Processing in Sensor Networks

Mathematical Problems in Engineering

Resource-Constrained Signal Processing in Sensor Networks

Guest Editors: Shuli Sun, Wendong Xiao, and Kung Yao

Editorial Board

Contents

Hindawi Publishing Corporation
Mathematical Problems in Engineering
Volume 2014, Article ID 756196, 2 pages
http://dx.doi.org/10.1155/2014/756196

Editorial
Resource-Constrained Signal Processing in Sensor Networks

Shuli Sun,[1] Wendong Xiao,[2] and Kung Yao[3]

[1] *School of Electronics Engineering, Heilongjiang University, Harbin 150080, China*
[2] *School of Automation and Electrical Engineering, University of Science and Technology Beijing, Beijing 100083, China*
[3] *Electrical Engineering Department, University of California, Los Angeles, CA 90095-1594, USA*

Correspondence should be addressed to Shuli Sun; sunsl@hlju.edu.cn

Received 13 February 2014; Accepted 13 February 2014; Published 17 March 2014

Sensor network is composed of spatially distributed sensor nodes to monitor the phenomenon of interest, where each sensor node takes measurements and transmits them to the data-processing center (fusion center). The main advantages of sensor network include its low cost, rapid deployment, self-organization, flexibility, and fault tolerance. Sensor networks, especially wireless sensor networks, have attracted significant research interests due to their wide applications and technological opportunities challenged by the limited resources, such as the battery-powered node energy and wireless bandwidth. Usually wireless channel in the network is also unreliable, which results in random transmission delays and packet losses when the sensor data are exchanged among nodes or sent to the data-processing center. Moreover, the quantization or compression of the sensor data is desired to tradeoff between the signal processing performance and the required network resources. It is very important to design collaborative signal processing algorithms and systems with network and sensor resource management under the uncertain network environment featured with the delayed, lost, or/and quantized data.

The main focus of this special issue will be on the new results of resource-constrained signal processing in sensor networks. It will provide an international platform for researchers to summarize the most recent development in the field. After a rigorous peer-reviewing process, 9 papers have been selected for publication. These papers cover the topics including compressed sensing, data compression, distributed estimation, consensus, and tracking.

In the paper entitled "*IDMA-based compressed sensing for ocean monitoring information acquisition with sensor networks*" by G. Liu and W. Kang, an interleave-division multiple-access- (IDMA-) based compressed sensing scheme is proposed for underwater sensor networks with applications to underwater environmental monitoring. The proposed scheme consists of three components: data sampling with randomly selected sensors, interleave-division multiple-access of the sampled packets, and information recovery with the successfully accessed measurements after chip-by-chip (CBC) multiuser detection (MUD). In the paper entitled "*Data reduction with quantization constraints for decentralized estimation in wireless sensor networks*" by Y. Weng, the unknown vector estimation problem is considered for bandwidth constrained wireless sensor network. Due to the power and communication bandwidth limitations, each sensor node must compress its data and transmit them to the fusion center. Both centralized and decentralized estimation frameworks are developed. The closed-form solution for the centralized estimation framework is proposed. The computational complexity of decentralized estimation problem is proven to be NP-hard and a Gauss-Seidel algorithm is also proposed to search for an optimal solution. In the paper entitled "*Weighted measurement fusion quantized filtering with bandwidth constraints and missing measurements in sensor networks*" by J. Ding et al., the estimation problem of a dynamic stochastic variable in a sensor network is studied, where the quantization of scalar measurement, the optimization of the bandwidth scheduling, and the characteristic of transmission channels are considered. Two weighted measurement fusion (WMF) quantized Kalman filters based on the quantized measurements arriving at the fusion center are presented for the imperfect channels with

missing measurements in sensor networks. It is shown that they have the reduced computational cost and the same accuracy as the corresponding centralized fusion filter. The approximate solution for the optimal bandwidth-scheduling problem is given under a limited bandwidth constraint. In the paper entitled "*Distributed fusion estimation for multisensor multirate systems with stochastic observation multiplicative noises*" by F. Peng and S. Sun, a distributed fusion estimation algorithm is presented for a class of multisensor multirate systems with observation multiplicative noises. Sampling period of each sensor is uniform and the integer multiple of the state updates period. Moreover, different sensors have different sampling rates and observations of sensors are subject to the stochastic uncertainties of multiplicative noises. In the paper entitled "*Average consensus analysis of distributed inference with uncertain Markovian transition probability*" by W. I. Kim et al., the average consensus problem is studied for the distributed inference in a wireless sensor network under the Markovian communication topology with uncertain transition probability. A sufficient condition is presented for the average consensus of linear distributed inference algorithm. Based on linear matrix inequalities and numerical optimization, a design method is provided for fast distributed inference. In the paper entitled "*IMM filter based human motion tracking using a wireless sensor network*" by S. Zhang and W. Xiao, using low cost range wireless sensor nodes, an novel sensor selection algorithm is proposed for human tracking based on the interacting multiple model filter (IMM) techniques and considering both the tracking accuracy and the energy cost. In the paper entitled "*Unknown clutter estimation by FMM approach in multitarget tracking algorithm*" by N. Lv et al., a multitarget tracking algorithm based on clutter model estimation is proposed to deal with severe bias caused by unknown and complex clutters. Multitarget likelihood function is established with FMM. In this frame, the algorithm of expectation maximum (EM) and Markov Chain Monte Carlo (MCMC) are both consulted in FMM parameters estimation. Furthermore, target number and multitarget states can be estimated precisely after the clutter model is fitted. In the paper entitled "*Models and algorithms for tracking target with coordinated turn motion*" by X. Yuan et al., firstly a number of widely used models are compared under the single model tracking framework, and the suggestions on the choice of models for different practical target tracking problems are given; then, in the multiple models (MM) framework, the algorithm based on expectation maximization (EM) algorithm is derived, including both the batch form and the recursive form. In the paper entitled "*Self-similarity super resolution for resource-constrained image sensor node in wireless sensor networks*" by Y. Wang et al., a self-similarity super resolution with low computation cost and high recovery performance is proposed. In the self-similarity image super resolution model, a small size sparse dictionary is learned from the image itself. The most similar patch is searched and specially combined during the sparse regulation iteration to preserve the detailed information.

The guest editors hope that this special issue can provide a snapshot of the latest advances in sensor networks and stimulate more research interest and efforts in sensor network research and development. They would like to acknowledge all authors for their efforts in submitting high-quality papers and are also very grateful to the reviewers for their professional contributions.

Shuli Sun
Wendong Xiao
Kung Yao

Hindawi Publishing Corporation
Mathematical Problems in Engineering
Volume 2014, Article ID 938242, 11 pages
http://dx.doi.org/10.1155/2014/938242

Research Article

Unknown Clutter Estimation by FMM Approach in Multitarget Tracking Algorithm

Ning Lv,[1,2] Feng Lian,[1] and Chongzhao Han[1]

[1] *The Institute of Integrated Automation, MOE KLINNS Lab, School of Electronics and Information, Xi'an Jiaotong University, Xi'an 710049, China*
[2] *Xi'an Research Institute of Hi-Tech, Hongqing Town, Xi'an 710025, China*

Correspondence should be addressed to Feng Lian; lianfeng1981@mail.xjtu.edu.cn

Received 28 August 2013; Accepted 19 December 2013; Published 16 March 2014

Academic Editor: Shuli Sun

Finite mixture model (FMM) approach is a research focus in multitarget tracking field. The clutter was treated as uniform distribution previously. Aiming at severe bias caused by unknown and complex clutter, a multitarget tracking algorithm based on clutter model estimation is put forward in this paper. Multitarget likelihood function is established with FMM. In this frame, the algorithms of expectation maximum (EM) and Markov Chain Monte Carlo (MCMC) are both consulted in FMM parameters estimation. Furthermore, target number and multitarget states can be estimated precisely after the clutter model fitted. Association between target and measurement can be avoided. Simulation proved that the proposed algorithm has a good performance in dealing with unknown and complex clutter.

1. Introduction

Multiple target tracking (MTT), for its important theoretical significance and widely applied engineering background, is a research focus in tracking field in recent years [1–3]. In MTT problems, measurement set of sensors contains not only the measurements from target, but also massive clutters from interference caused by meteorological phenomena, electromagnetism environment, and false target. In addition, measurements from target and clutter cannot be distinguished usually. How to estimate target number and multitarget states using these mixture measurements is the key.

Until now, MTT solutions could be concluded in two classes. The first is data association solutions, such as the nearest neighbor (NN) method [4], the joint probabilistic data association (JPDA) method [5], and the multiple hypothesis tracking (MHT) method [6]. In this class, corresponding relationship between target and measurement should be established before target number and multitarget states estimate. While the second solution dealing with MTT problems is random finite sets (RFS) method based solutions, such as the probability hypothesis density (PHD) filter [7] and the cardinalized probability hypothesis density (CPHD) filter [8]. Target state set can be updated with measurement set directly. MTT in frame of RFS does not need data association consequently.

The mentioned MTT solutions are all based on the known clutter model. For randomness of clutter, its distribution model usually includes clutter number and clutter position. If there is not so many interference factors in surveillance area, clutter number could be considered to obey Poisson distribution, while clutter position obeys uniform distribution. But in many actual scenes, especially ground and sea level surveillance, even battlefield surveillance, the clutter model appears to be unknown and more complex as results of complicated landform, jamming station, and unidentified interference source such as electronic countermeasure systems. In this case, assumptions of Poisson and uniform distribution which the clutter model satisfied will lead to severe bias estimated by the filter.

A novel MTT algorithm based on clutter model estimation is put forward in the light of the problems mentioned above. In this algorithm, multitarget likelihood function is

established with finite mixture model (FMM) [9], whose parameters can be estimated by the algorithms of expectation maximum (EM) and Markov Chain Monte Carlo (MCMC). Furthermore, target number and multitarget states can be estimated as well as the clutter model fitted. Similarly with the RFS based solution, association between target and measurement can be avoided in this algorithm. Compared with the MTT solution without clutter model fitting, it can be proved from a simulation that the algorithm proposed in this paper is more efficient.

2. Problem Description

2.1. Target Motion Model. Suppose that the sensor was monitoring a fixed region. For situation of spontaneous birth, spawned by existent targets and extinction, the number of target detected over the surveillance region varies with time. Supposing that t_k is the number of existing targets at time k, we model the motion of the multitarget system as

$$\mathbf{x}_{k+1}^i = f_k^i\left(\mathbf{x}_k^i\right) + \boldsymbol{\omega}_k^i, \quad i = 1, \ldots, t_k, \tag{1}$$

where $\mathbf{x}_k^i = [x_k^i, \dot{x}_k^i, \ddot{x}_k^i, y_k^i, \dot{y}_k^i, \ddot{y}_k^i]^T$ represents the state vector of target i, including position, velocity, and acceleration information and $X_k = \{\mathbf{x}_k^1, \ldots, \mathbf{x}_k^{T_k}\}$ represents multitarget state set at time k, while $\boldsymbol{\omega}_k^i$ represents the process noise vector, obeying Gaussian distribution $\boldsymbol{\omega}_k^i \sim \mathcal{N}(\mathbf{0}, Q_k^i)$, where Q_k^i denotes the variance matrix of process noise.

2.2. Measurement Model. The measurement set received by sensor at time k could be represented as $Z_k = \{\mathbf{z}_k^1, \ldots, \mathbf{z}_k^{n_k}\}$, where n_k denotes the number of measurement at time k. Sensor measurements are generally regarded as a mixture of target-originated measurement and clutter-originated measurement. Measurements from different targets and clutters are statistically independent in this paper without additional illustration.

2.2.1. Target-Originated Measurement. Supposing that measurement j is originated from target i,

$$\mathbf{z}_k^j = \mathbf{h}_k\left(\mathbf{x}_k^i\right) + \boldsymbol{v}_k^j, \quad \mathbf{z}_k^j \in Z_k, \tag{2}$$

where $\mathbf{h}_k(\cdot)$ denotes the measurement function of sensor and $\boldsymbol{v}_k^j$ denotes the measurement noise vector, obeying Gaussian distribution $\boldsymbol{v}_k^j \sim \mathcal{N}(\mathbf{0}, R_k)$ as well, where R_k denotes the variance matrix of measurement noise.

2.2.2. Clutter Model. Assume that at time k $\mathcal{F}_{c,k}$ denotes the model of clutter position distribution, and measurement j is originated from clutter, then

$$\mathbf{z}_k^j \sim \mathcal{F}_{c,k}, \quad \mathbf{z}_k^j \in Z_k, \tag{3}$$

where $\mathcal{F}_{c,k}$ is unknown and varies with time.

So far as mentioned above, at time k, the information needed to be estimated includes the distribution model of clutter position $\mathcal{F}_{c,k}$, target number t_k, and multitarget state set X_k. In addition, the number model of clutter need not be estimated, because this algorithm is adapted to any variation of the clutter number.

3. Multitarget Likelihood Function Based on FMM

Given the measurement set Z_k and condition of independence, the multitarget likelihood function at time k can be described by FMM [9, 10] as

$$\mathcal{L}_k\left(Z_k; \boldsymbol{\psi}_k\right) = \prod_{j=1}^{n_k}\left(\mathcal{F}_{c,k}\left(\mathbf{z}_k^i; \boldsymbol{\psi}_{c,k}\right) + \mathcal{F}_{t,k}\left(\mathbf{z}_k^i; \boldsymbol{\psi}_{t,k}\right)\right). \tag{4}$$

Finite mixture model is considered an effective method dealing with multitarget tracking problem, especially under complex unknown clutter environment. Distribution model of target-originated measurement and clutter measurement could be described as a superposition of some normative distribution. Taking complex clutter, for example, it can be considered as a superposition of uniform and finite Gaussian models. By estimating the parameters of these potential models, we can get the multitarget state ultimately.

Formula (4) could be explained as follows:

$\mathcal{F}_{c,k}(\cdot; \boldsymbol{\psi}_{c,k})$ denotes the distribution model of clutter position at time k. Considering the complexity of clutter distribution model, multiple Gaussian models and one uniform model will be used to fit this clutter model:

$$\mathcal{F}_{c,k}\left(\cdot; \boldsymbol{\psi}_{c,k}\right) = \pi_{c,k}^1 \mathcal{U}(\cdot) + \sum_{i=2}^{g_{c,k}} \pi_{c,k}^i \mathcal{N}\left(\cdot; \boldsymbol{\theta}_{c,k}^i\right), \tag{5}$$

where $\boldsymbol{\psi}_{c,k} = \{g_{c,k}, \pi_{c,k}^1, \ldots, \pi_{c,k}^{g_{c,k}}, \boldsymbol{\theta}_{c,k}^2, \boldsymbol{\theta}_{c,k}^{g_{c,k}}\}$, $g_{c,k}$ denotes the number of clutter model, $\pi_{c,k}^i$ denotes the weights of clutter model, and $\boldsymbol{\theta}_{c,k}^i = (\boldsymbol{\mu}_{c,k}^i, \Sigma_{c,k}^i)$, composed of the mean vector and the covariance matrix, denotes the parameters of clutter model.

$\mathcal{F}_{t,k}(\cdot; \boldsymbol{\psi}_{t,k})$ denotes the distribution model of target-originated measurement position at time k. Assuming that the number of existing targets in surveillance region is t_k,

$$\mathcal{F}_{t,k}\left(\cdot; \boldsymbol{\psi}_{t,k}\right) = \sum_{i=1}^{g_{t,k}} \pi_{t,k}^i f_{t,k}^i\left(\cdot; \boldsymbol{\theta}_{t,k}^i\right), \tag{6}$$

where $\boldsymbol{\psi}_{t,k} = \{g_{t,k}, \pi_{t,k}^1, \ldots, \pi_{t,k}^{g_{t,k}}, \boldsymbol{\theta}_{t,k}^t, \boldsymbol{\theta}_{t,k}^{g_{t,k}}\}$ and $g_{t,k} = t_k$, which means that the number of models is equal to the number of targets. $\pi_{t,k}^i$ denotes the weights of target model, $f_{t,k}^i(\cdot; \boldsymbol{\theta}_{t,k}^i)$ denotes the distribution model of measurement from a single target, and $\boldsymbol{\theta}_{t,k}^i$ denotes the relevant parameters.

Letting $g_k = g_{c,k} + g_{t,k}$, all parameters to be estimated in the mixture model can be represented as $\boldsymbol{\psi}_k = \{g_k, \pi_k^1, \ldots, \pi_k^{g_k}, \boldsymbol{\theta}_k^1, \boldsymbol{\theta}_k^{g_k}\}$. consequently, (4) can be rewritten as

$$\mathcal{L}_k\left(Z_k; \boldsymbol{\psi}_k\right) = \prod_{j=1}^{n_k}\sum_{i=1}^{g_k} \pi_k^i f_k^i\left(\mathbf{z}_k^i; \boldsymbol{\theta}_k^i\right), \qquad \sum_{i=1}^{g_k} \pi_k^i = 1, \tag{7}$$

where $\pi_k^i n_k$ is the number of targets at time k.

EM and MCMC are the approaches most widely consulted in FMM parameters estimation. Until now, EM approach is considered a standard algorithm, but it is sensitive to initial value. The iteration will converge to some local extremum caused by worse initialization. Meanwhile the convergence rate will be affected. Comparatively, MCMC belongs to a stochastic algorithm, which is insensitive to initial value. In addition, for some complex situation, MCMC algorithm will lead a better global Convergence. In fact, if the Markov chain is long enough, MCMC approach can obtain massive information of posterior distribution, so local extremum could be avoided. Above all, robustness of MCMC is better than EM, nevertheless, computational complexity of MCMC is larger than EM. Now we will present these two approaches, respectively, in Sections 4 and 5.

4. FMM Parameters Estimation by EM Approach

4.1. Parameters Initialization. Parameters in FMM should be well initialized as much as possible before estimation in EM algorithm. Initializations of clutter model and target-originated measurement model were discussed, respectively.

4.1.1. Initialization of Clutter Model. Considering that the clutter model could vary with time, the initialization process at time k is listed as follows.

Inheritance of the value estimated at time t_{k-1} is

$$\boldsymbol{\mu}_{c,k}^{i}(0) = \widehat{\boldsymbol{\mu}}_{c,k-1}^{i}, \quad \Sigma_{c,k}^{i}(0) = \widehat{\Sigma}_{c,k-1}^{i}, \quad i = 1, \ldots, \widehat{g}_{c,k-1}. \tag{8}$$

Then add some clutter points randomly; the number of the clutter points is g_0. The initialization average $\boldsymbol{\mu}_{c,k}^{i}(0)$ can be got from these chosen points in surveillance region S. The covariance matrix could be initialized as $\Sigma_{c,k}^{i}(0) = \sigma^2 I$, $i = \widehat{g}_{c,k-1} + 1, \ldots, \widehat{g}_{c,k-1} + g_0$, where

$$\sigma^2 = \frac{1}{10d}\operatorname{trace}\left(\frac{1}{n_k}\sum_{j=1}^{n_k}\left(\mathbf{z}_k^j - \overline{\mathbf{z}}_k\right)\left(\mathbf{z}_k^j - \overline{\mathbf{z}}_k\right)^T\right), \tag{9}$$

where $\overline{\mathbf{z}}_k = \sum_{j=1}^{n_k}\overline{\mathbf{z}}_k^j/n_k$ denotes the average of measurement data.

Consequently, the number of clutter models in initialization process $g_{c,k}(0) = \widehat{g}_{c,k-1} + g_0$. In order to ensure the parameters of clutter models converging to the true value, the value of g_0 should be bigger than the number in reality.

4.1.2. Initialization of Target-Originated Measurement Model. At time k, targets totally are composed of survival targets and spontaneous birth targets and spawned by existent targets. So the number of target models in initialization process is

$$g_{t,k}(0) = g_{s,k}(0) + g_{b,k}(0) + g_{p,k}(0), \tag{10}$$

where $g_{s,k}(0)$ denotes the number of survival targets, $g_{b,k}(0)$ denotes the number of spontaneous birth targets, and $g_{p,k}(0)$ denotes the number of spawned by existent targets.

The initialization of target-originated measurement model at time k can be represented as

$$\begin{aligned}\mathcal{F}_{t,k}\left(\cdot;\boldsymbol{\psi}_{c,k}(0)\right) = {} & \mathcal{F}_{s,k}\left(\cdot;\boldsymbol{\psi}_{s,k}(0)\right) + \mathcal{F}_{b,k}\left(\cdot;\boldsymbol{\psi}_{b,k}(0)\right) \\ & + \mathcal{F}_{p,k}\left(\cdot;\boldsymbol{\psi}_{p,k}(0)\right).\end{aligned} \tag{11}$$

(a) To Survival Targets. Measurement noise obeys Gaussian distribution, as shown in (2), so $f_{s,k}^{i}(\cdot;\boldsymbol{\theta}_{s,k}^{i}) \sim \mathcal{N}(\cdot;\boldsymbol{\mu}_{s,k}^{i},\Sigma_{s,k}^{i})$. Furthermore, measurement model initialization of survival targets is

$$\mathcal{F}_{s,k}\left(\cdot;\boldsymbol{\psi}_{s,k}(0)\right) = \sum_{i=1}^{g_{s,k}(0)}\pi_{s,k}^{i}(0)\,\mathcal{N}\left(\cdot;\boldsymbol{\mu}_{s,k}^{i}(0),\Sigma_{c,k}^{i}(0)\right). \tag{12}$$

Let $g_{s,k}(0) = \widehat{g}_{t,k-1}$.

The initialization average $\boldsymbol{\mu}_{s,k}^{i}(0) = h_k(\widehat{\mathbf{x}}_{k|k-1}^{i})$ could be got from prediction of target state. The covariance is known, the same with measurement noise of the sensor, $\Sigma_{s,k}^{i}(0) = R_k$, $i = 1, \ldots, g_{s,k}(0)$.

(b) To Spontaneous Birth Targets. As is mentioned in [11–13], assume that the initial position model obeys Gaussian distribution either; that is,

$$\mathcal{F}_{b,k}\left(\cdot;\boldsymbol{\psi}_{b,k}(0)\right) = \sum_{i=1}^{g_{b,k}(0)}\pi_{b,k}^{i}(0)\,\mathcal{N}\left(\cdot;\boldsymbol{\mu}_{b,k}^{i}(0),\Sigma_{b,k}^{i}(0)\right), \tag{13}$$

where parameters of model initialization $g_{b,k}(0)$, $\boldsymbol{\mu}_{b,k}^{i}(0)$, $\Sigma_{b,k}^{i}(0)$ are all known, according to prior information.

(c) To Spawned by Existent Targets. Supposing that each original target can create p_k new targets at most, model initialization can be represented as [11–13]

$$\mathcal{F}_{p,k}\left(\cdot;\boldsymbol{\psi}_{p,k}(0)\right) = \sum_{j=1}^{p_k}\sum_{i=1}^{g_{p,k}(0)}\pi_{p,k}^{ij}(0)\,\mathcal{N}\left(\cdot;\boldsymbol{\mu}_{p,k}^{ij}(0),\Sigma_{p,k}^{ij}(0)\right). \tag{14}$$

The target number and state average can be assumed as $g_{p,k}(0) = p_k g_{s,k}(0)$, $\boldsymbol{\mu}_{p,k}^{i,j}(0) = h_k(\widehat{\mathbf{x}}_{k|k-1}^{i}) + \mathbf{d}_{p,k}^{j}$, where $i = 1, \ldots, g_{s,k}(0)$, $j = 1, \ldots, p_k$.

The parameters $\mathbf{d}_{p,k}^{j}$, $\Sigma_{p,k}^{ij}(0)$ could be valued according to prior information similarly.

The weights of models could be briefly treated as the same in initialization process:

$$\pi_k^{i}(0) = \frac{1}{g_k(0)}, \quad i = 1, \ldots, g_{c,k}(0) + g_{t,k}(0). \tag{15}$$

4.2. Estimation of FMM Parameters

4.2.1. EM Approach. As FMM Parameters Estimation with EM approach, the loss variables can be treated as element labeling $E_k = \{\mathbf{e}_k^1, \ldots, \mathbf{e}_k^{n_k}\}$, where $\mathbf{e}_k^1$ is a vector of n_k dimension. The element $e_k^{ij} = 1$ or 0 illustrates whether $\mathbf{z}_k^j$ is

originated from ith element of the FMM or not. So the complete dataset at time k is $Y_k = \{Z_k, E_k\}$, and logarithm likelihood function of the complete data is

$$\log \mathscr{C}_k\left(Y_k;\boldsymbol{\psi}_k\right) = \sum_{i=1}^{g_k}\sum_{j=1}^{n_k} e_k^{ij}\left\{\log \pi_k^i + \log f_k^i\left(z_k^j;\boldsymbol{\theta}_k^i\right)\right\}. \quad (16)$$

When the number of models g_k is known, EM algorithm can be iterated by E-step and M-step. But the number of models is unknown in this paper. Some criteria will be used for number estimation, such as minimum message length (MML) criterion and Bayesian information criterion (BIC) [10, 14]. Here in this paper, for the number of models in initialization being more than reality, the technology of model merging and pruning could be inserted into each step of iteration in EM algorithm. In this way, the number of FMM can be estimated. This method is more intuitive than those based on criteria. Now, this modified EM algorithm is described as follows:

(a) E-Step. Conditional expectations of $\mathscr{C}_k(Y_k;\boldsymbol{\psi}_k)$ will be iterated. The expectations of loss data e_k^{ij} at tth step is

$$\begin{aligned} E_{\boldsymbol{\psi}_k(t)}\left[e_k^{ij}; Z_k\right] &= \mathrm{pr}_{\boldsymbol{\psi}_k(t)}\left\{e_k^{ij} = 1 \mid Z_k\right\} \\ &= \tau_k^i\left(z_k^j;\boldsymbol{\psi}_k(t)\right) = \tau_k^{ij}(t), \end{aligned} \quad (17)$$

where $\tau_k^{ij}(t)$ represents the posterior probability of $\mathbf{z}_k^j$ belonging to model i. The formula for computing $\tau_k^{ij}(t)$ is

$$\tau_k^{ij}(t) = \frac{\pi_k^i(t)\, f_k^i\left(\mathbf{z}_k^j;\boldsymbol{\theta}_k^i(t)\right)}{\sum_{i=1}^{g_k(t)} \pi_k^i(t)\, f_k^i\left(\mathbf{z}_k^j;\boldsymbol{\theta}_k^i(t)\right)}. \quad (18)$$

According to the formula above, the conditional expectations of $\log \mathscr{C}_k(Y_k;\boldsymbol{\psi}_k)$ is

$$\begin{aligned} Q\left(\boldsymbol{\psi}_k;\boldsymbol{\psi}_k(t)\right) &= E_{\boldsymbol{\psi}_k(t)}\left\{\log \mathscr{C}_k\left(Y_k;\boldsymbol{\psi}_k\right) \mid Z_k\right\} \\ &= \sum_{i=1}^{g_k}\sum_{j=1}^{n_k} \tau_k^{ij}(t)\left\{\log \pi_k^i(t) + \log f_k^i\left(\mathbf{z}_k^j;\boldsymbol{\theta}_k^i(t)\right)\right\}. \end{aligned} \quad (19)$$

In fact, the loss variable has reflected the association relationship between the measurement and target, that is, why association process can be avoided in this algorithm.

(b) M-Step. The value of $\boldsymbol{\psi}_k$ will be estimated throught global maximum of $Q(\boldsymbol{\psi}_k;\boldsymbol{\psi}_k(t))$. By solving $\partial Q_k(\boldsymbol{\psi}_k,\boldsymbol{\psi}_k(t))/\partial\boldsymbol{\psi}_k = 0$, the weights of all models will be reestimated as

$$\pi_k^i(t) = \frac{1}{n_k}\sum_{j=1}^{n_k} \tau_k^{ij}(t). \quad (20)$$

Estimation for the average of FMM is

$$\boldsymbol{\mu}_k^i(t) = \frac{\sum_{j=1}^{n_k} \tau_k^{ij}(t)\,\mathbf{z}_k^j}{\sum_{j=1}^{n_k} \tau_k^{ij}(t)}, \quad i = 1,\ldots,g_k(t). \quad (21)$$

Considering the estimation for the covariance of FMM, because the covariance of target-originated measurement model is known or initialized, only covariance of clutter model needs to be estimated here:

$$\Sigma_{c,k}^i(t) = \frac{\sum_{j=1}^{n_k} \tau_k^{ij}(t)\left(\mathbf{z}_k^j - \boldsymbol{\mu}_{c,k}^i(t)\right)\left(\mathbf{z}_k^j - \boldsymbol{\mu}_{c,k}^i(t)\right)^T}{\sum_{j=1}^{n_k} \tau_k^{ij}(t)}, \quad (22)$$

where $i = 1,\ldots,g_{c,k}(t)$.

4.3. Component Management Step. The component management step of model is completed by the technology of model merging and pruning [12].

Notification. Models between clutter and target-originated measurement cannot merge each other.

To clutter model, the process of merging and pruning is listed as follows:

(a) Merging Step. Given the merging threshold U, let the set $I_k = \{1,\ldots,g_{c,k}(t)\}$, $l = 0$, circulate

$l = l + 1$, $j = \mathrm{argmax}_{i\in I_k}\pi_{c,k}^i$; take a model $i \in I_k$, for example,

if $d_k^{ij}(t) \le U$, where

$$d_k^{ij}(t) = \left(\boldsymbol{\mu}_{c,k}^i(t) - \boldsymbol{\mu}_{c,k}^j(t)\right)^T\left(\Sigma_{c,k}^j(t)\right)^{-1}\left(\boldsymbol{\mu}_{c,k}^i(t) - \boldsymbol{\mu}_{c,k}^j(t)\right). \quad (23)$$

Then let $i \in L_k$, and merge the models in set L_k, with the following merging formula:

$$\begin{aligned} \widetilde{\pi}_{c,k}^l(t+1) &= \sum_{i\in L_k} \pi_{c,k}^i(t), \\ \widetilde{\boldsymbol{\mu}}_{c,k}^l(t+1) &= \frac{1}{\widetilde{\pi}_{c,k}^l(t+1)}\sum_{i\in L_k} \pi_{c,k}^i(t)\,\boldsymbol{\mu}_{c,k}^i(t+1), \\ \widetilde{\Sigma}_{c,k}^l(t+1) &= \frac{1}{\widetilde{\pi}_{c,k}^l(t+1)} \\ &\quad\times \sum_{i\in L_k} \pi_{c,k}^i(t)\left(\Sigma_{c,k}^i(t) + \widetilde{\boldsymbol{\mu}}_{c,k}^l(t+1) - \boldsymbol{\mu}_{c,k}^i(t)\right) \\ &\quad\times \left(\widetilde{\boldsymbol{\mu}}_{c,k}^l(t+1) - \boldsymbol{\mu}_{c,k}^i(t)\right)^T. \end{aligned} \quad (24)$$

Let $I_{k,t+1} = I_{k,t} - L_{k,t}$; repeat this process until the set $I_k = \Phi$; the merging ends.

(b) Pruning Step. If the weight $n_k\widetilde{\pi}_{c,k} < D_c (i = 1,\ldots,l)$, where D_c denotes the pruning threshold of clutter model, the corresponding model should be pruned.

Then let $l = l-1$. Finally we can get the clutter model after merging and pruning, with the target number $g_{c,k}(t+1) = l$.

To target-originated measurement model, the process of merging and pruning is similar to the clutter model above. But the difference is that a target can not generate more measurements except one, the pruning gate D_t should be set far less than D_c in clutter model.

Iteration among the three steps above circulates until $\mathscr{L}_k(Y_k;\boldsymbol{\psi}_k(t+1)) - \mathscr{L}_k(Y_k;\boldsymbol{\psi}_k(t))$ is under the convergence threshold ε of EM or MCMC algorithm. Then we can get $\widehat{\boldsymbol{\psi}}_k$, the estimation of parameter value in FMM at the time k. Furthermore, the estimation of clutter model $\widehat{\mathscr{F}}_{c,k}(\cdot;\widehat{\boldsymbol{\psi}}_{c,k})$, target number $\widehat{g}_{t,k}$ and average value of target-originated measurement model $\widehat{\boldsymbol{\mu}}_{t,k}^{i}$ $(i = 1,\ldots,\widehat{g}_{t,k})$ are all obtained.

FMM Parameters Estimation by EM approach over Section 4 could be described by Algorithm 1.

5. FMM Parameters Estimation by MCMC Approach

MCMC is an approach which obtains a Markov chain sampling from posterior distribution. We can extract information of posterior distribution through this Markov chain. Gibbs sampling method is one of MCMC approach. In order to solve the uncertainty of element number in mixture distribution, merging and pruning technology was consulted after each sampling step instead of RJMCMC method [15].

5.1. Posterior Distribution of FMM. Parameters to be estimated consist of the weight of models π_j, the element labeling $e_{i,j}$, variance $\boldsymbol{\sigma}_j^2$, and average value $\boldsymbol{\mu}_j$. In order to get posterior distribution in Bayesian frame, prior distribution of these parameters is necessary [10].

Let the weight of models π_j obey Dirichelet distribution:

$$(\pi_1,\cdots\pi_m) \sim \mathscr{D}(a_1 + l_1,\cdots a_m + l_m), \tag{25}$$

where $a_j > 0$ is constant and l_j is the number of measurements which belong to model j.

The element labeling $e_{i,j}$ could be estimated by Bayes formula:

$$\widehat{e}_{i,j} = \frac{\pi_j f(\mathbf{y}_i \mid \theta_j)}{\sum_{j=1}^{k} \pi_j f(\mathbf{y}_i \mid \theta_j)}, \qquad l_j = \sum_{i=1}^{n} \widehat{e}_{i,j}. \tag{26}$$

Let variance $\boldsymbol{\sigma}_j^2$ obey Wishart distribution:

$$\begin{aligned} \boldsymbol{\sigma}_j^2 &\sim \text{Wishart}\left(\alpha_0 + \frac{l_j}{M_0}, \beta_0 + \frac{\boldsymbol{\kappa}_j^2}{N_0}\right) \\ \boldsymbol{\kappa}_j^2 &= \frac{\sum_{i=1}^{n} (\mathbf{y}_i - \boldsymbol{\mu}_i)(\mathbf{y}_i - \boldsymbol{\mu}_i)^T \cdot \widehat{e}_{i,j}}{\sum_{i=1}^{n} \widehat{e}_{i,j}}, \end{aligned} \tag{27}$$

where α_0 and β_0 are positive constant, M_0 and N_0 are positive number.

The average value $\boldsymbol{\mu}_j$ obey Gaussian distribution:

$$\boldsymbol{\mu}_j \sim \mathscr{N}(\boldsymbol{\xi}_j, \boldsymbol{\sigma}_j^2), \tag{28}$$

where $\boldsymbol{\xi}_j = \sum_{i=1}^{n} \mathbf{y}_i \cdot \widehat{e}_{i,j} / \sum_{i=1}^{n} \widehat{e}_{i,j}$.

5.2. Parameters Initialization. Easier than those of EM approach, in MCMC approach, initial values can be randomly selected in parameter space. While the number of models should be larger than expected value.

5.2.1. Gibbs Sampling Method. Circulate

$$\begin{aligned} e_{i,j}^{(t)} &= \frac{\pi_i^j p(\mathbf{y}_i \mid \theta(t-1))}{\sum_{j=1}^{k_{\max}} \pi_i^j p(\mathbf{y}_i \mid \theta(t-1))}, \qquad l_j^{(t)} = \sum_{i=1}^{n} \widehat{e}_{i,j}^{(t)}, \\ \boldsymbol{\mu}_j^{(t)} &= \sum_{i=1}^{n} \frac{\mathbf{y}_i \cdot e_{i,j}^{(t)}}{l_j^{(t)}}, \\ \boldsymbol{\xi}_j^{(t)} &= \sum_{i=1}^{n} (\mathbf{y}_i - \boldsymbol{\mu}_j^{(t)}) \cdot e_{i,j}^{(t)}, \\ \boldsymbol{\kappa}_j^{(t)2} &= \frac{\sum_{i=1}^{n} (\mathbf{y}_i - \boldsymbol{\mu}_j^{(t)})(\mathbf{y}_i - \boldsymbol{\mu}_j^{(t)})^T \cdot e_{i,j}^{(t)}}{\sum_{i=1}^{n} e_{i,j}^{(t)}}, \\ \boldsymbol{\sigma}_j^{(t)2} &\sim \text{Wishart}\left(\alpha_0 + \frac{l_j^{(t)}}{M_0}, \beta_0 + \frac{\boldsymbol{\kappa}_j^{(t)^2}}{N_0}\right), \\ \boldsymbol{\mu}_j^{(t)} &\sim \mathscr{N}(\boldsymbol{\xi}_j^{(t)}, \boldsymbol{\sigma}_j^{(t)^2}), \\ (\pi_1^{(t)},\ldots,\pi_m^{(t)}) &\sim \mathscr{D}(a_1 + l_1^{(t)},\ldots,a_m + l_m^{(t)}). \end{aligned} \tag{29}$$

5.3. Management of Model Number. Choosing proper thresholds λ_π, λ_μ, and λ_σ, use merging and pruning technology for reference from EM approach. In this way, algorithm becomes more concise ignoring jumping in parameter space.

6. Multitarget State Estimation

6.1. Equivalent Measurement of Target. The real measurement originated from target is hardly obtained because of the effect from clutter in MTT. In many circumstances, the real measurement is always replaced by equivalent measurement of target. Taking JPDA algorithm for example, the equivalent measurement could be obtained by probability weighted moments from actual measurement in the gate. To the algorithm proposed in this paper, association probability of target and measurement is represented by so-called loss variable, so average value of target-originated measurement model, that is, $\widehat{\boldsymbol{\mu}}_{t,k}^{i}$ $(i = 1,\ldots,\widehat{g}_{t,k})$, represents the equivalent measurement of target i, with variance R_k still. And the so-called gate is extended to the global surveillance region.

6.2. Multitarget State Estimation. Suppose that the state and measurement functions are both of the linear systems. That is,

$$f_k^i(\mathbf{x}_k^i) = F_k^i, \quad h_k^i(\mathbf{x}_k^i) = H_k^i(\mathbf{x}_k^i), \quad i = 1,\ldots,t_k. \tag{30}$$

By substitution of the equivalent measurement $\widehat{\boldsymbol{\mu}}_{t,k}^{i}$ into Kalman filter, state estimation of target i is acquired. The algorithm of Kalman filter is

Input: the convergence threshold ε, the estimation of clutter model parameters at time t_{k-1},

$$\boldsymbol{\mu}^i_{c,k}(0) = \widehat{\boldsymbol{\mu}}^i_{c,k-1}, \qquad \Sigma^i_{c,k}(0) = \widehat{\Sigma}^i_{c,k-1}, \quad i = 1, \ldots, \widehat{g}_{c,k-1}.$$

Initialization step:

(A) Initialization of Clutter Model:

sample some clutter points randomly $\mathscr{P}_k = \{p^i_k\}_{i=1}^{g_0}$, the number of the clutter points is g_0,

For $i = \widehat{g}_{c,k-1} + 1, \ldots, \widehat{g}_{c,k-1} + g_0$, do,

$$\boldsymbol{\mu}^i_{c,k}(0) = \overline{p_k}, \qquad \Sigma^i_{c,k}(0) = \sigma^2 I, \quad i = \widehat{g}_{c,k-1} + 1, \ldots, \widehat{g}_{c,k-1} + g_0$$

where $\sigma^2 = (1/10d)\ \mathrm{trace}((1/n_k)\sum_{j=1}^{n_k}(z^j_k - \overline{z}_k)(z^j_k - \overline{z}_k)^T)$

end for i. $g_{c,k}(0) = \widehat{g}_{c,k-1} + g_0$.

(B) Initialization of Target-Originated Measurement Model:

To survival targets, $g_{s,k}(0) = \widehat{g}_{t,k-1}$, for $i = 1, \ldots, g_{s,k}(0)$, do

$$\boldsymbol{\mu}^i_{s,k}(0) = h_k(\widehat{x}^i_{k|k-1}), \qquad \Sigma^i_{s,k}(0) = R_k, \quad (i = 1, \ldots, g_{s,k}(0))$$

$$\mathscr{F}_{s,k}\left(\cdot; \boldsymbol{\psi}_{s,k}(0)\right) = \sum_{i=1}^{g_{s,k}(0)} \pi^i_{s,k}(0)\mathscr{N}(\cdot; \boldsymbol{\mu}^i_{s,k}(0), \Sigma^i_{c,k}(0)).\ \text{end for } i.$$

To Spontaneous Birth Targets, $g_{b,k}(0)$, $\boldsymbol{\mu}^i_{b,k}(0)$, $\Sigma^i_{b,k}(0)$ will be set according to prior information, for $i = 1, \ldots, g_{b,k}(0)$, do

$$\mathscr{F}_{b,k}\left(\cdot; \boldsymbol{\psi}_{b,k}(0)\right) = \sum_{i=1}^{g_{b,k}(0)} \pi^i_{b,k}(0)\mathscr{N}(\cdot; \boldsymbol{\mu}^i_{b,k}(0), \Sigma^i_{b,k}(0)).\ \text{end for } i.$$

To Spawned by Existent Targets, $g_{p,k}(0) = p_k g_{s,k}(0)$, for $i = 1, \ldots, g_{s,k}(0)$, $j = 1, \ldots, p_k$, do

$$\boldsymbol{\mu}^{i,j}_{p,k}(0) = h_k(\widehat{x}^i_{k|k-1}) + d^j_{p,k},\ \mathscr{F}_{p,k}(\cdot; \boldsymbol{\psi}_{p,k}(0)) = \sum_{j=1}^{p_k}\sum_{i=1}^{g_{p,k}(0)} \pi^{ij}_{p,k}(0)\mathscr{N}(\cdot; \boldsymbol{\mu}^{ij}_{p,k}(0), \Sigma^{ij}_{p,k}(0)).$$

end for j; end for i.

$g_{t,k}(0) = g_{s,k}(0) + g_{b,k}(0) + g_{p,k}(0)$. $\quad g_k(0) = g_{c,k}(0) + g_{t,k}(0) \quad \pi^i_k(0) = 1/g_k(0)$. Set $t := 0$.

Repeat:

Expectation-step: calculate the conditional expectation of missing-data $E_k = \{e^1_k, \ldots, e^{n_k}_k\}$

For $i = 1, \ldots, g_k$, $j = 1, \ldots, n_k$, do

$$E_{\boldsymbol{\psi}_k(t)}[e^{ij}_k; Z_k] = \tau^{ij}_k(t) = \left(\pi^i_k(t) f^i_k(z^j_k; \boldsymbol{\theta}^i_k(t))\right) / \left(\sum_{i=1}^{g_k(t)} \pi^i_k(t) f^i_k(z^j_k; \boldsymbol{\theta}^i_k(t))\right).\ \text{end for } j;\ \text{end for } i.$$

calculate the conditional expectation of complete-data log likelihood given $\mathscr{P}_k$ and $\boldsymbol{\psi}_k(t)$

$$Q(\boldsymbol{\psi}_k; \boldsymbol{\psi}_k(t)) = E_{\boldsymbol{\psi}_k(t)}\left\{\log \mathscr{C}_k(Y_k; \boldsymbol{\psi}_k) \mid Z_k\right\} = \sum_{i=1}^{g_k}\sum_{j=1}^{n_k} \tau^{ij}_k(t)\left\{\log \pi^i_k(t) + \log f^i_k(z^j_k; \boldsymbol{\theta}^i_k(t))\right\}$$

Maximization-step: require the global maximization of $Q(\boldsymbol{\psi}_k; \boldsymbol{\psi}_k(t))$ with respect to $\boldsymbol{\psi}_k$ over the parameter space to give the updated estimate $\widehat{\boldsymbol{\psi}}_k(t) = \arg \max_{\boldsymbol{\psi}_k} Q(\boldsymbol{\psi}_k; \boldsymbol{\psi}_k(t))$.

for $i = 1, \ldots, g_k$, $\quad j = 1, \ldots, n_k$, do

$$\pi^i_k(t) = \frac{1}{n_k}\sum_{j=1}^{n_k} \tau^{ij}_k(t), \quad \boldsymbol{\mu}^i_k(t) = \frac{\sum_{j=1}^{n_k} \tau^{ij}_k(t) z^j_k}{\sum_{j=1}^{n_k} \tau^{ij}_k(t)}, i = 1, \ldots, g_k(t), \quad \sum_{c,k}^{i}(t) = \frac{\sum_{j=1}^{n_k} \tau^{ij}_k(t)(z^j_k - \boldsymbol{\mu}^i_{c,k}(t))(z^j_k - \boldsymbol{\mu}^i_{c,k}(t))^T}{\sum_{j=1}^{n_k} \tau^{ij}_k(t)}$$

end for j; end for i.

Component management step: manage the components of the set $\widehat{\boldsymbol{\psi}}_k(t) = \{\widehat{\pi}^i_k(t), \widehat{\boldsymbol{\mu}}^i_k(t), \widehat{\Sigma}^i_k(t)\}_{i=1}^{g_k}$ according to the merging and pruning strategy described in IV.C.

Update $g_k(t+1)$ and let $\boldsymbol{\psi}_k(t+1) = \{\pi^i_k(t+1), \boldsymbol{\mu}^i_k(t+1), \Sigma^i_k(t+1)\}_{i=1}^{g_k(t+1)}$. denote the managed component number and parameter set. Set $t := t + 1$.

Until $\left|\mathscr{L}_k(Y_k; \boldsymbol{\psi}_k(t+1)) - \mathscr{L}_k(Y_k; \boldsymbol{\psi}_k(t))\right| < \varepsilon \mathscr{L}_k(Y_k; \boldsymbol{\psi}_k(t))$.

Output: the set of estimated parameters $\widehat{\boldsymbol{\psi}}_k = \boldsymbol{\psi}_k(t+1)$

Algorithm 1: FMM Parameters Estimation by EM approach.

(1) Prediction Step

$$\widehat{\mathbf{x}}^i_{k|k-1} = F^i_{k-1}\widehat{\mathbf{x}}^i_{k-1},$$
$$P^i_{k|k-1} = Q^i_{k-1} + F^i_{k-1}P^i_{k-1}\left(F^i_{k-1}\right)^T. \tag{31}$$

(2) Update Step

$$K^i_k = P^i_{k|k-1}H^T_k\left(H_k P^i_{k|k-1}H^T_k\right)^{-1},$$
$$\widehat{\mathbf{x}}^i_k = \widehat{\mathbf{x}}^i_{k|k-1} + K^i_k\left(\widehat{\boldsymbol{\mu}}^i_{c,k} - H_k\widehat{\mathbf{x}}^i_{k|k-1}\right), \tag{32}$$
$$P^i_k = \left(I - K^i_k H_k\right)P^i_{k|k-1}.$$

If the state function or measurement function cannot meet linear condition, nonlinear filter methods such as extended Kalman filter (EKF) and unscented filter (UF) [16] will make contribution.

7. Simulation

7.1. Scene Generation. The motion model of the targets can be described as

$$\widehat{\mathbf{x}}^i_k = F^i_{k-1}\widehat{\mathbf{x}}^i_{k-1} + \boldsymbol{\omega}^i_{k-1}, \quad i = 1, \ldots, t_k, \tag{33}$$

where t_k denotes the target number at time k, $\mathbf{x}^i_k = [x^i_k, \dot{x}^i_k, \ddot{x}^i_k, y^i_k, \dot{y}^i_k, \ddot{y}^i_k]$ denotes the state vector of target i, F^i_k denotes

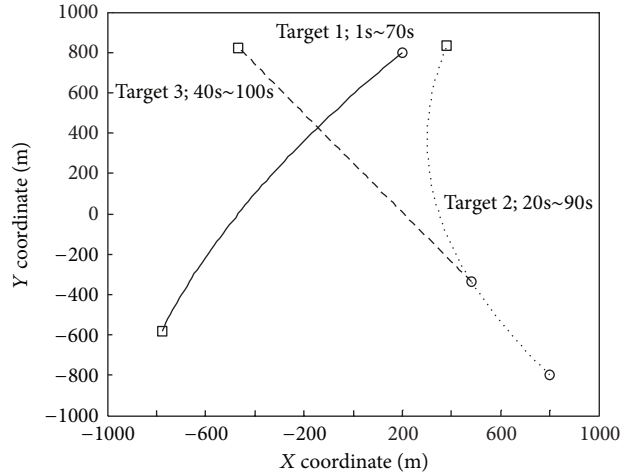

Figure 1: Tracks of targets.

the state transition matrix, and $\boldsymbol{\omega}_k^i \sim \mathcal{N}(\mathbf{0}, Q_k^i)$ denotes the process noise. The tracking process lasted for 100 s with a sampling interval 1 s. In two-dimensional coordinate system, the surveillance region is $[-1000\,\text{m}, 1000\,\text{m}] \times [-1000\,\text{m}, 1000\,\text{m}]$. The flight track is shown in Figure 1.

In Figure 1, the circle denotes starting point, while the rectangular denotes the end points of a track. The solid line is the track of target 1, which was born at time 1 and disappeared at time 70. The dotted line is the track of target 2, which was born at time 20 and disappeared at time 90. The dashed line is the track of target 3, which was spawned by target 2 and disappeared at time 100.

Target 1 and target 2 moved with constant acceleration (CA). The state transition matrix F_k^i and variance matrix of process noise Q_k^i [17] are

$$F_k^i = \begin{bmatrix} F_{\text{CA}} & \\ & F_{\text{CA}} \end{bmatrix}, \qquad Q_k^i = \begin{bmatrix} Q_{\text{CA}} & \\ & Q_{\text{CA}} \end{bmatrix}, \tag{34}$$

where

$$F_{\text{CA}} = \begin{bmatrix} 1 & T & \frac{T^2}{2} \\ & 1 & T \\ & & 1 \end{bmatrix}, \qquad Q_{\text{CA}} = \sigma_\omega^2 \begin{bmatrix} \frac{T^4}{4} & \frac{T^3}{2} & \frac{T^2}{2} \\ \frac{T^3}{2} & \frac{T^2}{2} & T \\ \frac{T^2}{2} & T & 1 \end{bmatrix}. \tag{35}$$

Target 3 moved with constant velocity (CV). The state transition matrix F_k^3 and variance matrix of process noise Q_k^3 are

$$F_k^3 = \begin{bmatrix} F_{\text{CV}} & \\ & F_{\text{CV}} \end{bmatrix}, \qquad Q_k^3 = \begin{bmatrix} Q_{\text{CV}} & \\ & Q_{\text{CV}} \end{bmatrix}, \tag{36}$$

where

$$F_{\text{CV}} = \begin{bmatrix} 1 & T & 0 \\ & 1 & 0 \\ & & 0 \end{bmatrix}, \qquad Q_{\text{CV}} = \sigma_\omega^2 \begin{bmatrix} \frac{T^4}{4} & \frac{T^3}{2} & 0 \\ \frac{T^3}{2} & T^2 & 0 \\ 0 & 0 & 0 \end{bmatrix}, \tag{37}$$

Table 1: Elliptic range of the complex clutter.

Model	Weight	Center ($\times 10^2$ m)	Long axis ($\times 10^2$ m)	Short axis ($\times 10^2$ m)
1	0.3	/	/	
2	0.3	[4, 2]	3	2
3	0.2	[−2, 4]	2	2
4	0.2	[2, −2]	2	2

where σ_ω denotes the standard deviation of process noise, $\sigma_\omega = 0.01\,\text{m/s}^2$.

Supposing that the measurement function is linear,

$$\mathbf{z}_k = \begin{bmatrix} 1 & 0 & 0 & 0 & 0 & 0 \\ 0 & 0 & 0 & 1 & 0 & 0 \end{bmatrix} \mathbf{x}_k + \boldsymbol{\upsilon}_k. \tag{38}$$

The sensor was in the origin of coordinate, with detection probability $p_D = 0.98$ and measurement noise $\boldsymbol{\upsilon}_k \sim \mathcal{N}(\mathbf{0}, R_k)$, where variance matrix of measurement noise $R_k = \sigma_\upsilon^2 I$, $\sigma_\upsilon = 12.5$ m.

Assume that the clutter model obeys stable Poisson distribution in this tracking process, with the number of clutters N_c and parameter $\lambda_c = 50$.

$$P\left(N_c = c_k\right) = \frac{e^{-\lambda_c} \lambda_c^{c_k}}{c_k!}, \tag{39}$$

where c_k is the number of clutters and $\lambda_c = 50$ denotes the average level that the sensor could receive 50 clutters each frame.

Assume that the position distribution of clutter model is

$$\mathcal{F}_{c,k}\left(\cdot; \boldsymbol{\theta}_c\right) = \pi_c^1 \mathcal{U}(\cdot) + \sum_{i=2}^{4} \pi_c^i \mathcal{D}(\cdot), \qquad \sum_{i=1}^{4} \pi_c^i = 1, \tag{40}$$

which is composed of one uniform distribution dispersed over the whole surveillance region and three groups of complex distribution concentrated in elliptic areas. Each group is a superposition of different types clutter model, not limited to uniform and Gaussian distribution, see in Figure 2.

Elliptic range of this complex clutter is listed as in Table 1.

7.2. Parameter Estimation in FMM. The effect of algorithm proposed in this paper is compared with Gaussian mixture PHD (GM-PHD) filter, which directly estimates the number and state of multitarget without clutter model fitting.

To spontaneous birth targets, the measurement model is represented by (13), with $g_{b,k}(0) = 2$, $\boldsymbol{\mu}_{b,k}^1(0) = [200, 800]^T$, $\boldsymbol{\mu}_{b,k}^2(0) = [800, -800]^T$, and $\Sigma_{b,k}^1(0) = \Sigma_{b,k}^2(0) = \text{diag}([100, 100])$. To the spawned targets generated from existent targets, the measurement model is represented by (14), with $p_k = 1$, $\mathbf{d}_{p.k}^1 = [0, 0]^T$, and $\Sigma_{p,k}^{i1} = \text{diag}([100, 100])$, $i = 1, \ldots, t_k$.

Let the merging threshold of the models $U = 4$, pruning threshold of clutter model $D_c = 3$, and pruning threshold of target-originated measurement model $D_t = 0.5$. With the algorithm proposed, estimation of clutter model can approximately converge to real model, as is shown in Figure 2.

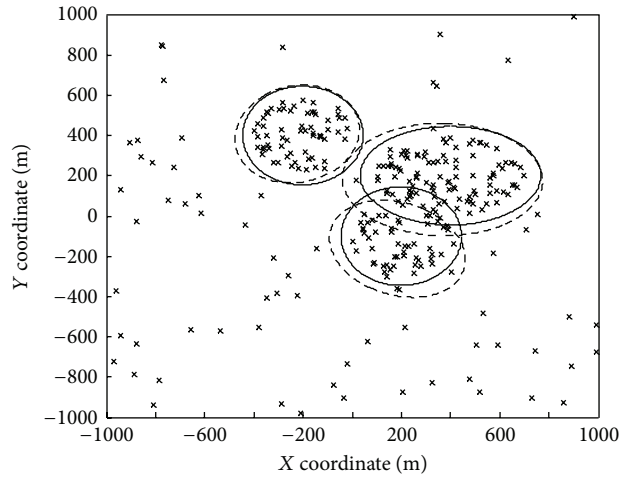

Figure 2: Fitted clutter model.

In Figure 2, the solid line illustrates 95% ellipse of the real clutter model, while the dotted line illustrates 95% ellipse of the estimation. Times of Monte Carlo simulations have shown that some estimation results could fit the region which the clutter concentrated according to Table 1, shown as Figure 2. But it does not exclude some results shown as Figure 3, caused by the complexity of clutter model. No matter how complex the clutter is, FMM algorithm would fit it as a linear superposition of one uniform and many Gaussian distributions, but the parameters may differ from each other, as shown by different dotted ellipse in Figure 3. Nevertheless, these situations do not affect the validity of FMM algorithm, with estimation accuracy satisfied.

7.2.1. Effect Comparison of Target Number Estimation. The target number estimated by GM-PHD filter is represented in Figure 4, while the algorithm proposed in Figure 5.

In Figures 4 and 5, the solid line illustrates the real target number varying with time, while it circles estimation. Apparently, effect of GM-PHD filter is worse. In circumstances of unknown complex clutter distribution, the assumption of uniform style will lead to serious error in target number estimation. Generally speaking, the more dense clutters the target passing and more time spent in this area, the more fake targets could emerge from estimation. As the algorithm proposed can fit clutter model synchronous with tracking, fake targets in high-density clutter area will decrease. Consequently, estimation accuracy of target number improved apparently. One attention: When target is passing high-density clutter area, the state estimation will get lost provisionally.

7.2.2. Effect Comparison of Target Position Estimation. Position estimation of multitarget by GM-PHD filter is represented in Figure 6, while the method is proposed in Figure 7.

In Figures 6 and 7, the solid line illustrates the real target track, while circles illustrate the position estimated. Similarly, the assumption of uniform style will lead to a crowd of fake targets emerging in high-density clutter area.

7.2.3. Evaluation of Effects. Different from single target tracking, root mean square error (RMSE) cannot measure error in multiple targets tracking quantitatively, [18] suggesting that Wasserstein distance can describe error in case of the number of target varying with time in MTT.

Suppose that $X_k = \{\mathbf{x}_k^1, \ldots, \mathbf{x}_k^{T_k}\}$ represents actual multitarget state set at time k; estimated state set $\widehat{X}_k = \{\widehat{\mathbf{x}}_k^1, \ldots, \widehat{\mathbf{x}}_k^{\widehat{T}_k}\}$, where T_k and $\widehat{T}_k$ denote the actual and estimated number of multitarget, respectively. The Wasserstein distance can be defined as

$$d_{p,k}\left(\widehat{X}_k, X_k\right) = \min_{C_k} \sqrt[p]{\sum_{i=1}^{|\widehat{X}_k||X_k|} \sum_{j=1} C_k^{ij} \left\|\widehat{\mathbf{x}}_k^i - \mathbf{x}_k^j\right\|^p}, \tag{41}$$

where C_k denotes transfer matrix with every element $C_k^{ij} \geq 0$, $\Sigma_{j=1}^{|X_k|} C_k^{ij} = 1/|\widehat{X}|$, and $\Sigma_{i=1}^{|X_k|} C_k^{ij} = 1/|X|$. Also, $|\cdot|$ represents cardinality and $\|\cdot\|^p$ represents norm with $p = 2$. When the set of X_k or $\widehat{X}_k$ is empty, Wasserstein distance can be assigned to 0. When the number of elements in X_k and $\widehat{X}_k$ is the same, Wasserstein distance is the best association distance.

Wasserstein distance varying with time of these two methods is shown in Figures 8 and 9. To punish the mistake in target number estimation, Wasserstein distance reaches peak value when the number is wrongly estimated. From Figures 8 and 9, Wasserstein distance of the latter is better than that of former, because the latter has more precise estimation. When the target number is correctly estimated, the value of Wasserstein distance is about 10 m, approximately the square root of trace($\Sigma_{b,k}^i(0)$) in Section 7.2.

8. Conclusion

FMM approach can solve unknown clutter problem in MTT. A novel MTT algorithm based on clutter model preestimation is put forward in this paper. In this algorithm, multitarget likelihood function is established with the finite mixture model (FMM), the parameters of which can be estimated by the algorithm of EM and MCMC. These two algorithms were put forward in the paper. Furthermore, target number and multitarget states can be estimated as well as the clutter model fitted. No matter how complex the clutter is, FMM algorithm would fit it as a linear superposition of one uniform and many Gaussian distributions, but the parameters may differ from each other, but it will not affect the validity of FMM algorithm.

Conflict of Interests

The authors declare that there is no conflict of interests regarding the publication of this paper.

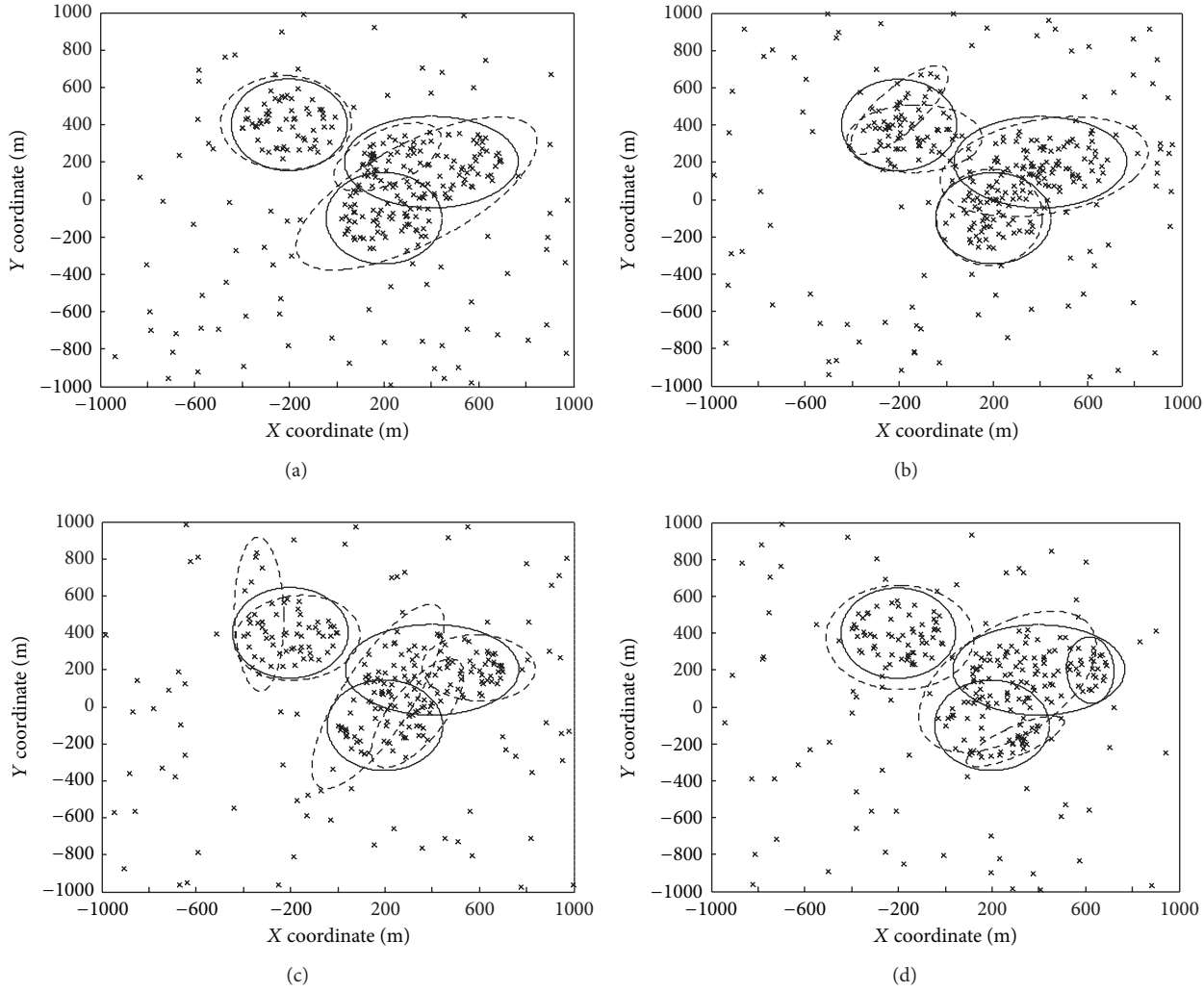

Figure 3: Other estimation result of complex clutter model.

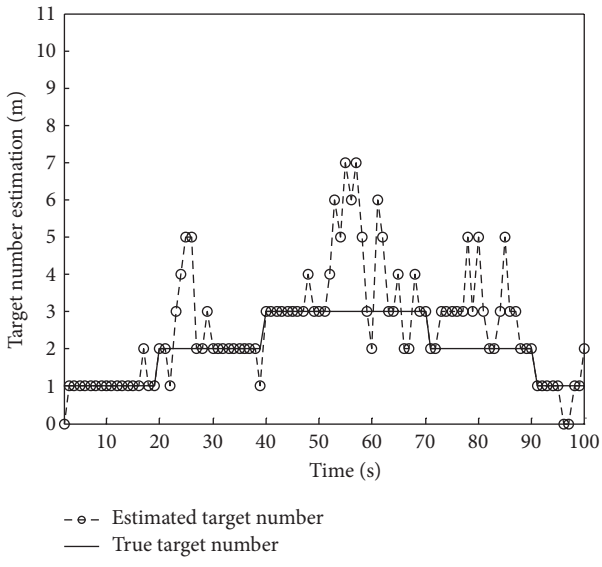

Figure 4: Target number estimation of GM-PHD filter.

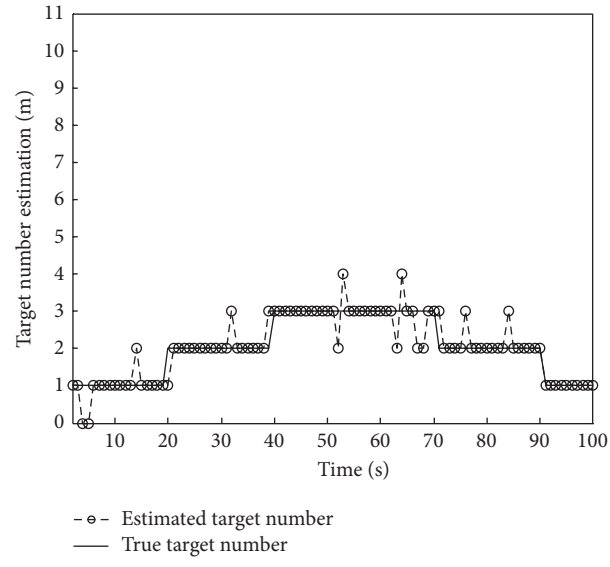

Figure 5: Target number estimation of the proposed method.

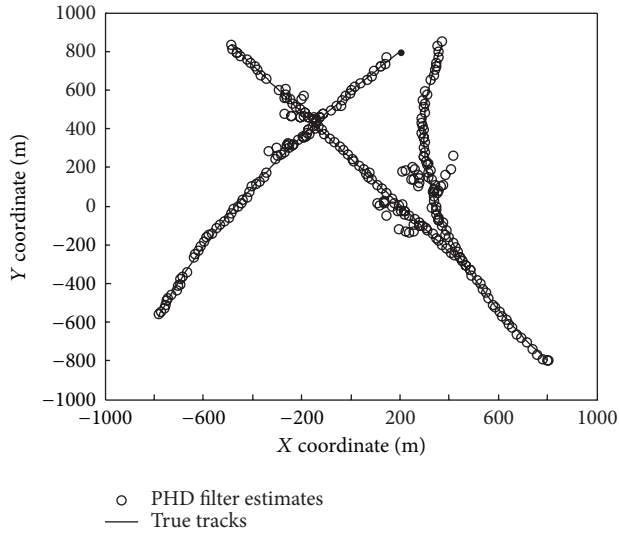

Figure 6: Target position estimation of GM-PHD filter.

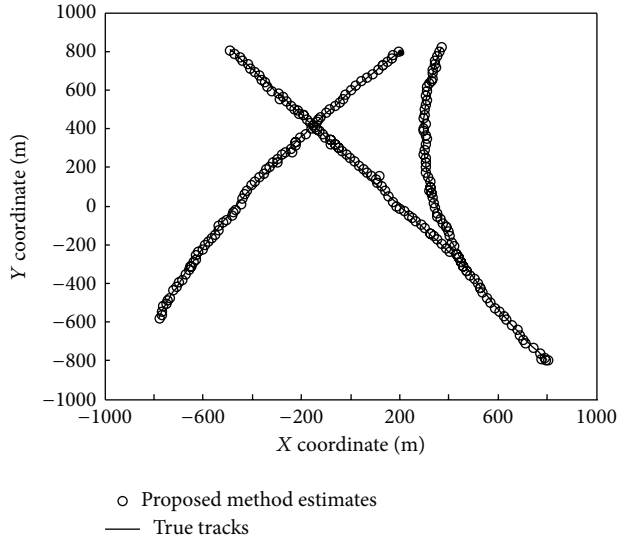

Figure 7: Target position estimation of the proposed method.

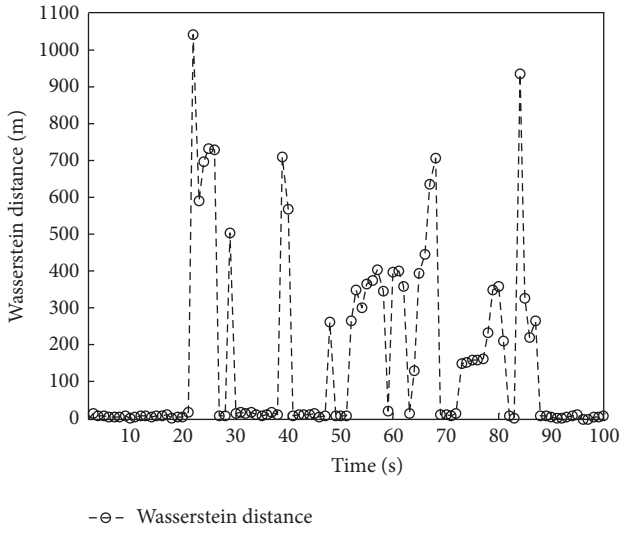

Figure 8: Wasserstein distance of GM-PHD filter.

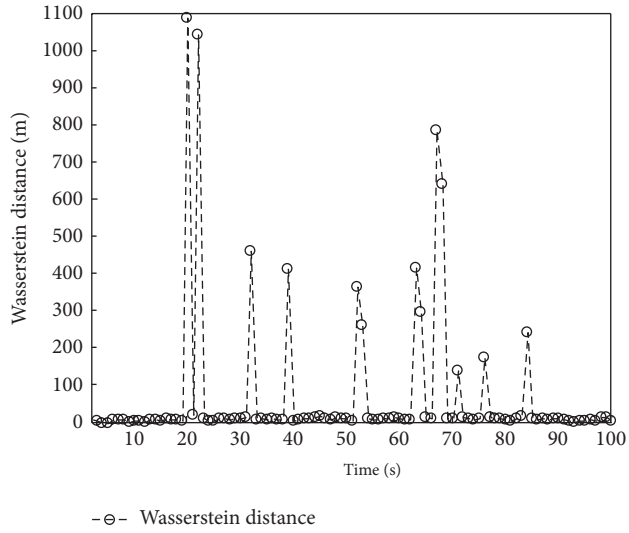

Figure 9: Wasserstein distance of the proposed method.

Acknowledgments

This work was sponsored by Foundation for Innovative Research Groups of the National Natural Science Foundation of China (61221063) and NSFC Grant (61074176).

References

[1] Y. Bar-Shalom and T. E. Fortmann, *Tracking and Data Association*, vol. 179, Academic Press, San Diego, Calif, USA, 1988.

[2] Y. Bar-Shalom and L. Xiao-Rong, *Multitarget-Multisensor Tracking: Principles and Techniques*, YBS Publishing, Storrs, Conn, USA, 1995.

[3] S. Blackman and R. Popoli, *Design and Analysis of Modern Tracking Systems*, Artech House, Boston, Mass, USA, 1999.

[4] H. Samet, "K-nearest neighbor finding using MaxNearestDist," *IEEE Transactions on Pattern Analysis and Machine Intelligence*, vol. 30, no. 2, pp. 243–252, 2008.

[5] S. P. Puranik and J. K. Tugnait, "Tracking of multiple maneuvering targets using multiscan JPDA and IMM filtering," *IEEE Transactions on Aerospace and Electronic Systems*, vol. 43, no. 1, pp. 23–35, 2007.

[6] H. Zhang, X.-P. Fan, and Z.-H. Qu, "Mobile robot adaptive monte carlo localization based on multiple hypothesis tracking," *Acta Automatica Sinica*, vol. 33, no. 9, pp. 941–946, 2007.

[7] R. P. S. Mahler, "Multitarget bayes filtering via first-order multitarget moments," *IEEE Transactions on Aerospace and Electronic Systems*, vol. 39, no. 4, pp. 1152–1178, 2003.

[8] R. Mahler, "PHD filters of higher order in target number," *IEEE Transactions on Aerospace and Electronic Systems*, vol. 43, no. 4, pp. 1523–1543, 2007.

[9] W. Liu and C. Han, "Multitarget tracking algorithm based on finite mixture models and equivalent measurement," in *Proceedings of the 11th International Conference on Information Fusion (FUSION '08)*, pp. 1544–1551, July 2008.

[10] G. McLachlan and D. Peel, *Finite Mixture Models*, Wiley-Interscience, New York, NY, USA, 2000.

[11] B.-N. Vo, S. Singh, and A. Doucet, "Sequential Monte Carlo methods for multi-target filtering with random finite sets," *IEEE*

Transactions on Aerospace and Electronic Systems, vol. 41, no. 4, pp. 1224–1245, 2005.

[12] B.-N. Vo and W.-K. Ma, "The Gaussian mixture probability hypothesis density filter," *IEEE Transactions on Signal Processing*, vol. 54, no. 11, pp. 4091–4104, 2006.

[13] K. Panta, B.-N. Vo, and S. Singh, "Novel data association schemes for the probability hypothesis density filter," *IEEE Transactions on Aerospace and Electronic Systems*, vol. 43, no. 2, pp. 556–570, 2007.

[14] M. A. T. Figueiredo and A. K. Jain, "Unsupervised learning of finite mixture models," *IEEE Transactions on Pattern Analysis and Machine Intelligence*, vol. 24, no. 3, pp. 381–396, 2002.

[15] P. J. Green, "Reversible jump Markov chain monte carlo computation and Bayesian model determination," *Biometrika*, vol. 82, no. 4, pp. 711–732, 1995.

[16] I. R. Goodman, R. P. S. Mahler, and H. T. Nguyen, *Mathematics of Data Fusion*, vol. 37, Kluwer Academic, Norwell, Mass, USA, 1997.

[17] X. R. Li and V. P. Jilkov, "Survey of maneuvering target tracking: dynamic models," in *Proceedings of the International Conference on Signal and Data Processing of Small Targets*, Proceedings of SPIE, pp. 212–235, April 2000.

[18] J. R. Hoffman and R. P. S. Mahler, "Multitarget miss distance via optimal assignment," *IEEE Transactions on Systems, Man, and Cybernetics A*, vol. 34, no. 3, pp. 327–336, 2004.

Hindawi Publishing Corporation
Mathematical Problems in Engineering
Volume 2014, Article ID 373270, 8 pages
http://dx.doi.org/10.1155/2014/373270

Research Article

Distributed Fusion Estimation for Multisensor Multirate Systems with Stochastic Observation Multiplicative Noises

Peng Fangfang and Sun Shuli

School of Electronics Engineering, Heilongjiang University, Harbin 150080, China

Correspondence should be addressed to Sun Shuli; sunsl@hlju.edu.cn

Received 27 August 2013; Accepted 29 December 2013; Published 12 February 2014

Academic Editor: Wendong Xiao

This paper studies the fusion estimation problem of a class of multisensor multirate systems with observation multiplicative noises. The dynamic system is sampled uniformly. Sampling period of each sensor is uniform and the integer multiple of the state update period. Moreover, different sensors have the different sampling rates and observations of sensors are subject to the stochastic uncertainties of multiplicative noises. At first, local filters at the observation sampling points are obtained based on the observations of each sensor. Further, local estimators at the state update points are obtained by predictions of local filters at the observation sampling points. They have the reduced computational cost and a good real-time property. Then, the cross-covariance matrices between any two local estimators are derived at the state update points. At last, using the matrix weighted optimal fusion estimation algorithm in the linear minimum variance sense, the distributed optimal fusion estimator is obtained based on the local estimators and the cross-covariance matrices. An example shows the effectiveness of the proposed algorithms.

1. Introduction

In networked systems or sensor networks, there often exist various uncertainties during the transmission process of signals due to the imperfection of the communication channels. It makes impossible to use linear model to describe some systems. The uncertainties can be approximated mathematically by an additive noise or a multiplicative noise [1–6]. These systems are widely used in petroleum seismic exploration, target detection, speech processing, and other areas; thus, the research on systems with multiplicative noise has the important practical significance. In the early references [1], the optimal linear filters have been proposed for systems with uncertain observations described by the multiplicative noise. For more general case with stochastic parameters, the optimal linear estimation is designed in [2]. References [3–5] study the polynomial filters; however, the proposed nonlinear filters have expensive computational cost. For networked systems with multiplicative noises and packet dropouts, optimal linear estimators including filter, predictor, and smoother have been proposed in [6]. However, the above-mentioned literatures are all concerned with single sensor case but do not take multiple sensors into account.

As the sensor technology is widely used in military, civilian, scientific research, and many other fields, single sensor has failed to meet the performance requirements in many aspects. Moreover, as the development of electronics technologies, various sensors have been developed and applied to many practical fields such as target tracking since they can provide more information than any single sensor. Therefore, multisensor information fusion has received considerable research attention in recent years [7]. For systems with a single sampling rate, the optimal state weighted fusion filter in the linear minimum variance sense [8] and the self-tuning fusion filter with unknown noise variances [9] have been presented. Recently, the multirate multisensor asynchronous fusion algorithms have been studied in [10–12]. References [13, 14] adopt the state augmentation approach to give the estimators with the expensive computational cost. Though [15, 16] adopt the nonaugmented approach to design the filters, a modeling error is made by ignoring the process noise. Therefore, there is the accuracy loss. By considering

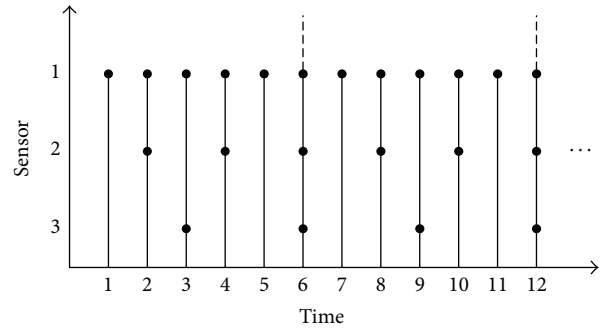

Figure 1: Sampling case of sensors.

the process noise to eliminate the modeling error, an optimal filter is presented to improve the estimation accuracy [17]. Furthermore, the missing measurements are also taken into account in [16, 18]. In [19], a multirate multisensor distributed fusion estimator is proposed for two-sensor systems with one-step cross-covariance noises. However, most of the above-mentioned literatures do not take the multiplicative noises into account. In sensor networks, there often exist various sensors with different sampling rates and stochastic uncertainty of multiplicative noises. It is significant to use the nonaugmented approach to deal with the multirate multisensor systems. This motivates our work.

This paper studies the fusion estimation problem of a class of multisensor multirate systems with observation multiplicative noises. State is sampled uniformly at the finest rate. Different sensors have different sampling periods that are integer multiples of the state update period. Local estimators at the state sampling points are obtained based on the local filters at the observation sampling points by the filtering and prediction. By using the distributed optimal weighted fusion estimation algorithm in the linear minimum variance sense [8], a distributed optimal fusion estimator is obtained. It avoids the state and observation augmentation. It has a good reliability since it has the distributed parallel structure. Moreover, the estimation error cross-covariance matrices between any two local estimators are derived according to the different sampling cases.

2. Problem Formulation

Consider the following multisensor multirate system with observation multiplicative noises:

$$x(t+1) = \Phi x(t) + \Gamma w(t), \tag{1}$$

$$y_i(l_i t) = \left(H_{0i} + \xi_i(l_i t) H_{1i}\right) x(l_i t) + v_i(l_i t), \quad i = 1, 2, \ldots L, \tag{2}$$

where $x(t)$ is the system state at time tT and T is the state update period. Φ, Γ, H_{0i}, and H_{1i} are constant matrices. $y_i(l_i t)$ is the observation of the ith sensor at time $l_i tT$; l_i is the ratio of the observation sampling period and the state update period. L is the number of sensors. $w(t)$ and $v_i(l_i t)$ are white noises with zero mean and variances Q_w and Q_{v_i}, respectively. The observation multiplicative noise $\xi_i(l_i t)$ is scalar white noise with zero mean and variance Q_{ξ_i}. $w(t)$, $v_i(l_i t)$, and $\xi_i(l_i t)$ are uncorrelated with each other. The initial state $x(0)$ is independent of $w(t)$, $v_i(l_i t)$, and $\xi_i(l_i t)$ and satisfies that $E\{x(0)\} = \mu_0$ and $E\{[x(0) - \mu_0][x(0) - \mu_0]^T\} = P_0$, where the symbol E is the mathematical expectation.

Remark 1. The sampling case of multisensor multirate systems can be described by Figure 1. The horizontal axis denotes time while the vertical axis denotes different sensors. Three sensors are shown in Figure 1. Black circle solid points represent the sampling time of different sensors. The sampling rate goes from the highest (sensor 1) to the lowest (sensor 3). As shown in Figure 1, the three sensors all sample uniformly. The first sensor has the same sampling rate as the state update rate; that is, the sampling period is T. The sampling period of the second sensor is $2T$ and the third is $3T$. It is clear that the least common multiple of three sample periods is $6T$. This means that the samplings of different sensors are asynchronous in each data block of the length $6T$.

The objective of this paper is to find the distributed optimal fusion estimator $\hat{x}_o(t)$ of $x(t)$ based on the local estimators $\hat{x}_i(t)$ from different sensors.

To obtain the distributed fusion estimator by using the optimal weighted fusion estimation algorithm in the linear minimum variance sense [8], we need to compute the local estimators and variance matrices from each sensor and the cross-covariance matrices between any two local estimators. In the latter text, we will give the computation of local estimators and cross-covariance matrices.

3. Local Filters at the Observation Sampling Points

At first, we give the filter at the observation sampling points of each sensor.

From the iteration of (1), we have

$$x(l_i t + l_i) = \Phi^{l_i} x(l_i t) + \sum_{m=0}^{l_i - 1} \Phi^m \Gamma w(l_i t + l_i - m - 1). \tag{3}$$

Let $\Phi_i = \Phi^{l_i}$ and $w_i(l_i t) = \sum_{m=0}^{l_i-1} \Phi^m \Gamma w(l_i t + l_i - m - 1)$; we have the state space model at the observation sampling points for the ith sensor as follows:

$$\begin{aligned} x(l_i t + l_i) &= \Phi_i x(l_i t) + w_i(l_i t), \\ y_i(l_i t) &= (H_{0i} + \xi_i(l_i t) H_{1i}) x(l_i t) + v_i(l_i t), \qquad (4) \\ & \qquad i = 1, 2, \ldots, L \end{aligned}$$

with the noise statistical information $Q_{w_i} = E\{w_i(l_i t) w_i(l_i t)^T\} = \sum_{m=0}^{l_i-1} \Phi^m \Gamma Q_w \Gamma^T (\Phi^m)^T$.

Then, we have the filter at the observation sampling points of each sensor based on the above model.

Lemma 2 (see [6]). *For system* (4)*, the local filters at the observation sampling points of the ith sensor are computed by*

$$\begin{aligned} \widehat{x}_i(l_i t \mid l_i t) &= \widehat{x}_i(l_i t \mid l_i t - l_i) + K_i(l_i t)\, \varepsilon_i(l_i t), \\ \widehat{x}_i(l_i t + l_i \mid l_i t) &= \Phi_i \widehat{x}_i(l_i t \mid l_i t), \\ \varepsilon_i(l_i t) &= y_i(l_i t) - H_{0i} \widehat{x}_i(l_i t \mid l_i t - l_i), \\ K_i(l_i t) &= P_i(l_i t \mid l_i t - l_i) H_{0i}^T Q_{\varepsilon i}^{-1}(l_i t), \\ Q_{\varepsilon i}(l_i t) &= H_{0i} P_i(l_i t \mid l_i t - l_i) H_{0i}^T \qquad (5) \\ &\quad + H_{1i} Q_{\xi_i} q_i(l_i t) H_{1i}^T + Q_{v_i}, \\ P_i(l_i t \mid l_i t) &= (I_n - K_i(l_i t) H_{0i}) P_i(l_i t \mid l_i t - l_i), \\ P_i(l_i t + l_i \mid l_i t) &= \Phi_i P_i(l_i t \mid l_i t) \Phi_i^T + Q_{w_i}, \\ q_i(l_i t) &= \Phi_i q_i(l_i t - l_i) \Phi_i^T + Q_{w_i}, \end{aligned}$$

where $\widehat{x}_i(l_i t \mid l_i t)$ and $\widehat{x}_i(l_i t \mid l_i t - l_i)$ are the filter and predictor at the observation sampling points, respectively. $P_i(l_i t \mid l_i t)$ and $P_i(l_i t \mid l_i t - l_i)$ are the corresponding covariance matrices. $\varepsilon_i(l_i t)$ is the innovation sequence with the covariance matrix $Q_{\varepsilon i}(l_i t)$. $K_i(l_i t)$ is the filtering gain matrix. $q_i(l_i t)$ is the state second-order moment. The initial values are $\widehat{x}_i(0 \mid 0) = \mu_0$, $P_i(0 \mid 0) = P_0$, and $q_i(0) = \mu_0 \mu_0^T + P_0$.

4. Local Estimators at the State Update Points

Based on the filters at the observation sampling points in Lemma 2, we have the following state estimation algorithms at the state update points.

Theorem 3. *For system* (1)-(2)*, the local estimators at the state update points of the ith sensor are computed by*

$$\widehat{x}_i(t) = \begin{cases} \widehat{x}_i(l_i l \mid l_i l), & t = l_i l,\ l = 0, 1, 2, \ldots \\ \Phi^p \widehat{x}_i(l_i l \mid l_i l), & t = l_i l + p,\ p = 1, 2, \ldots, l_i - 1. \end{cases} \qquad (6)$$

The estimation error covariance matrices are computed by

$$P_i(t) = \begin{cases} P_i(l_i l \mid l_i l), & t = l_i l,\ l = 0, 1, 2, \ldots \\ \Phi^p P_i(l_i l \mid l_i l) (\Phi^p)^T & \\ \quad + \sum_{m=0}^{p-1} \Phi^m \Gamma Q_w \Gamma^T (\Phi^m)^T, & t = l_i l + p,\ p = 1, 2, \ldots, l_i - 1, \end{cases} \qquad (7)$$

where $\widehat{x}_i(l_i l \mid l_i l)$ and $P_i(l_i l \mid l_i l)$ are computed by Lemma 2.

Proof. When $t = l_i l$, $l = 0, 1, 2, \ldots$, we have the filters $\widehat{x}_i(t) = \widehat{x}_i(l_i l \mid l_i l)$. When $t = l_i l + p$, $p = 1, 2, \ldots, l_i - 1$, we have the predictors $\widehat{x}_i(t) = \widehat{x}_i(l_i l + p \mid l_i l)$. Then from the iteration of (1), we have

$$\begin{aligned} x(l_i l + p) &= \Phi^p x(l_i l) \\ &\quad + \sum_{m=0}^{p-1} \Phi^m \Gamma w(l_i l + p - m - 1), \qquad (8) \\ & \qquad p = 1, 2, \ldots l_i - 1. \end{aligned}$$

Taking projection of both sides of (8) onto the linear space $\{y_i(0), y_i(l_i), \ldots, y_i(l_i l)\}$, we have the second equation of (6).

From (6) and (8), we easily obtain the estimation error equations:

$$\widetilde{x}_i(t) = \begin{cases} \widetilde{x}_i(l_i l \mid l_i l), & t = l_i l,\ l = 0, 1, 2, \ldots \\ \Phi^p \widetilde{x}_i(l_i l \mid l_i l) & \\ \quad + \sum_{m=0}^{p-1} \Phi^m \Gamma w(l_i l + p - m - 1), & t = l_i l + p,\ p = 1, 2, \ldots, l_i - 1, \end{cases} \qquad (9)$$

where the estimation error is $\widetilde{x}_i(t) = x(t) - \widehat{x}_i(t)$. Substituting (9) into $P_i(t) = E[\widetilde{x}_i(t) \widetilde{x}_i^T(t)]$, we have (7). This proof is completed. □

Remark 4. The local estimators at the state update points have been obtained by filtering and prediction based on the filter at the observation sampling points. State augmentation is avoided. They are simple and have a good real-time property.

Now, we have obtained the local estimators at the state update points based on the observations of each sensor. Next, we compute the cross-covariance matrices between any two local estimators.

5. Computation of Cross-Covariance Matrix

Theorem 5. *The estimation error cross-covariance matrices between any two local estimators can be computed in the following three cases.*

(i) *If the ith sensor and the jth sensor both have observations at time tT, the estimation error cross-covariance matrix is given as*

$$\begin{aligned} P_{ij}(t) &= \Phi P_{ij}(t-1)\Phi^T + \Gamma Q_w \Gamma^T \\ &\quad + K_i(t) H_{0i}\left(\Phi P_{ij}(t-1)\Phi^T + \Gamma Q_w \Gamma^T\right) H_{0j}^T K_j^T(t) \\ &\quad - \Phi P_{ij}(t-1)\Phi^T H_{0j}^T K_j^T(t) - \Gamma Q_w \Gamma^T H_{0j}^T K_j^T(t) \\ &\quad - K_i(t) H_{0i}\Phi P_{ij}(t-1)\Phi^T - K_i(t) H_{0i}\Gamma Q_w \Gamma^T. \end{aligned} \tag{10}$$

(ii) *If the ith sensor has an observation and the jth sensor does not have any observation at time tT, the estimation error cross-covariance matrix is given as*

$$\begin{aligned} P_{ij}(t) &= \Phi P_{ij}(t-1)\Phi^T + \Gamma Q_w \Gamma^T \\ &\quad - K_i(t) H_{0i}\Phi P_{ij}(t-1)\Phi^T - K_i(t) H_{0i}\Gamma Q_w \Gamma^T. \end{aligned} \tag{11}$$

(iii) *If both the ith sensor and the jth sensor do not have observations at time tT, the estimation error cross-covariance matrix is given as*

$$P_{ij}(t) = \Phi P_{ij}(t-1)\Phi^T + \Gamma Q_w \Gamma^T. \tag{12}$$

The initial value is $P_{ij}(0) = P_0$.

Proof. (i) If the ith sensor and the jth sensor both have observations at time tT, we have local filters as

$$\begin{aligned} \widehat{x}_i(t) &= \widehat{x}_i(t \mid t-1) + K_i(t)\varepsilon_i(t) \\ &= \Phi \widehat{x}_i(t-1) + K_i(t)\varepsilon_i(t), \\ \widehat{x}_j(t) &= \widehat{x}_j(t \mid t-1) + K_j(t)\varepsilon_j(t) \\ &= \Phi \widehat{x}_j(t-1) + K_j(t)\varepsilon_j(t), \end{aligned} \tag{13}$$

where

$$\begin{aligned} \widehat{x}_i(t-1) &= \widehat{x}_i\left(t-1 \mid t-l_i\right), \\ \widehat{x}_j(t-1) &= \widehat{x}_j\left(t-1 \mid t-l_j\right). \end{aligned} \tag{14}$$

Then we obtain the estimation error equation as

$$\begin{aligned} \widetilde{x}_i(t) &= \Phi \widetilde{x}_i\left(t-1 \mid t-l_i\right) \\ &\quad + \Gamma w(t-1) - K_i(t)\varepsilon_i(t), \\ \widetilde{x}_j(t) &= \Phi \widetilde{x}_j\left(t-1 \mid t-l_j\right) \\ &\quad + \Gamma w(t-1) - K_j(t)\varepsilon_j(t). \end{aligned} \tag{15}$$

The cross-covariance matrix can be computed by

$$\begin{aligned} P_{ij}(t) &= E\left[\widetilde{x}_i(t \mid t)\widetilde{x}_j^T(t \mid t)\right] \\ &= \Phi P_{ij}(t-1)\Phi^T + \Gamma Q_w \Gamma^T \\ &\quad + K_i(t) E\left\{\varepsilon_i(t)\varepsilon_j^T(t)\right\} K_j^T(t) \\ &\quad - \Phi E\left\{\widetilde{x}_i\left(t-1 \mid t-l_j\right)\varepsilon_j^T(t)\right\} K_j^T(t) \\ &\quad - \Gamma E\left\{w(t-1)\varepsilon_j^T(t)\right\} K_j^T(t) \\ &\quad - K_i(t) E\left\{\varepsilon_i(t)\widetilde{x}_j^T\left(t-1 \mid t-l_j\right)\right\}\Phi^T \\ &\quad - K_i(t) E\left\{\varepsilon_i(t) w^T(t-1)\right\}\Gamma^T, \end{aligned} \tag{16}$$

where

$$\begin{aligned} &E\left\{\varepsilon_i(t)\varepsilon_j^T(t)\right\} \\ &\quad = H_{0i}\left(\Phi P_{ij}\left(t-1 \mid t-l_i, t-l_j\right)\Phi^T + \Gamma Q_w \Gamma^T\right) H_{0j}^T, \\ &E\left\{w(t-1)\varepsilon_j^T(t)\right\} = Q_w \Gamma^T H_{0j}^T, \\ &E\left\{\varepsilon_i(t)\widetilde{x}_j^T\left(t-1 \mid t-l_j\right)\right\} \\ &\quad = H_{0i}\Phi P_{ij}\left(t-1 \mid t-l_i, t-l_j\right). \end{aligned} \tag{17}$$

Substituting (17) into (24) and noting that $P_{ij}(t-1) = P_{ij}(t-1 \mid t-l_i, t-l_j)$, (10) is obtained.

(ii) If the ith sensor has an observation and the jth sensor does not have any observation at time tT, we have local estimators as

$$\begin{aligned} \widehat{x}_i(t) &= \widehat{x}_i(t \mid t-1) + K_i(t)\varepsilon_i(t) \\ &= \Phi \widehat{x}_i(t-1) + K_i(t)\varepsilon_i(t), \\ \widehat{x}_j(t) &= \widehat{x}_j(t \mid t-1) = \Phi \widehat{x}_j(t-1). \end{aligned} \tag{18}$$

Then, we have the estimation error equation as

$$\begin{aligned} \widetilde{x}_i(t) &= \Phi \widetilde{x}_i\left(t-1 \mid t-l_i\right) \\ &\quad + \Gamma w(t-1) - K_i(t)\varepsilon_i(t), \\ \widetilde{x}_j(t) &= \widetilde{x}_j(t \mid t-1) \\ &= \Phi \widetilde{x}_j\left(t-1 \mid t-l_j\right) + \Gamma w(t-1). \end{aligned} \tag{19}$$

Similarly to the derivation of the case (i), (11) can be obtained by computing $P_{ij}(t) = E[\widetilde{x}_i(t)\widetilde{x}_j^T(t)]$.

(iii) If both the ith sensor and the jth sensor do not have observations at time tT, we have local estimators as

$$\begin{aligned} \widehat{x}_i(t) &= \widehat{x}_i(t \mid t-1) \\ &= \Phi \widehat{x}_i(t-1) = \Phi \widehat{x}_i\left(t-1 \mid t-l_i\right), \\ \widehat{x}_j(t) &= \widehat{x}_j(t \mid t-1) \\ &= \Phi \widehat{x}_j(t-1) = \Phi \widehat{x}_j\left(t-1 \mid t-l_j\right). \end{aligned} \tag{20}$$

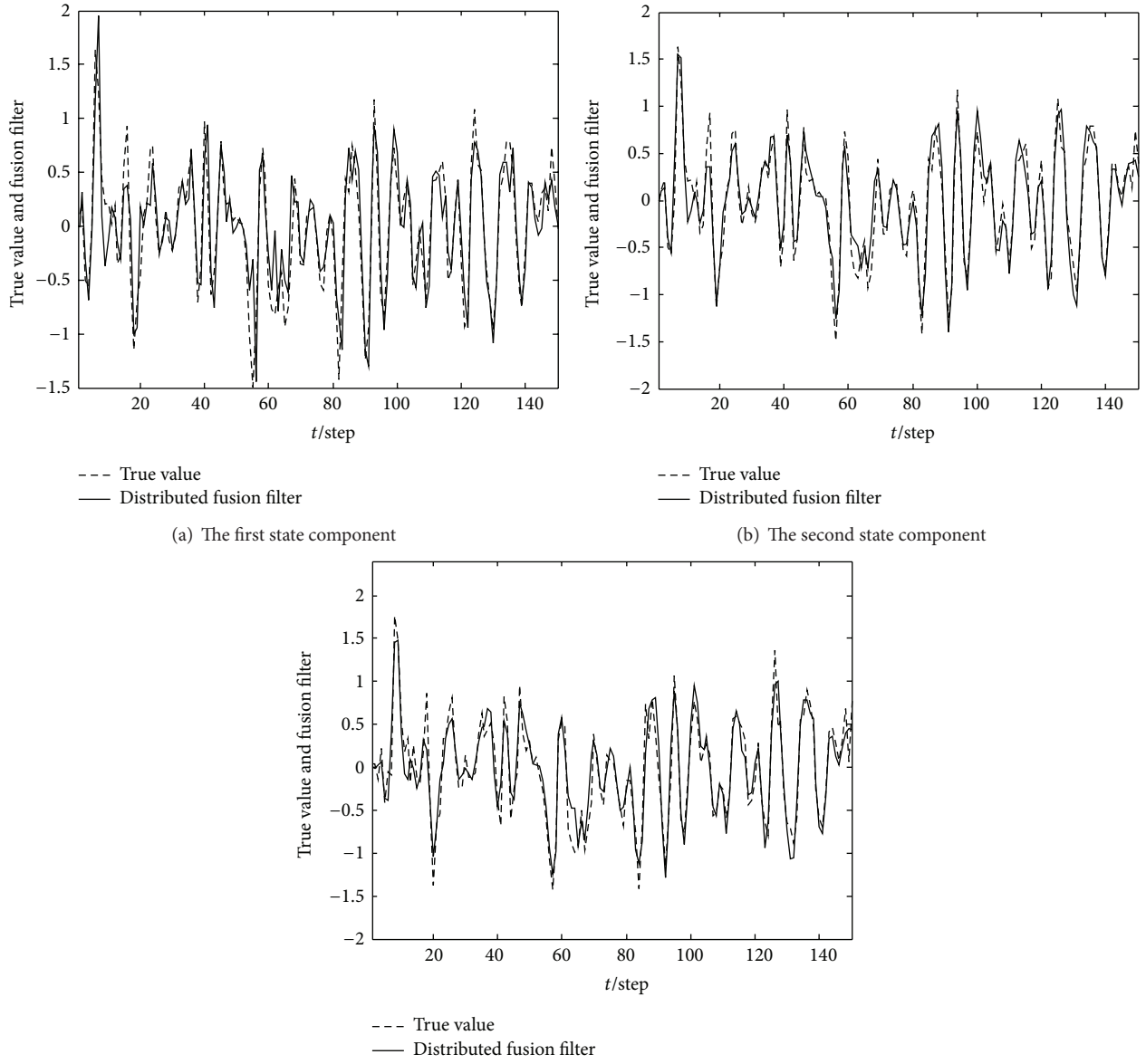

(a) The first state component

(b) The second state component

(c) The third state component

Figure 2: Distributed fusion filter.

We have the estimation error equation as

$$\begin{aligned}\widetilde{x}_i(t) &= \widetilde{x}_i(t \mid t-1)\\ &= \Phi\widetilde{x}_i\left(t-1 \mid t-l_i\right) + \Gamma w(t-1),\\ \widetilde{x}_j(t) &= \widetilde{x}_j(t \mid t-1)\\ &= \Phi\widetilde{x}_j\left(t-1 \mid t-l_i\right) + \Gamma w(t-1).\end{aligned} \tag{21}$$

Then (12) is obtained by computing $P_{ij}(t) = E[\widetilde{x}_i(t)\widetilde{x}_j^T(t)]$. This proof is completed. □

6. Distributed Fusion Estimator

In the preceding sections, we have obtained the local estimators at the state update points and their covariance matrices. Applying the distributed matrix weighted optimal fusion estimation algorithm in the linear minimum variance sense [8], we can obtain the distributed fusion estimator as follows:

$$\widehat{x}_o(t) = \sum_{i=1}^{L} A_i(t)\,\widehat{x}_i(t). \tag{22}$$

The optimal weighted matrices are computed by

$$\left[A_1(t), \ldots, A_L(t)\right] = \left(e^T P^{-1}(t)\, e\right)^{-1} e^T P^{-1}(t), \tag{23}$$

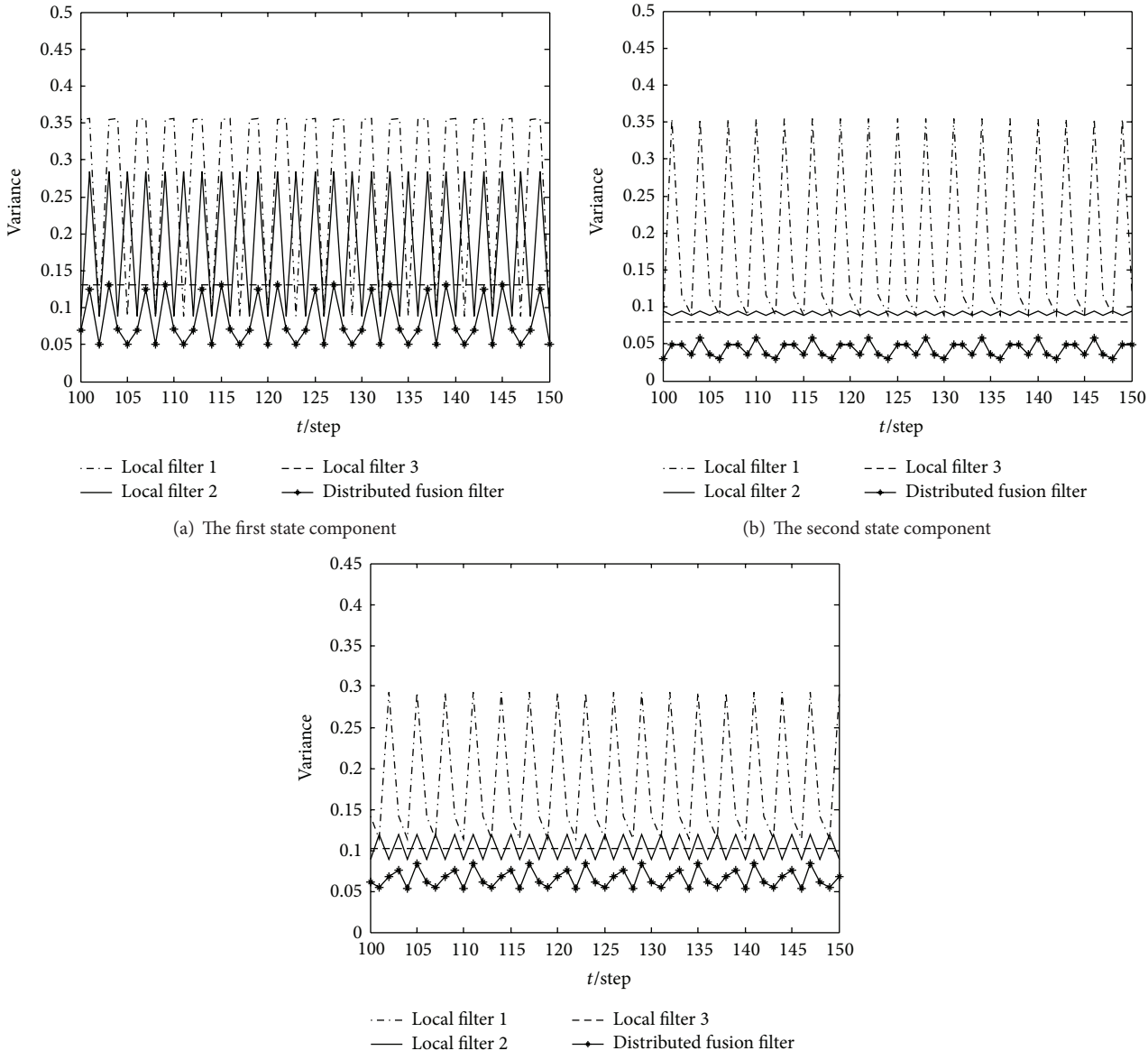

(a) The first state component

(b) The second state component

(c) The third state component

Figure 3: Comparison of variances of distributed fusion filter and local filters.

where $P(t) = (P_{ij}(t))$ is an $nL \times nL$ matrix whose (i, j) block is $P_{ij}(t)$ and $e = [I_n, \ldots, I_n]^T$ is an $nL \times n$ matrix. Then, the optimal fusion estimation error variance matrix is computed by

$$P_o(t) = \left(e^T P^{-1}(t)\, e\right)^{-1}. \tag{24}$$

Furthermore, we have $P_o(t) \leq P_i(t)$.

Remark 6. Compared to the centralized fusion estimator, the distributed fusion estimator has the flexibility, fault tolerance, and reliability since it has the distributed parallel structure [8].

7. Simulation

An uninterruptible power system (UPS) with three sensors subject to the multiplicative noises is taken as an example to demonstrate the effectiveness and applicability of the proposed method. We consider the UPS with 1KVA. The discrete-time model (1) can be obtained with sampling time 10 ms at half-load operating point as follows [20]:

$$x(t+1) = \begin{pmatrix} 0.9226 & -0.6330 & 0 \\ 1 & 0 & 0 \\ 0 & 1 & 0 \end{pmatrix} x(t) + \begin{pmatrix} 0.5 \\ 0 \\ 0.2 \end{pmatrix} w(t)$$

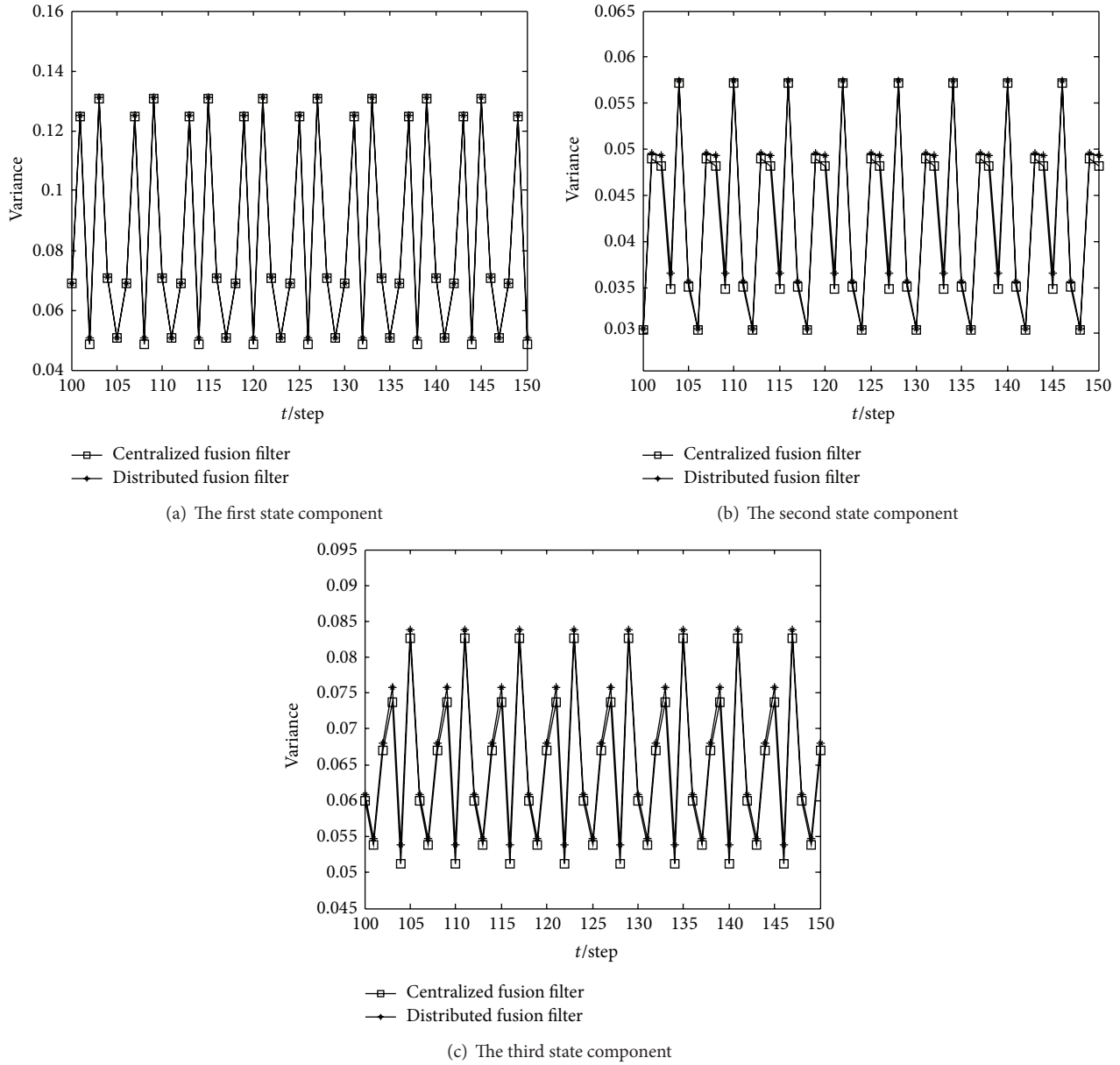

(a) The first state component

(b) The second state component

(c) The third state component

Figure 4: Comparison of variances of centralized and distributed fusion filters.

$$y_i(l_it) = \left(\left(23.738 \quad 20.287 \quad 0\right) + \xi_i(l_it) H_{1i}\right) x_i(l_it) + v_i(l_it), \quad i = 1, 2, 3, \tag{25}$$

where $w(t)$, $v_i(l_it)$, and $\xi_i(l_it)$ are uncorrelated white noises with zero mean and variances Q_w, Q_{v_i}, and Q_{ξ_i}. In simulation, we take $Q_w = 0.64$, $Q_{\xi_1} = 1.2$, $Q_{\xi_2} = 0.7$, $Q_{\xi_3} = 0.3$, $Q_{v_1} = 3$, $Q_{v_2} = 2$, $Q_{v_3} = 1$, $l_1 = 1$, $l_2 = 2$, $l_3 = 3$, $H_{11} = [8 \ 12 \ 6]$, $H_{12} = [10 \ 8 \ 5]$, $H_{13} = [8 \ 6 \ 10]$, the initial values $x(0) = 0$, and $P_0 = 0.1I_3$. The sampling case is shown in Figure 1. Figure 2 gives the distributed fusion estimator. We see that the fusion estimator has the effective estimation performance. Figure 3 gives the comparison of variances of the distributed fusion estimator and local estimators. We see that the proposed fusion estimator outperforms the local estimators. Figure 4 gives the comparison of variances of the distributed fusion estimator and centralized fusion estimator. We see that the distributed fusion estimator has the small accuracy loss. However, it is significant that the distributed fusion estimator has better reliability than the centralized fusion estimator since it is convenient to detect and isolate the faults of sensors from distributed structure.

8. Conclusion

A distributed fusion estimator has been designed for systems with multiple sensors of different sampling rates and observation multiplicative noises. Compared with the centralized

fusion estimator, it has the small accuracy loss and better reliability. Sampling period of each sensor is uniform and the integer multiple of the state update period. By establishing the state space model at the observation sampling points, the local filters at the observation sampling points are obtained. Further, the local estimators at the state update points are obtained by the filtering and prediction approach. They avoid the state augmentation and have a good real-time property. The cross-covariance matrices between any two local estimators are derived. The distributed fusion estimator is obtained by well-known weighted fusion estimation algorithm in linear minimum variance sense.

Conflict of Interests

The authors declare that there is no conflict of interests regarding the publication of this paper.

Acknowledgments

This work is supported by the Natural Science Foundation of China (NSFC-60874062 and NSFC-61174139), by the Program for New Century Excellent Talents in University (no. NCET-10-0133), by the Chang Jiang Scholar Candidates Program for Provincial Universities in Heilongjiang (no. 2013CJHB005), by Science and Technology Innovative Research Team in Higher Educational Institutions of Heilongjiang Province (No. 2012TD007), by the Program for High-qualified Talents (no. Hdtd2010-03), and by the Electronic Engineering Provincial Key Laboratory.

References

[1] N. Nahi, "Optimal recursive estimation with uncertain observation," *IEEE Transactions on Information Theory*, vol. 15, no. 4, pp. 457–462, 1969.

[2] W. L. de Koning, "Optimal estimation of linear discrete-time systems with stochastic parameters," *Automatica*, vol. 20, no. 1, pp. 113–115, 1984.

[3] F. Carravetta, A. Germani, and M. Raimondi, "Polynomial filtering of discrete-time stochastic linear systems with multiplicative state noise," *IEEE Transactions on Automatic Control*, vol. 42, no. 8, pp. 1106–1126, 1997.

[4] M. Basin, J. Pérez, and M. Skliar, "Optimal filtering for polynomial system states with polynomial multiplicative noise," *International Journal of Robust and Nonlinear Control*, vol. 16, no. 6, pp. 303–314, 2006.

[5] M. V. Basin and D. Calderón Álvarez, "Optimal filtering for incompletely measured polynomial systems with multiplicative noise," *Circuits, Systems, and Signal Processing*, vol. 28, no. 2, pp. 223–239, 2009.

[6] J. Ma and S. L. Sun, "Optimal linear estimation for systems with multiplicative noise uncertainties and multiple packet dropouts," *IET Signal Processing*, vol. 6, no. 9, pp. 839–848, 2012.

[7] Z. L. Deng, *Information Fusion Filtering Theory with Applications*, Harbin Institute of Technology Press, Harbin, China, 2007.

[8] S. L. Sun and Z. L. Deng, "Multi-sensor optimal information fusion Kalman filter," *Automatica*, vol. 40, no. 6, pp. 1017–1023, 2004.

[9] Z. L. Deng, Y. Gao, C. B. Li, and G. Hao, "Self-tuning decoupled information fusion Wiener state component filters and their convergence," *Automatica*, vol. 44, no. 3, pp. 685–695, 2008.

[10] C. L. Wen, B. Lu, and Q. B. Ge, "Data fusion algorithm based on filtering step by step," *Acta Electronica Sinica*, vol. 32, no. 8, pp. 1264–1267, 2004.

[11] Q. B. Ge, G. A. Wang, T. H. Tang, and C. Wen, "The research on asynchronous data fusion algorithm based on sampling of rational number times," *Acta Electronica Sinica*, vol. 34, no. 3, pp. 543–548, 2006.

[12] C. L. Wen, Z. G. Chen, L. P. Yan, and D. Zhou, "Multiscale recursive fusion estimation based on dynamic systems of multirate sensors," *Journal of Electronics and Information Technology*, vol. 25, no. 3, pp. 306–312, 2003.

[13] L. P. Yan, B. S. Liu, and D. H. Zhou, "The modeling and estimation of asynchronous multirate multisensor dynamic systems," *Aerospace Science and Technology*, vol. 10, no. 1, pp. 63–71, 2006.

[14] C. Y. Xiao, J. Ma, and S. L. Sun, "Design of information fusion filter for a class of multi-sensor asynchronous sampling systems," in *Proceedings of the Chinese Control and Decision Conference (CCDC '11)*, pp. 1081–1084, May 2011.

[15] L. P. Yan, B. S. Liu, and D. H. Zhou, "Asynchronous multirate multisensor information fusion algorithm," *IEEE Transactions on Aerospace and Electronic Systems*, vol. 43, no. 3, pp. 1135–1146, 2007.

[16] L. P. Yan, D. H. Zhou, M. Y. Fu, and Y. Q. Xia, "State estimation for asynchronous multirate multisensor dynamic systems with missing measurements," *IET Signal Processing*, vol. 4, no. 6, pp. 728–739, 2010.

[17] H. L. Lin, J. Ma, and S. L. Sun, "Optimal state filters for a class of non-uniform sampling systems," *Journal of Systems Science and Mathematics*, vol. 32, no. 6, pp. 768–779, 2012.

[18] Z. H. Deng, L. P. Yan, and M. Y. Fu, "Multirate multisensor data fusion based on missing measurements," *Systems Engineering and Electronics*, vol. 32, no. 5, pp. 886–958, 2010.

[19] Y. L. Liu, L. P. Yan, and Y. Q. Xia, "Multirate multisensor distributed data fusion algorithm for state estimation with cross-correlated noises," in *Proceedings of the 32nd Chinese Control Conference*, Technical Committee on Control Theory, Chinese Association of Automation, Xi'an, China, July 2013.

[20] Y. Rong, *The design of iterative learning control and its application to UPS [M.S. thesis]*, Fuzhou University, Fuzhou, China, 2003.

Hindawi Publishing Corporation
Mathematical Problems in Engineering
Volume 2014, Article ID 825809, 7 pages
http://dx.doi.org/10.1155/2014/825809

Research Article

Weighted Measurement Fusion Quantized Filtering with Bandwidth Constraints and Missing Measurements in Sensor Networks

Jian Ding, Jing Ma, and Shuli Sun

Department of Automation, Heilongjiang University, Harbin 150080, China

Correspondence should be addressed to Shuli Sun; sunsl@hlju.edu.cn

Received 14 September 2013; Accepted 29 December 2013; Published 4 February 2014

Academic Editor: Wendong Xiao

This paper is concerned with the estimation problem of a dynamic stochastic variable in a sensor network, where the quantization of scalar measurement, the optimization of the bandwidth scheduling, and the characteristic of transmission channels are considered. For the imperfect channels with missing measurements in sensor networks, two weighted measurement fusion (WMF) quantized Kalman filters based on the quantized measurements arriving at the fusion center are presented. One is dependent on the known message of whether a measurement is received. The other is dependent on the probability of missing measurements. They have the reduced computational cost and same accuracy as the corresponding centralized fusion filter. The approximate solution for the optimal bandwidth-scheduling problem is given under a limited bandwidth constraint. Furthermore, the vector measurement case is also discussed. The simulation research shows the effectiveness.

1. Introduction

In recent years, sensor networks have been widely investigated in decentralized estimation, detection, and control due to the significant applications in environmental monitoring, intelligent transportation, space exploration, and so forth [1]. In wireless sensor networks (WSN), a large number of sensors are spatially distributed to monitor the signal of interest. Each sensor makes a measurement of the signal and transmits it to the fusion center (data processing center). Due to a bandwidth constraint, each sensor is only able to transmit a finite number of bits. So the measurement must be quantized to adapt the limited bandwidth before it is transmitted. Due to the imperfection of networks, the quantized measurement can be lost during the transmission. Then the fusion centre will use the quantized measurements received to obtain a fusion estimate of the signal. WSN introduce many interesting research topics such as information fusion [2], network lifetime maximization [3], sensor coverage or scheduling [4], and optimization with bandwidth or energy-efficient constraints [5].

Various algorithms have been proposed for network estimation, detection, and control [5–18]. Decentralized detection is investigated in a sensor network where the communication channels between sensors and the fusion centre are bandwidth constrained [5]. Several distributed estimators for parameters have been designed in the presence of additive sensor noise [6–10]. A universal decentralized estimator taking into account local SNR and channel path loss in sensor networks is studied [11] where the power scheduling optimization is solved based on the Karush-Kuhn-Tucker (KKT) condition. Quantization approach in many references above is to quantize the sensor's measurements directly. A distributed estimation approach based on the sign of innovations (SOI) is developed in [12] where only the transmission of a single bit per measurement is required. However, the cost of saving more communication is more accuracy loss. As a generalization of [12], a multilevel quantized innovation filter is presented [13, 14]. The estimation and control based on the logarithm quantization approach are studied in [15, 16]. Quantized Kalman filters based on quantized scalar measurements and innovations are presented for perfect channels in sensor networks [17], respectively. However, the quantized estimation for imperfect channels with missing measurements is not taken into consideration. A centralized

fusion quantized filter dependent on the packet dropout rate is designed for sensor networks with packet dropouts [18]. However, it has the expensive computational burden due to the augmented measurements.

In this paper, the quantized estimation problem for a dynamic stochastic variable is studied in a sensor network. Due to the limited bandwidth constraint, the measurement of sensors is quantized uniformly according to a given optimal bandwidth scheduling. During the transmission of quantized measurements, there are possible losses due to imperfect channels. Due to the large number of data, the fusion center compresses the received measurements to produce a reduced dimensional fused measurement, based on which, two weighted measurement fusion quantized filters are presented. One is dependent on the knowledge of whether a packet is received. The other is dependent on the probabilities of missing measurements. The front has the better accuracy since more messages are used. They have the same accuracy as the corresponding centralized fusion filters.

2. Problem Formulation

Consider the discrete-time system in a sensor network with N sensors

$$x(t+1) = \Phi(t)\, x(t) + \Gamma(t)\, w(t) \tag{1}$$

$$y_i(t) = h_i(t)\, x(t) + v_i(t), \quad i = 1, 2, \ldots, N, \tag{2}$$

where $x(t) \in R^n$ is the state to be estimated, $y_i(t) \in R$ is the scalar measurement of the ith sensor, N is the number of sensors, and $\Phi(t)$, $\Gamma(t)$, $h_i(t)$ are time-varying matrices with appropriate dimensions.

Assumption 1. $w(t) \in R^r$ and $v_i(t) \in R$, $i = 1, 2, \ldots, N$ are uncorrelated white noises with zero mean and variances $Q_w(t)$ and $\sigma_{v_i}^2(t)$. The initial value $x(0)$ with mean μ_0 and variance P_0 is uncorrelated with $w(t)$ and $v_i(t)$.

Assumption 2. $y_i(t) \in [\underline{U}_i, \overline{U}_i]$, where $\underline{U}_i$ and $\overline{U}_i$, $i = 1, 2, \ldots, N$, are known constants.

The estimation problem considered is shown in Figure 1. Each sensor makes a measurement $y_i(t)$. Due to the limited bandwidth, it is quantized to produce a quantized measurement $m_i(t) = q(y_i(t))$ where $q(\cdot)$ is a quantized function. Then, $m_i(t)$ is transmitted to the fusion center by an imperfect channel where there are possible packet losses. We introduce a Bernoulli distributed random variable $\gamma_i(t)$ with the probabilities $\mathrm{Prob}\{\gamma_i(t) = 1\} = \alpha_i$ and $\mathrm{Prob}\{\gamma_i(t) = 0\} = 1 - \alpha_i$ to describe the phenomena of missing measurements. Namely, the data received by the fusion center is $m_i'(t) = \gamma_i(t) m_i(t)$, where $\gamma_i(t) = 1$ means the quantized measurement is received and $\gamma_i(t) = 0$ means loss. At last, the fusion center will combine the received data $m_i'(t)$ to give a final estimate for state $x(t)$. We assume that the fusion center knows all the parameters of system (1). If there is a sufficient bandwidth to be supplied and the channel is perfect, that is, in the case of $m_i'(t) = y_i(t)$, the standard Kalman filter can be used [19]. If the bandwidth is limited and the channel is perfect, that is, in the case of $m_i'(t) = m_i(t)$, the fusion center will make the estimate based on the received measurements $\{m_i(t),\ i = 1, 2, \ldots, N\}$. Otherwise, the fusion center has to make the estimate based on the received measurements $\{m_i'(t),\ i = 1, 2, \ldots, N\}$.

Our aim in this paper is to find the weighted measurement fusion quantized Kalman filters (WMF-QKF) under the limited bandwidth by imperfect channels. Two kinds of filters are designed. One is dependent on the values of $\gamma_i(t)$, the other is dependent on the probability of $\gamma_i(t)$.

3. WMF-QKF

3.1. Quantization and Bandwidth Scheduling. We adopt the uniform quantization strategy in [11]. Measurement $y_i(t)$ is quantized to $m_i(t)$ with the length of $b_i(t)$ bits, where $b_i(t)$ is to be determined later. We have $2^{b_i(t)}$ quantization points spaced uniformly within the interval $[\underline{U}_i, \overline{U}_i]$. The quantization noise $n_i(t) = m_i(t) - y_i(t)$ is uncorrelated white noise with zero mean and variance $\sigma_{n_i}^2(t) = \mathrm{E}(n_i(t))^2 = \mathrm{E}(m_i(t) - y_i(t))^2 \le \delta_i^2(t)$ where $\delta_i^2(t) = (\overline{U}_i - \underline{U}_i)^2 / [4(2^{b_i(t)} - 1)^2]$. Furthermore, $n_i(t)$, $v_i(t)$, $i = 1, 2, \ldots, N$, and $w(t)$ are uncorrelated with each other.

In sensor networks, the whole bandwidth of communication channels is bounded. Let B be the bits of the whole bandwidth and let $b_i(t)$ be the bits scheduled to the ith sensor. To obtain the good estimation performance under the constraint of bounded bandwidths, we adopt the following bandwidth scheduling strategy [17]:

$$\begin{aligned} \min \quad & \sum_{i=1}^{N} \frac{h_i(t)\, h_i^T(t)}{\sigma_{v_i}^2(t)} \delta_i^2(t) \\ \text{s.t.} \quad & \sum_{i=1}^{N} b_i(t) \le B, \quad b_i(t) \ge 0,\ i = 1, 2, \ldots, N, \end{aligned} \tag{3}$$

where $h_i(t) h_i^T(t) / \sigma_{v_i}^2(t)$ is the SNR (signal to noise ratio). Then the optimal solution of $b_i(t)$ is given as

$$\begin{aligned} b_i(t) &= \left\lceil \log_2 \left(\frac{\sqrt{\ln 2 h_i(t)\, h_i^T(t)}\, (\overline{U}_i - \underline{U}_i)}{\sigma_{v_i}(t) \sqrt{2\lambda(t)}} \right) \right\rceil, \\ \lambda(t) &= \frac{\ln 2 / 2 \prod_{i=1}^{N} \left(h_i(t)\, h_i^T(t) (\overline{U}_i - \underline{U}_i)^2 / \sigma_{v_i}^2(t) \right)^{1/N}}{2^{2B/N}}, \end{aligned} \tag{4}$$

where the symbol $\lceil \cdot \rceil$ denotes the least integer greater than $\cdot$.

3.2. Design of Two Kinds of WMF-QKF

3.2.1. Filter Design Dependent on Values of $\gamma_i(t)$. When the values of $\gamma_i(t)$ are known, that is, we know whether a packet is received or lost, which can be carried out by the information of time stamps, letting $L(t)$ be the number of measurements received by the fusion center at t time, then we have the augmented measurement equation in the fusion center:

$$m'(t) = h(t)\, x(t) + \eta(t), \tag{5}$$

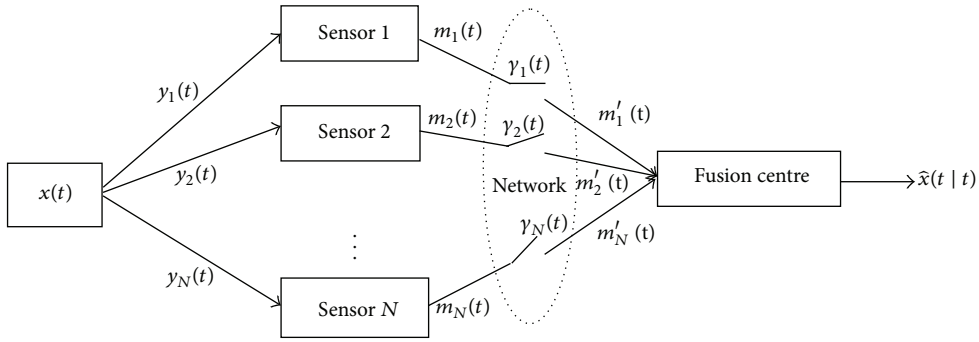

Figure 1: Distributed state estimation scheme based on quantized observations.

where the augmented quantized measurement received by the fusion center is $m'(t) = [m'_{k_1(t)}(t), m'_{k_2(t)}(t), \ldots, m'_{k_{L(t)}(t)}(t)]^T$, $1 \le k_1(t) < \cdots < k_{L(t)}(t) \le N$ and the integer $k_i(t)$ denotes the $k_i(t)$th sensor that arrives at the fusion center. The augmented measurement matrix is $h(t) = [h^T_{k_1(t)}(t), h^T_{k_2(t)}(t), \ldots, h^T_{k_{L(t)}(t)}(t)]^T$ and the noise is $\eta(t) = [\eta_{k_1(t)}(t), \eta_{k_2(t)}(t), \ldots, \eta_{k_{L(t)}(t)}(t)]^T$ with zero mean and variance matrix $Q_\eta(t) = \mathrm{diag}(\sigma^2_{\eta_{k_1(t)}}(t), \sigma^2_{\eta_{k_2(t)}}(t), \ldots, \sigma^2_{\eta_{k_{L(t)}(t)}}(t))$ where $\eta_{k_i(t)}(t) = v_{k_i(t)}(t) + n_{k_i(t)}(t)$ are uncorrelated with one another, with zero mean and variance $\sigma^2_{\eta_{k_i(t)}}(t) = \sigma^2_{v_{k_i(t)}}(t) + \sigma^2_{n_{k_i(t)}}(t) \le \sigma^2_{v_{k_i(t)}}(t) + \delta^2_{k_i(t)}(t)$. We approximately consider the measurement noise $\eta(t)$ to be the white noise. Then, the Kalman filtering can be used for the augmented systems (1) and (5) where the upper bound of variance of the quantized noise is used. However, the expensive computational cost is required due to the high-dimensional augmented measurement when the data of a large number of sensors arrive at the fusion center. To reduce the computational cost, we will present the WMF filter in the following text.

When $L(t) \ge 1$, that is, there are measurement data arriving at the fusion center at time t, then we can obtain the filter according to the following three cases.

(a) If $h(t)$ is full row rank, we can apply the standard Kalman filtering algorithm to obtain the fusion filter.

(b) If $h(t)$ is full column rank, we have that $h^T(t)Q_\eta^{-1}(t)h(t)$ is nonsingular. Then the WMF measurement equation is given as follows:

$$\overline{m}(t) = x(t) + \overline{\eta}(t), \tag{6}$$

where $\overline{m}(t) = [h^T(t)Q_\eta^{-1}(t)h(t)]^{-1}h^T(t)Q_\eta^{-1}(t)m'(t)$, $\overline{\eta}(t) = [h^T(t)Q_\eta^{-1}(t)h(t)]^{-1}h^T(t)Q_\eta^{-1}(t)\eta(t)$, $\overline{Q}_\eta^{-1}(t) = [h^T(t)Q_\eta^{-1}(t)h(t)]^{-1}$.

Then based on systems (1) and (6), we can apply the standard Kalman filtering algorithm to obtain the fusion filter.

(c) If $h(t)$ is not full rank, that is, $h^T(t)Q_\eta^{-1}(t)h(t)$ is singular, letting $\mathrm{rank}\{h(t)\} = p(t)$, $p(t) \le \min\{n, L(t)\}$, then there is full-rank decomposition [20]; that is,

$$h(t) = f(t)\overline{h}(t), \tag{7}$$

where $f(t) \in R^{L(t)\times p(t)}$ is full column rank and $\overline{h}(t) \in R^{p(t)\times n}$ is full row rank. $f^T(t)Q_\eta^{-1}(t)f(t)$ is a nonsingular matrix. So, we have the WMF measurement equation as

$$\overline{\overline{m}}(t) = \overline{h}(t)x(t) + \overline{\overline{\eta}}(t), \tag{8}$$

where $\overline{\overline{m}}(t) = [f^T(t)Q_\eta^{-1}(t)f(t)]^{-1}f^T(t)Q_\eta^{-1}(t)m'(t)$, $\overline{\overline{\eta}}(t) = [f^T(t)Q_\eta^{-1}(t)f(t)]^{-1}f^T(t)Q_\eta^{-1}(t)\eta(t)$, $Q_{\overline{\overline{\eta}}}(t) = [f^T(t)Q_\eta^{-1}(t)f(t)]^{-1}$.

Then based on systems (1) and (8), we can apply the standard Kalman filtering algorithm to obtain the fusion filter.

When $L(t) = 0$, that is, there are no measurement data arriving at the fusion center at time t, then, the Kalman predictor is used based on the last estimator.

Remark 3. From (6) and (8), we can know that the dimension of the compressed measurement $\overline{m}(t)$ or $\overline{\overline{m}}(t)$ is not greater than $\min\{n, L(t)\}$. When the number of sensors arriving at the fusion center is large, that is, $L(t) \gg n$, the proposed WMF-QKF with the computational order of magnitude $O(p^3(t))$ can obviously reduce the computational cost compared to the centralized fusion filter with the computational order of magnitude $O(L^3(t))$. However, they have the same accuracy; that is, WMF-QKF has the global optimality [20].

3.2.2. Filter Design Dependent on Probabilities of $\gamma_i(t)$. In this section, we will design the filter dependent on the probabilities of $\gamma_i(t)$. At each time, the measurement of each sensor arriving at the fusion center can be expressed as follows:

$$\begin{aligned} m'_i(t) &= \gamma_i(t)m_i(t) \\ &= \gamma_i(t)h_i(t)x(t) + \gamma_i(t)v_i(t) \\ &\quad + \gamma_i(t)n_i(t), \quad i = 1, 2, \ldots, N \end{aligned} \tag{9}$$

which can be rewritten as

$$m'_i(t) = \alpha_i h_i(t)x(t) + \zeta_i(t), \quad i = 1, 2, \ldots, N, \tag{10}$$

where $\zeta_i(t) = (\gamma_i(t) - \alpha_i)h_i(t)x(t) + \gamma_i(t)v_i(t) + \gamma_i(t)n_i(t)$, $i = 1, 2, \ldots, N$ are uncorrelated white noises with zero mean and

variances $\sigma^2_{\zeta_i}(t) = \alpha_i(1-\alpha_i)h_i(t)q(t)h_i^T(t) + \alpha_i\sigma^2_{v_i}(t) + \alpha_i\sigma^2_{n_i}(t)$; $q(t) = \mathrm{E}[x(t)x^T(t)]$ is the state second-order moment which can be computed by $q(t+1) = \Phi(t)q(t)\Phi^T(t) + \Gamma(t)Q_w(t)\Gamma^T(t)$ from (1).

Then the augmented measurements can be expressed as

$$M'(t) = \widetilde{h}(t)\,x(t) + \zeta(t), \tag{11}$$

where $M'(t) = \left[m_1'(t)\ m_2'(t)\ \cdots\ m_N'(t)\right]^T$, $\widetilde{h}(t) = \left[\alpha_1 h_1(t)\ \alpha_2 h_2(t)\ \cdots\ \alpha_N h_N(t)\right]^T$, $\zeta(t) = \left[\zeta_1(t)\ \zeta_2(t)\ \cdots\ \zeta_N(t)\right]^T$; $\zeta(t)$ and $w(t)$ are uncorrelated. The variance matrix of $\zeta(t)$ is $Q_\zeta(t) = \mathrm{diag}\left(\sigma^2_{\zeta_1}(t)\ \sigma^2_{\zeta_2}(t)\ \cdots\ \sigma^2_{\zeta_N}(t)\right)$ where the symbol $\mathrm{diag}(\cdot)$ denotes the diagonal matrix.

According to the different cases that the matrix $\widetilde{h}(t)$ is full row-rank, full column-rank, or not full-rank, we can obtain the WMF-QKF dependent on probabilities of $\gamma_i(t)$ similar to design of the above subsection.

Remark 4. Two kinds of WMF-QKFs have been proposed. The filter dependent on the values of $\gamma_i(t)$ (WMF-QKFV) has better accuracy than that dependent on the probabilities of $\gamma_i(t)$ (WMF-QKFP) since more information is used. However, WMF-QKFV requires the online computation since it is dependent on the stochastic variable $\gamma_i(t)$ at each time. WMF-QKFP can be computed offline since it is only dependent on the probabilities. Moreover, WMF-QKFP has the reduced online computational cost than WMF-QKFV.

3.3. Multiple Dimension Measurement Case. WMF-QKF with optimization problems has been solved for systems with scalar measurement in Sections 3.1 and 3.2. In this section, we consider the WMF-QKF for systems with multiple dimension measurements. We consider the system

$$\begin{aligned} x(t+1) &= \Phi(t)\,x(t) + \Gamma(t)\,w(t) \\ y_i(t) &= H_i(t)\,x(t) + v_i(t), \quad i = 1, 2, \ldots, N, \end{aligned} \tag{12}$$

where $y_i(t) \in R^{q_i}$ is the measurement vector of the ith sensor; other variables have the same definitions as Section 2. $H_i(t)$ is full row rank. We make the following assumptions.

Assumption 5. $w(t) \in R^r$ and $v_i(t) \in R^{q_i}$, $i = 1, 2, \ldots, N$, are uncorrelated white noises with zero mean and variance matrices $Q_w(t)$ and $Q_{v_i}(t)$, and their each component is uncorrelated with each other; that is, $Q_w(t)$ and $Q_{v_i}(t)$ are diagonal matrices.

Assumption 6. $y_i^{(k)}(t) \in [\underline{U}_i^{(k)}, \overline{U}_i^{(k)}]$, $k = 1, 2, \ldots, q_i$; $i = 1, 2, \ldots, N$, where $y_i^{(k)}(t)$ is the kth component of observation vector $y_i(t)$ and $\underline{U}_i^{(k)}$ and $\overline{U}_i^{(k)}$ are known constants.

The system structure is similar to Figure 1. For each component $y_i^{(k)}(t)$ of measurement $y_i(t)$ from the ith sensor, we quantize each component $y_i^{(k)}(t)$ to $m_i^{(k)}(t)$ with the length of $b_i^{(k)}(t)$ bits according to the quantized approach in Section 3.1. Let the quantized noise be $n_i^{(k)}(t) = m_i^{(k)}(t) - y_i^{(k)}(t)$; then the variance of the quantized noise $n_i^{(k)}(t)$ is $\sigma^2_{n_i^{(k)}}(t) \le \delta^2_{n_i^{(k)}}(t)$, $\delta^2_{n_i^{(k)}}(t) = (\overline{U}_i^{(k)} - \underline{U}_i^{(k)})^2/[4(2^{b_i^{(k)}(t)} - 1)^2]$. Furthermore, $n_i^{(k)}(t)$, $v_j^{(l)}(t)$, $i, j = 1, 2, \ldots, N$; $k = 1, 2, \ldots, q_i$; $l = 1, 2, \ldots, q_j$, and $w(t)$ are uncorrelated with each other. Then, similar to scalar measurement case, we can deal with the WMF-QKF. The detailed algorithm is omitted here.

Remark 7. For the case of multiple dimension measurements of each sensor, $H_i(t)$ is assumed to be full row rank. If not, the full-rank decomposition can be implemented. Then the measurement of each sensor can be compressed to a reduced dimension measurement without information loss. Or other compressed algorithms [21, 22] can be used for the multiple dimension measurements of each sensor. Then its each component is quantized and transmitted. Thus, the bandwidth can be saved.

4. Simulation Research

Consider a discrete-time system measured by five sensors:

$$\begin{aligned} x(t+1) &= \begin{bmatrix} 0.9226 & -0.633 & 0 \\ 1 & 0 & 0 \\ 0 & 1 & 0 \end{bmatrix} x(t) + \begin{bmatrix} 0.5 \\ 0 \\ 0.2 \end{bmatrix} w(t) \\ y_i(t) &= h_i x(t) + v_i(t), \quad i = 1, 2, 3, \end{aligned} \tag{13}$$

where $y_i(t)$ is the measurement signal and $v_i(t)$ is the measurement noise with mean zero and variance $\sigma^2_{v_i}$ and is independent with Gaussian noise $w(t)$ with mean zero and variance σ^2_w. Our goal is to find the WMF-QKF dependent on values (WMF-QKFV) of $\gamma_i(t)$ and WMF-QKF dependent on probabilities (WMF-QKFP) of $\gamma_i(t)$. In the simulation, we set noise variances $\sigma^2_w = 1$, $\sigma^2_{v_1} = 1$, $\sigma^2_{v_2} = 2$, $\sigma^2_{v_3} = 2.5$, $\sigma^2_{v_4} = 2.5$, $\sigma^2_{v_5} = 3$, measurement matrices $h_1 = h_2 = h_3 = \left[23.738\ \ 20.287\ \ 0\right]$ and $h_4 = h_5 = \left[0\ \ 20\ \ 23\right]$, the initial values $x(0) = \left[0\ \ 0\ \ 0\right]^T$ and $P_0 = 0.1I_3$, where I_3 is a 3×3 identity matrix, the bounds $\underline{U}_1 = \underline{U}_2 = \underline{U}_3 = \underline{U}_4 = \underline{U}_5 = -40$ and $\overline{U}_1 = \overline{U}_2 = \overline{U}_3 = \overline{U}_4 = \overline{U}_5 = 40$ for measurements of five sensors, the initial bandwidths $b_1 = b_2 = b_3 = b_4 = b_5 = 1$, and the probabilities $\alpha_1 = 0.5$, $\alpha_2 = 0.7$, $\alpha_3 = 0.8$, $\alpha_4 = 0.8$ and $\alpha_5 = 0.7$ and we take 100 sampling data.

We solve the optimization problem (3) with the bits of the whole bandwidth $B = 12$. We can compute the bandwidths $b_1 = 3$, $b_2 = 3$, $b_3 = 2$, $b_4 = 2$, and $b_5 = 2$. Tracking performance of WMF-QKFV and WMF-QKFP is shown in Figure 2 where bold curves denote the true value, dotted curves denote the estimates of WMF-QKFV, and dashed curves denote the estimates of WMF-QKFP. We see that WMF-QKFV has better accuracy than WMF-QKFP under the same bandwidth constraint. The comparison of mean square errors $\mathrm{MSE}_k = \left(\sum_{i=1}^{500}\left(\widehat{x}_k^{(i)}(t \mid t) - x_k(t)\right)^2\right)/500$ by 500 times Monte-Carlo test, $k = 1, 2, 3$, denoting the kth component of the state of all LFs, WMF-QKFV, and WMF-QKFP

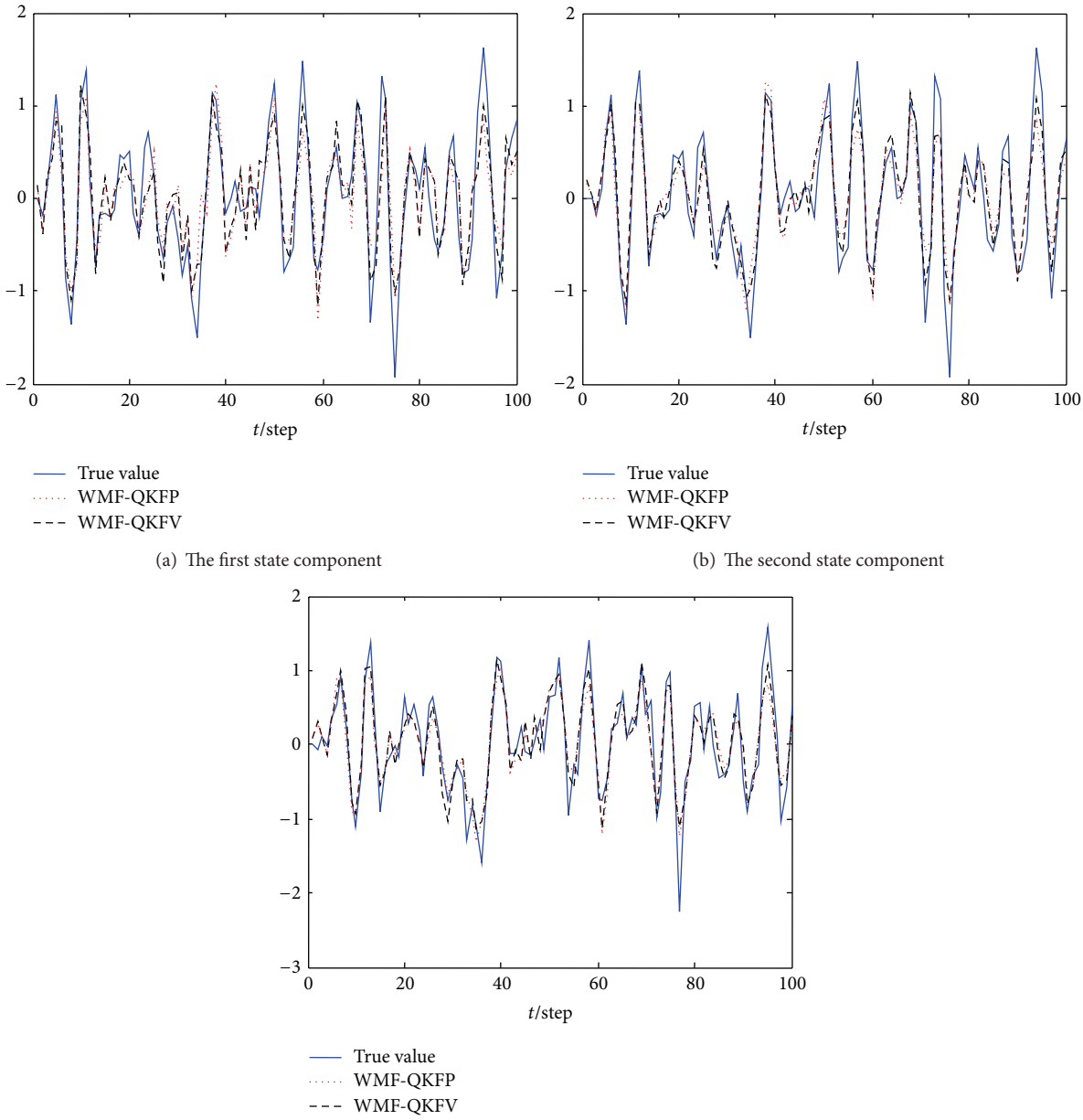

Figure 2: Comparison of tracking for WMF-QKFP and WMF-QKFV under whole bandwidth $B = 12$.

is shown in Figure 3. We see that WMF-QKFP and WMF-QKFV have better accuracy than any local filter and WMF-QKFV has better accuracy than WMF-QKFP. All simulations verify the effectiveness of the proposed algorithms.

5. Conclusion

The weighted measurement fusion quantized filtering problem is investigated in a sensor network with bandwidth constraint and imperfect channels of missing measurements. Using the knowledge of whether a measurement is lost at the present time or the probabilities of missing measurements, two weighted measurement fusion quantized Kalman filters are developed based on the quantized measurements received, respectively. They have the same accuracy as the corresponding centralized fusion estimators and have the reduced computational cost.

Conflict of Interests

The authors declare that there is no conflict of interests regarding the publication of this paper.

Acknowledgments

This work is supported by the Natural Science Foundation of China (NSFC-61174139), by Chang Jiang Scholar

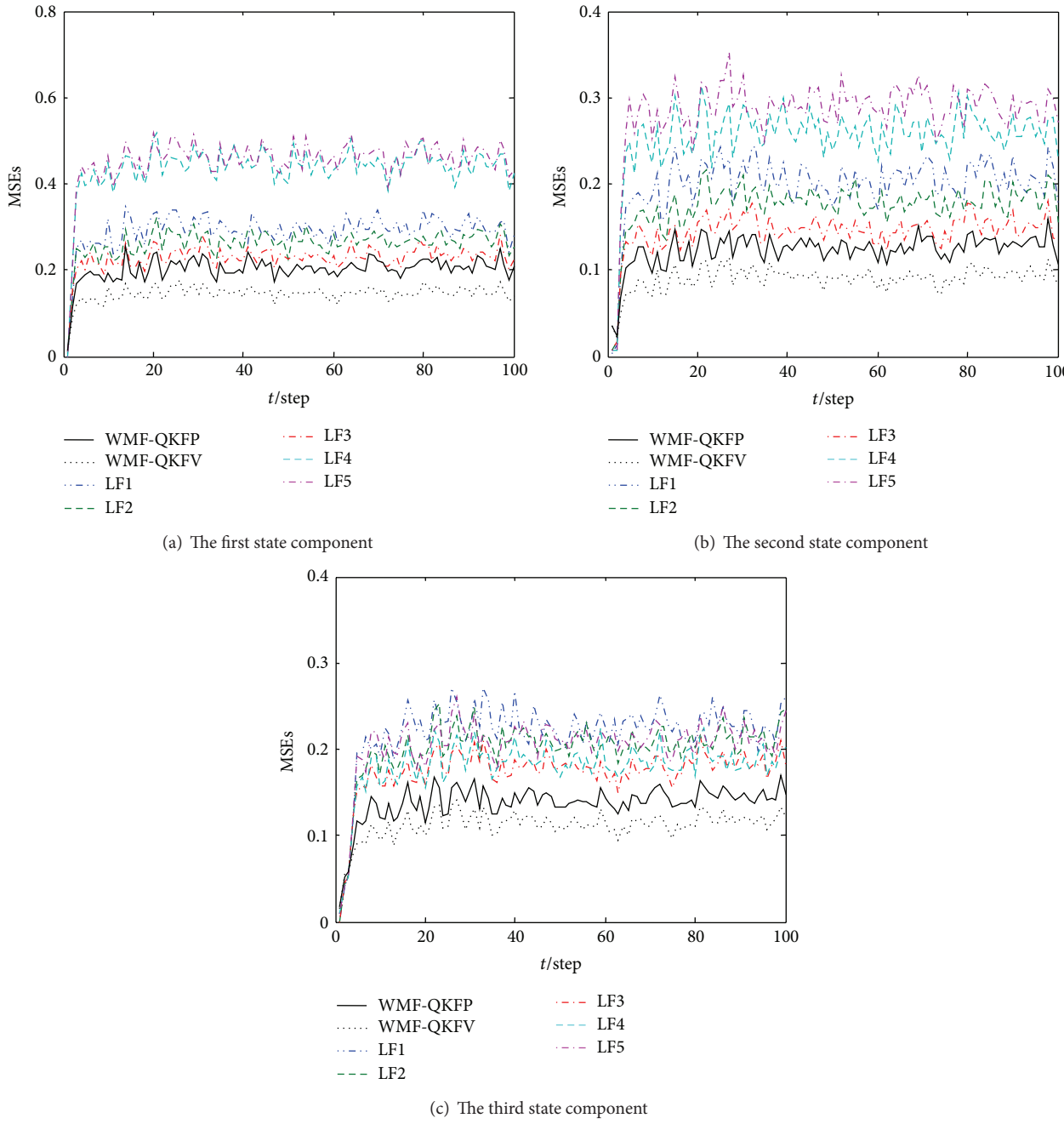

(a) The first state component

(b) The second state component

(c) The third state component

FIGURE 3: Comparison of accuracy of WMF-QKFP, WMF-QKFV, and all LFs under whole bandwidth $B = 12$ by 100 times Monte-Carlo test.

Candidates Program for Provincial Universities in Heilongjiang (no. 2013CJHB005), by Science and Technology Innovative Research Team in Higher Educational Institutions of Heilongjiang Province (no. 2012TD007), by the Program for New Century Excellent Talents in University for Heilongjiang Province (no. 1154-NCET-01), by the Program for High-qualified Talents (no. Hdtd2010-03), and by Electronic Engineering Provincial Key Laboratory.

References

[1] C.-Y. Chong and S. P. Kumar, "Sensor networks: evolution, opportunities, and challenges," *Proceedings of the IEEE*, vol. 91, no. 8, pp. 1247–1256, 2003.

[2] E. F. Nakamura, A. A. F. Loureiro, and A. C. Frery, "Information fusion for wireless sensor networks: methods, models, and classifications," *ACM Computing Surveys*, vol. 39, no. 3, Article ID 1267073, 2007.

[3] X. Ning and C. G. Cassandras, "On maximum lifetime routing in wireless sensor networks," in *Proceedings of the 48th IEEE Conference on Decision and Control*, pp. 3757–3762, Shanghai, China, December 2009.

[4] M. Cardei and J. Wu, "Energy-efficient coverage problems in wireless ad-hoc sensor networks," *Computer Communications*, vol. 29, no. 4, pp. 413–420, 2006.

[5] J. J. Xiao and Z. Q. Luo, "Universal decentralized detection in a bandwidth-constrained sensor network," *IEEE Transactions on Signal Processing*, vol. 53, no. 8, pp. 2617–2624, 2005.

[6] D. A. Castanon and D. Teneketzis, "Distributed estimation algorithms for nonlinear systems," *IEEE Transactions on Automatic Control*, vol. 30, no. 5, pp. 418–425, 1985.

[7] A. S. Willsky, M. G. Bello, D. A. Castanon, B. C. Levy, and G. C. Verghese, "Combining and updating of local estimates and regional maps along sets of one-dimensional tracks," *IEEE Transactions on Automatic Control*, vol. 27, no. 4, pp. 799–813, 1982.

[8] Z. Chair and P. K. Varshney, "Distributed Bayesian hypothesis testing with distributed data fusion," *IEEE Transactions on Systems, Man and Cybernetics*, vol. 18, no. 5, pp. 695–699, 1988.

[9] Z.-Q. Luo, "Universal decentralized estimation in a bandwidth constrained sensor network," *IEEE Transactions on Information Theory*, vol. 51, no. 6, pp. 2210–2219, 2005.

[10] Z.-Q. Luo, "An isotropic universal decentralized estimation scheme for a bandwidth constrained ad hoc sensor network," *IEEE Journal on Selected Areas in Communications*, vol. 23, no. 4, pp. 735–744, 2005.

[11] J.-J. Xiao, S. Cui, Z.-Q. Luo, and A. J. Goldsmith, "Power scheduling of universal decentralized estimation in sensor networks," *IEEE Transactions on Signal Processing*, vol. 54, no. 2, pp. 413–422, 2006.

[12] A. Ribeiro, G. B. Giannakis, and S. I. Roumeliotis, "SOI-KF: distributed Kalman filtering with low-cost communications using the sign of innovations," *IEEE Transactions on Signal Processing*, vol. 54, no. 12, pp. 4782–4795, 2006.

[13] K. You, L. Xie, S. Sun, and W. Xiao, "Multiple-level quantized innovation Kalman filter," in *Proceedings of the 17th World Congress, International Federation of Automatic Control (IFAC '08)*, pp. 1420–1425, July 2008.

[14] K. You, L. Xie, S. Sun, and W. Xiao, "Quantized filtering of linear stochastic systems," *Transactions of the Institute of Measurement and Control*, vol. 33, no. 6, pp. 683–698, 2011.

[15] M. Fu and C. E. de Souza, "State estimation for linear discrete-time systems using quantized measurements," *Automatica*, vol. 45, no. 12, pp. 2937–2945, 2009.

[16] M. Fu and L. Xie, "The sector bound approach to quantized feedback control," *IEEE Transactions on Automatic Control*, vol. 50, no. 11, pp. 1698–1711, 2005.

[17] S. Sun, J. Lin, L. Xie, and W. Xiao, "Quantized Kalman filtering," in *Proceedings of the IEEE 22nd International Symposium on Intelligent Control (ISIC '07)*, pp. 7–12, October 2007.

[18] N. Liu, J. Ma, and S. L. Sun, "Quantized Kalman filter for sensor networks with random packet dropouts," *Advanced Materials Research*, vol. 219-220, pp. 1040–1044, 2011.

[19] B. D. O. Anderson and J. B. Moore, *Optimal Filtering*, Prentice-Hall, Englewood Cliffs, NJ, USA, 1979.

[20] X. Wang, S. Sun, K. Ding, and J. Xue, "Weighted measurement fusion white noise deconvolution filter with correlated noise for multisensor stochastic systems," *Mathematical Problems in Engineering*, vol. 2012, Article ID 257619, 16 pages, 2012.

[21] K. Zhang, X. R. Li, P. Zhang, and H. Li, "Optimal linear estimation fusion—part 6: sensor data compression," in *Proceedings of the International Conference on Information Fusion*, pp. 221–228, 2003.

[22] E. Song, Y. Zhu, and J. Zhou, "Sensors' optimal dimensionality compression matrix in estimation fusion," *Automatica*, vol. 41, no. 12, pp. 2131–2139, 2005.

Hindawi Publishing Corporation
Mathematical Problems in Engineering
Volume 2014, Article ID 719408, 10 pages
http://dx.doi.org/10.1155/2014/719408

Research Article

Self-Similarity Superresolution for Resource-Constrained Image Sensor Node in Wireless Sensor Networks

Yuehai Wang,[1] Weidong Wang,[1] Shiying Cao,[1] Shiju Li,[1] Li Xie,[1] and Baocang Ding[2]

[1] *Department of Information Science and Electronic Engineering, Zhejiang Provincial Key Laboratory of Information Network Technology, Zhejiang University, Hangzhou 310027, China*
[2] *Department of Automation, School of Electronic and Information Engineering, Xi'an Jiaotong University, Xian 710049, China*

Correspondence should be addressed to Li Xie; xiehan@zju.edu.cn

Received 30 July 2013; Accepted 18 December 2013; Published 21 January 2014

Academic Editor: Wendong Xiao

Wireless sensor networks, in combination with image sensors, open up a grand sensing application field. It is a challenging problem to recover a high resolution (HR) image from its low resolution (LR) counterpart, especially for low-cost resource-constrained image sensors with limited resolution. Sparse representation-based techniques have been developed recently and increasingly to solve this ill-posed inverse problem. Most of these solutions are based on an external dictionary learned from huge image gallery, consequently needing tremendous iteration and long time to match. In this paper, we explore the self-similarity inside the image itself, and propose a new combined self-similarity superresolution (SR) solution, with low computation cost and high recover performance. In the self-similarity image super resolution model (SSIR), a small size sparse dictionary is learned from the image itself by the methods such as KSVD. The most similar patch is searched and specially combined during the sparse regulation iteration. Detailed information, such as edge sharpness, is preserved more faithfully and clearly. Experiment results confirm the effectiveness and efficiency of this double self-learning method in the image super resolution.

1. Introduction

Wireless sensor networks, in combination with image sensors, open up a grand sensing application field. Visual information provided by image sensor is the most intuitive information perceived by human, especially for recognition, monitoring, and surveillance. Low-cost and resource-constrained image sensors with limited resolution are mainly employed [1–3]. Recovery from low resolution to high resolution is the pressing need for image sensor node. Image super resolution (SR) receives more and more interests recently, which has lots of applications in image sensor, digital cameras, mobile phone, image enhancement, high definition TV [4–6], and so forth. It aims to reconstruct a high-resolution (HR) image from the low-resolution (LR) one based on reasonable assumptions or prior knowledge. From the view of the target HR image, the LR image can be generated after downsampling and some blurring operator. Hence, the SR work has always been formulated as an inverse problem:

$$Y = \Phi HX + N, \tag{1}$$

where X is the HR image to be recovered, Y is the known LR image, Φ is the downsampling operator, H is the blurring operator that minimizes the high frequency aliasing effect, and N is the noise. Traditionally, the downsampling operator Φ and blurring operator H are conducted at the same time. Hence, we can use the following formulation (2) instead of (1):

$$Y = \mathscr{H}X + N, \tag{2}$$

where $\mathscr{H} = \Phi H$ is the generalized blurring and downsampling operator. However, the detailed information, especially

the high frequency part, is lost after these two operations. Hence, image super resolution has become a highly underdetermined reconstruction problem.

The classical SR solutions are interpolation-based methods, including bilinear, bicubic, spline interpolation and some other improved versions [7, 8]. These methods tend to generate overly smooth HR images with ringing and jaggy effects. Their visual clarity is very limited. Edge preserving and directional interpolators have been proposed to improve the reconstruction image's visual clarity [9–11]. However, the blurring and noises are still obstacles to overcome.

Sparse representation-based SR methods are becoming more popular recently since the issue of sparse representation is consistent with (2). Sparse representation provides a different perspective in solving the underdetermined problems [12–15]. This powerful and promising tool has proven to be effective for a wide range of problems, such as sub-Nyquist sensing of signals and coding, image denoising, and deblurring [16–23]. Several sparse representation based SR algorithms have been proposed with superior results reported [12, 22, 24, 25]. Most of them need training dictionaries based on a large scale external image gallery, which have limited matching degree to the target image and time consuming. Another issue is that the external dictionary depends on the blurring modal with less generality. Self-learning SR algorithms, lately emerged, show that the internal statistics in the image itself often have stronger prediction power than the external statistics and can give more powerful image-specific priors [26, 27].

In this paper, we explore the self-similarity inside the image and propose a new combined self-similarity super resolution (SR) solution, which successfully restores the missing detailed image information. In this self-similarity image super resolution model (SSIR), the patches from the LR image are downsampled firstly to form smaller LR patches (SLR). Small-sized sparse dictionary is learned from the image itself by methods such as KSVD. Then, a most similar patch for the unrecovered LR patch is searched and combined, during the sparse iteration, to preserve the faithful detailed information. Experiment results confirm the effectiveness and efficiency of the double self-similarity learning method in the image super resolution.

The rest of this paper is organized as follows. Section 2 describes our approach of SSIR framework with self-learning dictionary. In Section 3, experiments are taken to compare the proposed method with other ones. The conclusions are finally given in Section 4.

2. The Proposed Self-Similarity-Based Image Super Resolution Approach

2.1. Sparse Representation of Image Super Resolution. For sparse representation-based SR methods, high resolution image X can be represented by sparse coefficients α under dictionary D as follows:

$$X = D\alpha. \tag{3}$$

Hence, the HR image recovering procedure can be seen as the minimization of the l_1-norm problem:

$$\widehat{\alpha} = \arg\min \|\alpha\|_1 \quad \text{s.t. } Y = \mathscr{H}X = \mathscr{H}D\alpha, \tag{4}$$

where Y is the LR image and $\mathscr{H}$ is the generalized blurring and downsampling degradation matrix. The quality of recover HR image is always determined by the details, such as edges and contrast. However, such details are lost when the HR image is downsampled. Hence, small patch based recovery is more popular than the whole image based ones to prevent large scale details losing. We follow the patch based learning strategy in our approach. For $N \times N$ sized LR image, the atoms in D are learned by patches sized by $n \times n$, where n can be 8, 10, and so forth. Then the sparse representation (4) can be rewritten as

$$\widehat{\alpha}_k = \arg\min \|\alpha_k\|_1 \quad \text{s.t. } y_k = \mathscr{H}x_k = \mathscr{H}D\alpha_k, \tag{5}$$

where y is the LR patch with size of (1/scale) $\times\, n \times n$, x_k is the HR patch, α_k is the coefficient of the patch, and $\mathscr{H}$ and D are corresponding patch with the size of $n \times n$. The image reconstruction scheme based on self-learning dictionary can be presented more intuitively by

$$\widehat{\alpha} = \arg\min \|y - \mathscr{H}D\alpha\|_F^2 + \lambda\|\alpha\|_1. \tag{6}$$

2.2. Internal Dictionary Learning. Most of the sparse representation SR methods are based on dictionary learning from the external image library [12, 22, 25]. The number of the atoms in dictionary D should be huge enough to confirm the sparsity of α and avoid image hallucination and blurring [16]. Normally, the dimension of external dictionary should be above thousand and the recovery time is huge. For various natural images, especially the high-gradient ones, high recover performance could not be easily and fast reached if the dictionary is learned from the outside image gallery. External dictionary approaches are not suitable for the resource-constrained image sensor node. A different idea is that we should make full use of the information inside of the image itself as shown in [26, 27]. The feature of the same structure textures or patterns can be more easily found within the image. For the destination image, the dictionary does not need to be tremendous to mate different kinds of natural images. Inspired by [26, 27], the dictionary D is learned firstly from LR image in our approach to classify the local structures.

The internal training patches are extracted from LR image and then used to generate an overcomplete dictionary $D \in R^{n\times n\times K}$ which contains K atoms. It is assumed that a training patch y_{TS} can be represented as $y_{\mathrm{TS}} = D\beta$, which satisfies $\|y_{\mathrm{TS}} - D\beta\| < \varepsilon$. Hence, the training dictionary is the solution of

$$[D, \beta] = \arg\min \|y_{\mathrm{TS}} - D\beta\| \quad \text{s.t.} \|\beta\|_0 < K. \tag{7}$$

Iterative optimization is used to solve this dictionary training problem. The iteration consists of two basic steps: (1) sparse coding: fix the dictionary D and search for the sparse representation of β and (2) dictionary update: update

Table 1: HR patch, corresponding LR patch, and reconstruction patch under KSVD dictionary.

HR patch								LR patch				Reconstruction patch under KSVD dictionary							
100	99	96	91	90	88	85	83	99	95	89	84	100	99	96	94	91	88	84	84
98	100	98	93	90	87	84	83	98	93	88	85	101	99	96	92	90	86	83	84
99	99	96	92	89	86	85	84	99	94	90	84	100	98	95	92	88	85	84	85
100	96	93	91	89	87	85	85	99	94	87	85	99	97	94	92	90	87	84	85
99	97	95	95	91	88	85	83					100	97	94	93	92	88	85	85
101	99	95	91	91	89	86	84					101	99	96	93	91	88	85	84
101	99	95	91	89	88	86	85					100	99	96	92	89	87	85	84
98	97	96	93	88	85	84	84					99	98	96	92	88	86	86	85

the dictionary atoms $\{d_j\}_{j=1}^{K}$ and their corresponding coefficients β one by one. Inspired by [28, 29], we use orthogonal matching pursuit (OMP) algorithm in the sparse coding step and K-singular value decomposition (K − SVD) based iterative optimization in dictionary update step, respectively. These two steps run iteratively until the maximum iteration or the convergence is reached.

Typically, the self-leaning dictionary size K is set below 256 in our approach, and we get similar recovery performance with the external dictionary. Detailed comparison is illustrated in Section 3.

2.3. Self-Similarity Regulation Scheme. Local image structures in LR image can be classified by the patch dictionary learned from itself. However, detailed information, such as sharp edges and corners, could not be clustered perfectly by limit atoms and may be lost for some extent after downsampled from the HR patch. The following Table 1 demonstrates a real HR patch in Lena, its corresponding LR patch, and reconstruction patch by self-learning KSVD dictionary with 256 atoms. From Table 1, the rich variation between the HR pixels is omitted in LR patch and smoothed in the reconstruction patch. The reason of smooth effect under KSVD dictionary is mainly that the dictionary atoms are trained not only for the special patch, but also for all the patches in the image.

Hence, accurate reconstruction for each patch is tough even under the sparse self-learning dictionary. More prior information should be incorporated into the recover procedure to improve the HR image quality. Several additional parameters have been studied such as frequency, histogram, low-pass, nonlocal means constraints [22, 25]. Unlike these statistic constraints, we consider true information inside of the image as the regulation index.

As aforementioned, distinct edges and corners become blur after downsample operation. The information loss phenomenon appears when the HR image is downsampled to LR image. Similar information loss phenomenon also appears when the LR image is down-sampled to an even lower resolution image. The lost information during the latter procedure can be recovered from the image before down-sample. It provides a learning way to recover more realistic HR patches. A new self-similarity regulation scheme is proposed based on finding image patch similar to the destination HR patch. The new sparse regulation scheme can be formulated as

$$\widehat{\alpha} = \arg\min \left\| y - \mathcal{H} D\alpha \right\|_F^2 + \lambda \|\alpha\|_1 + \gamma_{\text{similar}} \|J(\alpha)\|_1, \quad (8)$$

where γ_{similar} is the regulation threshold and $J(\alpha)$ is the similarity prior. We divide the whole sparse regulation into two steps: self-similarity regulation and sparse dictionary regulation. The self-similarity regulation step can be seen as an internal regulation step to compensate the sharpness of the edges. The sparse dictionary regulation step provides the basic framework to enlarge the LR image.

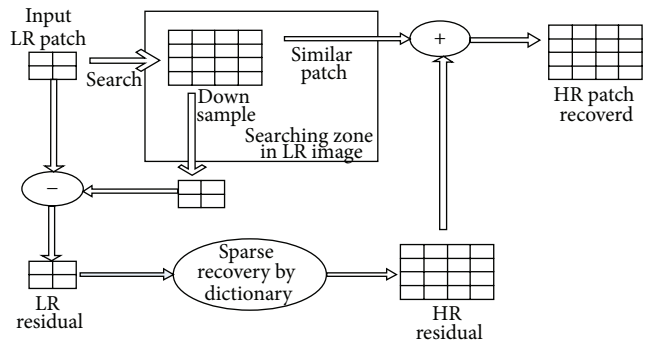

Figure 1: Self-similarity regulation step.

The detailed self-similarity regulation step is described in Figure 1. Firstly, the input unrecovered LR patch, named as y_{LR}, is upscaled by bicubic operator. Then, a similar HR patch of the same up-scaled size, named as S_{HR}, is searched around the LR patch y_{LR} inside of LR image Y. If a similar HR patch S_{HR} is found, we can get its corresponding down-sampled LR patch S_{LR}. The true HR patch x_{HR} is approximated by the similar HR patch S_{HR}. This recovered HR patch $\widetilde{x}_{\text{HR}}$ coming from real pixels can be closer to the ground truth x_{HR} than that recovered by statistic constraints studied previously. During approximation, the similar down-sampled LR patch S_{LR} is firstly subtracted from the unrecovered LR patch y_{LR}. Then, the above difference is estimated from the residual RS_{LR} by the self-learning sparse dictionary, which is named as RS_{HR}. At last, the recovered HR patch $\widetilde{x}_{\text{HR}}$ is computed by adding the similar patch S_{HR} and the difference estimation RS_{HR}. The well-known sparse regulation methods,

Input: LR image Y, LR image patches' size m and HR image patches' size n, the degradation matrix $\mathscr{H}$.
Output: HR image X
Step 1. Extract patches $y_{\mathrm{LR}} \in R^m$ from LR image Y, follow the raster-scan order, and start from the upper-left corner (some pixel overlap in each direction is allowed).
Step 2. Recover HR image patches x_{HR} iteratively by Steps 2.1 and 2.2, until the maximum iteration times or convergence is reached.
Step 2.1 Self-similarity regulation step:
Step 2.1.1. Use bicubic method to up scale the unrecovered LR patch y_{LR} to the same size n as HR patch, defined as y_{HR}.
Step 2.1.2. Searching for a similar n sized patch in y_{LR}'s neighbor:
Step 2.1.2.1. Compute each searching patch's SSE as the self-similarity prior $J(\alpha)$,
$$J(\alpha) = \mathrm{SSE} = \sum_l \sum_k (B_{lk} - \widehat{B}_{lk})^2$$
Step 2.1.2.2. Find the least SSE patch, and compare its SSE with the adaptive threshold $\alpha\,\mathrm{Var} + \beta$. If $\mathrm{SSE} < \alpha\,\mathrm{Var} + \beta$, define this least SSE patch as the similar patch S_{HR}.
Step 2.1.3. Use degradation matrix $\mathscr{H}$ to down sample similar patch S_{HR}, define as S_{LR}.
Step 2.1.4. Subtract S_{LR} from LR patch y_{LR}, and get the residual $RS_{\mathrm{LR}} = y_{\mathrm{LR}} - S_{\mathrm{LR}}$.
Step 2.1.5. Recover the residual RS_{LR} to RS_{HR} using IRLS algorithm according (9).
Step 2.1.6. Add the RS_{HR} to S_{HR}, according to (10).
Step 2.2 Sparse dictionary regulation step: update $\widetilde{x}_{\mathrm{HR}}^{l+1}$ according to (11).
Step 3. Ensemble all $\widetilde{x}_{\mathrm{HR}}$ to recover HR image X (if there is pixel overlap, the weighted average method is needed).

Algorithm 1: Self-similarity regulation scheme.

like IRLS and OMP, can be used in the recovery procedure [27–30].

The above self-similarity regulation step can be represented as

$$RS_{\mathrm{HR}}^l = D_H * \mathrm{IRLS}\left(y_{\mathrm{LR}} - \mathscr{H} S_{\mathrm{HR}}^l, D_L\right),$$
$$\widetilde{x}_{\mathrm{HR}}^{l+1/2} = S_{\mathrm{HR}}^l + RS_{\mathrm{HR}}^l, \tag{9}$$

where l is the current iteration index, S_{HR}^l is the most similar patch found in lth iteration, RS_{HR}^l is the recovered difference between S_{HR}^l and $\widetilde{x}_{\mathrm{HR}}$, $\widetilde{x}_{\mathrm{HR}}^{l+1/2}$ represents updated $\widetilde{x}_{\mathrm{HR}}$, and D_L and D_H are dictionary trained for low-resolution patch and high-resolution patch, respectively.

We introduced sum square error (SSE) as the self-similarity prior $J(\alpha)$ and use it to decide which patch is the most matching one. The definition of the SSE is given by

$$J(\alpha) = \mathrm{SSE} = \sum_l \sum_k \left(B_{lk} - \widehat{B}_{lk}\right)^2, \tag{10}$$

where B_{lk} is the pixels taken from y_{LR} neighbor patch in the searching zone and $\widehat{B}_{lk}$ is the pixels taken from the bicubic up-scaled patch y_{HR}. Both have the same size as the output HR patch $\widetilde{x}_{\mathrm{HR}}$. The patches we searched for come from the LR image, so the fidelity can be guaranteed.

Sparse threshold $\gamma_{\mathrm{similar}}$ is used to decide whether a patch is similar to destination HR patch. $\gamma_{\mathrm{similar}}$ is adaptive to y_{LR}, instead of being a fixed value. The adaptive threshold $\gamma_{\mathrm{similar}}$ is defined as $\alpha\,\mathrm{Var} + \beta$, where Var is variance of the processing patch y_{LR} and α, β are associated parameters. If the minimum $J(\alpha)$ within the searching zone is smaller than $\gamma_{\mathrm{similar}}$, its corresponding patch is named as the most similar patch S_{HR}.

The sparse dictionary regulation step is then performed under self-learned dictionary, which can be represented by

$$\widetilde{x}_{\mathrm{HR}}^{l+1} = \widetilde{x}_{\mathrm{HR}}^{l+1/2} + \lambda D_H * \mathrm{IRLS}\left(y_{\mathrm{LR}} - \mathscr{H}\widetilde{x}_{\mathrm{HR}}^{l+1/2}, D_L\right). \tag{11}$$

The above two regulation steps are performed until the maximum iteration times or the convergence is reached.

The procedure of self-similarity regulation scheme is described in detail by Algorithm 1.

2.4. Overall Diagram of Self-Similarity Based Image Super Resolution Approach. After all the analyses above, the overall diagram of self-similarity based image super resolution approach is shown in Figure 2. Firstly, the input LR image Y, regarded as a down-sampled version from corresponding HR image X, is segmented into patches y_{LR}. Then the sparse representation dictionaries D_L and D_H are trained by these internal patches. Next, the self-similarity regulation scheme is applied to find a matching patch S_{HR}. Afterwards, HR patch $\widehat{x}_{\mathrm{HR}}$ is recovered by sparse regulation based on the self-learning dictionary. At last, we ensemble all these recovered HR patches $\widehat{x}_{\mathrm{HR}}$ to get a high-quality HR image X.

3. Experimental Results

3.1. Experimental Background. In this section, several experimental results for the proposed method are given. All the simulations are conducted in MATLAB 7.5 on PC with Intel Core2/1.6 GHz/1 GB. The test LR images include several typical 256 × 256 natural images. We aim to recover their 512 × 512HR images. The input LR images with different degradation matrix $\mathscr{H}$ (direct downsampling degradation matrix $\mathscr{H}_d$ and blur down-sampling degradation matrix $\mathscr{H}_b$) are tested. Every experiment is evaluated from the luminance peak signal-to-noise ratio (Y_PSNR) and SSIM

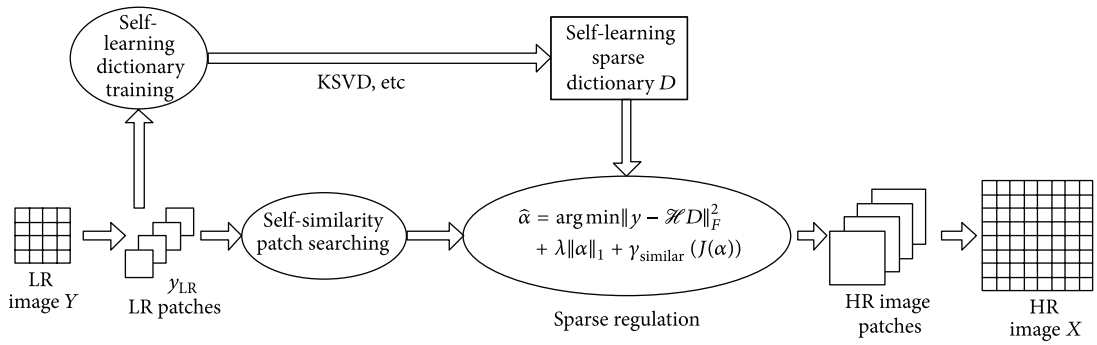

Figure 2: The overall diagram of the self-similarity-based image super resolution.

Figure 3: Experiment results on image Lena, from left to right: (a) original 512×512 HR image, (b) $\mathcal{H}_b$ sampled Bicubic (PSNR = 34.87 dB), and (c) $\mathcal{H}_b$ sampled Yang et al.'s [24] (PSNR = 35.75 dB), (d) $\mathcal{H}_b$ sampled Proposed method (PSNR = 35.80 dB), (e) Dong et al.'s [25] NCSR (PSNR = 35.45 dB), (f) $\mathcal{H}_d$ sampled Bicubic (PSNR = 30.96 dB), (g) $\mathcal{H}_d$ sampled Yang et al's. [24] (PSNR = 29.09 dB), and (h) $\mathcal{H}_d$ sampled proposed method (PSNR = 33.82 dB).

and is compared with the state of the art methods such as Yang et al.'s [12, 22], Dong et al.'s [25]. We thank the above authors to provide their program codes.

3.2. Experiments on Different Downsampled Image. In this test, our method is tested on several 512 × 512 common experimental natural images such as Lena, Plane, and Pepper. The input 256×256 LR image is down-sampled from the original 512 × 512 HR image. We use both direct downsampling degradation matrix $\mathcal{H}_d$ and blur downsampling degradation matrix $\mathcal{H}_b$ to test the algorithm's adaptability. At first, a sparse dictionary is trained by the 8×8 patches taken from input LR image. The dictionary has 128 atoms. Hence, the dictionary is a 64 × 128 matrix. Then, the 8 × 8 HR image patches are recovered by 4×4 LR image patches under our self-similarity based SR approach. We set 3 pixels overlap in LR patches by default. The neighbor searching zone is set to 10 × 10.

Figure 3 shows the experiment on the image Lena under different downsampling matrix. Figure 3(a) plots the original Lena image. Figures 3(b)–3(d) plot the HR Lena images recovered from $\mathcal{H}_b$ down-sampled LR image, respectively, by Bicubic, Yang et al.'s [24], and our proposed methods. Recovered image by Dong et al.'s [25] NCSR method is also illustrated in Figure 3(e), which uses the elaborate Gaussian low-pass filter. Figures 3(e)–3(g) show the recovered HR Lena images from $\mathcal{H}_d$ down-sampled LR image, respectively, by Bicubic, Yang et al.'s [24] method, and the proposed method. Dong et al.'s [25] NCSR method cannot get acceptable performance without Gaussian low-pass filter, which is not illustrated in Figure 3. These experimental results show that our method has better performance than the state of the art methods [12, 24, 25] in both cases. The Bicubic method could not recover the high frequency details in both cases. Although Yang et al.'s [24] method can recover the blur downsampled-LR image very well but produce too much artifact and fake high frequency details in the direct downsampling case.

Experiment result on image Pepper is shown in Figure 4. Pepper has lots of edge, which is a preferable image

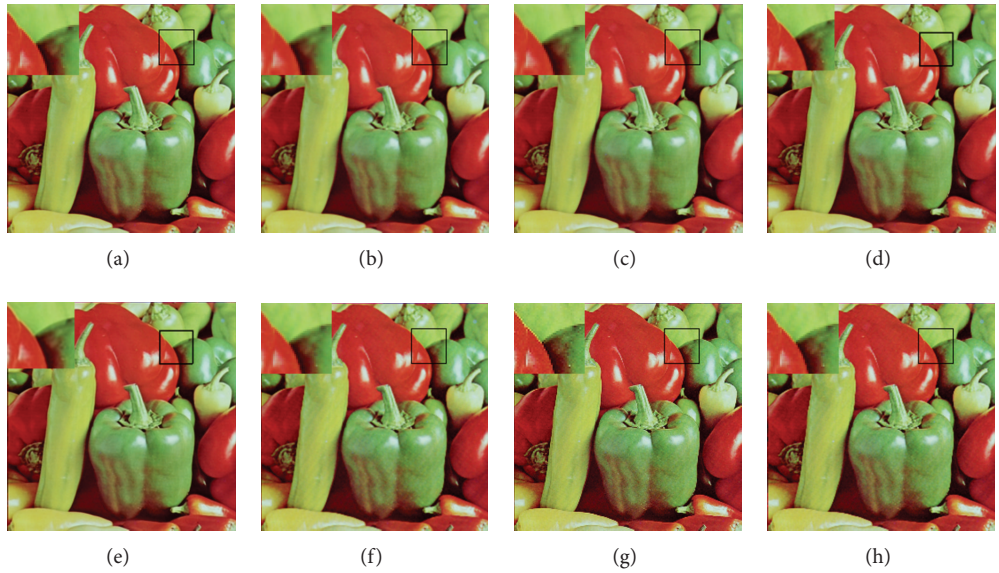

FIGURE 4: Experiment results on image Pepper, from left to right: (a) original 512×512HR image, (b) $\mathcal{H}_b$ sampled Bicubic (PSNR = 33.08 dB), (c) $\mathcal{H}_b$ sampled Yang et al.'s [24] (PSNR = 33.84 dB), (d) $\mathcal{H}_b$ sampled proposed method (PSNR = 35.68 dB), (e) Dong et al.'s [25] NCSR (PSNR = 34.92 dB) (f), $\mathcal{H}_d$ sampled bicubic (PSNR = 29.78 dB), (g) $\mathcal{H}_d$ sampled Yang et al.'s [24] (PSNR = 28.3943 dB), and (h) $\mathcal{H}_d$ sampled proposed method (PSNR = 33.25 dB).

TABLE 2: Comparison results of different SR methods.

Image	Downsampling matrix	Measures	Methods			
			Bicubic	Yang et al. [24]	Dong et al. [25]	Proposed
Lena	Blur	PSNR (dB)	34.8671	35.7477	35.46	35.8
		SSIM	0.8538	0.8586	0.9067	0.9237
	Direct	PSNR (dB)	30.964	29.0875		33.8206
		SSIM	0.7873	0.7322		0.8098
Plane	Blur	PSNR (dB)	32.6525	33.5788	34.05	34.9828
		SSIM	0.9341	0.9369	0.9487	0.9629
	Direct	PSNR (dB)	28.8573	27.5349		31.5616
		SSIM	0.8985	0.8525		0.9141
Pepper	Blur	PSNR (dB)	33.0847	33.8412	34.92	35.6808
		SSIM	0.8382	0.8474	0.9028	0.9173
	Direct	PSNR (dB)	29.7824	28.3943		33.2525
		SSIM	0.7712	0.7229		0.7754
Sailboat	Blur	PSNR (dB)	31.065	31.6411	32.05	32.1125
		SSIM	0.8143	0.8294	0.8826	0.8979
	Direct	PSNR (dB)	27.7443	26.0675		30.0478
		SSIM	0.7537	0.6893		0.756
Baboon	Blur	PSNR (dB)	25.0694	25.0966	25.13	25.4071
		SSIM	0.7068	0.7388	0.7375	0.7479
	Direct	PSNR (dB)	22.661	20.5052		23.6535
		SSIM	0.611	0.5595		0.6217

to test the recover effect about edge. Similar result is derived. The edge recovered by Yang et al.'s [24] method is not clear when LR image is down-sampled by $\mathcal{H}_d$. This failure may be caused by the inconsistency between Yang et al.'s [24] pair of HR and LR dictionaries. In comparison, our proposed method can preserve the edge's sharpness well. Besides the edge's sharpness, recovered information by self-learning is more faithful to the true HR details.

More bench-mark comparisons are illustrated in Table 2. Our proposed method shows high recovery performance

Table 3: Recovery PSNR of three sparse based SR methods with different dictionary sizes.

Image	Bicubic (dB)	Yang et al. [24] (dB) 1024 atoms	Yang et al. [22] (dB) 500 atoms	Proposed (dB) 128 atoms
Lena	29.8545	33.4116	33.4302	33.6360
Pepper	28.8546	31.4435	31.5071	31.9216
Boat	26.7158	30.4966	30.5984	30.8878

Table 4: Recovery effects of different size searching zones on image Tank.

Searching zone	8×8	10×10	12×12	14×14
PSNR (dB)	34.4982	34.6764	34.8211	34.8985
SSIM	0.9057	0.9085	0.9106	0.9114

under both kinds of downsampling degradation matrix. The comparison shows that self-similarity is a powerful image-specific prior for sparse representation SR method.

Images produced by industrial environment sensors are tested too, as shown below in Figures 5 and 6. Recovered high resolution images in Figure 6 show the effectiveness of our approach.

Furthermore, we do experiments on Forman video sequence to test the stability of our algorithm. All the frames are processed as an image. Figure 7 shows the PSNR comparison between the proposed method and Bicubic method. The proposed approach stably outperforms the Bicubic method. From about the 210th frame, recovery performance decays rapidly, since the followed frames are full of wild high frequency details.

3.3. Influence of Different Parameters. To further observe different parameter's impact, several comparison experiments are conducted.

3.3.1. Influence of Dictionary Size. Another advantage of the proposed approach is that the sparse dictionary only needs a small amount of atoms. 128 atoms are enough to get a favorable result for the proposed method. Meanwhile, Yang et al.'s method [12, 24] needs to train external dictionaries at least 512 atoms. In [22], Yang et al. propose a CS-based SR method, which also needs to train a dictionary with 500 atoms by external database. Comparison experiments are conducted on gray 512×512 natural images, including Lena, Pepper, and Boat. Table 3 shows the recovery PSNR of three sparse based SR methods with different dictionary sizes. The proposed method can recover favorable HR images by the smallest dictionary. Test results show that the proposed self-similarity learning method is more suitable for resource-constrained image sensor node.

For external dictionary based SR method, the recovery performance gets better as the dictionary size is growing larger. Figure 8 shows another comparison on Lena between Yang et al.'s method [24] and the proposed method. Yang et al.'s method [24] is conducted by a series of dictionary sizes of 256, 512, 1024, and 2048. The proposed method is conducted by different dictionary sizes of 64, 128, 256, and 512. We use the increment PSNR to Bicubic method as the comparison index. As PSNR growth curve shown in Figure 8, we can see that the recovery performance of Yang et al.'s method relies much more on the dictionary size. Its dictionary size should be three times larger than the dictionary size in the proposed method. By contrast, our approach gives a stable performance on different dictionary sizes.

Figure 5: Low resolution test images from industrial environment sensors.

3.3.2. Influence of Self-Similarity Searching Zone. Self-similarity is introduced as the sparse regulation prior in our approach. The above tests show its effectiveness and stability in preserving the detailed information such as

Figure 6: Recovered high resolution test images from industrial environment sensors scale factor = 2.

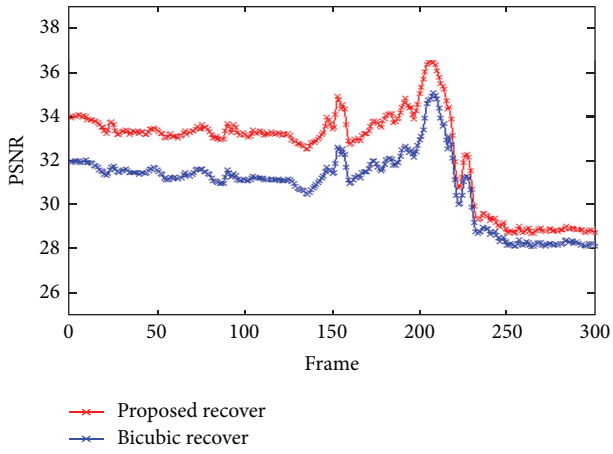

Figure 7: Self-similarity based SR performance on Foreman video sequence.

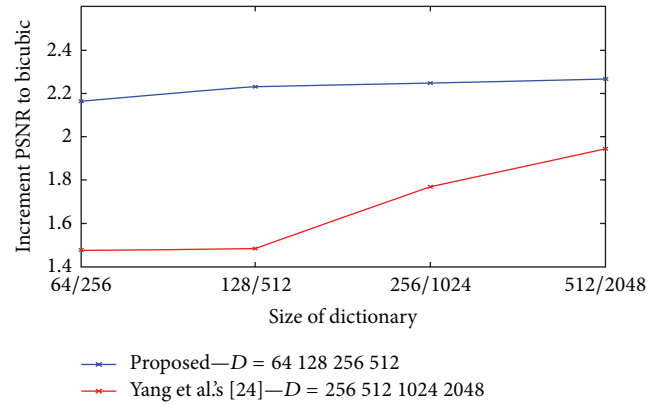

Figure 8: Recovery performance comparison over different dictionary sizes.

edge sharpness. The size of self-similarity searching zone is tested here, using test image Tank from 8×8 to 14×14 neighborhood. Results are illustrated in Table 4 and Figure 9. The similar patches found are shown in Figure 10. The experiment tells us that more edge patches can be found, and the recovery performance gets better, when the searching zone size increases.

3.4. Limitation and Further Research Direction. Although we have shown the outstanding performance of the proposed

(a) (b) (c) (d)

Figure 9: Recovery effects of different sized searching zones on image Tank, from left to right: (a) 8 × 8, (b) 10 × 10, (c) 12 × 12, and (d) 14 × 14.

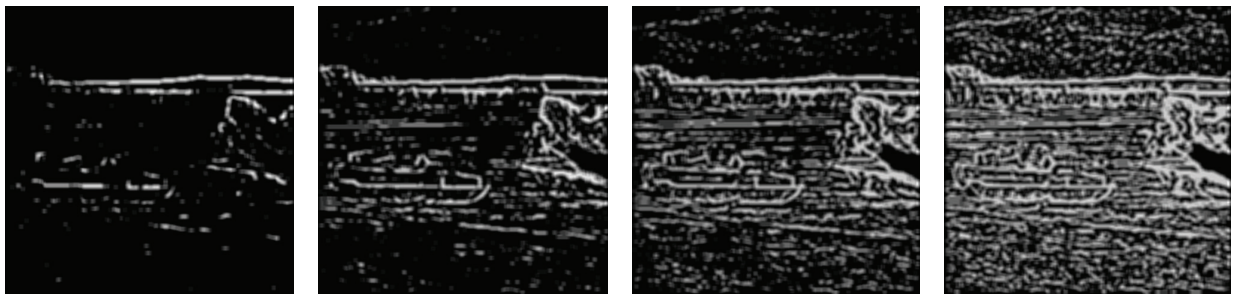

(a) (b) (c) (d)

Figure 10: Similar patches found by different sized searching zones, from left to right: (a) 8 × 8, (b) 10 × 10, (c) 12 × 12, and (d) 14 × 14.

self-similarity super resolution approach, there are still some limitation that should be considered. The proposed method assumes that the blur matrix is known as most SR methods. Further research should consider how to estimate the optimal blur kernel under the blind circumstance. Another point is that the SSE self-similarity prior used in the proposed algorithm is quite simple. We will use more delicate prior such as Parzen window estimation [31], BM3D [32], and so forth, to get a better match with the destination HR patch.

4. Conclusion

This paper has presented a novel double self-similarity super resolution approach for the resource-constrained image sensor node in the wireless sensor networks. The proposed method does not need external database and only uses the LR image itself as the training sample for sparse representation dictionary with a small number of atoms. Self-similarity sparse prior is combined in the regulation iteration to preserve the detailed information. Experiments are conducted on bench-mark test images. The effects of different parameters have been surveyed. Comparative tests show the effectiveness and stability of the proposed method over the state of the art sparse based SR methods.

Conflict of Interests

The authors declare that there is no conflict of interests regarding the publication of this paper.

Acknowledgments

This work is supported by the Open Research Fund of Zhejiang Network Media Cloud Processing Technology Center (no. 2012E10023-1) and NSFC (no. 61179006).

References

[1] H. Lee, C. Wu, and H. Aghajan, "Vision-based user-centric light control for smart environments," *Pervasive and Mobile Computing*, vol. 7, no. 2, pp. 223–240, 2011.

[2] P. Kulkarni, D. Ganesan, P. Shenoy, and Q. Lu, "SensEye: a multi-tier camera sensor network," in *Proceedings of the 13th Annual ACM International Conference on Multimedia (MULTIMEDIA '05)*, pp. 229–238, New York, NY, USA, 2005.

[3] K. Dong, Y. Liu, L. Guo, and M. Hu, "An array computer for low- and intermediate-level image processing," in *Proceedings of the IEEE International Conference on Networking, Architecture, and Storage*, pp. 447–451, Hunan, China, 2009.

[4] T. M. Lehmann, C. Gönner, and K. Spitzer, "Survey: interpolation methods in medical image processing," *IEEE Transactions on Medical Imaging*, vol. 18, no. 11, pp. 1049–1075, 1999.

[5] E. Meijering, "A chronology of interpolation: from ancient astronomy to modern signal and image processing," *Proceedings of the IEEE*, vol. 90, no. 3, pp. 319–342, 2002.

[6] M. Unser, "Splines: a perfect fit for signal and image processing," *IEEE Signal Processing Magazine*, vol. 16, no. 6, pp. 22–38, 1999.

[7] J. Sun, J. Sun, Z. Xu, and H.-Y. Shum, "Image super-resolution using gradient profile prior," in *Proceedings of the IEEE Conference on Computer Vision and Pattern Recognition (CVPR '08)*, pp. 1–8, Anchorage, AK, USA, 2008.

[8] S. Dai, M. Han, W. Xu, Y. Wu, and Y. Gong, "Soft edge smoothness prior for alpha channel super resolution," in *Proceedings of the IEEE Computer Society Conference on Computer Vision and Pattern Recognition (CVPR '07)*, pp. 1–8, Minneapolis, Minn, USA, 2007.

[9] X. Li and M. T. Orchard, "New edge-directed interpolation," *IEEE Transactions on Image Processing*, vol. 10, no. 10, pp. 1521–1527, 2001.

[10] L. Zhang and X. Wu, "An edge-guided image interpolation algorithm via directional filtering and data fusion," *IEEE Transactions on Image Processing*, vol. 15, no. 8, pp. 2226–2238, 2006.

[11] X. Zhang and X. Wu, "Image interpolation by adaptive 2-D autoregressive modeling and soft-decision estimation," *IEEE Transactions on Image Processing*, vol. 17, no. 6, pp. 887–896, 2008.

[12] J. Yang, J. Wright, T. Huang, and Y. Ma, "Image super-resolution as sparse representation of raw image patches," in *Proceedings of the IEEE Conference on Computer Vision and Pattern Recognition (CVPR '08)*, pp. 1–8, Anchorage, AK, USA, 2008.

[13] E. J. Candès, *Compressive Sampling*, International Congress of Mathematicians, 2006.

[14] E. J. Candès, J. Romberg, and T. Tao, "Robust uncertainty principles: exact signal reconstruction from highly incomplete frequency information," *IEEE Transactions on Information Theory*, vol. 52, no. 2, pp. 489–509, 2006.

[15] D. L. Donoho, M. Elad, and V. N. Temlyakov, "Stable recovery of sparse overcomplete representations in the presence of noise," *IEEE Transactions on Information Theory*, vol. 52, no. 1, pp. 6–18, 2006.

[16] D. Takhar, V. Bansal, and M. Wakin, "A compressed sensing camera: new theory and an implementation using digital micro mirrors," in *Electronic Imaging: Computational Imaging*, vol. 4 of *Proceedings of the SPIE*, San Jose, Calif, USA, 2006.

[17] R. Baraniuk and P. Steeghs, "Compressive radar imaging," in *Proceedings of the IEEE Radar Conference*, pp. 128–133, Boston, Mass, USA, 2007.

[18] M. Herman and T. Strohmer, "High-resolution radar via compressed sensing," *IEEE Transactions on Signal Processing*, vol. 57, no. 6, pp. 2275–2284, 2009.

[19] M. Lustig, D. Donoho, and J. M. Pauly, "Sparse MRI: the application of compressed sensing for rapid MR imaging," *Magnetic Resonance in Medicine*, vol. 58, no. 6, pp. 1182–1195, 2007.

[20] W. Bajwa, J. Haupt, A. Sayeed, and R. Nowak, "Compressive wireless sensing," in *Proceedings of the 5th International Conference on Information Processing in Sensor Networks (IPSN '06)*, pp. 134–142, New York, NY, USA, 2006.

[21] J. Laska, S. Kirolos, Y. Massoud et al., "Random sampling for analog to information conversion of wideband signals," in *Proceedings of the IEEE Dallas Circuits and Systems Workshop on Design, Applications, Integration and Software (DCAS '06)*, pp. 119–122, Dallas, Tex, USA, 2006.

[22] S. Yang, M. Wang, Y. Sun, F. Sun, and L. Jiao, "Compressive sampling based single-image super-resolution reconstruction by dual-sparsity and non-local similarity regularizer," *Pattern Recognition Letters*, vol. 33, no. 9, pp. 1049–1059, 2012.

[23] N. Kulkarni, P. Nagesh, R. Gowda, and B. Li, "Understanding compressive sensing and sparse representation-based super-resolution," *IEEE Transactions on Circuits and Systems for Video Technology*, vol. 22, no. 5, pp. 778–789, 2012.

[24] J. Yang, J. Wright, T. S. Huang, and Y. Ma, "Image super-resolution via sparse representation," *IEEE Transactions on Image Processing*, vol. 19, no. 11, pp. 2861–2873, 2010.

[25] W. Dong, L. Zhang, G. Shi, and X. Li, "Nonlocally centralized sparse representation for image restoration," *IEEE Transactions on Image Processing*, vol. 22, no. 4, pp. 1620–1630, 2013.

[26] D. Glasner, S. Bagon, and M. Irani, "Super-resolution from a single image," in *Proceedings of the 12th International Conference on Computer Vision (ICCV '09)*, pp. 349–356, Kyoto, Japan, 2009.

[27] M. Zontak and M. Irani, "Internal statistics of a single natural image," in *Proceedings of the IEEE Conference on Computer Vision and Pattern Recognition (CVPR '11)*, pp. 977–984, 2011.

[28] M. Aharon, M. Elad, and A. Bruckstein, "K-SVD: an algorithm for designing overcomplete dictionaries for sparse representation," *IEEE Transactions on Signal Processing*, vol. 54, no. 11, pp. 4311–4322, 2006.

[29] R. Chartrand and W. Yin, "Iteratively reweighted algorithms for compressive sensing," in *Proceedings of the IEEE International Conference on Acoustics, Speech and Signal Processing (ICASSP '08)*, pp. 3869–3872, 2008.

[30] J. A. Tropp and A. C. Gilbert, "Signal recovery from random measurements via orthogonal matching pursuit," *IEEE Transactions on Information Theory*, vol. 53, no. 12, pp. 4655–4666, 2007.

[31] E. Parzen, "On estimation of a probability density function and mode," *Annals of Mathematical Statistics*, vol. 33, no. 3, pp. 1065–1076, 1962.

[32] K. Dabov, A. Foi, V. Katkovnik, and K. Egiazarian, "Image denoising by sparse 3-D transform-domain collaborative filtering," *IEEE Transactions on Image Processing*, vol. 16, no. 8, pp. 2080–2095, 2007.

Hindawi Publishing Corporation
Mathematical Problems in Engineering
Volume 2014, Article ID 649276, 10 pages
http://dx.doi.org/10.1155/2014/649276

Research Article

Models and Algorithms for Tracking Target with Coordinated Turn Motion

Xianghui Yuan, Feng Lian, and Chongzhao Han

Ministry of Education Key Laboratory for Intelligent Networks and Network Security (MOE KLINNS), School of Electronics and Information Engineering, Xi'an Jiaotong University, Xi'an 710049, China

Correspondence should be addressed to Feng Lian; lianfeng1981@mail.xjtu.edu.cn

Received 23 July 2013; Accepted 15 December 2013; Published 12 January 2014

Academic Editor: Shuli Sun

Tracking target with coordinated turn (CT) motion is highly dependent on the models and algorithms. First, the widely used models are compared in this paper—coordinated turn (CT) model with known turn rate, augmented coordinated turn (ACT) model with Cartesian velocity, ACT model with polar velocity, CT model using a kinematic constraint, and maneuver centered circular motion model. Then, in the single model tracking framework, the tracking algorithms for the last four models are compared and the suggestions on the choice of models for different practical target tracking problems are given. Finally, in the multiple models (MM) framework, the algorithm based on expectation maximization (EM) algorithm is derived, including both the batch form and the recursive form. Compared with the widely used interacting multiple model (IMM) algorithm, the EM algorithm shows its effectiveness.

1. Introduction

The problem of tracking a single target with coordinated turn (CT) motion is considered. The motion of a civil aircraft can usually be modeled as moving by constant speed in straight lines and circle segments. The former is known as constant velocity (CV) model and the latter is coordinated turn model. In tracking applications, only the position part of the state can be measured by the sensor and the turn rate ω is often unknown. So the measurement data can be seen as the incomplete data. This is a resource-constrained problem for tracking target with coordinated turn motion.

CT model is highly dependent on the choice of state components [1]. The turn rate ω can be augmented in the CT model, called ACT model. There are two types of ACT models: ACT model with Cartesian velocity and ACT model with polar velocity. The state vectors are $[x, y, \dot{x}, \dot{y}, \omega]'$ and $[x, y, v, \phi, \omega]'$, respectively. The two are both nonlinear models and have been compared in [2, 3] based on EKF. For unscented Kalman filter (UKF) is a very efficient tool for nonlinear estimation [4, 5], here the two models are compared based on UKF.

When the target with CT motion has a constant speed, it satisfies a kinematic constraint: $V \cdot A = 0$, where V is the target velocity vector and A is the target acceleration vector. If the dynamic model incorporates the constraint directly, it will become a highly nonlinear one. To avoid this nonlinearity, the kinematic constraint was incorporated into a pseudomeasurement model [6–8].

A maneuver-centered model is introduced in [9]. The state components are $[r, \theta, \omega]'$. The model's state equation has a linear form, but its measurement equation is pseudolinear because the noise covariance is actually state dependent [10]. The center of the turn should be accurately determined, which is inherently a nonlinear problem.

Target dynamic models and tracking algorithms have intimate ties [1]. In the single model tracking framework, the tracking algorithms are interpreted and compared.

The interacting multiple model (IMM) approach has been generally considered to be the mainstream approach to maneuvering target tracking. It utilizes a bank of N Kalman filters, each designed to model a different maneuver [11]. IMM algorithm is a suboptimal algorithm based on the minimum mean square error (MMSE) criterion. Under the MMSE criterion, to get the optimal estimation of the target state, the computational load grows exponentially when the measurements are increasing. In recent years, tracking target based on maximum a posteriori (MAP) criterion has received a lot of

interest [12–17]. Expectation maximization (EM) algorithm is the state estimation approach based on MAP criterion. Us ing EM algorithm, the computational load grows linearly during per iteration and the optimal estimation based on MAP criterion can be achieved finally.

The existing EM algorithm to track maneuvering target can be classified into two categories: one formulates the maneuver as the unknown input [12–14] and the other formulates the maneuver as the system's process noise [15]. Aiming at the problem to track a target with CT maneuver, an EM algorithm is presented. The maneuver is formulated by the turn rate. First, the turn rate sequence is estimated using the EM algorithm. Then, with the estimated turn rate sequence, the target state sequence is estimated accurately.

The rest of this paper is organized as follows. Section 2 presents all the CT models' state equations and measurement equations. The tracking algorithms based on single model are interpreted in Section 3; the simulations are also presented. In Section 4, the batch and recursive EM algorithms are derived and compared with the IMM algorithm in simulation. Section 5 provides the paper's conclusions.

2. Dynamic Models for CT Motion

A maneuvering target can be modeled by

$$\begin{aligned} X_{k+1} &= f_k\left(X_k\right) + w_k, \\ z_k &= h_k\left(X_k\right) + e_k, \end{aligned} \tag{1}$$

where X_k and z_k are target state and observation, respectively, at discrete time t_k; w_k and e_k are process noise and measurement noise sequences, respectively; f_k and h_k are vector-valued functions.

2.1. CT Model with Known Turn Rate. The coordinated turn motion can be described by the following equation:

$$X_{k+1} = F\left(\omega_k\right) X_k + w_k. \tag{2}$$

The measurement equation is:

$$z_k = H_{\mathrm{CT}} X_k + e_k. \tag{3}$$

The components of state are $X = \begin{bmatrix} x & \dot{x} & y & \dot{y} \end{bmatrix}'$. ω_k stands for the turn rate in time k.

Where

$$F\left(\omega_k\right) = \begin{bmatrix} 1 & \dfrac{\sin\left(\omega_k T\right)}{\omega_k} & 0 & -\dfrac{1-\cos\left(\omega_k T\right)}{\omega_k} \\ 0 & \cos\left(\omega_k T\right) & 0 & -\sin\left(\omega_k T\right) \\ 0 & \dfrac{1-\cos\left(\omega_k T\right)}{\omega_k} & 1 & \dfrac{\sin\left(\omega_k T\right)}{\omega_k} \\ 0 & \sin\left(\omega_k T\right) & 0 & \cos\left(\omega_k T\right) \end{bmatrix} \tag{4}$$

$$w = \begin{bmatrix} w_x & w_y \end{bmatrix}'$$

$$E\left[w_k\right] = 0, \qquad E\left[w_k w_l'\right] = Q_{\mathrm{CT}}\delta_{kl}.$$

Assume only position could be measured, where

$$\begin{aligned} H_{\mathrm{CT}} &= \begin{bmatrix} 1 & 0 & 0 & 0 \\ 0 & 0 & 1 & 0 \end{bmatrix} \\ E\left[e_k\right] &= 0, \qquad E\left[e_k e_l'\right] = R\delta_{kl}. \end{aligned} \tag{5}$$

This model assumes that the turn rate is known or could be estimated. When the range rate measurements are available, the turn rate could be estimated by using range rate measurements [18, 19]. The tracking performance will be deteriorated when the assumed turn rate is far away from the true one. This model is usually used as one of the models in a multiple models framework.

2.2. ACT Model with Cartesian Velocity. In this model, the state vector is chosen to be $X = [x, y, \dot{x}, \dot{y}, \omega]'$; the state space equation can be written as

$$X_{k+1} = f_{\mathrm{ACT1}}\left(X_k\right) + G_{\mathrm{ACT1}} w_k, \tag{6}$$

where

$$f_{\mathrm{ACT1}}(X) = \begin{bmatrix} x + \dfrac{\dot{x}}{\omega}\sin(\omega T) - \dfrac{\dot{y}}{\omega}(1-\cos(\omega T)) \\ y + \dfrac{\dot{x}}{\omega}(1-\cos(\omega T)) + \dfrac{\dot{y}}{\omega}(\sin(\omega T)) \\ \dot{x}\cos(\omega T) - \dot{y}\sin(\omega T) \\ \dot{x}\sin(\omega T) + \dot{y}\cos(\omega T) \\ \omega \end{bmatrix}, \tag{7}$$

$$G_{\mathrm{ACT1}} = \begin{bmatrix} \dfrac{T^2}{2} & 0 & T & 0 & 0 \\ 0 & \dfrac{T^2}{2} & 0 & T & 0 \\ 0 & 0 & 0 & 0 & 1 \end{bmatrix}', \tag{8}$$

$$w = \begin{bmatrix} w_x & w_y & w_\omega \end{bmatrix}', \tag{9}$$

$$E\left[w_k\right] = 0, \qquad E\left[w_k w_l'\right] = Q_{\mathrm{ACT1}}\delta_{kl}. \tag{10}$$

Assume only position could be measured, the measurement equation can be written as

$$z_k = H_{\mathrm{ACT1}} X_k + e_k, \tag{11}$$

where

$$H_{\mathrm{ACT1}} = \begin{bmatrix} 1 & 0 & 0 & 0 & 0 \\ 0 & 1 & 0 & 0 & 0 \end{bmatrix}, \tag{12}$$

$$E\left[e_k\right] = 0, \qquad E\left[e_k e_l'\right] = R\delta_{kl}. \tag{13}$$

2.3. ACT Model with Polar Velocity. This model's state vector is $X = [x, y, v, \phi, \omega]'$, and the dynamic state equation is given by

$$X_{k+1} = f_{\mathrm{ACT2}}\left(X_k\right) + G_{\mathrm{ACT2}} w_k, \tag{14}$$

where

$$f_{\mathrm{ACT2}}(X) = \begin{bmatrix} x + \left(\frac{2v}{\omega}\right)\sin\left(\frac{\omega T}{2}\right)\cos\left(\phi + \frac{\omega T}{2}\right) \\ y + \left(\frac{2v}{\omega}\right)\sin\left(\frac{\omega T}{2}\right)\sin\left(\phi + \frac{\omega T}{2}\right) \\ v \\ \phi + \omega T \\ \omega \end{bmatrix} \tag{15}$$

$$G_{\mathrm{ACT2}} = \begin{bmatrix} 0 & 0 & T^2 & 0 & 0 \\ 0 & 0 & 0 & \frac{T^2}{2} & T^2 \end{bmatrix}'$$

$$w = \begin{bmatrix} w_v & w_\omega \end{bmatrix}'$$

$$E[w_k] = 0, \qquad E\left[w_k w_l'\right] = Q_{\mathrm{ACT2}}\delta_{kl}.$$

However the measurement equation is the same as (11) to (13).

2.4. Kinematic Constraint Model. For a constant speed target, the acceleration vector is orthogonal to the velocity vector:

$$C(X) = V \cdot A = 0, \tag{16}$$

where V is the target velocity vector and A is the target acceleration vector.

This kinematic constraint can be used as a pseudomeasurement. The state vector is chosen to be $X = \begin{bmatrix} x & \dot{x} & \ddot{x} & y & \dot{y} & \ddot{y} \end{bmatrix}'$. So the dynamic model is the constant acceleration (CA) model, given by

$$X_{k+1} = FX_k + Gw_k, \tag{17}$$

where

$$F = \begin{bmatrix} 1 & T & \frac{T^2}{2} & 0 & 0 & 0 \\ 0 & 1 & T & 0 & 0 & 0 \\ 0 & 0 & 1 & 0 & 0 & 0 \\ 0 & 0 & 0 & 1 & T & \frac{T^2}{2} \\ 0 & 0 & 0 & 0 & 1 & T \\ 0 & 0 & 0 & 0 & 0 & 1 \end{bmatrix}$$

$$G = \begin{bmatrix} \frac{T^2}{2} & T & 1 & 0 & 0 & 0 \\ 0 & 0 & 0 & \frac{T^2}{2} & T & 1 \end{bmatrix}' \tag{18}$$

$$w = \begin{bmatrix} w_x & w_y \end{bmatrix}'$$

$$E[w_k] = 0, \qquad E\left[w_k w_l'\right] = Q_{\mathrm{CA}}\delta_{kl}.$$

The measurement equation is given by

$$z_k = Hx_k + e_k, \tag{19}$$

where

$$H = \begin{bmatrix} 1 & 0 & 0 & 0 & 0 & 0 \\ 0 & 0 & 0 & 1 & 0 & 0 \end{bmatrix}$$

$$E[e_k] = 0, \qquad E\left[e_k e_l'\right] = R\delta_{kl}. \tag{20}$$

The pseudomeasurement is

$$\frac{V_{k|k}}{S_{k|k}} \cdot A_k + \mu_k = 0, \tag{21}$$

where $V_{k|k} = \begin{bmatrix} \dot{x}_{k|k} & \dot{y}_{k|k} \end{bmatrix}'$ and $A_k = \begin{bmatrix} \ddot{x}_k & \ddot{y}_k \end{bmatrix}'$.

$S_{k|k}$ is the filtered speed at time k :

$$S_{k|k} = \sqrt{\dot{x}_{k|k}^2 + \dot{y}_{k|k}^2}, \tag{22}$$

$$\mu_k \sim N\left(0, R_k^\mu\right), \tag{23}$$

$$R_k^\mu = r_1(\delta)^k + r_0, \quad 0 \le \delta < 1, \tag{24}$$

where r_1 is chosen to be large for initialization and r_0 is chosen for steady-state conditions.

2.5. Maneuver-Centered CT Model. This model's state vector is given by $X = \begin{bmatrix} r & \theta & \omega \end{bmatrix}'$. The process state space equation is

$$X_{k+1} = \Phi X_k + \Gamma w_k, \tag{25}$$

where

$$\Phi = \begin{bmatrix} 1 & 0 & 0 \\ 0 & 1 & T \\ 0 & 0 & 1 \end{bmatrix}$$

$$\Gamma = \begin{bmatrix} 1 & 0 \\ 0 & \frac{T}{2} \\ 0 & 1 \end{bmatrix} \tag{26}$$

$$w = \begin{bmatrix} w_r & w_\omega \end{bmatrix}'$$

$$E[w_k] = 0, \qquad E\left[w_k w_l'\right] = Q_m\delta_{kl}.$$

Assume the center of the CT motion is $(\hat{x}_c, \hat{y}_c)$. The transformation between Cartesian coordinates and maneuver-centered coordinates is given by

$$r = \sqrt{(x - \hat{x}_c)^2 + (y - \hat{y}_c)^2}$$

$$\theta = \tan^{-1}\left(\frac{y - \hat{y}_c}{x - \hat{x}_c}\right). \tag{27}$$

So the measurement equation is given by

$$z_k = H^m X_k + e_k, \tag{28}$$

where

$$H^m = \begin{bmatrix} 1 & 0 & 0 \\ 0 & 1 & 0 \end{bmatrix}$$

$$E\left[e_k e_l'\right] = R^m = J_{r\theta} R J_{r\theta}'. \tag{29}$$

$J_{r\theta}$ is the Jacobian matrix based on (27), which leads to

$$J_{r\theta} = \begin{bmatrix} \cos\theta & \sin\theta \\ -\sin\frac{\theta}{r} & \cos\frac{\theta}{r} \end{bmatrix}. \tag{30}$$

3. Tracking Algorithms in a Single Model Framework

3.1. UKF Filter with ACT Models. If the turn rate is augmented to the state vector, it will become a nonlinear problem. The extended Kalman filter (EKF) has been used to track this kind of motion. Since unscented Kalman filter (UKF) is very suitable for nonlinear estimation [4, 5], here the UKF algorithm is introduced.

(i) Calculate the Weights of Sigma Points

$$\begin{aligned} W_0^m &= \frac{\lambda}{(n+\lambda)} W_0^c \\ &= \frac{\lambda}{(n+\lambda)} + \left(1 - \alpha^2 + \beta\right) W_i^m \\ &= W_i^c = \frac{0.5}{(n+\lambda)}, \quad i = 1, 2, \ldots 2n, \end{aligned} \tag{31}$$

where n is the dimension of the state vector. $\lambda = \alpha^2(n + \kappa) - n$ is a scaling parameter. α determines the sigma points around $\overline{x}$ and is usually set to a small positive value (e.g., $1e - 3$). κ is a secondary scaling parameter which is usually set to 0, and $\beta = 2$ is optimal for Gauss distributions. Where the $\left(\sqrt{(n+\lambda)P_x}\right)_i$ is the ith row of the matrix square root.

(ii) Calculate the Sigma Points

$$\begin{aligned} \xi_{k-1|k-1}^0 &= \widehat{X}_{k-1|k-1} \\ \xi_{k-1|k-1}^{(i)} &= \widehat{X}_{k-1|k-1} + \left(\sqrt{(n+\lambda)\,P_x}\right)_i \quad i = 1, 2, \ldots, n \\ \xi_{k-1|k-1}^{(i)} &= \widehat{X}_{k-1|k-1} - \left(\sqrt{(n+\lambda)\,P_x}\right)_i \\ & \qquad i = n+1,\ n+2, \ldots, 2n. \end{aligned} \tag{32}$$

(iii) Time Update

$$\begin{aligned} \xi_k^{(i)} &= f_k\left(\xi_{k-1|k-1}^{(i)}\right), \quad i = 0, 1, \ldots 2n \widehat{X}_{k|k-1} \\ &= \sum_{i=0}^{2n} W_i^m \xi_k^{(i)} P_{k|k-1} \\ &= \sum_{i=0}^{2n} W_i^c \left(\xi_k^{(i)} - \widehat{X}_{k|k-1}\right)\left(\xi_k^{(i)} - \widehat{X}_{k|k-1}\right)' + GQ_{k-1}G'. \end{aligned} \tag{33}$$

(iv) Measurement Update. Because we assume the measurement equation is linear, the following is just the same as the traditional Kalman filter:

$$\begin{aligned} \widehat{z}_{k|k-1} &= H\widehat{X}_{k|k-1} S_k \\ &= HP_{k|k-1}H' + R_k K_k \\ &= P_{k|k-1}H' S_k^{-1} \widehat{X}_{k|k} \\ &= \widehat{X}_{k|k-1} + K_k\left(z_k - z_{k|k-1}\right) P_{k|k} \\ &= P_{k|k-1} - K_k S_k K_k'. \end{aligned} \tag{34}$$

For the cases where the measurement equation is also nonlinear, the measurement update can be referred to [10] for details.

3.2. Kinematic Constraint Tracking Filter. The Kalman filtering equations for processing this kinematic constraint as a pseudomeasurement are given below, where the filtered state estimate and error covariance after the constraint have been applied are denoted by $X_{k|k}^C$ and $P_{k|k}^C$, respectively [8].

(i) Time Update

$$\begin{aligned} \widehat{X}_{k|k-1} &= F\widehat{X}_{k-1|k-1}^C \\ P_{k|k-1} &= FP_{k-1|k-1}^C F' + GQ_{k-1}G'. \end{aligned} \tag{35}$$

(ii) Measurement Update. The measurement update is the same as (34).

(iii) Constraint Update

$$\begin{aligned} K_k^C &= P_{k|k}C_k^T\left[C_k P_{k|k} C_k' + R_k^\mu\right]^{-1} \widehat{X}_{k|k}^C \\ &= \left[I - K_k^C C_k\right] \widehat{X}_{k|k} P_{k|k}^C \\ &= \left[I - K_k^C C_k\right] P_{k|k}, \end{aligned} \tag{36}$$

where

$$C_k = \frac{1}{S_{k|k}}\left[0 \;\; 0 \;\; \hat{x}_{k|k} \;\; 0 \;\; 0 \;\; \hat{y}_{k|k}\right]. \tag{37}$$

3.3. Maneuver-Centered Tracking Filter

(i) Estimating Center of Maneuver. The center of the maneuver should be estimated from the measurements. It can be estimated through least square method which requires an iterative search procedure. The following simple geometrically oriented procedure of estimating the center was proposed in [9]. The main idea is as follows: if two points are on a circle then the perpendicular bisector of the chord between those points will pass through the center of the circle. The slope (m) and y intercept (b) of the perpendicular bisector is given by

$$\begin{aligned} m &= \frac{(x_1 - x_2)}{(y_2 - y_1)} \\ b &= \frac{(y_1 + y_2)}{2} - m\frac{(x_1 + x_2)}{2}, \end{aligned} \tag{38}$$

where (x_1, y_1) and (x_2, y_2) are the coordinates of the two points. The center can be given by

$$\begin{aligned} \widehat{x}_c &= \frac{(b_1 - b_2)}{(m_2 - m_1)} \\ \widehat{y}_c &= \frac{(m_1 b_2 - m_2 b_1)}{(m_1 - m_2)}. \end{aligned} \tag{39}$$

(ii) Maneuver Detection. In the absence of a maneuver, the target is assumed to be traveling in a straight line and modeled by a constant velocity (CV) motion. (CV model is very simple and commonly used, which will not be listed here.) When the maneuver is detected, the filter switches to the maneuver-center CT model. While the end of a maneuver is detected, the filter will then switch back to CV model.

Here a fading memory average of the innovations is used to detect if a maneuver occurs. The equation is given by

$$u_k = \rho u_{k-1} + d_k \tag{40}$$

with

$$d_k = \nu_k' S_k^{-1} \nu_k, \tag{41}$$

where $0 < \rho < 1$, ν_k is the innovation vector, and S_k is its covariance matrix.

u_k will have a chi-squared distribution with degrees

$$n_u = n_z \frac{1 + \rho}{1 - \rho}, \tag{42}$$

where n_z is the dimension of the measurement vector. When u_k exceeds a threshold (e.g., 95% or 99% confidence interval), then a maneuver onset is declared. The end time of a maneuver will be determined in a similar fashion. The procedure can be referred to [9] for details.

3.4. Simulation Results

(i) The Scenario. The scenario simulated here is very similar to that described in [20]. It includes few rectilinear stages and few CT maneuvers. Four consecutive 180° turns with rates $\omega = 1.87, -2.8, 5.6, -4.68$ are simulated, respectively, for scans [56, 150], [182, 245], [285, 314], and [343, 379]. The target trajectory can be seen in Figure 1.

The initial target position and velocities are $X_0 = 60$ km, $Y_0 = 40$ km, $\dot{X}_0 = -172$ km, and $\dot{Y}_0 = 246$ km. It is assumed that the sensor measures Cartesian coordinates X and Y directly. It is also assumed that $\sigma_X = \sigma_Y = 100$ m and the sample rate $T = 1$.

(ii) Algorithms' Parameters. UKF controlled ACT model's parameter:

$$\begin{aligned} &\alpha = 10^{-3}, \qquad \beta = 2, \qquad \kappa = 0 \\ &Q_{\text{ACT1}} = \text{diag}\{1 \quad 1 \quad 10^{-4}\} \\ &Q_{\text{ACT2}} = \text{diag}\{1 \quad 10^{-4}\}. \end{aligned} \tag{43}$$

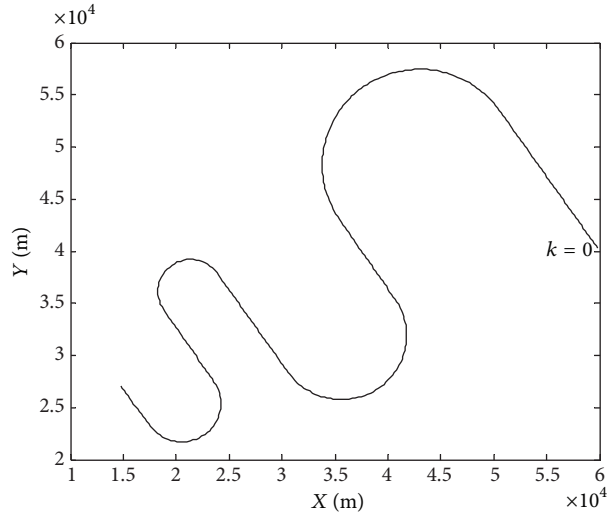

Figure 1: The test trajectory.

Kinematic constraint model's parameter:

$$\begin{aligned} &Q_{\text{CA}} = \text{diag}\{1 \quad 1\} \\ &\delta = 0.92, \qquad r_0 = 1, \qquad r_1 = 200. \end{aligned} \tag{44}$$

Maneuver centered model's parameter:

$$\begin{aligned} &Q_m = \text{diag}\{10^6 \quad 10^{-4}\} \\ &\rho = 0.8. \end{aligned} \tag{45}$$

(iii) Results. The four models are listed as follows.

Method 1: ACT model with Cartesian velocity.

Method 2: ACT model with polar velocity.

Method 3: kinematic constraint model.

Method 4: maneuver-centered CT model.

Root mean squared errors (RMSE) are used here for comparison. The RME position errors are defined as follows:

$$\text{RMS.P.E}(k) = \sqrt{\frac{1}{M}\sum_{i=1}^{M}\left[\left(x_k^i - \widehat{x}_k^i\right)^2 + \left(y_k^i - \widehat{y}_k^i\right)^2\right]}, \tag{46}$$

where $M = 200$ are the Monte-Carlo simulation runs. x_k^i and y_k^i stand for the true position, while $\widehat{x}_{k|k}^i$ and $\widehat{y}_k^i$ are the position estimates.

The RMS position errors of all but the first ten are shown in Figure 2.

Table 1 summarizes the average RMS of the position errors.

Table 2 summarizes the relative computational complexity, normalized to method 4.

It can be seen from the figure and tables that method 2 has the best performance and its computational load is roughly

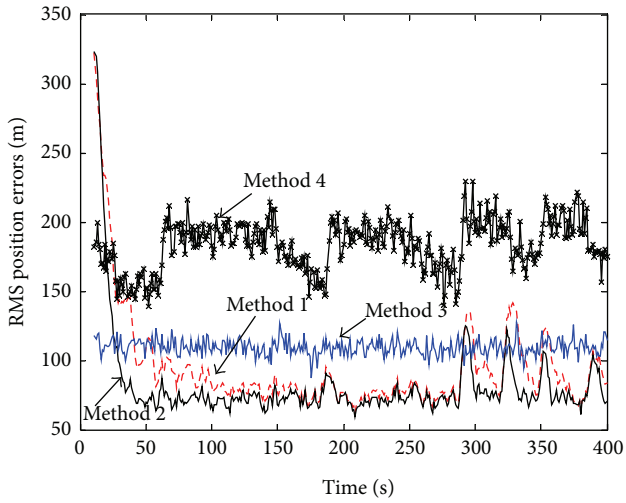

Figure 2: RMS position errors of the four methods.

Table 1: Average RMS of position errors.

Method	Average RMS of position errors (m)
1	94.26
2	81.57
3	109.51
4	183.46

Table 2: Relative computational load.

Method	Relative computational load
1	7.26
2	7.07
3	1.42
4	1

the same as method 1. So we can conclude that ACT model with polar velocity is better than ACT model with Cartesian velocity. Method 4 has the least computational load but its performance is poor. Method 3 is slightly more complex than method 4 but can decrease the error greatly. So if the computational load is of great concern, kinematic constraint model is a good choice.

4. The Expectation Maximization (EM) Algorithm for Tracking CT Motion Target

In this part, the model in Section 2.1 is used.

The turn rate ω_k can be described by a Markov chain [21, 22] and has r possible values:

$$\omega_k \in M_r = \{\omega(1), \omega(2), \ldots, \omega(r)\}. \quad (47)$$

Assume the initial probability τ_i and the one-step transition matrix are known, as follows:

$$\tau_i = p(\omega_0 = \omega(i)), \quad i = 1, 2, \ldots, r$$
$$\pi_{i,j} = p(\omega_{k+1} = \omega(j) \mid \omega_k = \omega(i)), \quad i, j = 1, 2, \ldots, r. \quad (48)$$

The measurement sequence is defined by $Z_{1:N} = \{z_1, z_2, \ldots, z_N\}$, state sequence is $X_{1:N} = \{X_1, X_2, \ldots, X_N\}$, and maneuver sequence is $\Omega_{1:N} = \{\omega_1, \omega_2, \ldots, \omega_N\}$.

4.1. Batch EM Algorithm. Assume the measurement sequence is known, this algorithm focuses on finding the best maneuver sequence based on MAP criterion. There is one best maneuver sequence $\Omega_{1:N}^{(\mathbf{B})}$ in r^N possible sequences that makes the conditional probability density function be the maximum. When $\Omega_{1:N}^{(\mathbf{B})}$ is achieved, the state sequence $X_{1:N}$ can be estimated accurately.

According to EM algorithm, $Z_{1:N}$ is considered to be the incomplete data, $X_{1:N}$ to be the "lost" data, and $\Omega_{1:N}$ to be the data that needs to be estimated. EM algorithm carries out the following two steps iteratively.

(1) Expectation Step (E step)

$$J\left(\Omega_{1:N}, \Omega_{1:N}^{(j)}\right) = E_{\mathbf{X}_{1:N}}\left\{\ln p\left(X_{1:N}, Z_{1:N}, \Omega_{1:N}\right) \mid Z_{1:N}, \Omega_{1:N}^{(j)}\right\}, \quad (49)$$

where $J(\Omega_{1:N}, \Omega_{1:N}^{(j)})$ is defined as the cost function, $\Omega_{1:N}^{(j)}$ is the maneuver sequence estimation after j times iteration.

(2) Maximization step (M step)

$$\Omega_{1:N}^{(j+1)} = \arg\max_{\Omega_{1:N}} J\left(\Omega_{1:N}, \Omega_{1:N}^{(j)}\right). \quad (50)$$

If the initial value is given, the above E step and M step are carried out repeatedly, until convergence.

(i) E step. The union probability density function can be decomposed as follows:

$$p\left(X_{1:N}, Z_{1:N}, \Omega_{1:N}\right) = \prod_{k=1}^{N} p\left(z_k \mid X_k\right) \times \prod_{k=1}^{N} p\left(X_k \mid X_{k-1}, \omega_{k-1}\right) \times p\left(X_0\right) \times \prod_{i=1}^{N} p\left(\omega_i \omega_{i-1}\right) \times p\left(\omega_0\right). \quad (51)$$

$p(X_k \mid X_{k-1}, \omega_{k-1})$ and $p(\omega_i \mid \omega_{i-1})$ rely on the maneuver sequence $\Omega_{1:N}$. The state equation is Gaussian distribution:

$$p\left(X_k \mid X_{k-1}, \omega_{k-1}\right) = N\left\{X_k - F\left(\omega_{k-1}\right) X_{k-1}, Q_k\right\}, \quad (52)$$

where $N\{\mu; \Sigma\}$ is the Gaussian probability density function with mean μ and covariance Σ.

From the above analysis,

$$\begin{aligned} J\left(\Omega_{1:N}, \Omega_{1:N}^{(j)}\right) &= E_{X_{1:N}}\left\{\ln p\left(X_{1:N}, Z_{1:N}, \Omega_{1:N}\right) \mid Z_{1:N}, \Omega_{1:N}^{(j)}\right\} \\ &= \sum_{k=1}^{N}\left\{\ln p\left(\omega_k \mid \omega_{k-1}\right) - \frac{1}{2}\left(\widehat{X}_{k|N} - F(\omega_{k-1})\widehat{X}_{k-1|N}\right)' \right. \\ &\qquad \left. \times Q_k^{-1}\left(\widehat{X}_{k|N} - F\left(\omega_{k-1}\right)\widehat{X}_{k-1|N}\right)\right\}, \end{aligned} \tag{53}$$

where

$$\widehat{X}_{k|N} = E\left[X_k \mid Z_{1:N}, \Omega_{1:N}^{(j)}\right]. \tag{54}$$

Those terms which are independent of $\Omega_{1:N}$ are omitted here.

In the E step, if $\Omega_{1:N}^{(j)}$ is given, the cost function can be achieved using Kalman smoothing algorithm.

(ii) M step. In the maximization step, a new $\Omega_{1:N}$ is chosen for a higher conditional probability. Then a better parameter estimation is achieved compared to the former iteration. The following Viterbi algorithm can solve this problem perfectly.

Viterbi algorithm is a recursive algorithm looking for the best path. As shown in Figure 3, the path connects the adjacent points with the weights to be the logarithm function of the likelihood, named cost. The path's total cost is the sum of its each point's cost. The best path has the maximum cost. The detailed method to find the best path can be found in [12].

(iii) Calculating Algorithm

(1) *Initialization:* the initial maneuver sequence $\Omega_{1:N}^{(1)}$ and threshold ε should be given.

(2) *Iteration:* for each circle ($j = 1, 2, \ldots$), carry out the following steps: (1) E step, according to (53), calculate the cost between the adjacent point. (2) M step, according to Viterbi algorithm, find a better maneuver sequence.

(3) *Stop:* if $\|\Omega_{1:N}^{(j+1)} - \Omega_{1:N}^{(j)}\| \le \varepsilon$, then stop the iteration. The best maneuver sequence is $\Omega_{1:N}^{(\mathbf{B})} = \Omega_{1:N}^{(j+1)}$; then the state estimation sequence is calculated according to $\Omega_{1:N}^{(\mathbf{B})}$.

4.2. Recursive EM Algorithm. In target tracking applications, the target's state always needs online estimation. So a recursive EM algorithm is needed for calculating ω_k.

(i) Recursive Equation. Under the MAP criterion,

$$\Omega_{1:k}^{(\mathbf{B})} = \arg\max_{\Omega_{1:k}}\left\{p\left(\Omega_{1:k} \mid Z_{1:k}\right)\right\}, \tag{55}$$

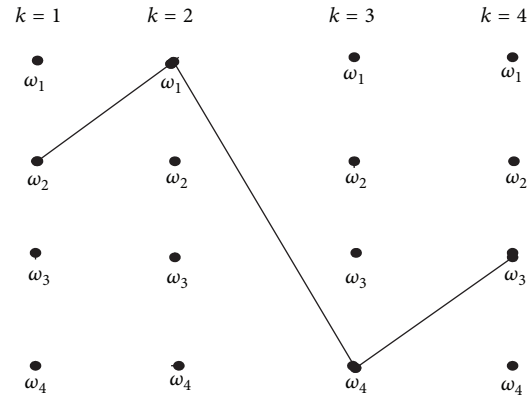

Figure 3: Viterbi algorithm for path following.

where $p(\Omega_{1:k} \mid Z_{1:k})$ can be calculated online.

$$\begin{aligned} p\left(\Omega_{1:k} \mid Z_{1:k}\right) &= p\left(\Omega_{1:k} \mid z_k, Z_{1:k-1}\right) \\ &= \frac{p\left(z_k \mid \Omega_k, Z_{1:k-1}\right) p\left(\Omega_k \mid Z_{1:k-1}\right)}{p\left(z_k \mid \Omega_{1:k-1}\right)} \\ &= p\left(z_k \mid \Omega_{1:k}, Z_{1:k-1}\right) p\left(\omega_k \mid \Omega_{1:k-1}\right) \\ &\quad \times p\left(\Omega_{1:k-1} \mid Z_{1:k-1}\right)\left(p\left(z_k \mid Z_{1:k-1}\right)\right)^{-1}. \end{aligned} \tag{56}$$

Because $\Omega_{1:k}$ is Markov chain,

$$p\left(\omega_k \mid \Omega_{1:k-1}\right) = p\left(\omega_k \mid \omega_{k-1}\right). \tag{57}$$

The possible maneuver sequence grows exponentially as the time grows. For the computation to be feasibility, it is assumed that

$$\begin{aligned} p\left(z_k \mid \Omega_{1:k}, Z_{1:k-1}\right) &\approx p\left(z_k \mid \omega_k, Z_{1:k-1}\right) \\ &= N\left(\boldsymbol{v}_k, \mathbf{S}_k\right), \end{aligned} \tag{58}$$

where $\boldsymbol{v}_k$ is the Kalman filter's innovation and $\mathbf{S}_k$ is the covariance of the innovation.

The cost function is defined as

$$J\left(\omega_k(i)\right) = \ln p\left(\Omega_{1:k}, \omega_k(i) Z_{1:k}\right), \quad i = 1, 2, \ldots, r, \tag{59}$$

which stands for the cost to model i until time k.

From (57) to (59),

$$\begin{aligned} J\left(\omega_k(j)\right) &= J\left(\omega_{k-1}(i)\right) + \ln \pi_{ij} \\ &\quad - \frac{1}{2}\boldsymbol{v}_k'(i,j)\,\mathbf{S}_k^{-1}(i,j)\,\boldsymbol{v}_k(i,j) \quad i, j = 1, 2, \ldots, r, \end{aligned} \tag{60}$$

where $\boldsymbol{v}_k(i, j)$ stands for the innovation when model i is chosen in time $k-1$ and model j is chosen in time k. $\mathbf{S}_k(i, j)$ is the corresponding covariance.

Because of using the assumption (58), the iteration algorithm is not the optimal algorithm under MAP criterion, but a suboptimal one.

(ii) Calculating Algorithm. Only one-step iteration is listed here.

(1) *E Step Calculation*. Using (10), calculate each cost from time $k-1$ to k; r^2 costs are needed.

(2) *M Step Calculation*. According to Viterbi algorithm, find out the maximum cost $J_{\max}(\omega_k(i))$ related to each model. $J_{\max}(\omega_k(i))$ is the initial value to be the next iteration.

(3) *Filtering*. According to the path which reaches each model, calculate each model's state estimation $\widehat{X}_k(i)$ and covariance $P_{k|k}(i)$, $i = 1, 2, \ldots, r$.

(4) *The Final Results*. From $J_{\max}(\omega_k(i))$, $i = 1, 2, \ldots, r$, choose the maximum one as the final filtering result:

$$j = \arg\max_i \left\{J_{\max}\left(\omega_k(i)\right)\right\}_{i=1}^{r}. \tag{61}$$

$$\widehat{X}_k^{(\mathbf{B})} = \widehat{X}_k\left(j\right), \qquad P_{k|k}^{(\mathbf{B})} = P_{k|k}\left(j\right). \tag{62}$$

4.3. Simulation Results

(i) Simulation Scenario. Target initial state is $X_0 = [60000\,\text{m} \;\; -172\,\text{m/s} \;\; 40000\,\text{m} \;\; 246\,\text{m/s}]'$. The sample rate $T = 1$ s. The covariance of process noise

$$Q = \begin{bmatrix} Q_x & 0 \\ 0 & Q_y \end{bmatrix}, \qquad Q_x = Q_y = \begin{bmatrix} \frac{T^4}{3} & \frac{T^3}{2} \\ \frac{T^3}{2} & T^2 \end{bmatrix}. \tag{63}$$

Assume only position can be measured, the measurement equation is the following:

$$z_k = \begin{bmatrix} 1 & 0 & 0 & 0 \\ 0 & 0 & 1 & 0 \end{bmatrix} X_k + v_k. \tag{64}$$

The covariance of measurement noise $R = 2500\mathbf{I}$, where $\mathbf{I}$ is the 2×2 unit matrix.

The simulation lasts for 300 s. Target's true turn rate is

$$\omega_k = \begin{cases} 0 & 0 \le k < 103 \\ 0.033\,\text{rad/s} & 104 \le k < 198 \\ 0 & 198 \le k < 300. \end{cases} \tag{65}$$

Figure 4 gives the target's true trajectory.

Assume target's maximum centripetal acceleration is $30\,\text{m/s}^2$. Under the speed 300 m/s, the corresponding turn rate is 0.1 rad/s. Seven models are used for this simulation. From -0.1 to 0.1, the seven models are distributed evenly. Their values are −0.1, −0.067, −0.033, 0, 0.033, 0.067, and 0.1. The initial probability matrix is

$$\tau = \left[\frac{1}{7} \;\; \frac{1}{7} \;\; \frac{1}{7} \;\; \frac{1}{7} \;\; \frac{1}{7} \;\; \frac{1}{7} \;\; \frac{1}{7}\right]. \tag{66}$$

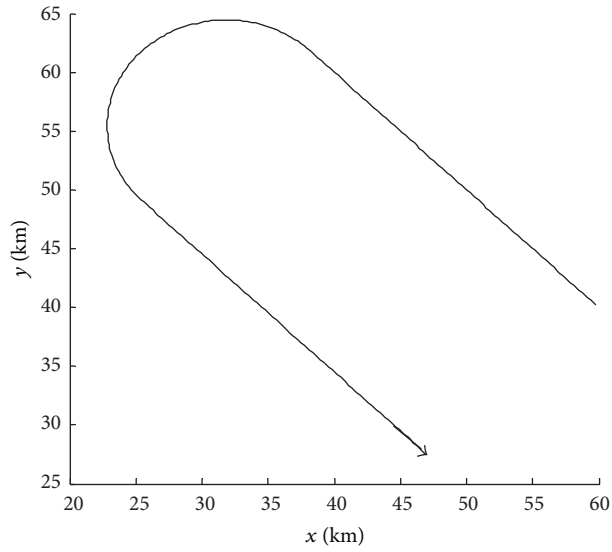

Figure 4: Target trajectory.

The model transition matrix is

$$\pi_{i,j} = \begin{cases} 0.7 & i = j \\ 0.05 & i \ne j \end{cases} \qquad i, j = 1, 2, \ldots, 7. \tag{67}$$

(ii) Simulation Results and Analysis. Batch EM algorithm, recursive algorithm, and IMM algorithm are compared in this scenario. Root mean squared errors (RMSE) are used here for comparison. The RME position errors are defined as (46) and velocity error are defined as follows:

$$\text{RMS.V.E}\,(k) = \sqrt{\frac{1}{M}\sum_{i=1}^{M}\left[\left(\dot{x}_k^i - \widehat{\dot{x}}_k^i\right)^2 + \left(\dot{y}_k^i - \widehat{\dot{y}}_k^i\right)^2\right]}, \tag{68}$$

where $M = 200$ are Monte-Carlo simulation runs and $\dot{x}_k^i$, $\dot{y}_k^i$ and $\widehat{\dot{x}}_k^i$, $\widehat{\dot{y}}_k^i$ stand for the true and estimated velocity at time k in the ith simulation runs, respectively.

Figures 5 and 6 show the position and velocity performance comparison. It can be concluded that the batch EM algorithm has much less tracking errors compared to IMM algorithm. During maneuver onset time and termination time, the IMM algorithm is better than recursive EM algorithm. But on stable period, the recursive EM algorithm performs better.

5. Conclusions

Aiming at the CT motion target tracking, several models and algorithms are introduced and simulated in this paper.

In single model framework, four CT models have been compared for tracking applications: ACT model with Cartesian velocity, ACT model with polar velocity, kinematic constraint model, and maneuver-centered model. The Monte-Carlo simulations show that the ACT model with polar

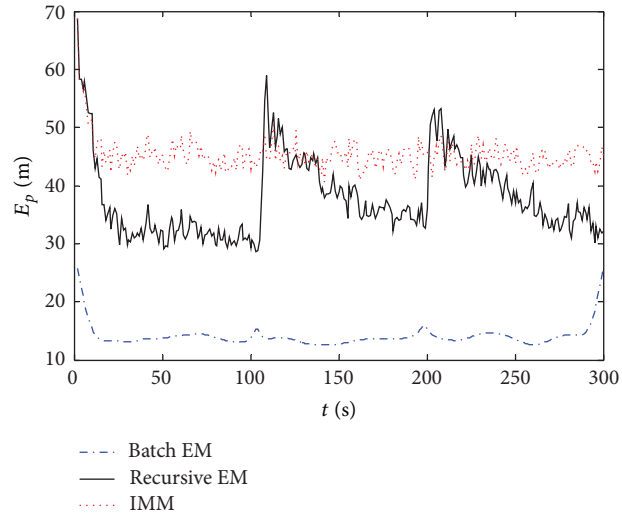

Figure 5: Position performance comparison.

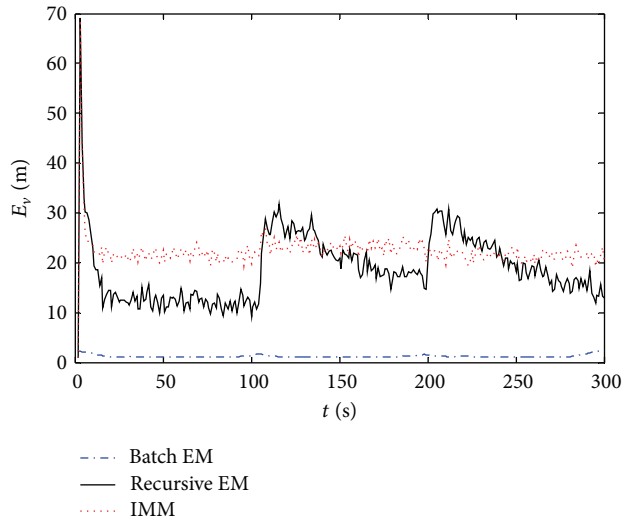

Figure 6: Velocity performance comparison.

velocity has the best tracking performance but the computational load is a bit heavier. The kinematic constraint model has a moderate tracking performance, but its computational load decreases greatly compared with UKF controlled ACT model. So if the computational load is of a great concern, the kinematic constraint model is suggested. If the tracking performance is very important and the computational load is not a problem, the ACT model with polar velocity is suitable.

In multiple models framework, EM algorithm is used for tracking CT motion target. First a batch EM algorithm is derived. The turn rate is acted as the maneuver sequence and estimated based on the MAP criterion. Under the E step, the cost function is calculated using the Kalman smoothing algorithm. Under the M step, Viterbi algorithm is used for path following to find out the path with maximum cost. Simulation results show that the Batch EM algorithm has better tracking performance than IMM algorithm. Through modification of the cost function, a recursive EM algorithm is presented. The algorithm can track the target online. Compared with the IMM algorithm, on the stable period, the recursive EM algorithm has better tracking performance.

Conflict of Interests

The authors declare that there is no conflict of interests regarding the publication of this paper.

Acknowledgments

This research work was supported by the National Key Fundamental Research & Development Programs (973) of China (2013CB329405), Foundation for Innovative Research Groups of the National Natural Science Foundation of China (61221063), Natural Science Foundation of China (61203221, 61004087), Ph.D. Programs Foundation of Ministry of Education of China (20100201120036), China Postdoctoral Science Foundation (2011M501442, 20100481338), and Fundamental Research Funds for the Central University.

References

[1] X. R. Li and V. P. Jilkov, "Survey of maneuvering Target Tracking—part I: dynamic models," *IEEE Transactions on Aerospace and Electronic Systems*, vol. 39, no. 4, pp. 1333–1364, 2003.

[2] F. Gustafsson and A. J. Isaksson, "Best choice of coordinate system for tracking coordinated turns," in *Proceedings of the 35th IEEE Conference on Decision and Control*, pp. 3145–3150, Kobe, Japan, December 1996.

[3] A. J. Isaksson and F. Gustaffsson, "Comparison of some Kalman filter based on methods for maneuver tracking and detection," in *Proceedings of the 34th IEEE Conference on Decision and Control*, pp. 1525–1530, New Orleans, La, USA, December 1995.

[4] S. Julier, J. Uhlmann, and H. F. Durrant-Whyte, "A new method for the nonlinear transformation of means and covariances in filters and estimators," *IEEE Transactions on Automatic Control*, vol. 45, no. 3, pp. 477–482, 2000.

[5] S. J. Julier and J. K. Uhlmann, "Unscented filtering and nonlinear estimation," *Proceedings of the IEEE*, vol. 92, no. 3, pp. 401–422, 2004.

[6] M. Tahk and J. L. Speyer, "Target Tracking problems subject to kinematic constraints," *IEEE Transactions on Automatic Control*, vol. 35, no. 3, pp. 324–326, 1990.

[7] A. T. Alouani and W. D. Blair, "Use of a kinematic constraint in tracking constant speed, maneuvering targets," in *Proceedings of the 30th IEEE Conference on Decision and Control*, pp. 1055–1058, Brighton, UK, December 1991.

[8] A. T. Alouani and W. D. Blair, "Use of a kinematic constraint in tracking constant speed, maneuvering targets," *IEEE Transactions on Automatic Control*, vol. 38, no. 7, pp. 1107–1111, 1993.

[9] J. A. Roecker and C. D. McGillem, "Target Tracking in maneuver-centered coordinates," *IEEE Transactions on Aerospace and Electronic Systems*, vol. 25, no. 6, pp. 836–843, 1989.

[10] X. R. Li and V. P. J. ILkov, "A Survey of maneuvering Target Tracking—part III: measurement models," in *Conference on Signal and Data Processing of Small Targets*, vol. 4437 of *Proceeding of SPIE*, pp. 423–446, San Diego, Calif, USA, 2001.

[11] Y. Bar-Shalom, K. C. Chang, and H. A. P. Blom, "Tracking a maneuvering target using input estimation versus the interacting multiple model algorithm," *IEEE Transactions on Aerospace and Electronic Systems*, vol. 25, no. 2, pp. 296–300, 1989.

[12] A. Averbuch, S. Itzikowitz, and T. Kapon, "Radar Target Tracking—viterbi versus IMM," *IEEE Transactions on Aerospace and Electronic Systems*, vol. 27, no. 3, pp. 550–563, 1991.

[13] G. W. Pulford and B. F. La Scala, "MAP estimation of target manoeuvre sequence with the expectation-maximization algorithm," *IEEE Transactions on Aerospace and Electronic Systems*, vol. 38, no. 2, pp. 367–377, 2002.

[14] A. Logothetis, V. Krishnamurthy, and J. Holst, "A Bayesian EM algorithm for optimal tracking of a maneuvering target in clutter," *Signal Processing*, vol. 82, no. 3, pp. 473–490, 2002.

[15] P. Willett, Y. Ruan, and R. Streit, "PMHT: problems and some solutions," *IEEE Transactions on Aerospace and Electronic Systems*, vol. 38, no. 3, pp. 738–754, 2002.

[16] Z. Li, S. Chen, H. Leung, and É. Bossé, "Joint data association, registration, and fusion using EM-KF," *IEEE Transactions on Aerospace and Electronic Systems*, vol. 46, no. 2, pp. 496–507, 2010.

[17] D. L. Huang, H. Leung, and E. Boose, "A pseudo-measurement approach to simultaneous registration and track fusion," *IEEE Transactions on Aerospace and Electronic Systems*, vol. 48, no. 3, pp. 2315–2331, 2012.

[18] X. Yuan, C. Han, Z. Duan, and M. Lei, "Adaptive turn rate estimation using range rate measurements," *IEEE Transactions on Aerospace and Electronic Systems*, vol. 42, no. 4, pp. 1532–1540, 2006.

[19] V. B. Frencl and J. B. R. do Val, "Tracking with range rate measurements: turn rate estimation and particle filtering," in *Proceedings of the IEEE Radar Conference*, pp. 287–292, Atlanta, Ga, USA, May 2012.

[20] E. Semerdjiev, L. Mihaylova, and X. R. Li, "Variable- and fixed-structure augmented IMM algorithms using coordinated turn model," in *Proceedings of the 3rd International Conference on Information Fusion*, pp. 10–13, Paris, France, July 2000.

[21] Y. Bar-shalom, X. R. Li, and T. Kirubarajan, *Estimation with Applications to Tracking and Navigation: Theory, Algorithms and Software*, John Wiley & Sons, New York, NY, USA, 2001.

[22] J. P. Iielferty, "Improved tracking of maneuvering targets: the use of turn-rate distributions for acceleration modeling," *IEEE Transactions on Aerospace and Electronic Systems*, vol. 32, no. 4, pp. 1355–1361, 1996.

Hindawi Publishing Corporation
Mathematical Problems in Engineering
Volume 2014, Article ID 932358, 8 pages
http://dx.doi.org/10.1155/2014/932358

Research Article

Data Reduction with Quantization Constraints for Decentralized Estimation in Wireless Sensor Networks

Yang Weng

College of Mathematics, Sichuan University, Chengdu, Sichuan 610064, China

Correspondence should be addressed to Yang Weng; wengyang@scu.edu.cn

Received 22 August 2013; Revised 15 December 2013; Accepted 19 December 2013; Published 9 January 2014

Academic Editor: Shuli Sun

The unknown vector estimation problem with bandwidth constrained wireless sensor network is considered. In such networks, sensor nodes make distributed observations on the unknown vector and collaborate with a fusion center to generate a final estimate. Due to power and communication bandwidth limitations, each sensor node must compress its data and transmit to the fusion center. In this paper, both centralized and decentralized estimation frameworks are developed. The closed-form solution for the centralized estimation framework is proposed. The computational complexity of decentralized estimation problem is proven to be NP-hard and a Gauss-Seidel algorithm to search for an optimal solution is also proposed. Simulation results show the good performance of the proposed algorithms.

1. Introduction

The developments in microelectromechanical systems technology, wireless communications, and digital electronics have enabled the deployment of low-cost wireless sensor networks (WSNs) in large scale using small size sensor nodes [1]. In such networks, the distributed sensors collaborate with a fusion center to jointly estimate the unknown parameter. If fusion center receives all measurement data from all sensors directly and processes them in real time, the corresponding processing of sensor data is known as the centralized estimation, which has several serious drawbacks, including poor survivability and reliability, heavy communications, and computational burdens. Since all sensors have limited battery power, their computation and communication capability are severely limited; the decentralized estimation methods are widely discussed in recent years [2–6]. In the decentralized estimation framework, every sensor is also a subprocessor. It first preprocesses the measurements in terms of a criterion and then transmits its local compression data to the fusion center. Upon receiving the sensor messages, the fusion center combines them according to a fusion rule to generate the final result. In such networks, less information is transmitted leading to a significant power-saving advantage which is very important in the case of WSNs.

To minimize the communication cost, only limited amount of information is allowed to be transmitted through networks; dimensionality reduction estimation methods have attracted considerable attentions [7–9]. The basic idea of the dimensionality reduction estimation strategy is to prefilter the high-dimensional observation vector by a linear transformation (matrix) to project the observation onto the subspace spanned by basis vectors and filter the result with a low-rank estimation. Indeed, dimensionality reduction estimation and filtering are important for a wide range of signal processing applications where data reduction, robustness against noise, and high computational efficiency are desired.

Quantization has been viewed as a fundamental element in saving bandwidth by reducing the amount of data to represent a signal and well studied in digital signal processing and control where a signal with continuous values is quantized due to a finite word-length of microprocessor [10]. In WSNs, quantization is also necessary to reduce the energy consumption as communications consume the most energy as the amount of energy consumed is related to the amount of data transmitted. An interesting distributed estimation approach based on the sign of innovation (SOI) has been developed for dynamic stochastic systems in [11] where only transmission of innovation of a single bit is required. A general multiple-level quantized innovation Kalman filter for

estimation of linear dynamic stochastic systems has been presented in [12]. The solution to the optimal filter is given in terms of a simple Riccati recursion as in the standard Kalman filter. A random field estimation problem with quantized measurements in sensor networks has been considered in [13]. In the early work [14], the trade-off between dimension reduction and quantization in minimum mean squared error estimation problem is investigated.

In this paper, different from the existing work, the dimensionality reduction and quantization for local data compression are considered in an integrated way. Data reduction with quantization constraints estimation for an unknown vector is formulated as an optimization problem. Both centralized and decentralized estimation frameworks are developed. The closed-form solution for the centralized estimation framework is proposed. By using computational complexity theory, the intractability of decentralized estimation problem is established. A Gauss-Seidel type iteration algorithm to search for an optimal solution is also proposed for the decentralized estimation problem.

The rest of this paper is organized as follows. With given communication bandwidth, the bits allocation problem has been formulated as an optimization problem in Section 2. The closed-form solution for the centralized estimation framework is proposed in Section 3. The computational complexity of decentralized estimation problem is proved to be NP-hard and a Gauss-Seidel algorithm to search for an optimal solution is also proposed in Section 4. Simulation results are reported in Section 5 to show the performance of our methods. Concluding remarks are given in Section 6.

2. Problem Formulation

Consider a sensor network deployed with L sensor nodes. Each sensor, say the ith sensor, can take observation $y_i \in \mathscr{R}^{n_i}$ which is correlated with an unknown random parameter $x \in \mathscr{R}^m$. The observations will be transmitted to a fusion center to estimate the unknown parameter x under some certain criterion. In this paper, we consider the minimum mean squared error (MMSE) criterion [15, 16].

Through a transform matrix $K_i \in \mathscr{R}^{r_i \times n_i}$, $r_i \leq n_i$, each sensor transforms the observation into a $r_i \times 1$ vector $K_i y_i$, whereafter the transformed vector will be quantized into several bits and transmited to the fusion center. In this paper, we assume that there is no information exchange among sensors. We also assume without loss of generality that the unknown parameter x and observations y_i are zeromean. The auto- and cross-covariance matrices $R_{xx}, R_{xy_i}, R_{y_i y_j}$, $\forall i, j \in \{1, \ldots, L\}$ are available at the FC. The role of FC is to combine the received quantization information

$$\left\{Q\left(K_1 y_1\right), Q\left(K_2 y_2\right), \ldots, Q\left(K_L y_L\right)\right\}, \tag{1}$$

according to

$$\widehat{x} = f\left(Q\left(K_1 y_1\right), Q\left(K_2 y_2\right), \ldots, Q\left(K_L y_L\right)\right), \tag{2}$$

where $f(\cdot)$ is the fusion function and $Q(\cdot)$ is a given quantizer. Our goal is to design the linear transforms $\{K_1, \ldots, K_L\}$ and the fusion function $f(\cdot)$ such that the mean squared error (MSE) is as small as possible under the constraint that the total number of bits can be transmitted to FC. Throughout this work, we will focus only on the linear design of fusion function $f(\cdot)$ which can be represented in the form

$$\begin{aligned}\widehat{x} &= f\left(Q\left(K_1 y_1\right), Q\left(K_2 y_2\right), \ldots, Q\left(K_L y_L\right)\right) \\ &= \sum_{i=1}^{L} C_i Q\left(K_i y_i\right).\end{aligned} \tag{3}$$

The given quantizer $Q(\cdot)$ is considered as a minimum squared error distortion quantizer [17]. We assume that the quantizer input vector $Z = (z_1, \ldots, z_r)^T$ is a random vector with uncorrelated components. Each component has zero mean and variance σ_i^2. Under the Gaussian assumption, the quantizer output $Q(Z)$ is treated as a noise source that introduces independent white noise v as

$$Z = Q(Z) + v, \tag{4}$$

whose mean is zero and covariance is [17]

$$\begin{aligned}\Sigma_{vv} &= E\left(vv^T\right) \\ &= \operatorname{diag}\left\{\gamma_1^2, \ldots, \gamma_r^2\right\} \\ &= \operatorname{diag}\left\{\sigma_1^2 2^{-2B_1}, \ldots, \sigma_r^2 2^{-2B_r}\right\},\end{aligned} \tag{5}$$

where $\gamma_i^2 = \sigma_i^2 2^{-2B_i}$ is the squared error distortion for the ith component and B_i is the bits used by the the ith component z_i.

Therefore, the mean squared error at the fusion center can be calculated as follows:

$$\begin{aligned}E\|x - \widehat{x}\|^2 &= E\left\|x - \sum_{i=1}^{L} C_i Q\left(K_i y_i\right)\right\|^2 \\ &= E\left\|x - \sum_{i=1}^{L} C_i\left(K_i y_i - v_i\right)\right\|^2 + \sum_{i=1}^{L} E\left\|C_i v_i\right\|^2 \\ &= E\left\|x - \sum_{i=1}^{L} C_i K_i y_i\right\|^2 + \sum_{i=1}^{L}\sum_{s=1}^{m}\sum_{t=1}^{r_i} c_{st}^i \gamma_{it}^2 \\ &= E\left\|x - \sum_{i=1}^{L} C_i K_i y_i\right\|^2 + \sum_{i=1}^{L}\sum_{s=1}^{m}\sum_{t=1}^{r_i} c_{st}^i \sigma_{it}^2 2^{-2B_{it}},\end{aligned} \tag{6}$$

where K_i is the local linear transform operator, $C_i = \{c_{st}^i\}_{m \times r_i}$ is the fusion operator at the fusion center and B_{it} is the quantization bits for the tth elements of vector $K_i y_i$. The optimal estimation of random vector x under individual sensor bandwidth constraint can be formulated as follows:

$$\begin{aligned}&\text{minimize} \quad E\left(\|x - \widehat{x}\|^2\right) \\ &\text{subject to} \quad \sum_{i=1}^{L}\sum_{t=1}^{r_i} B_{it} \leq B, \quad C_i \in \mathscr{R}^{m \times r_i}, \quad K_i \in \mathscr{R}^{r_i \times n_i}.\end{aligned} \tag{7}$$

By appropriate pre- and postwhitening process if necessary, we assume without loss of generality that the auto- and cross-covariance matrices $R_{xx}, R_{xy_i}, R_{y_iy_j}, \forall\, i, j \in \{1, \ldots, L\}$ have full rank and the elements of observation vector taken by each sensor are uncorrelated [18].

3. Centralized Data Reduction with Quantization Constraints

In this section, we consider a simple centralized framework where the entire data is available at a single sensor node and the centralized case of optimization problem (7) can be simplified as follows:

$$\begin{aligned} &\text{minimize} \quad E\|x-\hat{x}\|^2 = E\left\|x - K(r)\, y\right\|^2 + \sum_{i=1}^{r}\sigma_i^2 2^{-2B_i} \\ &\text{subject to} \quad \sum_{i=1}^{r} B_i \le B, \quad K(r) \in \mathscr{R}^{m\times n}, \end{aligned} \tag{8}$$

where $K(r)$ is the approximation matrix and B is the total bits to be transmitted.

The optimal estimation without observation compression in the MMSE sense is as follows:

$$\hat{x} = R_{xy}R_{yy}^{-1}y = Ky, \tag{9}$$

with estimation error covariance matrix

$$P = R_{xx} - R_{xy}R_{yy}^{-1}R_{yx}, \tag{10}$$

where K is called optimal estimation matrix. We write formula (9) as a linear model by introducing an estimation error e as

$$x = \hat{x} + e = R_{xy}R_{yy}^{-1}y + e. \tag{11}$$

We consider the problem that the optimal estimation matrix K is replaced by an approximating matrix $K(r)$ with lower rank $r < n$. With a given compressed dimension r, we want to find an optimal $K(r)$ such that the MMSE is as small as possible. The linear model (11) is modified as

$$x = \hat{x}(r) + e(r) = K(r)\, y + e(r). \tag{12}$$

The estimation error covariance matrix can be calculated as follows:

$$\begin{aligned} P(r) &= E\left(e(r)\, e(r)^T\right) \\ &= E\left(\left(e + Ky - K(r)\, y\right)\left(e + Ky - K(r)\, y\right)^T\right) \\ &= P + (K - K(r))\, R_{yy}(K - K(r))^T. \end{aligned} \tag{13}$$

Therefore, the approximation matrix $K(r)$ introduces an extra variance term

$$\begin{aligned} \varepsilon^2 &= \operatorname{tr}\left[(K - K(r))\, R_{yy}(K - K(r))^T\right] \\ &= \operatorname{tr}\left[\left(KR_{yy}^{1/2} - K(r)\, R_{yy}^{1/2}\right)\left(KR_{yy}^{1/2} - K(r)\, R_{yy}^{1/2}\right)^T\right]. \end{aligned} \tag{14}$$

The matrix $KR_{yy}^{1/2} = R_{xy}R_{yy}^{-1/2}$ has an SVD of the form

$$KR_{yy}^{1/2} = U\Sigma V^T. \tag{15}$$

By minimizing ε^2, it is not hard to show that the best approximation matrix is

$$K(r) = U\Sigma(r)\, V^T R_{yy}^{1/2}. \tag{16}$$

The extra variance is then

$$\varepsilon^2 = \sum_{i=r+1}^{m}\lambda_i^2, \tag{17}$$

where $\lambda_{r+1}, \ldots, \lambda_m$ are the smallest $m - r$ singular values of $KR_{yy}^{1/2}$.

Therefore the optimization problem (18) is as follows:

$$\begin{aligned} &\text{minimize} \quad \sum_{i=r+1}^{m}\lambda_i^2 + \sum_{i=1}^{r}\sigma_i^2 2^{-2B_i} \\ &\text{subject to} \quad \sum_{i=1}^{r} B_i \le B, r. \end{aligned} \tag{18}$$

If r is given, we can solve this optimization problem by a Laplacian multiplier [19].

4. Decentralized Data Reduction with Quantization Constraints

Let us now consider the estimation framework in a multisensor setup, under a total available rate B which has to be shared among all sensors. In the decentralized manner, the ith sensor transforms the observation $y_i \in \mathscr{R}^{n_i}$ into a $r_i \times 1$ vector $K_i y_i$ through a transform matrix $K_i \in \mathscr{R}^{r_i\times n_i}$, $r_i \le n_i$, whereafter the transformed vector will be quantized into several bits and transmited to the fusion center. By the linear fusion rule at the fusion center, the mean squared error at the fusion center can be calculated as follows:

$$\begin{aligned} E\|x-\hat{x}\|^2 &= E\left\|x - \sum_{i=1}^{L} C_i Q\left(K_i y_i\right)\right\|^2 \\ &= E\left\|x - \sum_{i=1}^{L} C_i K_i y_i\right\|^2 + \sum_{i=1}^{L}\sum_{s=1}^{m}\sum_{t=1}^{r_i} c_{st}^i \sigma_{it}^2 2^{-2B_{it}}, \end{aligned} \tag{19}$$

where K_i is the local linear transform operator, $C_i = \{c_{st}^i\}_{m\times r_i}$ is the fusion operator at the fusion center and B_{it} is the quantization bits for the tth elements of vector $K_i y_i$. Therefore, the decentralized estimation of random vector x under

individual sensor bandwidth constraint can be formulated as follows:

$$\begin{aligned}\text{minimize}\quad & E\|x-\widehat{x}\|^2 = E\left\|x-\sum_{i=1}^{L}C_iK_iy_i\right\|^2 \\ & \quad +\sum_{i=1}^{L}\sum_{s=1}^{m}\sum_{t=1}^{r_i}c_{st}^{i}\sigma_{it}^{2}2^{-2B_{it}} \\ \text{subject to}\quad & \sum_{i=1}^{L}\sum_{t=1}^{r_i}B_{it}\le B,\quad C_i\in\mathscr{R}^{m\times r_i},\quad K_i\in\mathscr{R}^{r_i\times n_i}.\end{aligned} \tag{20}$$

Theorem 1. *The computational complexity of solving problem* (20) *is NP-hard even in the case with absence of channel distortions for quantization of each sensor.*

Proof. We present the simplified formulations to analyze the computation complexity of problem (7). Let the L distributed sensor nodes make observations on a common random parameter vector $x\in\mathscr{R}^m$ according to

$$y_i = H_ix+v_i,\quad i=1,2,\ldots,L, \tag{21}$$

where $H_i\in\mathscr{R}^{m_i\times m}$ is the observation matrix and $v_i\in\mathscr{R}^{m_i}$ is the additive noise which is zero mean and spatially uncorrelated. According to [18], we can assume that the sensor noises are uncorrelated with the input signal x. Without loss of generality, we can assume that the unknown parameter vector x has an autocovariance matrix $R_{xx}=I_m$ and the noise covariance matrix is $R_{v_i}=I_{m_i}$.

The MSE at the FC can be calculated as follows:

$$\begin{aligned}E\|x-\widehat{x}\|^2 &= E\left\|x-\sum_{i=1}^{L}C_iQ\left(K_iy_i\right)\right\|^2 \\ &= E\left\|x-\sum_{i=1}^{L}C_iK_iy_i\right\|^2+\sum_{i=1}^{L}\sum_{s=1}^{m}\sum_{t=1}^{r_i}c_{st}^{i}\sigma_{it}^{2}2^{-2B_{it}}.\end{aligned} \tag{22}$$

In the absence of channel distortions, the MSE at the FC can be simplified as

$$\begin{aligned}E\left(\|x-\widehat{x}\|^2\right) &= E\left\|x-\sum_{i=1}^{L}C_iQ\left(K_iy_i\right)\right\|^2 \\ &= E\left\|x-\sum_{i=1}^{L}C_i\left(K_iy_i-v_i\right)\right\|^2+\sum_{i=1}^{L}E\|C_iv_i\|^2 \\ &= E\left\|x-\sum_{i=1}^{L}C_iK_iy_i\right\|^2+\sum_{i=1}^{L}\sum_{s=1}^{m}\sum_{t=1}^{r_i}c_{st}^{i}\gamma_{it}^{2} \\ &= E\left\|x-\sum_{i=1}^{L}C_iK_iy_i\right\|^2 \\ &= E\left\|x-\sum_{i=1}^{L}C_iK_i\left(H_ix+v_i\right)\right\|^2 \\ &= E\left(x-\sum_{i=1}^{L}C_iK_i\left(H_ix+v_i\right)\right)^T \\ &\quad\times\left(x-\sum_{i=1}^{L}C_iK_i\left(H_ix+v_i\right)\right) \\ &= \mathrm{Tr}\left(E\left(x-\sum_{i=1}^{L}C_iK_i\left(H_ix+v_i\right)\right)\right. \\ &\quad\left.\times\left(x-\sum_{i=1}^{L}C_iK_i\left(H_ix+v_i\right)\right)^T\right) \\ &= \mathrm{Tr}\left[\left(I_m-\sum_{i=1}^{L}C_iK_iH_i\right)E\left(xx^T\right)\right. \\ &\quad\times\left(I_m-\sum_{i=1}^{L}C_iK_iH_i\right)^T \\ &\quad\left.+\sum_{i=1}^{L}\left(C_iK_iE\left(v_iv_i^T\right)K_i^TC_i^T\right)\right] \\ &= \mathrm{Tr}\left[\left(I_m-\sum_{i=1}^{L}C_iK_iH_i\right)\left(I_m-\sum_{i=1}^{L}C_iK_iH_i\right)^T\right. \\ &\quad\left.+\sum_{i=1}^{L}\left(C_iK_iK_i^TC_i^T\right)\right] \\ &= \left\|I_m-\sum_{i=1}^{L}C_iK_iH_i\right\|_F^2+\sum_{i=1}^{L}\mathrm{Tr}\left(C_iK_iK_i^TC_i^T\right),\end{aligned} \tag{23}$$

where the last step follows from the independence assumptions and the fact that the autocovariance of x and v_i is normalized to I_m and I_{m_i}, respectively; the notation $\mathrm{Tr}(\cdot)$ denotes the trace of a matrix, and the subscript F denotes the usual Frobenius norm of a matrix. Therefore, the optimal linear DES design problem under individual sensor power constraint can be formulated as follows:

$$\begin{aligned}\text{minimize}\quad & E\|x-\widehat{x}\|^2 = \left\|I-\sum_{i=1}^{L}C_iK_iH_i\right\|_F^2 \\ & \quad +\sum_{i=1}^{L}\mathrm{Tr}\left(C_iK_iK_i^TC_i^T\right) \\ \text{subject to}\quad & \sum_{i=1}^{L}\mathrm{Tr}\left(K_iK_i^T\right)\le k,\quad C_i\in\mathscr{R}^{m\times r_i}, \\ & \quad K_i\in\mathscr{R}^{r_i\times n_i},\end{aligned} \tag{24}$$

where k is the total rate constraint since the transmission power for sensor i to send K_iy_i to fusion center is linearly proportional to $\mathrm{Tr}(K_iK_i^T)$.

From (23), the MSE at the FC can be written as

$$E\left(\|x-\hat{x}\|^2\right) = \mathrm{Tr}\left[\left(I_m-\sum_{i=1}^{L}C_iK_iH_i\right)\left(I_m-\sum_{i=1}^{L}C_iK_iH_i\right)^T + \sum_{i=1}^{L}\left(C_i^TK_i^TK_iC_i\right)\right]. \tag{25}$$

Following the fact of matrix derivatives of traces [20],

$$\frac{\partial}{\partial X}\mathrm{Tr}\left(XA\right) = A^T, \qquad \frac{\partial}{\partial X}\mathrm{Tr}\left(X^TBX\right) = BX + B^TX, \tag{26}$$

we can eliminate variables $\{C_i\}$ by minimizing $E\|x-\hat{x}\|^2$ with respect to $\{C_i\}$. As a result, the optimization problem (24) is equivalent to

$$\begin{aligned} &\text{minimize} \quad \mathrm{Tr}\left(I+\sum_{i=1}^{L}H_i^TK_i^T\left(K_i^TK_i\right)^{-1}K_iH_i\right)^{-1} \\ &\text{subject to} \quad \sum_{i=1}^{L}\mathrm{Tr}\left(K_iK_i^T\right)\le k, \quad K_i\in\mathscr{R}^{r_i\times n_i}. \end{aligned} \tag{27}$$

When K_i is a vector, problem (27) is equivalent to "*minimum sum of squares*" problem which is NP-complete [21].

Therefore, the computational complexity of solving problem (20) is NP-hard even in the case with absence of channel distortions for quantization of each sensor. □

Remark 2. The NP-completeness of optimization problem (20) leads to the intractability of finding the globally optimal solution in polynomial time. Instead of finding a globally optimal solution, a locally optimal solution may be sufficient in many applications. An effective heuristic algorithm should be proposed to search for the optimal solution of optimization problem (20).

An algorithm that could be used to search for the optimal solution is the Gauss-Seidel type iteration algorithm which may converge to a locally optimal solution and widely used in estimation, detection, and classification with sensor networks [22–27]. In this paper, a Gauss-Seidel type iteration algorithm is proposed to search the optimal solution for that problem sensor by sensor.

Suppose that all sensor nodes except node j have fixed transformation matrix K_l, $l\neq j$, $l = 1,\ldots,L$. The goal is to determine the optimal K_j. From the perspective of a selected node j, suppose that all other nodes have decided on (arbitrary) suitable approximations of their observations, and the question becomes to optimally choose the approximation to be provided by terminal j, where we without loss of generality set $j = 1$. Observations taken by sensor node 1 are denoted by y_1. The remaining observations which may be thought of as being merged into one node are denoted by y_2. In line with this, we can partition the covariance matrix of the entire vector into four parts, according to

$$R_y = \begin{pmatrix} R_{y_1} & R_{y_1y_2} \\ R_{y_2y_1} & R_{y_2} \end{pmatrix}. \tag{28}$$

Denoting $\xi = x - C_1K_1y_1$, $\eta = K_2y_2$, the distortion by dimension reduction is

$$E\|x-\hat{x}\|^2 = E\left\|x-\left(C_1K_1y_1+C_2K_2y_2\right)\right\|^2 = E\left\|\xi-C_2\eta\right\|^2. \tag{29}$$

The optimal estimation matrix is

$$\begin{aligned} C_2 &= R_{\xi\eta}R_\eta^{-1} \\ &= E\left[\left(x-C_1K_1y_1\right)\left(K_2y_2\right)^T\right]\left(E\left(K_2y_2\right)\left(K_2y_2\right)^T\right)^{-1} \\ &= \left(R_{xy_2}K_2^T-C_1K_1R_{y_1y_2}K_2^T\right)\left(K_2R_{y_2}K_2^T\right)^{-1}K_2y_2. \end{aligned} \tag{30}$$

Take (30) into (29) as

$$\begin{aligned} &E\|x-\hat{x}\|^2 \\ &\quad= \left\|x-C_1K_1y_1-\left(R_{xy_2}K_2^T-C_1K_1R_{y_1y_2}K_2^T\right)\right. \\ &\qquad\left.\times\left(K_2R_{y_2}K_2^T\right)^{-1}K_2y_2\right\|^2 \\ &\quad= \left\|\zeta-C_1K_1\nu\right\|^2. \end{aligned} \tag{31}$$

Denote

$$\zeta = x-R_{xy_2}K_2^T\left(K_2R_{y_2}K_2^T\right)^{-1}K_2y_2, \qquad \nu = y_1-R_{y_1y_2}K_2^T\left(K_2R_{y_2}K_2^T\right)^{-1}K_2y_2. \tag{32}$$

Equation (31) is simplified as

$$E\|x-\hat{x}\|^2 = \left\|\zeta-C_1K_1\nu\right\|^2. \tag{33}$$

Obviously, the optimal solution of sensor by sensor optimization problem can be solved because the question has been reduced to that in the centralized case. Based on the previous analysis, it is easy to construct a Gauss-Seidel type iteration algorithm to search for an optimal solution of optimization problem (20). We omit it here.

5. Simulations

In this section, we implement several simulations to show the performance of our proposed method. Both centralized and decentralized estimation frameworks are considered.

5.1. Centralized Estimation Framework. In centralized estimation framework, entire data is available at a single sensor

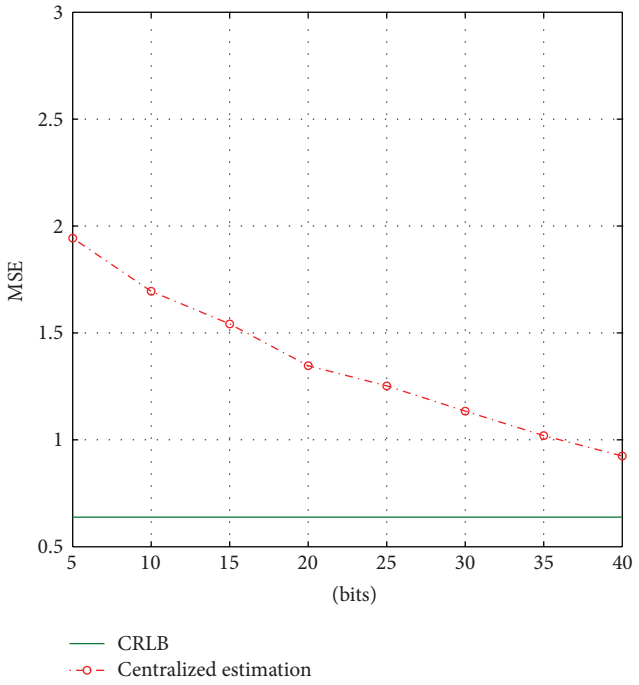

Figure 1: Estimation performance for centralized estimation with different bandwidth constraints.

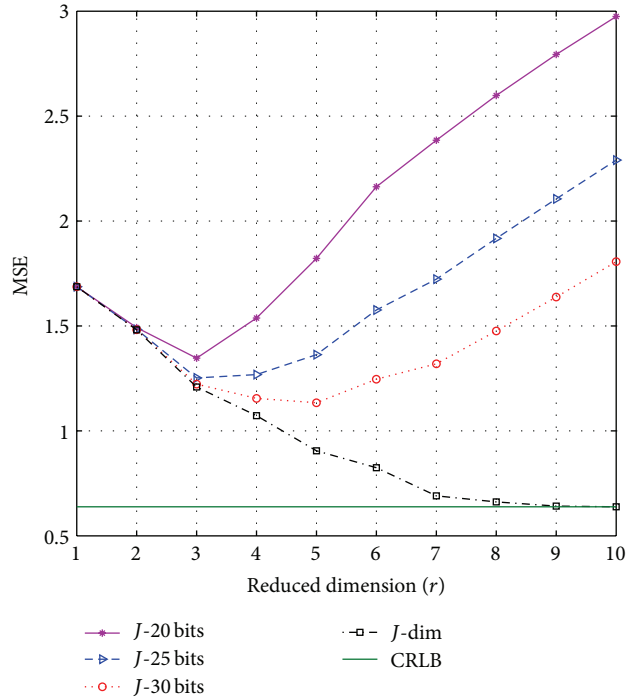

Figure 2: Comparison of estimation performance with different reduced dimensions.

and the observation data compression is needed in order to reduce communication requirement. Consider a linear model

$$y = Hx + \varepsilon, \quad H \in \mathcal{R}^{n\times m}, \tag{34}$$

where $H \in \mathcal{R}^{n\times m}$ and ε is a white noise with covariance matrix $\Sigma_\varepsilon = \sigma^2 I$. In addition, x and ε are uncorrelated. In simulation, we set $n = 50$, $m = 10$, $\sigma^2 = 1$, and $\Sigma_x = RR^T$, where R is drawn from a standard normal distribution. The estimation performance for centralized estimation framework with different bandwidth constraints is shown in Figure 1. The bottom solid line is the Cramer-Rao lower bound (CRLB). The dimension reduction and quantization lead to the gap between the centralized estimation curve and CRLB.

We plot the estimation performance for different reduced dimensions in Figure 2. Three cases of bandwidth constraint are considered ($B = 20, 25, 30$). The bottom solid line is the CRLB. The blue line with circle is the MSE for the data only with dimension reduction. When quantization is implemented after dimension reduction, the optimal strategy allocates the bandwidth to the most important dimension. Do not waste the bandwidth on the less important dimension which would leads to bad performance.

The comparison of estimation performance for different signal-to-noise ratios (SNR) is shown in Figure 4. The SNR is defined as

$$\text{SNR} = \frac{\text{Tr}\left(H\Sigma_y H^T\right)}{n\sigma^2}. \tag{35}$$

5.2. Decentralized Estimation Framework. In decentralized estimation framework, the distributed sensors collaborate with a fusion center to jointly estimate the parameter s. Since all sensors have limited battery power, their computation and communication capability are severely limited. As a result, local data compression is needed in order to reduce communication requirement.

Let the 3 distributed sensor nodes make observations on a common random parameter vector $x \in \mathcal{R}^m$ according to

$$y_i = H_i x + v_i, \quad i = 1, 2, 3, \tag{36}$$

where $H_i \in \mathcal{R}^{m_i\times m}$ is the observation matrix and $v_i \in \mathcal{R}^{m_i}$ is the additive noise which is zero mean and spatially uncorrelated. In addition, x and v_i are uncorrelated. In simulation, we set $m_i = 15$, $m = 10$, $\sigma^2 = 1$, and $\Sigma_x = RR^T$, where R is drawn from a standard normal distribution.

The comparison of centralized and decentralized estimation performance is shown in Figure 3. The bottom solid line is the CRLB. The estimation for centralized and decentralized framework are plotted in red dash line with circle and blue dot line with square for different bandwidth constraints, respectively. The decentralized estimation performance is slightly worse than the centralized estimation since the Gauss-Seidel method cannot guarantee the optimal solution [22].

6. Conclusion

In this paper, we have considered a bandwidth constrained sensor network in which a set of distributed sensors and

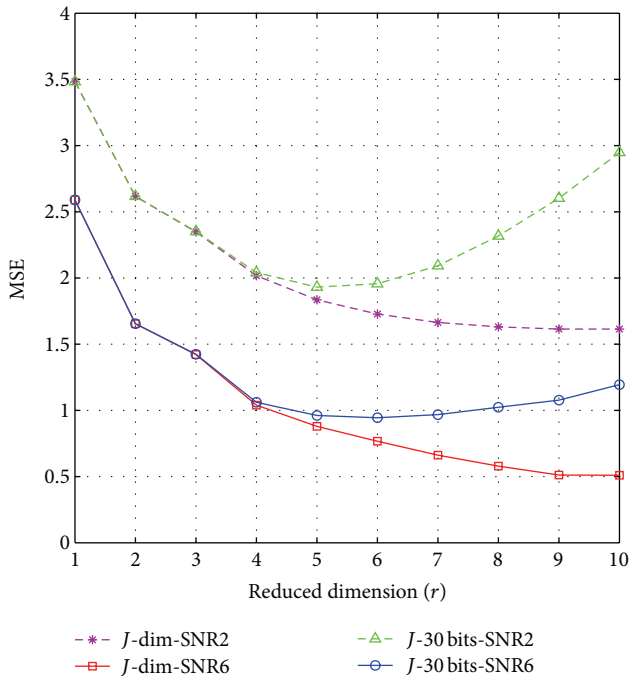

Figure 3: Comparison of estimation performance with different SNR.

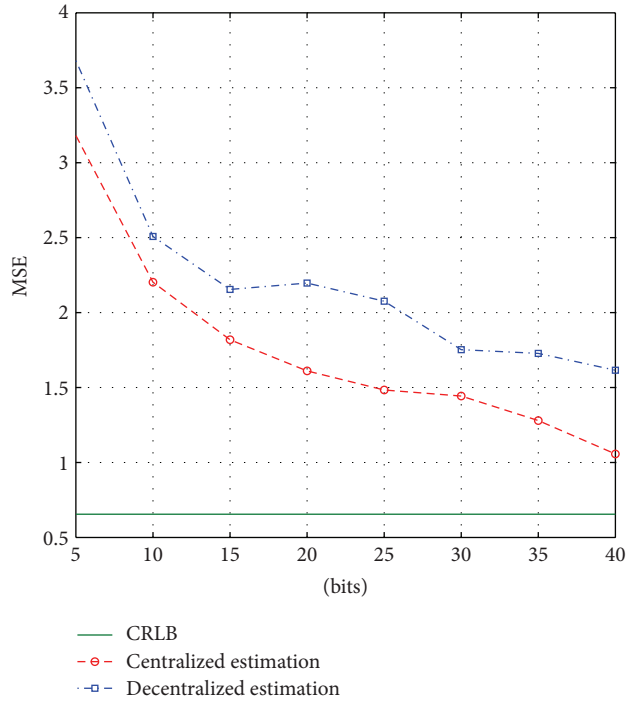

Figure 4: Comparison of estimation performance for centralized and decentralized framework.

a fusion center collaborate to estimate an unknown vector. With given communication bandwidth, the bits allocation problem has been formulated as an optimization problem. Both centralized and decentralized estimation frameworks have been developed. The closed-form solution for the centralized estimation framework has been proposed. The computational complexity of decentralized estimation problem has been proved to be NP-hard and a Gauss-Seidel type iteration algorithm to search for an optimal solution has been also proposed. Simulation results show the good performance of the proposed algorithms.

Conflict of Interests

The authors declares that there is no conflict of interests regarding the publication of this paper.

Acknowledgments

This work is supported by the National Natural Science Foundation of China under Grant no. 61203219 and the National Natural Science Foundation of China-Key Program under Grant no. 61032001.

References

[1] I. F. Akyildiz, W. Su, Y. Sankarasubramaniam, and E. Cayirci, "Wireless sensor networks: a survey," *Computer Networks*, vol. 38, no. 4, pp. 393–422, 2002.

[2] W.-M. Lam and A. R. Reibman, "Design of quantizers for decentralized estimation systems," *IEEE Transactions on Communications*, vol. 41, no. 11, pp. 1602–1605, 1993.

[3] M. Mallick, S. Coraluppi, and C. Carthel, "Advances in asynchronous and decentralized estimation," in *Proceedings of the IEEE Aerospace Conference*, vol. 4, pp. 873–888, IEEE, March 2001.

[4] Z.-Q. Luo, "Universal decentralized estimation in a bandwidth constrained sensor network," *IEEE Transactions on Information Theory*, vol. 51, no. 6, pp. 2210–2219, 2005.

[5] Z.-Q. Luo, "An isotropic universal decentralized estimation scheme for a bandwidth constrained ad hoc sensor network," *IEEE Journal on Selected Areas in Communications*, vol. 23, no. 4, pp. 735–744, 2005.

[6] T. C. Aysal and K. E. Barner, "Constrained decentralized estimation over noisy channels for sensor networks," *IEEE Transactions on Signal Processing*, vol. 56, no. 4, pp. 1398–1410, 2008.

[7] Y. Hua, M. Nikpour, and P. Stoica, "Optimal reduced-rank estimation and filtering," *IEEE Transactions on Signal Processing*, vol. 49, no. 3, pp. 457–469, 2001.

[8] Y. Zhu, E. Song, J. Zhou, and Z. You, "Optimal dimensionality reduction of sensor data in multisensor estimation fusion," *IEEE Transactions on Signal Processing*, vol. 53, no. 5, pp. 1631–1639, 2005.

[9] H. Zhu, I. D. Schizas, and G. B. Giannakis, "Power-efficient dimensionality reduction for distributed channel-aware kalman tracking using WSNs," *IEEE Transactions on Signal Processing*, vol. 57, no. 8, pp. 3193–3207, 2009.

[10] D. Williamson, *Digital Control and Implementation*, Prentice-Hall, 1991.

[11] A. Ribeiro, G. B. Giannakis, and S. I. Roumeliotis, "SOI-KF: distributed Kalman filtering with low-cost communications using the sign of innovations," *IEEE Transactions on Signal Processing*, vol. 54, no. 12, pp. 4782–4795, 2006.

[12] K. You, L. Xie, S. Sun, and W. Xiao, "Multiple-level quantized innovation Kalman filter," in *Proceedings of the 17th IFAC World Congress*, pp. 1420–1425, July 2008.

[13] Y. Weng, L. Xie, and W. Xiao, "Random field estimation with quantized measurements in sensor networks," in *Proceedings of the 29th Chinese Control Conference (CCC '10)*, pp. 6203–6208, IEEE, July 2010.

[14] Y. Weng, "Trade-off between dimensionality reduction and quantization in minimum mean square error estimation," in *Proceedings of the 32nd Chinese Control Conference (CCC '13)*, pp. 4803–4806, IEEE, 2013.

[15] C. R. Rao, *Linear Statistical Inference and Its Applications*, John Wiley & Sons, New York, NY, USA, 2nd edition, 1973.

[16] S. Kay, *Fundamentals of Statistical Signal Processing: Estimation Theory*, Prentice Hall, 1993.

[17] T. M. Cover and J. A. Thomas, *Elements of Information Theory*, John Wiley & Sons, Hoboken, NJ, USA, 2nd edition, 2006.

[18] Y. Weng, Y. Zhu, and E. Song, "Two new results of linear minimum variance estimation," in *Proceedings of the 5th International Conference on Control and Automation (ICCA '05)*, vol. 1, pp. 230–233, IEEE, June 2005.

[19] S. Boyd and L. Vandenberghe, *Convex Optimization*, Cambridge University Press, Cambridge, UK, 2004.

[20] X. Magnus and H. Neudecker, *Matrix Differential Calculus*, Wiley, New York, NY, USA, 1988.

[21] M. R. Garey and D. S. Johnson, *Computers and Intractability: A Guide to the Theory of NP-Completeness*, W. H. Freeman, San Francisco, Calif, USA, 1979.

[22] P. K. Varshney, "Distributed detection theory and data fusion," Tech. Rep., 1995.

[23] K. Zhang, X. R. Li, P. Zhang, and H. Li, "Optimal linear estimation fusion?—part VI: sensor data compression," in *Proceedings of the 6th International Conference on Information Fusion*, vol. 1, pp. 221–228, July 2003.

[24] E. Song, Y. Zhu, and J. Zhou, "Sensors' optimal dimensionality compression matrix in estimation fusion," *Automatica*, vol. 41, no. 12, pp. 2131–2139, 2005.

[25] Z.-B. Tang, K. R. Pattipati, and D. L. Kleinman, "An algorithm for determining the decision thresholds in a distributed detection problem," *IEEE Transactions on Systems, Man and Cybernetics*, vol. 21, no. 1, pp. 231–237, 1991.

[26] B. Liu and B. Chen, "Channel-optimized quantizers for decentralized detection in sensor networks," *IEEE Transactions on Information Theory*, vol. 52, no. 7, pp. 3349–3358, 2006.

[27] T.-Y. Wang, Y. S. Han, P. K. Varshney, and P.-N. Chen, "Distributed fault-tolerant classification in wireless sensor networks," *IEEE Journal on Selected Areas in Communications*, vol. 23, no. 4, pp. 724–734, 2005.

Hindawi Publishing Corporation
Mathematical Problems in Engineering
Volume 2014, Article ID 430275, 13 pages
http://dx.doi.org/10.1155/2014/430275

Research Article

IDMA-Based Compressed Sensing for Ocean Monitoring Information Acquisition with Sensor Networks

Gongliang Liu and Wenjing Kang

School of Information and Electrical Engineering, Harbin Institute of Technology, No. 2 West Wenhua Road, Weihai 264209, China

Correspondence should be addressed to Wenjing Kang; kangwj@163.com

Received 27 June 2013; Accepted 28 November 2013; Published 9 January 2014

Academic Editor: Shuli Sun

The ocean monitoring sensor network is a typically energy-limited and bandwidth-limited system, and the technical bottleneck of which is the asymmetry between the demand for large-scale and high-resolution information acquisition and the limited network resources. The newly arising compressed sensing theory provides a chance for breaking through the bottleneck. In view of this and considering the potential advantages of the emerging interleave-division multiple access (IDMA) technology in underwater channels, this paper proposes an IDMA-based compressed sensing scheme in underwater sensor networks with applications to environmental monitoring information acquisition. Exploiting the sparse property of the monitored objects, only a subset of sensors is required to measure and transmit the measurements to the monitoring center for accurate information reconstruction, reducing the requirements for channel bandwidth and energy consumption significantly. Furthermore, with the aid of the semianalytical technique of IDMA, the optimal sensing probability of each sensor is determined to minimize the reconstruction error of the information map. Simulation results with real oceanic monitoring data validate the efficiency of the proposed scheme.

1. Introduction

With the ever-increasing demand for marine exploitation and the rapid development of network communication technologies, underwater sensor network (UWSN) [1] has become a new research hotspot in recent years. As the extension of wireless sensor networks (WSN) into ocean, UWSN has potential values in the wide application fields, such as oceanographic information collection, hydrological and environmental monitoring, resources exploration, disaster forecast, underwater navigation, and military defense. This paper focuses on the ocean environmental monitoring application. In this kind of UWSN, a large number of underwater sensor nodes are deployed in the concerned area, which measure the required physical, chemical, or biological phenomena and transmit the measurements to the monitoring center. Then, the monitoring center forms the information map of the monitoring area according to the measurements it received. Due to the particularity of underwater environments [2], wireless acoustic communication is believed as the most suitable physical layer transmission technology in underwater networks. However, wireless acoustic communication has some distinct disadvantages in the following aspects: (1) low carrier frequency leads to limited available bandwidth; (2) low propagation speed of sound leads to long end-to-end delay. Furthermore, considering the application environment of UWSN, the batteries of sensor nodes can hardly be replaced. According to the above analysis, UWSN is believed to be a typical energy-limited and bandwidth-limited system.

In order to distinguish the measurements of different sensors from each other, the multiple access scheme is an important issue in underwater sensor networks, as well as in other communication systems with multiple users. Time-division multiple access (TDMA) is a popular scheme in the existing underwater networks, but it has some insurmountable disadvantages. (1) TDMA scheme is based on the accurate synchronization. The long propagation delay and large amount of sensors bring great difficulties for the timing system, especially when the system has a large number of sensors. (2) TDMA mechanism has feeblish capability against interference and multipath fading and

cannot accommodate to the complicated and time-varying underwater environment. (3) The capacity of TDMA system is restricted by the factors such as frame architecture and channel rate. Hence, the network scale is difficult to be extended. In recent years, code-division multiple access (CDMA) has been regarded as the promising multiple access scheme for underwater sensor networks. With the aid of multiuser detection (MUD) technologies, CDMA outperforms TDMA in the aspects of frequency utilization, feasibility, multiple access interference (MAI) suppression capability, and immunity against multipath effects. However, most of the MUD algorithms have high-computational complexity, and the detection cost increases greatly with the amount of sensor nodes. Therefore, a simple and efficient multiple access scheme is required for the large-scale underwater sensor networks. This requirement is expected to be realized with the emergence of interleave-division multiple access (IDMA) [3] technology.

IDMA is a relative new multiple access scheme, which employs random interleavers as the only method for user separation. As a particular case of CDMA, IDMA inherits many distinguished features of the well-studied CDMA. Furthermore, it allows a low-cost turbo-type chip-by-chip (CBC) multiuser detection (MUD) algorithm applicable to system with a large number of users, which is crucial for the large-scale underwater sensor networks.

With applications to wide area ocean monitoring, underwater sensor networks are usually required to deploy a large amount of sensor nodes in the concerned region. Due to the rigorous limitations on bandwidth and energy of the underwater sensor networks, there is an asymmetry between the requirement for high-rate sampling and the restricted network resources. This becomes the technical bottleneck of developing a practical large-scale underwater sensor network for ocean monitoring. The traditional information acquisition methods cannot solve the above problem, while the newly arising compressed sensing (CS) technology [4–6] provides a potentially reasonable solution. Different from the traditional Nyquist sampling theory, the CS theory is concerned more with the information structure rather than the signal bandwidth. According to the CS theory, if a signal is sparse or compressible in a certain domain (e.g., spatial domain or frequency domain), it can be accurately reconstructed from a small number of nonadaptive, randomized linear projection measurements by solving an optimization problem.

Fortunately, most of the nature phenomena are sparse in an appropriate basis, so the sparsity of the nature phenomena provides the feasibility to widely apply CS theory into practical engineering field. In the last few years, the researchers have attempted to utilize CS technology in the aspects of wireless communications [7], image processing [8], compressive radar [9], and so on. To the best of our knowledge, [10] is the first attempt for CS-based network data processing, which is followed by a series of influential work. References [11, 12] investigate the routing issue in wireless networks under the framework of compressed sensing. Reference [13] focuses on the CS-based target detection scheme in wireless sensor networks, where the observed signal is spatially sparse. A compressed sensing framework for on-off random access channels is provided in [14], and the theoretical bounds for channel capacity are given after thorough derivation. In [15], authors proposed an energy-efficient random access compressed sensing (RACS) scheme for underwater sensor networks, which is the most important work for applying CS theory into underwater sensor networks so far. However, the authors of [15] did not take the effect of channel error into consideration, which is in fact a crucial issue affecting the quality of reconstructed information map. Reference [16] proposed a CS-based multiple access control (MAC) scheme and provided the in-depth analysis from a physical layer perspective. However, the effects of multiple access interference (MAI) are not considered in this paper. In our previous work of [17], we have proposed a novel CS-based information collection scheme for the large-scale underwater networks, which realized accurate "information collection" for the large-scale underwater sensor network with a reduced number of measurements, instead of the traditional "data collection" methods. However, this scheme is based on the traditional TDMA technology, which has some insurmountable disadvantages as mentioned above. Moreover, [17] did not consider the issue of optimal sensing probability. These problems will be solved in this paper.

Inspired by the theory of compressed sensing and the above extensive applications, in this paper, we propose an IDMA-based compressed sensing information acquisition scheme for the large-scale underwater sensor networks. After a subrate sampling step with the random selected sensor nodes, the measurements are transmitted to the monitoring center through the underwater multiple access channel (MAC) with IDMA method. Then, the monitoring center distinguishes the reduced-dimensional measurements from each other with online CBC MUD. Finally, the monitoring center reconstructs the information map according to the output of MUD. On the framework of compressed sensing and by the aid of signal-to-interference-plus-noise ratio (SINR) evolution semianalytical technique of IDMA, we further investigate the problem of optimal sensing probability at each sensor, with which the minimal reconstruction error will be achieved. To the best of our knowledge, our work introduced compressed sensing into the IDMA system for the first time, and we made the first attempt in studying the optimal sensing probability of CS-based information acquisition scheme by exploiting the advantages of the specific SINR evolution semianalytical technique of IDMA system. The remainder of this paper is organized as follows. In Section 2, the system model and problem description are given. After introducing the mathematical foundations of compressed sensing and IDMA in Section 3, the CS-IDMA scheme is proposed in Section 4. Then, thorough analytical observations on reconstruction error and resource requirements of our scheme are given in Section 5. In Section 6, simulation results and performance evaluation are provided to validate the proposed scheme. Finally, the paper concludes in Section 7.

2. System Model and Problem Description

Consider a 2-dimensional underwater monitoring area, with L sensor nodes in x direction and W sensor nodes in y direction, as shown in Figure 1. The sensors are regularly deployed to collect some kinds of ocean monitoring elements, such as temperature, salinity, and ocean current, and transmit the measurements to the monitoring center by one hop. The distance between two neighbor nodes is D, the both in x and y directions. The monitored plane where the sensor is located is H (meters) under the ocean surface.

In this paper, the simple single-path multiple access underwater channel model is taken into consideration. Suppose ideal power control is adopted and the required power of each sensor at the receiver side (sink node) is P_0, the distance between the sender and the receiver is d (km), and the carrier frequency is f (kHz). In order to achieve the required BER, the transmitted power should be $P_0 \cdot A(d, f)$, where

$$A(d, f) = d^c \cdot a(f)^d. \tag{1}$$

The constant c is usually set as 1.5, and

$$a(f) = 10^{\alpha(f)/10}, \tag{2}$$

where $\alpha(f)$ is the absorption coefficient, with an experiential formula as follows [18]:

$$\alpha(f) = \frac{0.11 f^2}{1 + f^2} + \frac{44 f^2}{4100 + f^2} + \frac{2.75 f^2}{10^4} + 0.003. \tag{3}$$

For such an ocean monitoring application, the traditional method is to collect the measurements from all sensors to form an information map about certain characteristic, for example, temperature, salinity, or ocean current. However, with the augment of network scale, more sensors are required to measure and transmit together, leading to a burdensome energy consumption and bandwidth cost. Furthermore, in a quasi-orthogonal network, such as a CDMA or IDMA network, the performance of bit error rate (BER) and packet error rate (PER) will turn worse significantly when the number of nodes increases. Although a long spread sequence is helpful for interference suppression, it leads to higher demand for the channel bandwidth, which is severely limited in the underwater sensor networks. In view of the above facts, this paper aims to find an efficient information acquisition approach for the large-scale ocean monitoring underwater sensor networks as shown in Figure 1. As an emerging information sample theory, compressed sensing provides a novel perspective to the potential solution.

3. Preliminaries

3.1. Mathematical Foundation of Compressed Sensing. The core of CS theory is briefly expressed as follows [4]: consider a discrete signal $\mathbf{X} = [x_1, x_2, \ldots, x_n]^{\mathrm{T}}$, which is an $n \times 1$ vector; that is, $\mathbf{X} \in \mathbb{R}^n$. According to the compressed sensing theory, if $\mathbf{X}$ is sparse or compressible in a certain transform domain, it can be accurately recovered from a compressed

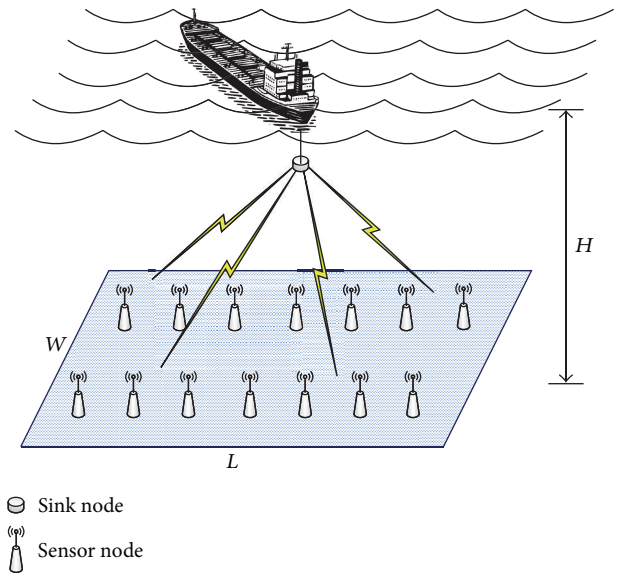

Figure 1: Two-dimensional underwater sensor network for ocean monitoring applications.

measurement $\mathbf{Y} = [y_1, y_2, \ldots, ym]^{\mathrm{T}}$, which is an $m \times 1$ vector, $m \ll n$. The framework of compressed sensing theory mainly consists of three steps: (1) sparse transformation, (2) reduced-dimensional observation, and (3) signal recovery.

Sparse Transformation. Suppose the original signal $\mathbf{X} \in \mathbb{R}^n$ is s-sparse ($s \leq n$) on the orthogonal basis of $\mathbf{\Psi}$, $\mathbf{\Psi} := [\mathbf{\Psi}_1, \mathbf{\Psi}_2, \ldots, \mathbf{\Psi}_n]$, where $\mathbf{\Psi}_i \in \mathbb{R}^n$, $i = 1, 2, \ldots, n$. As shown in (4), $\mathbf{X}$ can be expressed as the linear combination of a subset of basis vector:

$$\mathbf{X} = \sum_{i=1}^{n} \theta(i)\, \mathbf{\Psi}_i = \sum_{l=1}^{s} \theta(i_l)\, \mathbf{\Psi}_{i_l}, \tag{4}$$

where $\{i_l\}$ is the set of serial number with the selected basis vectors. The $n \times 1$ transform coefficient vector, $\mathbf{\Theta} = \mathbf{\Psi}^{\mathrm{T}}\mathbf{X}$, is the sparse representation of $\mathbf{X}$, which has s none-zero elements.

Reduced-Dimensional Observation. Design an $m \times n$ ($m \ll n$) independent identically distributed (i.i.d.) matrix $\mathbf{\Phi}$, which is independent from $\mathbf{\Psi}$. Using $\mathbf{\Phi}$, an m-length measurement vector is obtained by

$$\mathbf{Y} = \mathbf{\Phi\Theta} = \mathbf{\Phi\Psi}^{\mathrm{T}}\mathbf{X} = \mathbf{RX}, \tag{5}$$

where $\mathbf{R} = \mathbf{\Phi\Psi}^{\mathrm{T}}$ is the CS matrix from $\mathbf{X}$ to $\mathbf{Y}$.

Signal Reconstruction. The last step of compressed sensing is to recover the original n-length signal $\mathbf{X}$ from the compressed m-length measurement vector $\mathbf{Y}$. Because m is smaller than n, (5) is originally undetermined and has no unique definite solution. However, the s-sparsity characteristic of $\mathbf{X}$ makes the signal reconstruction realizable. If the matrix $\mathbf{R}$ or $\mathbf{\Phi}$ satisfies the restricted isometry property (RIP) [5], the original

signal $\mathbf{X}$ can be recovered from the compressed measurement $\mathbf{Y}$ by solving the following optimization problem:

$$\begin{aligned} &\arg\min \quad \left\|\boldsymbol{\Psi}^{\mathrm{T}}\mathbf{X}\right\|_1 \\ &\text{subject to} \quad \mathbf{Y} = \mathbf{R}\mathbf{X}, \end{aligned} \tag{6}$$

where $\|\boldsymbol{\Psi}^{\mathrm{T}}\mathbf{X}\|_1 = \|\boldsymbol{\Theta}\|_1 = \sum_{i=1}^{n} \theta_i$ denotes the ℓ_1-norm of $\boldsymbol{\Theta}$.

In the application of ocean monitoring with underwater sensor networks, the ultimate purpose is to acquire the concerned information of the monitored area by means of data collection and transmission. Because most of the ocean elements (temperature, ocean current, etc.) are sparse in an appropriate domain (such as Fourier domain), it is realizable to reconstruct the information map with reduced measurements under the theoretical framework of compressed sensing.

3.2. Interleave-Division Multiple Access. IDMA is a relatively new multiple access scheme, in which user-specific interleavers are adopted as the only method for user separation. Compared to CDMA, it has smaller MUD complexity and higher bandwidth utilization and power efficiency. In view of this, IDMA is a promising candidate for the resource-limited underwater sensor networks and is adopted in the uplink channels for the random selected underwater sensors in our scheme. As the background of our work, here we first elaborate on the concept of IDMA [3].

3.2.1. IDMA Model and CBC Algorithm. In this study, the IDMA-CBC MUD channel model and its operational principles are confined to single-path synchronous channel and BPSK modulation. Figure 2 illustrates the generic transmitter and the IDMA-CBC MUD receiver with K simultaneous users. The input data sequence of user-k is first encoded by a forward error correction (FEC) code. After spreading, the respective chips are interleaved by user-specific interleaver π_k, producing $x_k \equiv [x_k(1), \ldots, x_k(j), \ldots, x_k(J)]$. The main difference between CDMA and IDMA at the transmitter side is the position exchange of spreader and interleaver, leading to chip-level interleaving for IDMA and bit-level interleaving for the CDMA. Compared with CDMA, the distinguished feature of IDMA is that different interleavers are used to separate signals from different users. Thus, the adjacent chips from the same users are approximately uncorrelated, which facilitates the simple chip-by-chip multiuser detection scheme discussed below.

As illustrated in Figure 2, an iterative suboptimal receiver structure is adopted, consisting of an elementary signal estimator (ESE) and K single-user *a posteriori* probability decoders (DECs). In the global turbo-type iterative process, the ESE and DECs exchange extrinsic log-likelihood ratios (LLRs) about $\{x_k(j)\}$, defined as follows:

$$e\left(x_k\left(j\right)\right) \equiv \log\left(\frac{\Pr\left(\mathbf{y} \mid x_k\left(j\right) = +1\right)}{\Pr\left(\mathbf{y} \mid x_k\left(j\right) = -1\right)}\right), \quad \forall k, j. \tag{7}$$

The CBC MUD algorithm contains two parts, listed as follows [3].

(1) The basic ESE function. The jth received chip from K users can be written as

$$r\left(j\right) = h_k x_k\left(j\right) + \zeta_k\left(j\right) \tag{8}$$

with

$$\zeta_k\left(j\right) = \sum_{\substack{k'=1 \\ k' \neq k}}^{K} h_{k'} x_{k'}\left(j\right) + n\left(j\right), \tag{9}$$

where $\zeta_k(j)$ is the distortion (including interference-plus-noise) with respect to user-k, h_k is a priori channel coefficient at the receiver side, and $n(j)$ is sample of an AWGN with variance $\sigma^2 = N_0/2$.

Step i. Estimation of interference mean and variance:

$$\begin{aligned} E\left(r\left(j\right)\right) &= \sum_{k=1}^{K} h_k E\left(x_k\left(j\right)\right), \quad \forall j \\ \mathrm{Var}\left(r\left(j\right)\right) &= \sum_{k=1}^{K} \left|h_k\right|^2 \mathrm{Var}\left(x_k\left(j\right)\right) + \sigma^2, \quad \forall j \\ E\left(\zeta_k\left(j\right)\right) &= E\left(r\left(j\right)\right) - h_k E\left(x_k\left(j\right)\right), \quad \forall k, j \\ \mathrm{Var}\left(\zeta_k\left(j\right)\right) &= \mathrm{Var}\left(r\left(j\right)\right) - \left|h_k\right|^2 \mathrm{Var}\left(x_k\left(j\right)\right), \quad \forall k, j \end{aligned} \tag{10}$$

Step ii. LLR generation:

$$e_{\mathrm{ESE}}\left(x_k\left(j\right)\right) = 2h_k \cdot \frac{r\left(j\right) - E\left(\zeta_k\left(j\right)\right)}{\mathrm{Var}\left(\zeta_k\left(j\right)\right)}, \quad \forall k, j. \tag{11}$$

(2) *The DEC Function.* The DECs in Figure 2 implement APP decoding with the output of the ESE as the input. Their output is the extrinsic LLRs $e_{\mathrm{DEC}}(x_k(j))$, generating the following statistics:

$$\begin{aligned} E\left(x_k\left(j\right)\right) &= \tanh\left(\frac{e_{\mathrm{DEC}}\left(x_k\left(j\right)\right)}{2}\right), \\ \mathrm{Var}\left(x_k\left(j\right)\right) &= 1 - \left(E\left(x_k\left(j\right)\right)\right)^2. \end{aligned} \tag{12}$$

As discussed above, $\{E(x_k(j))\}$ and $\{\mathrm{Var}(x_k(j))\}$ will be used in the ESE to update the interference mean and variance in the next iteration. APP decoding is a standard operation; thus, we will not discuss it in detail.

The DEC cost is dominated by the APP decoding cost. Compared with CDMA, the extra cost the MUD described above is mainly related to the ESE, while it costs seven multiplications and five additions per coded bit per user in the ESE, which is very modest. Thus, the overall complexity of the multiuser detector can be roughly comparable to that of a single-user one. This is considerably lower than those of other schemes, for example, the well-known MMSE algorithm with a complexity of $O(K^2)$ and the MAP MUD algorithm with a complexity of $O(2^K)$.

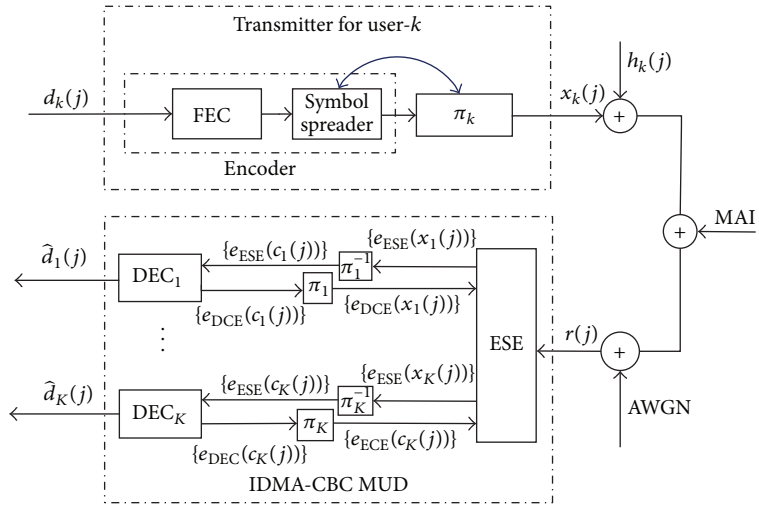

Figure 2: Transmitter and receiver structure of IDMA.

3.2.2. Performance Comparison between IDMA and CDMA. It is interesting to compare the performance of IDMA and CDMA using the same detection algorithm. Figure 3 illustrates such performance comparison for different number of users with the same spreading length $L = 15$. For CDMA, m-sequence is employed as the spreading sequence, while for IDMA, $[+1, -1, +1, -1, \ldots]$ is adopted. The length of the information block is $N = 1500$. As we can see, the performance advantage of IDMA increases with the number of users. When the number of users is small, the performance of IDMA and CDMA is almost the same. However, the performance of CDMA becomes worse when the number of users is larger than 15. IDMA can achieve near single-user performance even for $K = 24$. Thus, compared with CDMA, IDMA can achieve better performance with low computational cost.

4. IDMA-Based Compressed Sensing Information Acquisition Scheme

In this section, the IDMA-based compressed sensing (CS-IDMA) information acquisition scheme is proposed and illustrated for the large-scale ocean monitoring underwater sensor networks.

The framework of the proposed scheme is simple and clear. As shown in Figure 4, the proposed scheme consists of three main components: (1) data sensing with randomly selected sensors; (2) interleave-division multiple access to the monitoring center over noisy channels; (3) information recovery with the available measurements. Under the compressed sensing framework, the procedure of random sampling and the following multiple access is mapped to the mathematical operation of reduced-dimensional observation. The performance of IDMA multiuser detection determines the precision of the reconstructed information map.

4.1. Random Sensing at Sensor Side. In order to prolong the lifetime of the underwater sensor networks, in each monitoring round only a subset of the sensor nodes is randomly selected to make sensing and transmit the measurement to the monitoring center. The number of active nodes in one round is determined by a parameter named sensing probability p.

According to the compressed sensing theory, in order to realize accurate recovery, the sensing matrix $\mathbf{R}$ should satisfy two basic conditions: the independency between $\mathbf{R}$ and $\mathbf{\Psi}$ and the RIP property. The commonly used sensing matrixes include random Gaussian matrix, random Bernoulli matrix, and partial Hadamard matrix. However, they cannot contribute to energy and bandwidth saving for the considered scenario. In view of this, a simple and efficient sensing matrix, random extractive matrix, is used in this paper. The random extractive matrix is easily formed by randomly selecting m rows from the $n \times n$ identity matrix, where n is the number of sensors in the monitored area and m is the number of the selected sensors in one round. The elements in the random extractive matrix have the following property:

$$\sum_{i=1}^{m} r_{ij} \le 1, \quad j = 1, 2, \ldots, n,$$
$$\sum_{j=1}^{n} r_{ij} = 1, \quad i = 1, 2, \ldots, m. \tag{13}$$

4.2. Interleave-Division Multiple Access over Noisy Channels. Suppose there are N underwater sensor nodes deployed in the monitoring area. In one round of information acquisition, each node performs measurement with probability p. Then, the random $K = pN$ measurements will be transmitted to the monitoring center simultaneously. In this study, IDMA is employed to distinguish the measurements from each other.

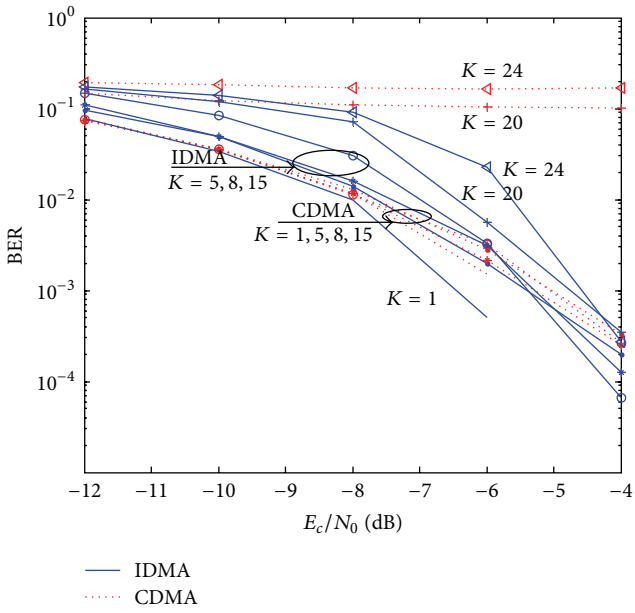

FIGURE 3: Performance comparison between IDMA and CDMA systems.

Compared to CDMA, the transmitter of IDMA system exchanges the sequence of the spreader and interleaver; that is, it employs a chip-level interleaver to randomize the chip-level information. Consequently, the MAI in IDMA system can be regarded as the additive Gaussian white noise (AWGN), which is not reasonable in the traditional CDMA system. Similar to Turbo decoding, IDMA-CBC MUD is an iterative procedure with two decoding components, namely, an elementary signal estimator (ESE) and K a posteriori probability (APP) decoders (DECs). During each iteration, they exchange extrinsic log-likelihood ratios (LLRs) about $x_k(j)$, which is the jth chip output from the user-k dependent permutation. From the central limited theorem, the MAI of every chip is reasonably approximated by a Gaussian distribution. Furthermore, the key principle of IDMA is that the user separation is made possible by using different interleavers invoked after the spreading, and chip-level interleaving makes MAI appear as an additive uncorrelated Gaussian process. Based on the above assumptions, the extrinsic LLRs about each chip become equivalent to the mean and variance of $x_j(k)$ upon iteration convergence. The complete computational procedure of IDMA-CBC MUD has been given in Section 3.2.1.

The choice of interleaver is an important problem for the IDMA system. In theory, the user-specific interleavers can be generated independently and randomly, while for the considered underwater sensor networks, the monitoring center has to use a considerable amount of memory to store these interleavers, which may cause serious concern when the number of users is large. Furthermore, during the initial link setting-up phase, a large number of messages are changed between the sensors and the monitoring center to inform each other about their interleavers. Extra bandwidth resource will be consumed for this purpose if the interleavers used by the sensors and the monitoring center are long and randomly generated. The case will be more serious for the long-propagation-delay, bandwidth-limited, and energy-limited underwater sensor networks. In view of this, the power-interleaver method [19] is employed in our scheme as follows.

Assume that we have a master interleaver ϕ. Then the K interleavers for each sensor can be generated as

$$\pi_k \equiv \phi^k, \tag{14}$$

where $\phi^k(c)$ is defined as

$$\phi^k(c) \equiv \begin{cases} \phi(c), & k = 1 \\ \phi\left(\phi^{k-1}(c)\right), & k = 2, \ldots, K. \end{cases} \tag{15}$$

In this way, every interleaver is a "power" of ϕ. The rationale for this method is that if ϕ is an "ideal" random permutation, so are all $\{\phi^k\}$, and these permutations are also approximately independent of each other. Based on this method, we simply assume that the monitoring center assigns the power index k to each user k, and then ϕ^k will be generated at the sensor nodes for user k accordingly. Considering that the number of active sensors is usually large in the ocean monitoring sensor networks, the uplink frame will be split into several subframes and IDMA scheme is operated in each subframe. The procedure is illustrated in Figure 5. At the beginning of each monitoring round, the monitoring center broadcasts a downlink control information packet to the underwater sensors. The control information packet contains the following contents: (1) ID of each selected sensor according to a given sensing probability p; (2) subframe index assigned to each selected sensor; (3) power index assigned to each selected sensor. Then, the selected sensors perform sampling and transmit the measurements with the allocated interleavers at the corresponding subframes. Next, the iterative CBC MUD algorithm is carried out in the monitoring center.

4.3. Reconstructing the Information Map. The output of MUD is used for reconstructing the information map. Traditionally, if barely K ($K \ll N$) measurements are obtained for the monitoring field, it is insurmountable to achieve the required monitoring resolution. Furthermore, due to the effect of MAI and AWGN, some of the measurements may be destroyed in the multiple access procedure. The packet error rate (PER) is affected by the SINR of uplink channels, the length of the uplink data packet, and the error correction code it used. Detailed analysis will be given in Section 5.

However, in view of the fact that most of the monitored underwater characteristics are sparse in the spatial domain (e.g., the objective tracking information) or the frequency domain (such as the temperature, salinity, and sea currents), the CS theory provides the possibility to reconstruct a high-resolution information map of the monitoring field with N elements. For a frequency-sparse scenario, in which the Fourier coefficients of the original signal $\mathbf{X}$ make up an

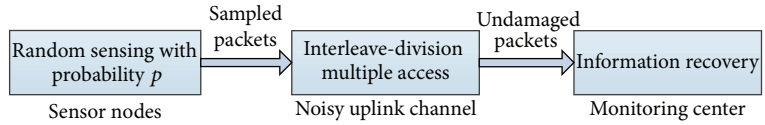

Figure 4: CS-IDMA framework.

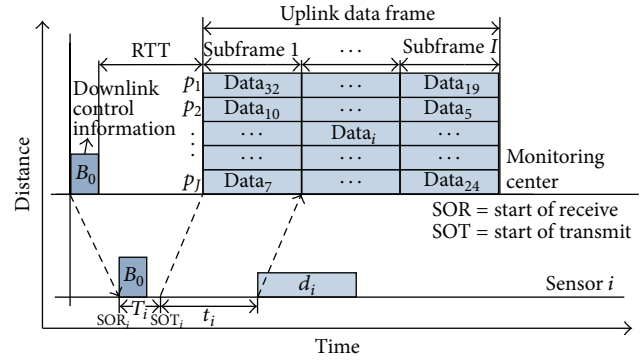

Figure 5: The architecture of uplink data frame.

$N \times 1$ vector $\boldsymbol{\Theta}$ with only s none-zero elements, the transform matrix $\boldsymbol{\Psi}$ consists of N orthogonal Fourier basis shown as follows:

$$\mathbf{X} = \boldsymbol{\Psi}\boldsymbol{\Theta},$$
$$\boldsymbol{\Psi} = \left[\boldsymbol{\Psi}_1, \boldsymbol{\Psi}_2, \ldots, \boldsymbol{\Psi}_N\right], \tag{16}$$
$$\boldsymbol{\Psi}_i(k) = e^{-j2\pi ik/N}, \quad i = 1, 2, \ldots, N;\ k = 1, 2, \ldots, N.$$

According to the CS theory, if the sensing matrix is random and independent from $\boldsymbol{\Psi}$ and the number of measurements exceeds a certain threshold N_s, the original data of $\mathbf{X}$ can be reconstructed by solving the problem of (6). Considering that the active sensors are selected randomly and the packet error is random in the multiple access procedure, the corresponding sensing matrix is feasible for information recovery under CS framework. Several simpler and practicable methods have been proposed to solve this problem, such as BP (Basic Pursuit) [5], OMP (Orthogonal Matching Pursuit) [20], and BCS (Bayesian Compressed Sensing) [21]. In this paper, the OMP algorithm is adopted for information recovery, by which the theoretical threshold is $N_s = 2k\ln(N)$ [20].

5. Analytical Observations

5.1. Consideration of Optimal Sensing Probability. As mentioned above, among the N underwater sensor nodes deployed in the monitoring area, only K nodes are active in one monitoring round. The active nodes are selected randomly by the monitoring center according to the sensing probability p. During the multiple access phase, part of the K transmitted measurements will be dropped for packet error due to the adverse effects such as thermal noise and multiple access interference (MAI). Obviously, when the sensing probability p turns larger, the MAI will be more severe, and, consequently, the packet error rate (PER) will increase. The amount of available measurements for information reconstruction is expressed as follows:

$$N_{\text{avl}} = N_{\text{act}} p_{\text{suc}} = pN\left(1 - \text{PER}\right), \tag{17}$$

where $N_{\text{act}} = pN$ is the number of active sensors in one round of information gathering and $p_{\text{suc}} = 1 - \text{PER}$ is the probability that the measurements are successfully received after noisy multiple access channel.

In our compressed sensing information acquisition scheme, the performance of reconstruction error P_e is one of the most important evaluating indicators. Let us define it as a function of the sensing probability p:

$$P_e = f\left(p\right). \tag{18}$$

Obviously, p_e decreases with larger N_{avl}. However, the relationship between N_{avl} and p is not clear. In (17), N_{avl} is a linearly increasing function of p, while p_{suc} is a decreasing function of p. Therefore, the authors wonder whether an optimal sensing probability p exists, which leads to the minimal reconstruction error under CS framework. This is a key perspective of this paper.

Without loss of generality, supposing a BCH(m,n,t) FEC code is used in IDMA system, followed by a length-r repetition code, as shown in Figure 2, then the PER can be calculated as

$$\text{PER} = \sum_{s=t+1}^{m} \mathrm{C}_m^s p_b^s (1 - p_b)^{m-s}, \tag{19}$$

where p_b is the bit error ratio after the decoding of repetition code, which is a function of the chip error ration p_c and the repletion code length r. Given p_c and r, the solution of p_b is detailed as follows:

$$p_b = \sum_{i=\lceil r/2 \rceil}^{r} \mathrm{C}_r^i p_c^i (1 - p_c)^{r-i}. \tag{20}$$

Suppose BPSK modulation with coherent demodulation is adopted and AWGN channel is taken into consideration. Then, the channel error ration, that is, the chip error ration p_c, is theoretically expressed as

$$p_c = \frac{1}{2}\operatorname{erfc}\left(\sqrt{\gamma}\right), \tag{21}$$

where γ is the signal-to-noise ratio (SNR) of single-user system, or the signal-to-interference-plus-noise ratio (SINR) at the iteration convergence point, that is, after multiuser detection.

It is usually difficult to evaluate the efficiency of MUD accurately for a quasi-orthogonal multiuser system. Fortunately, the SINR evolution technique of IDMA system provides a simple semianalytical method to solve this problem, which in turn helps to build the relationship between the reconstruction error and sensing probability p under CS-IDMA framework.

5.2. Semianalytical Method Based on SINR Evolution. We now outline a performance evaluation technique for IDMA-CBC multiuser detection algorithm. The performance of IDMA-CBC detection scheme at the iteration convergence point is concerned, which depends on the amount of cancelled MAI, equivalently, the amount of variance reduced from chip $\{x_k(j), \forall k, j\}$ variables [21]:

$$V_k = 1 - \tanh^2\left(\frac{Y_{\mathrm{SINR}_k}}{2}\right), \quad k = 1, \ldots, K. \tag{22}$$

For each user-k, a fixed received power, P_k, can be maintained under the perfect power control (PPC). Thus, the total interference power received by user-k can be estimated as

$$I_k = P_N + \sum_{i \neq k} P_i \cdot E\left(V_i\right), \tag{23}$$

where P_N is the thermal background noise, and by (22), we define

$$f\left(\mathrm{SINR}_k, r\right) = E\left(V_k\right) = 1 - E\left[\tanh^2\left(\frac{Y_{\mathrm{SINR}_k}}{2}\right)\right], \quad k = 1, \ldots, K. \tag{24}$$

It is shown in [22], for large number of chips and BPSK with repetition code (each bit is replicated r times over the symbol chips), that Y_{SINR_k} is approximately Gaussian with mean and variance $2(r-1)\mathrm{SINR}_k$ and $4(r-1)\mathrm{SINR}_k$, respectively. Thus, the average variance of an arbitrary chip from user-k, $f(\mathrm{SINR}_k, r)$, is a function of SINR_k, which by definition is the uncancelled percentage of the interference power introduced by user-k. The corresponding MUD efficiency in the uplink is equivalent to $1 - f(\mathrm{SINR}, r)$. Generally, $f(\mathrm{SINR}, r)$ does not have an analytical expression, but it can be easily obtained by the Monte Carlo method, which is depicted in Figure 6 as the solid curve. In the situation of perfect power control, the SINR evolution for the iterative process can be expressed as

$$\mathrm{SINR}_{k\_\mathrm{new}} = \frac{1}{(K-1)\, f\left(\mathrm{SINR}_{k\_\mathrm{old}}\right) + \sigma^2}. \tag{25}$$

At the start, we initialize $f(\mathrm{SINR}_{k\_\mathrm{old}}) = 1$ for all k. Repeating (25), SINR_k will converge towards a steady value and we call it $\mathrm{SINR}_{k\_\mathrm{final}}$. Thus, at the convergence point, we have

$$\mathrm{SINR}_{k\_\mathrm{final}} \approx \frac{1}{(K-1)\, f\left(\mathrm{SINR}_{k\_\mathrm{final}}\right) + \sigma^2}. \tag{26}$$

The above expression can be modified as

$$f\left(\mathrm{SINR}_{k\_\mathrm{final}}\right) \approx \left(\frac{1}{\mathrm{SINR}_{k\_\mathrm{final}}} - \sigma^2\right)\frac{1}{K-1}. \tag{27}$$

The above function is depicted in Figure 6 as the dashed curve. Obviously, the cross point of the solid curve and the dashed curve corresponds to the final SINR value after CBC iterative MUD in IDMA system, which is the required value of γ in (21). Substituting the value of γ into (21) and by using (20), (19), and (17), we can solve the number of available measurements for reconstructing an information map. Thus, based on this special semianalytical technique of IDMA system, SINR evolution, we can further optimize system performance in a simple way. Using the above method, the optimal sensing probability will be observed in Section 6.

5.3. Resource Requirements. In this section, we give a thorough analysis of the resource requirements for the proposed scheme. Suppose the channel rate (digital bandwidth) is R_B and a frame is divided into I subframes; in each subframe K/I measurements are distinguished by different interleavers. As mentioned above, a BCH(m,n,t) FEC code followed by a length-r repetition code is used, in which an n-bit block is coded as an m-bit block, and a corrupted packet with no more than t bit errors can be corrected after decoding. Thus, the subframe length is calculated as

$$\mathrm{T}_p = \frac{mr}{R_B}. \tag{28}$$

And the frame length for one monitoring period is

$$\mathrm{T}_f = \mathrm{RTT} + I \cdot \mathrm{T}_p + (I-1)\,\mathrm{T}_g, \tag{29}$$

where RTT is the maximal round trip time between the sink node and the sensors and T_g is the guard time between two neighboring subframes.

If the monitored element has a correlation time of T_s, equivalently, the signal is stationary during T_s, one round of information acquisition should be completed in this correlation time. So we have

$$\mathrm{T}_f \leq \mathrm{T}_s. \tag{30}$$

Substituting (29) into (30), we get

$$\mathrm{T}_p \leq \frac{\mathrm{T}_s - \mathrm{RTT} - (I-1)\,\mathrm{T}_g}{I}. \tag{31}$$

Combining (28) and (31), we get the requirement for the digital bandwidth of the underwater channel:

$$R_B \geq \frac{mrI}{\mathrm{T}_s - \mathrm{RTT} - (I-1)\,\mathrm{T}_g}. \tag{32}$$

Considering that the transmitted signal is shaped by a square root raised cosine filter with a roll-off factor equivalent to β, the minimal requirement for the occupied bandwidth is as follows:

$$B_{\text{req}} = \frac{R_{B,\text{req}}(1+\beta)}{\log_2 M} = \frac{mrI(1+\beta)}{\left[\text{T}_s - \text{RTT} - (I-1)\,\text{T}_g\right]\log_2 M}, \tag{33}$$

where $M = 2$ for the BPSK method.

Similarly, we can get the requirement for energy consumption. Supposing the consumed energy of each sensor for one round of data sampling is E_g, the average energy cost for transmitting one bit is E_t, and the average energy cost for receiving a downlink control packet is E_r, then the total energy cost of the whole network during one monitoring round is

$$E = NE_r + K\left(E_g + mE_t\right). \tag{34}$$

Thus, the average energy consumption per sensor per round is

$$\widetilde{E} = \frac{E}{N} = E_r + p\left(E_g + mE_t\right). \tag{35}$$

According to the channel model described in Section 2, we have

$$E_t = A(d, f)\cdot E_b, \tag{36}$$

where E_b is the required energy per bit at the receiver side.

6. Performance Evaluation and Discussion

In order to evaluate the performance of the CS-IDMA scheme in underwater sensor networks, necessary simulations are carried out in this section. The ocean environmental data is available from the website of NASA JPL (http://ourocean.jpl.nasa.gov/). In the following simulations, the simple single-path multiple access underwater channel model with ideal power control is taken into consideration.

The main simulation parameters are given in Table 1.

6.1. Simulation Results on 2D Real Data. We take the real ocean meridional current data of Monterey Bay as the experimental subject. The data is obtained by the Regional Ocean Modeling System (ROMS) at 3GMT 05/13/2012. The monitored region is 100 meters below the sea surface and ranged over [–122.8°E,–122.6°E] in longitude and [36.6°N, 36.8°N] in latitude, and the required spatial resolution is 0.01°× 0.01°. In the traditional method, we should divide the concerned area into 20 × 20 grids, and, in each grid, a sensor node is deployed for data sampling in order to build an information map of the monitored region. It should be noticed that any data missing will destroy the integrality of the information map. On the contrary, the proposed CS-IDMA scheme needs much fewer measurements for reconstructing an information map of the concerned area with the same spatial resolution. Moreover, data loss is tolerable with our scheme.

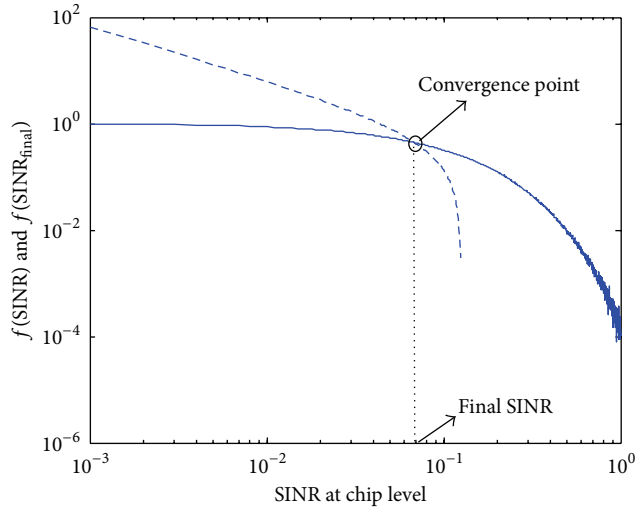

Figure 6: f (SINR) and f (SINR$_{\text{final}}$) versus chip level SINR, with $r = 16$, $K = 16$, and $E_b/N_0 = 4$ dB.

Table 1: Simulation parameters.

Parameters	Value
Data packet length	16 bits
Forward error correction coding	BCH (34, 16, 3)
Repetition code length	16
Average energy cost for receiving a downlink control packet, E_r	100 nJ
Average energy cost of each sensor for one round data sampling, E_g	1000 nJ
Number of sensors in the region	400
Number of sumframes, I	20
Roll-off factor of the square root raised cosine filter, β	0.98
Correlation time of the monitored element, T_s	100 s
Maximal round trip time	10 s
Guard time, T_g	20 ms
Noise power spectral density, N_0	–100 dBm
Carrier frequency	10 kHz

Figure 7(a) is the original information map of the given region, with a spatial resolution of 0.01°× 0.01°; Figure 7(b) illustrates the compressed sensing measurements by the 100 random selected sensors; Figure 7(c) describes the successfully received data after CBC iterative MUD; and Figure 7(d) shows the reconstructed result with OMP algorithm. In this simulation, E_b/N_0 at the sink side is set to be 8 dB. The simulation result of packet loss rate (PER) is 0.1055. As a result, about 90 of the 100 random measurements are available for the information reconstruction procedure, leading

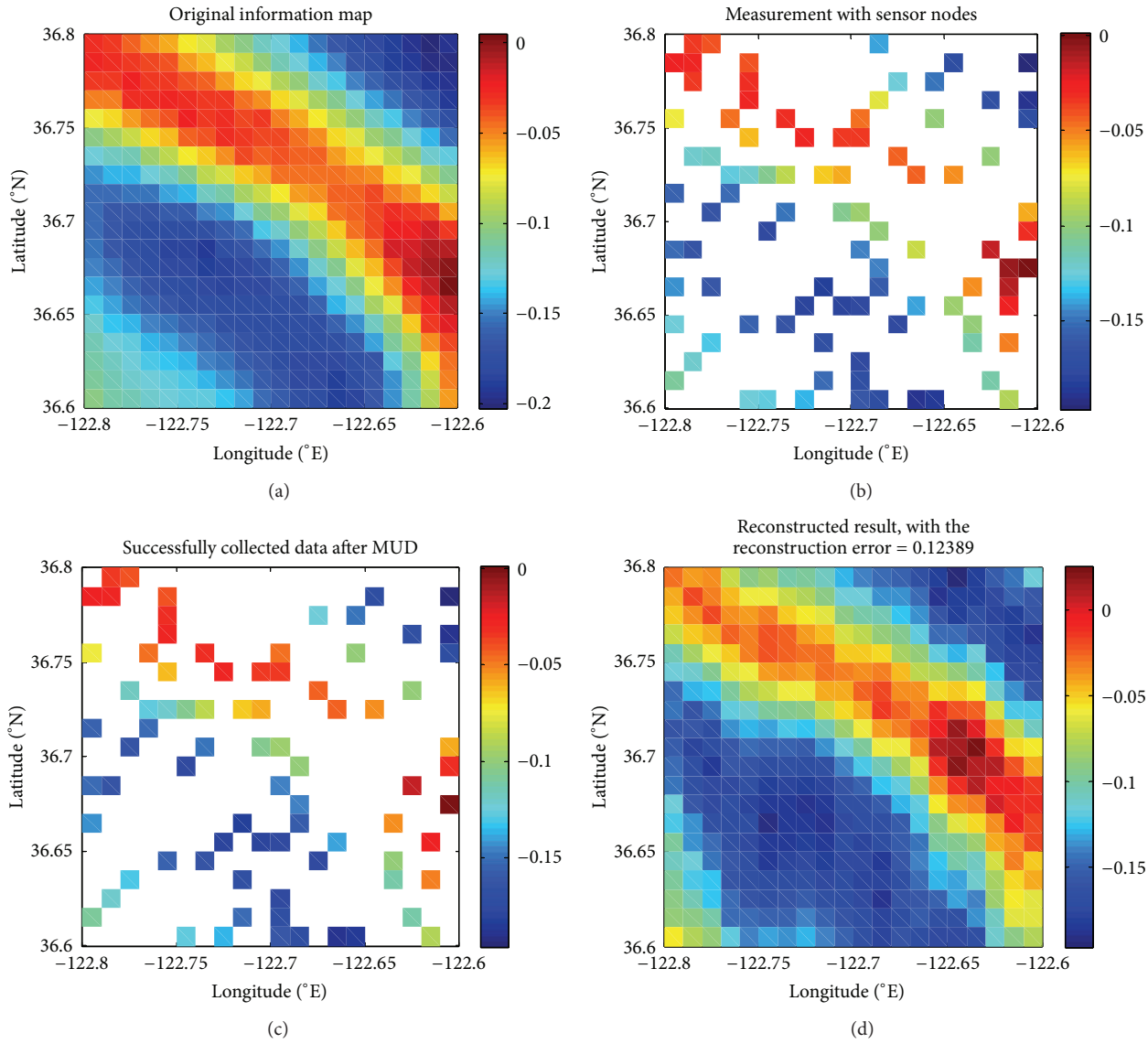

FIGURE 7: Information map about ocean meridional current of the given area. (a) Original information map; (b) measurement with random selected sensor nodes; (c) successfully collected data after CBC MUD; (d) reconstructed information map with OMP algorithm.

to a reconstruction error of 0.12389. Here, the reconstruction error P_e is defined as

$$P_e = \frac{\left\|\widehat{\mathbf{X}} - \mathbf{X}\right\|_2}{\|\mathbf{X}\|_2} = \frac{\sqrt{\sum_{i=1}^{n} \left(\widehat{x}_i - x_i\right)^2}}{\sqrt{\sum_{i=1}^{n} x_i^2}}. \tag{37}$$

6.2. Optimal Sensing Probability and Resource Requirements. As mentioned above, the relationship between the reconstruction error P_e and the sensing probability p is not clear originally, while by using the semianalytical method peculiar to IDMA, we can plot the relationship curve in Figure 8. An interesting phenomenon is observed where, as the sensing probability increases from 0.1 to 1, the reconstruction error declines at the beginning phase and ascends quickly after a turning point. The turning point varies with different channel conditions. The larger the value of E_b/N_0 is, the latter the turning point appears. Consequently, for a given channel condition, there exists an optimal sensing probability. This result is significant for system designing.

It can also be seen from Figure 8 that the reconstruction error decreases evidently with the increase of E_b/N_0, due to the higher packet loss rate. However, higher E_b/N_0 means that more energy consumption is required, as shown in Figure 9. In system designing, the performance tradeoff between resource requirement and quality of reconstructed information map should be considered according to the simulation results.

Furthermore, we discuss the issue of bandwidth requirement of our scheme. From (33) we can find the relationship between the minimum required bandwidth and the number of subframes. Meanwhile, given the number of active sensors,

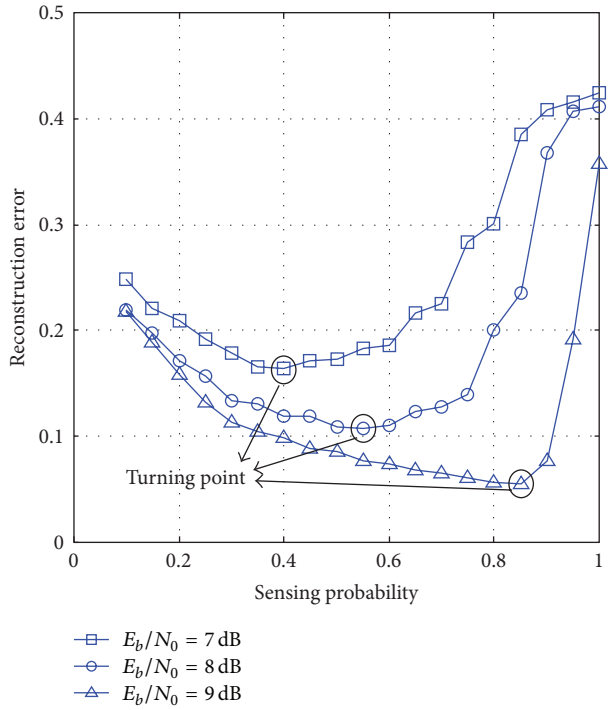

Figure 8: Reconstruction error versus sensing probability.

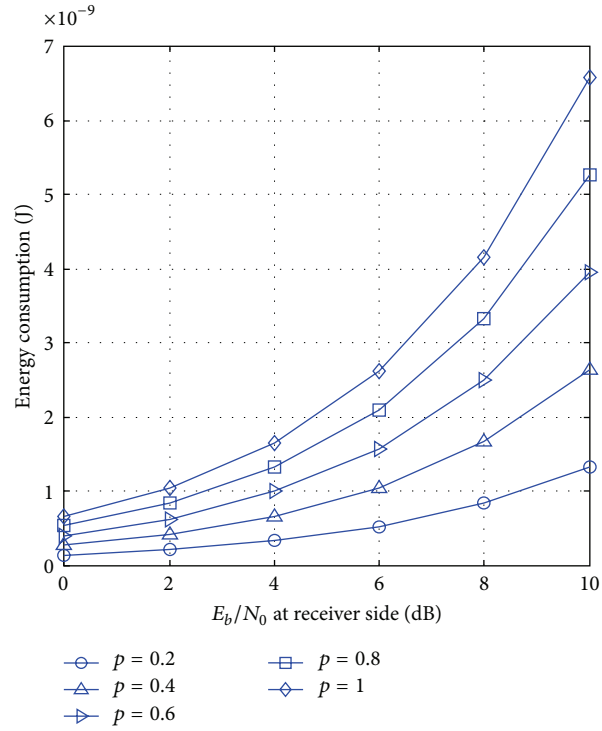

Figure 9: Average energy consumption per sensor versus E_b/N_0 at receiver side.

the number of subframes will affect the MAI of IDMA system and hence lead to different BER performance. As a result, the relationship between the reconstructed error and the minimum required bandwidth is given in Figure 10, where $E_b/N_0 = 8$ dB and $p = 0.6$. We can see from Figure 10 that, in order to reconstruct an information map with reconstruction error below 0.1, at least 0.265 kHz bandwidth is required for the uplink multiple access channel. If more bandwidth is available, the reconstruction error keeps smooth because enough measurements are already provided for information reconstruction with the minimal required bandwidth. It should be noticed that the issue of overdesigning should be considered in real applications.

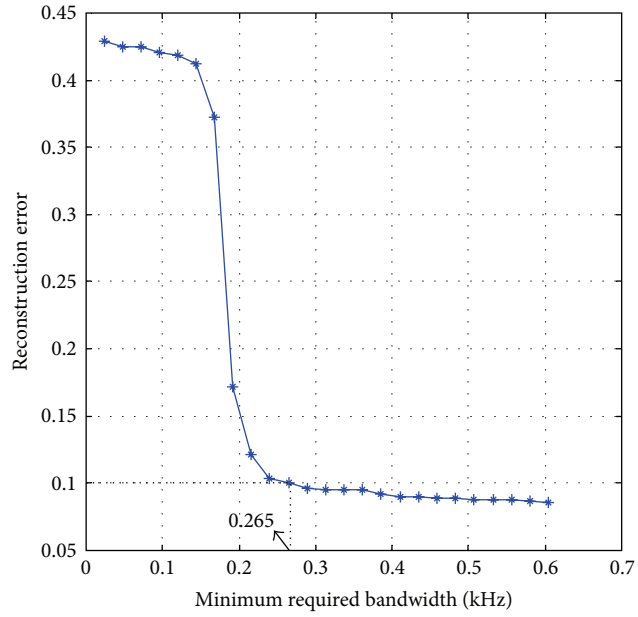

Figure 10: Reconstruction error versus minimum required bandwidth.

6.3. Comparisons with the Traditional Method. In order to illustrate the advantages of compressed sensing in resource saving, the energy and bandwidth costs of the proposed CS-based scheme and the traditional information acquisition scheme are given in Figures 11 and 12, respectively. From the figures we can find that, if an information map with the reconstruction error of no more than 0.1 is needed for the tested area, the CS-based new scheme requires far less network resources than the traditional scheme, saving 65% energy and 88% bandwidth, respectively.

6.4. Simulation Result on 3D Real Data. The above research is carried out on the two-dimensional scenario; however, the proposed scheme is also suitable for the three-dimensional environment. In order to prove it, reconstruction experiment is implemented on the zonal current data collected at South California Bay at 3 GMT on May 16, 2012, at latitude [34.3°, 34.5°], longitude [−122.2°, −122.0°], and depth [100 m, 600 m]. The original information map and reconstructed information map with optimal sensing probability are given in Figure 13. The reconstruction error is only 0.1136, with 62% energy saving and 75% bandwidth saving, respectively.

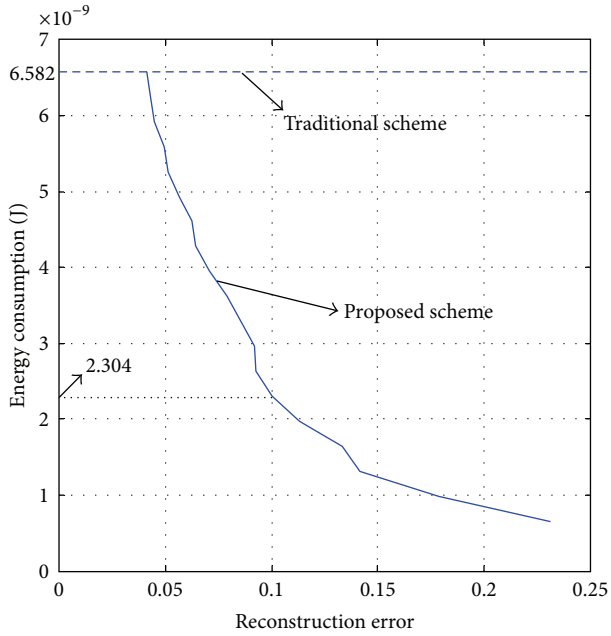

Figure 11: Comparison on energy cost between the proposed and traditional schemes.

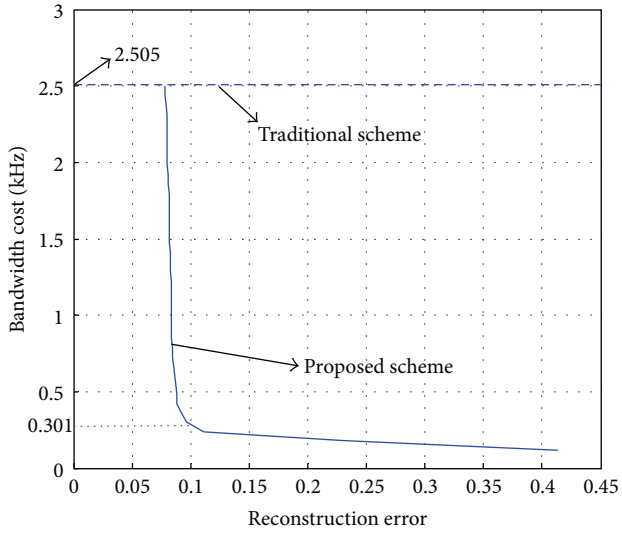

Figure 12: Comparison on bandwidth cost between the proposed and traditional schemes.

7. Conclusions

In this paper, a novel information acquisition scheme, CS-IDMA, is proposed for the large-scale ocean monitoring sensor networks. Exploiting the advantages of compressed sensing in low-sampling signal reconstruction and the advantages of IDMA in low-complexity multiuser detection, the proposed scheme can realize high-resolution information reconstruction with lower network cost, and the packet error during transmission can be greatly tolerant. With the aid of the particular semianalytical method based on SINR evolution, we give elaborate analytical observations on the proposed scheme. The simulation results carried on real ocean monitoring data show that our scheme can realize accurate information map reconstruction with much fewer measurements compared to the traditional method in which all sensors should participate in data sampling and transmitting, leading to less energy consumption and bandwidth requirement. Furthermore, an interesting phenomenon is observed where an optimal sensing probability exists for a given value of E_b/N_0 at the receiver side, with which the minimal reconstruction error is achieved. This result is significant for system designing.

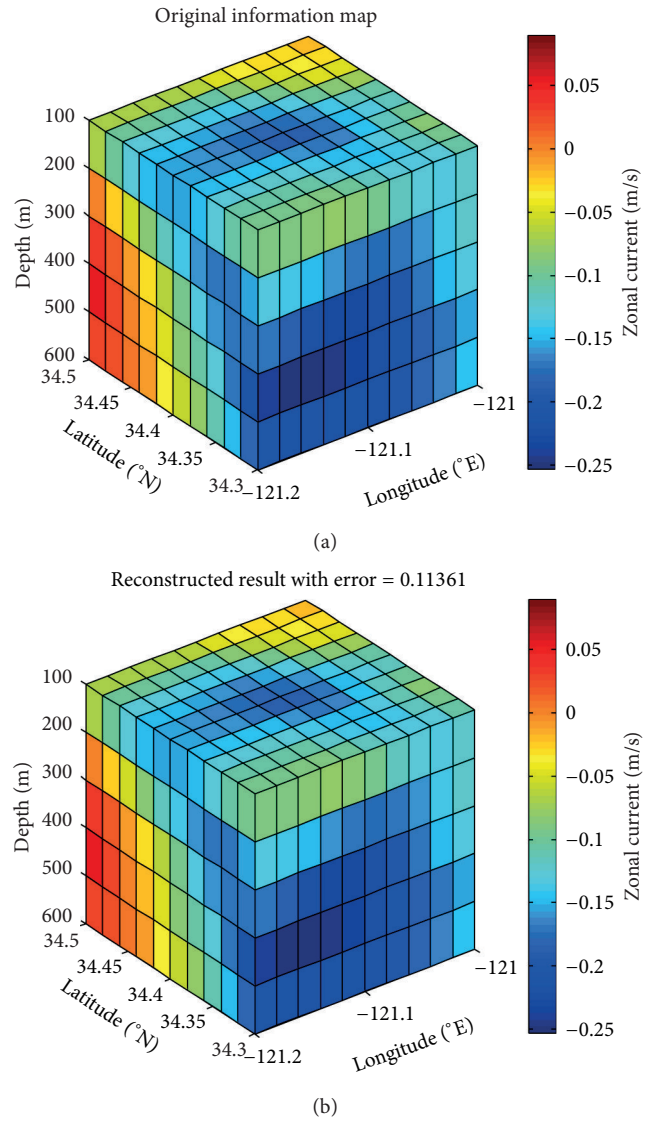

Figure 13: Simulation result on 3D zonal current data. (a) Original information map; (b) reconstructed result.

Conflict of Interests

The authors declare that there is no conflict of interests regarding the publication of this paper.

Acknowledgments

The presented work is sponsored by the National Natural Science Foundation of China (61371100, 61001093), the Promotive Research Fund for Excellent Young and Middle-Aged Scientist of Shandong Province (BS2012DX001), the Natural Scientific Research Innovation Foundation in Harbin Institute of Technology (HIT.NSRIF.2011114), and the Fundamental Research Funds for the Central Universities (HIT.NSRIF.2013136).

References

[1] J. Heidemann, U. Mitra, J. Preisig, M. Stojanovic, M. Zorzi, and L. Cimini, "Underwater wireless communication networks," *IEEE Journal on Selected Areas in Communications*, vol. 26, no. 9, pp. 1617–1619, 2008.

[2] J. Heidemann, M. Stojanovic, and M. Zorzi, "Underwater sensor networks: applications, advances and challenges," *Philosophical Transactions of the Royal Society A*, vol. 370, no. 1958, pp. 158–175, 2012.

[3] L. Ping, L. Liu, K. Wu, and W. K. Leung, "Interleave-division multiple-access," *IEEE Transactions on Wireless Communications*, vol. 5, no. 4, pp. 938–947, 2006.

[4] D. L. Donoho, "Compressed sensing," *IEEE Transactions on Information Theory*, vol. 52, no. 4, pp. 1289–1306, 2006.

[5] E. J. Candès, J. Romberg, and T. Tao, "Robust uncertainty principles: exact signal reconstruction from highly incomplete frequency information," *IEEE Transactions on Information Theory*, vol. 52, no. 2, pp. 489–509, 2006.

[6] R. G. Baraniuk, "Compressive sensing," *IEEE Signal Processing Magazine*, vol. 24, no. 4, pp. 118–124, 2007.

[7] M. Mishali and Y. C. Eldar, "Wideband spectrum sensing at sub-nyquist rates," *IEEE Signal Processing Magazine*, vol. 28, no. 4, pp. 102–135, 2011.

[8] M. Rostami, O. Michailovich, and Z. Wang, "Image deblurring using derivative compressed sensing for optical imaging application," *IEEE Transactions on Image Processing*, vol. 21, no. 7, pp. 3139–3149, 2012.

[9] J. Zhang, D. Zhu, and G. Zhang, "Adaptive compressed sensing radar oriented toward cognitive detection in dynamic sparse target scene," *IEEE Transactions on Signal Processing*, vol. 60, no. 4, pp. 1718–1729, 2012.

[10] J. Haupt, W. U. Bajwa, M. Rabbat, and R. Nowak, "Compressed sensing for networked data: a different approach to decentralized compression," *IEEE Signal Processing Magazine*, vol. 25, no. 2, pp. 92–101, 2008.

[11] S.-Y. Shih and K.-C. Chen, "Compressed sensing construction of spectrum map for routing in cognitive radio networks," in *Proceedings of the IEEE 73rd Vehicular Technology Conference (VTC '11)*, Budapest, Hungary, May 2011.

[12] X. Wang, Z. Zhao, Y. Xia, and H. Zhang, "Compressed sensing for efficient random routing in multi-hop wireless sensor networks," *International Journal of Communication Networks and Distributed Systems*, vol. 7, no. 3-4, pp. 275–292, 2011.

[13] H. Zheng, S. Xiao, and X. Wang, "Sequential compressive target detection in wireless sensor networks," in *Proceedongs of the IEEE International Conference on Communications (ICC '11)*, Kyoto, Japan, June 2011.

[14] A. K. Fletcher, S. Rangan, and V. K. Goyal, "On-off random access channels: a compressed sensing framework," submitted to *IEEE Transaction on Information Theory*, http://arxiv.org/abs/0903.1022.

[15] F. Fazel, M. Fazel, and M. Stojanovic, "Random access compressed sensing for energy-efficient underwater sensor networks," *IEEE Journal on Selected Areas in Communications*, vol. 29, no. 8, pp. 1660–1670, 2011.

[16] T. Xue, X. Dong, and Y. Shi, "Multiple access and data reconstruction in wireless sensor networks based on compressed sensing," *IEEE Transactions on Wireless Communications*, vol. 12, pp. 3399–3411, 2013.

[17] W. J. Kang and G. L. Liu, "Super-resolution information collection in underwater sensor networks with random node deployment: a compressed sensing approach," *Journal of Networks*, vol. 7, pp. 1280–1287, 2012.

[18] E. M. Sozer, M. Stojanovic, and J. G. Proakis, "Underwater acoustic networks," *IEEE Journal of Oceanic Engineering*, vol. 25, no. 1, pp. 72–83, 2000.

[19] H. Wu, L. Ping, and A. Perotti, "User-specific chip-level interleaver design for IDMA systems," *Electronics Letters*, vol. 42, no. 4, pp. 233–234, 2006.

[20] R. Saab, R. Chartrand, and Ö. Yilmaz, "Stable sparse approximations via nonconvex optimization," in *Proceedings of the IEEE International Conference on Acoustics, Speech and Signal Processing (ICASSP '08)*, pp. 3885–3888, Las Vegas, Nev, USA, April 2008.

[21] S. Lee and M. Eskenazi, "Incremental sparse bayesian method for online dialog strategy learning," *IEEE Journal on Selected Topics in Signal Processing*, vol. 6, pp. 903–916, 2012.

[22] Z. Rosberg, "Optimal transmitter power control in interleave division multiple access (IDMA) spread spectrum uplink channels," *IEEE Transactions on Wireless Communications*, vol. 6, no. 1, pp. 192–200, 2007.

Hindawi Publishing Corporation
Mathematical Problems in Engineering
Volume 2014, Article ID 895971, 8 pages
http://dx.doi.org/10.1155/2014/895971

Research Article

IMM Filter Based Human Tracking Using a Distributed Wireless Sensor Network

Sen Zhang,[1] Wendong Xiao,[1] and Jun Gong[2]

[1] *School of Automation and Electrical Engineering, University of Science and Technology Beijing, 30 Xueyuan Road, Haidian District, Beijing 100083, China*
[2] *School of Information and Science Engineering, Northeastern University, Shenyang 110031, China*

Correspondence should be addressed to Wendong Xiao; wdxiao@ustb.edu.cn

Received 2 September 2013; Revised 21 November 2013; Accepted 1 December 2013; Published 8 January 2014

Academic Editor: Shuli Sun

This paper proposes a human tracking approach in a distributed wireless sensor network. Most of the efforts on human tracking focus on vision techniques. However, most vision-based approaches to moving object detection involve intensive real-time computations. In this paper, we present an algorithm for human tracking using low-cost range wireless sensor nodes which can contribute lower computational burden based on a distributed computing system, while the centralized computing system often makes some information from sensors delay. Because the human target often moves with high maneuvering, the proposed algorithm applies the interacting multiple model (IMM) filter techniques and a novel sensor node selection scheme developed considering both the tracking accuracy and the energy cost which is based on the tacking results of IMM filter at each time step. This paper also proposed a novel sensor management scheme which can manage the sensor node effectively during the sensor node selection and the tracking process. Simulations results show that the proposed approach can achieve superior tracking accuracy compared to the most recent human motion tracking scheme.

1. Introduction

In the daily life surveillance system, if the human actions can be tracked accurately, the results can help greatly and readily improve the ability of the identification of the whole system. Therefore, devices that can accurately track human motion in space are essential components of such a surveillance system. A complete model of human consists of both the movements and the shape of the body. Many of the available systems consider the two modeling processes as separate even if they are very close. In our study, the movement of the body is the target.

There have been some approaches to the human motion tracking. Most of the human motion tracking systems are based on vision sensors. The camera-based human tracking system is much more popular nowadays. Some of the proposed approaches present systems that are capable of segmenting, detecting, and tracking people using multiple synchronized surveillance cameras located far from each other. But they try to hand off image-based tracking from camera to camera without recovering real-world coordinates [1–3]. Some other work has to deal with large video sequences involved when the image capture time interval is short [4, 5]. However, most vision-based approaches to moving human tracking are computationally intensive and costly expensive [6]. For example, they often involve intensive real-time computations such as image matching, background subtraction, and overlapping identification [6]. In fact, in many cases, due to the availability of prior knowledge on target motion kinematics, the intensive and expensive imaging detector array appears inefficient and unnecessary. For example, a video image consisting of 100×100 pixels with 8-bit gray level contains 80 kbits of data, while the position and velocity can be represented by only a few bits [7].

Recently wireless sensor network (WSN) technique has been developed quickly. A WSN consists of many low-cost spatially dispersed position sensor nodes. Each node can process information that it collected and received and exchange information with its neighboring nodes or the fusion center. Although there are many applications of WSNs on target

tracking [8–12], few papers can be found on human motion tracking in real-time systems [13, 14]. The recent proposed low-resolution camera-based WSNs for people tracking [15, 16] are still very computational and energy expensive. In this paper, we will develop an energy-efficient WSN technique for human motion tracking using low-cost ranging sensors.

Due to the limited resources of the sensor nodes for sensing, computation, and communication, the WSN will rely on collaborative information processing among sensor nodes to manage network resources and process the related information from different sensor nodes. Although various data fusion schemes and techniques have been proposed for combining measurements from many sensing nodes with limited accuracy and reliability, to achieve better accuracy and more robustness [14, 17, 18], the tracking accuracy is still limited due to the high maneuvering property of the human target. In this paper, an interacting multiple model (IMM) filter is employed to estimate the velocity and position of the human trajectory. IMM filter has the ability to switch between a high-process noise (or alternatively, higher order or turn) model in the presence of maneuvers and a low-process noise model in the absence of maneuvers. This gives the IMM filter its advantage over simpler estimators like the Kalman filter and extended Kalman filter (EKF). Based on the IMM filter, an adaptive sensor selection scheme is proposed in this paper for the tracking framework in order to save energy. Verified by simulations and a real testbed, the proposed algorithm can achieve more accurate estimation performance for human motion tracking compared to EKF [14].

The layout of the paper is arranged as follows. Section 2 presents the multiple models for human motion tracking. Section 3 presents the IMM estimator for our application. Section 4 proposes the sensor node selection method. Section 5 presents the simulation results and experimental results. Conclusions and future work are given in Section 6.

2. Problem Formulation

We consider the human moving in a 2D Cartesian coordinate system. The target state includes the human velocity, the human position in the coordinate, and the turn rate when the trajectory is along a curve. Assuming the human target has a nearly constant velocity and a nearly constant angular rate, we can build up the system models in this section.

2.1. Constant Velocity Model. Denote the human's position at time step k in the coordinate system as $(P_x(k), P_y(k))$, the velocity as $(V_x(k), V_y(k))$, and the sampling time interval as T. A constant velocity model that describes the human movement with a nearly constant velocity is

$$\mathbf{x}_1(k+1) = \mathbf{F}_1\left(\mathbf{x}_1(k)\right) + \mathbf{G}_1\mathbf{v}_1(k), \tag{1}$$

where $x_1(k) = [P_x(k) \;\; V_x(k) \;\; P_y(k) \;\; V_y(k)]^T$,

$$\mathbf{F}_1(\mathbf{x}(k)) = \left[P_x(k) + T \cdot V_x(k)\, V_x(k)\, P_y(k) \;\; +T \cdot V_y(k)\, V_y(k)\right], \tag{2}$$

and $\mathbf{v}_1(k)$ is the process noise which reflects possible imperfection of the assumption of the constant velocity. For convenience, we assume that $\mathbf{v}_1$ is a zero-mean Gaussian white noise with variance $\mathbf{Q}_1(k)$.

2.2. Coordinated Turn Model. In order to describe the human's more complex trajectory, such as turn left or turn right, here we adopt the coordinated turn model similar to [11]:

$$\mathbf{x}_2(k+1) = \mathbf{F}_2\left(\mathbf{x}_2(k)\right) + \mathbf{G}_2\mathbf{v}_2(k), \tag{3}$$

where $\mathbf{x}_2(k) = [P_x(k) \;\; V_x(k) \;\; P_y(k) \;\; V_y(k) \;\; \omega(k)]^T$,

$$\mathbf{F}_2\left(\mathbf{x}_2(k)\right) = \begin{bmatrix} P_x(k) + \dfrac{\sin\omega(k)T}{\omega(k)} \cdot V_x(k) - \dfrac{1-\cos\omega(k)T}{\omega(k)} \cdot V_y(k) \\ \cos\omega(k)T \cdot V_x(k) - \sin\omega(k)T \cdot V_y(k) \\ P_y(k) + \dfrac{1-\cos\omega(k)T}{\omega(k)} \cdot V_x(k) + \dfrac{\sin\omega(k)T}{\omega(k)} \cdot V_y(k) \\ \sin\omega(k)T \cdot V_x(k) + \cos\omega(k)T \cdot V_y(k) \\ \omega(k) \end{bmatrix},$$

$$\mathbf{G}_2(K) = \begin{bmatrix} \frac{1}{2}T^2 & T & 0 & 0 & 0 \\ 0 & 0 & \frac{1}{2}T^2 & T & 0 \\ 0 & 0 & 0 & 0 & T \end{bmatrix}^T. \tag{4}$$

Here $\omega(k)$ is the unknown constant turn rate and $\mathbf{v}_2(k)$ is the process noise. Although the actual turn rate is not exactly a constant, we can assume that it is not changed in a very short time interval. For convenience, we assume that $\mathbf{v}_2$ is a zero-mean Gaussian white noise with variance $\mathbf{Q}_2(k)$.

Since the above model is nonlinear, the estimation of the state will be done via EKF when the IMM is applied during the subprediction for different models. This needs the linearization of the system model. Thus the Jacobian matrix Jaco(k) of (3) is given by

$$\text{Jaco}(k) = \begin{bmatrix} 1 & \dfrac{\sin(\widehat{\omega}(k)T)}{\widehat{\omega}(k)} & 0 & -\dfrac{1-\cos(\widehat{\omega}(k)T)}{\widehat{\omega}(k)} & f_{\omega 1}(k) \\ 0 & \cos(\widehat{\omega}(k)T) & 0 & -\sin(\widehat{\omega}(k)T) & f_{\omega 2}(k) \\ 0 & \dfrac{1-\cos(\widehat{\omega}(k)T)}{\widehat{\omega}(k)} & 1 & \dfrac{\sin(\widehat{\omega}(k)T)}{\widehat{\omega}(k)} & f_{\omega 3}(k) \\ 0 & \sin(\widehat{\omega}(k)T) & 0 & \cos(\widehat{\omega}(k)T) & f_{\omega 4}(k) \\ 0 & 0 & 0 & 0 & 1 \end{bmatrix}, \tag{5}$$

where

$$f_{\omega 1}(k) = \frac{\cos(\widehat{\omega}(k)T)\,TV_x(k)}{\widehat{\omega}(k)} + \frac{\sin(\widehat{\omega}(k)T)\,V_x(k)}{\widehat{\omega}(k)^2} - \frac{\sin(\widehat{\omega}(k)T)\,TV_y(k)}{\widehat{\omega}(k)} - \frac{-1+\cos(\widehat{\omega}(k)T)\,V_y(k)}{\widehat{\omega}(k)^2},$$

$$f_{\omega 2}(k) = -\sin(\widehat{\omega}(k)T)\,TV_x(k) - \cos(\widehat{\omega}(k)T)\,TV_y(k),$$

$$f_{\omega 3}(k) = \frac{\sin(\widehat{\omega}(k)T)\,TV_x(k)}{\widehat{\omega}(k)} + \frac{1-\cos(\widehat{\omega}(k)T)\,V_x(k)}{\widehat{\omega}(k)^2} + \frac{\cos(\widehat{\omega}(k)T)\,TV_y(k)}{\widehat{\omega}(k)} - \frac{\sin(\widehat{\omega}(k)T)\,V_y(k)}{\widehat{\omega}(k)^2},$$

$$f_{\omega 4}(k) = \cos(\widehat{\omega}(k)T)\,TV_x(k) - \sin(\widehat{\omega}(k)T)\,TV_y(k),$$

$$R_1 = \widehat{x}_2(k)^2 + \widehat{x}_3(k)^2 - 2\widehat{x}_2(k)\,\widehat{x}_3(k)\cos\gamma,$$

$$R_2 = \widehat{x}_3(k)\cos\gamma - \widehat{x}_2(k)\cos(2\gamma),$$

$$R_3 = \widehat{x}_2(k) - \widehat{x}_3(k)\cos\gamma,$$

$$R_4 = -\widehat{x}_2(k)\,\widehat{x}_3(k)\cos\left(2\widehat{x}_1(k)\right)\cos^2\gamma + \widehat{x}_2(k)\,\widehat{x}_3(k)\cos(2\gamma) + \cos\gamma\left[-\widehat{x}_3(k)^2 + \left(\widehat{x}_2(k)^2 + \widehat{x}_3(k)^2\right)\cos^2\widehat{x}_1(k) - \widehat{x}_2(k)^2\cos 2\gamma\right]. \tag{6}$$

2.3. System Observation Model. Let $Z_j(k)$ denote the k-th measurement of the target at time step t_k if sensor j is used. The measurement model is given by

$$Z_j(k) = h_j(x(k)) + v_j(k), \tag{7}$$

where h_j is a (generally nonlinear) measurement function depending on sensor j's measurement characteristic and parameters (e.g., its location). $v_j(k)$ is the measurement noise of sensor j which is assumed independent and to be zero-mean Gaussian white noise with covariance $R_j(k)$.

Based on the above velocity constant model, the coordinated constant turn model, and the system observation model, the interacting multiple model filter is applied to estimate the system state variable which includes the human's position coordinate and velocity.

2.4. IMM Filter. The basic IMM algorithm (one cycle) is as follows.

Step 1. We calculate the mixing probabilities and interaction between different models:

$$\mu_{i'|j'}(k \mid k) = \frac{1}{\bar{c}_{j'}} p_{i'j'}\mu_{i'}(k),$$

$$\bar{c}_{j'} = \sum_{i'} p_{i'j'}\mu_{i'}(k),$$

$$\widehat{x}_{0j'}(k \mid k) = \sum_{i'} \widehat{x}_{i'}(k \mid k)\,\mu_{i'|j'}(k \mid k),$$

$$P_{0j'}(k \mid k) = \sum_{i'} \left\{P_{i'}(k \mid k) + \left[\widehat{x}_{i'}(k \mid k) - \widehat{x}_{0j'}(k \mid k)\right] \times \left[\widehat{x}_{i'}(k \mid k) - \widehat{x}_{0j'}(k \mid k)\right]^T\right\} \times \mu_{i'|j'}(k \mid k). \tag{8}$$

In these equations, $\mu_{i'|j'}(k \mid k)$ is the mixing probability at time k (the weights with which the estimates from the previous cycle are given to each filter at the beginning of the current cycle); $\widehat{x}_{0j'}(k \mid k)$ and $P_{0j'}(k \mid k)$ are the mixed initial condition for mode-matched filter j' at time k; $p_{i'j'}$ is the transition probability between mode i' and mode j'. $\mu_{i'}(k)$ is the mode i' probability at time k.

Step 2. Prediction and filtering are as follows:

$$\widehat{x}_{j'}(k+1 \mid k) = F_{j'}\widehat{x}_{0j'}(k \mid k) + \Gamma_{j'}(k)\,\overline{v}_{j'}(k),$$

$$P_{j'}(k+1 \mid k) = F_{j'}P_{0j'}(k \mid k)\,F_{j'}^T + \Gamma_{j'}(k) \times Q_j(k)\,\Gamma_{j'}(k)^T,$$

$$\widehat{x}_{j'}(k+1 \mid k+1) = \widehat{x}_{j'}(k+1 \mid k) + W_{j'}(k) \times r_{j'}(k+1),$$

$$P_{j'}(k+1 \mid k+1) = P_{j'}(k+1 \mid k)\,F_{j'}^T - W_{j'}(k) \times S_{j'}(k)\,W_{j'}(k)^T, \tag{9}$$

where $\widehat{x}_{j'}(k+1 \mid k)$ and $P_{j'}(k+1 \mid k)$ are the state estimate and its covariance in model-matched filter j' at time step $k+1$. $F_{j'}(k+1)$ is the Jacobin matrix of the system model j'.

The observation residenital is

$$r_{j'}(k+1 \mid k+1) = z(k+1) - \widehat{z}_{j'}(k+1 \mid k). \tag{10}$$

The measurement prediction is

$$\widehat{z}_{j'}(k+1 \mid k) = H_{j'}(k+1)\,\widehat{x}_{j'}(k+1 \mid k), \tag{11}$$

where $H_{j'}(k+1)\widehat{x}_{j'}(k+1 \mid k)$ is Jacobin matrix of the system observation model of sensor j'.

The residential covariance is

$$S_{j'}(k+1 \mid k) = H_{j'}(k+1)\,P_{j'}(k+1 \mid k) \times H_{j'}(k+1)^T + R_{j'}(k+1),$$

$$W_{j'}(k+1) = P_{j'}(k+1 \mid k)\,H_{j'}(k+1)^T \times S_{j'}(k+1)^{-1}. \tag{12}$$

The likelihood function for filter j' is

$$\Lambda_{j'}(k+1) = N\left(r_{j'}(k+1); 0, S_{j'}(k+1)\right). \quad (13)$$

The mode j' probability at time k is

$$\mu_{j'} = \frac{1}{c}\Lambda_{j'}(k+1)\sum_{i'} p_{i'j'}\mu_{i'}(k), \quad (14)$$

where c is a normalizing factor. $\hat{x}_{j'}(k+1 \mid k+1)$ and $P_{j'}(k+1 \mid k+1)$ are the state estimate and its covariance in mode-matched filter j' at time $k+1$.

Step 3. Combination of the different mode update results is

$$\begin{aligned}
&\hat{x}(k+1 \mid k+1) = \sum_{j'} \hat{x}_{j'}(k+1 \mid k+1)\,\mu_{j'}(k+1),\\
&P(k+1 \mid k+1)\\
&\quad = \sum_{j'} \Big\{ P_{j'}(k+1 \mid k+1)\\
&\qquad + \left[\hat{x}_{j'}(k+1 \mid k+1) - \hat{x}(k+1 \mid k+1)\right]\\
&\qquad \times \left[\hat{x}_{j'}(k+1 \mid k+1) - \hat{x}(k+1 \mid k+1)\right]^{T} \Big\}\\
&\qquad \times \mu_{j'}(k+1).
\end{aligned} \quad (15)$$

In this paper for human motion tracking, we adopt 2 models in IMM to estimate the system state variable including the target's position coordinate and velocity, that is, the constant velocity model and the coordinated constant turn model introduced in Section 2.

3. Adaptive Sensor Selection Scheme

The sensor node selection scheme based on the IMM filter for maneuvering target tracking framework will be proposed in this section. We assumed that each sensor node can detect the human target and determine the range of the sensor node, and the locations of all the sensor nodes are known. The popular approach only selects the sensor nodes which are closest to the predicted human location as estimated by the estimator such as EKF [14]. One of the shortcomings of this "closest" node approach is that it does not consider its contribution to the tracking accuracy and the energy consumption quantitatively and simultaneously but simply selects the sensor nodes. Therefore, we proposed an adaptive sensor selection scheme in this paper, which is similar to the work in [19]. In our proposed method, IMM filter will be applied instead of EKF in order to avoid the maneuvering property of the human target. The approach jointly selects the next tasking sensor node and automatically determines the sampling time interval simultaneously based on both of the prediction of the tracking accuracy and tracking energy cost.

Tracking accuracy can be measured by various criteria, such as the trace and the determinant of the covariance matrix and Fisher information defined on the Fisher information matrix. In our proposed approach, the tracking accuracy is reflected by tracking error $\phi(k)$ at time step k which is defined as the trace of the covariance matrix $P(k \mid k)$; that is,

$$\phi(k) = \text{trace}\left(P(k \mid k)\right). \quad (16)$$

Given a predefined threshold $\phi_0(k)$, the tracking accuracy at time step k is considered to be satisfactory if

$$\phi(k) < \phi_0(k); \quad (17)$$

otherwise it is considered to be unsatisfactory.

Energy consumption is a main consideration in this paper. We utilize the following energy model. If current sensor i selects sensor j as the next tasking sensor, then the total energy consumed by sensor i in transmission is

$$E_t(i,j) = \left(e_t + e_d r_{ij}^{\alpha}\right) b_c, \quad (18)$$

where e_t and e_d are decided by the specifications of the transceivers used by the nodes, r_{ij} is the distance between sensor i and sensor j, b_c is the number of bits sent, and α depends on the channel characteristics and is assumed to be time invariant. Energy consumed in receiving is

$$E_r(j) = e_r b_c, \quad (19)$$

where e_r is decided by the specification of the receiver of sensor j. The energy spent in sensing/processing data of b_s bits by sensor j is

$$E_s(j) = e_s b_s. \quad (20)$$

Therefore the total energy consumption is

$$E(i,j) = E_t(i,j) + E_r(j) + E_s(j). \quad (21)$$

In this paper, we will ignore the energy consumption for idling state of the node.

Suppose the current time step is k and the current tasking sensor is the sensor i which receives state estimation $\hat{x}(k-1 \mid k-1)$ and estimation covariance matrix $P(k-1 \mid k-1)$ of the time step $k-1$ from its parent tasking sensor. It first updates the state estimation by incorporating its new measurement $Z_j(k)$ using IMM algorithm described in Section 2. Then it uses the sensor scheduling algorithm to select the next tasking sensor j and the next sampling interval Δt_k such that the sensor j can undertake the sensing task at the time $t_{k+1} = t_k + \Delta t_k$. We suppose Δt_k should be in the range $[T_{\min}, T_{\max}]$, where $T_{\min}$ and $T_{\max}$ are the minimal and maximal sampling intervals, respectively. If sensor j is selected with the sampling interval Δt_k, its associated predicted objective function is defined as

$$J(j, \Delta t_k) = w\Phi_j(k) + (1-w)\frac{E(i,j)}{\Delta t_k}, \quad (22)$$

where $\Phi_j(k)$ is the predicted tracking accuracy according to the IMM algorithm, $E(i,j)$ is the corresponding predicted cost given by (21), is the averaged energy consumption over the period. $w \in [0,1]$ is the weighting parameter used to balance the tracking accuracy and the energy consumption.

The sensors are scheduled in the following two tracking methods.

(1) After prediction, none of the sensors can achieve the satisfactory tracking accuracy using any sampling interval in $T_{\min}$ and $T_{\max}$. In this case, Δt_k is set to the minimal sampling interval $T_{\min}$ and the sensor is selected by

$$j^* = \arg\min_{j \subset A} \{J(j, T_{\min})\}, \tag{23}$$

where A is the candidate sensors that can be selected by sensor i. Generally in (23), $w \neq 0$. The purpose of this mode is to drive the tracking accuracy to be satisfactory as soon as possible with consideration of the energy consumption.

(2) After prediction, at least one sensor can achieve the satisfactory tracking accuracy. In this case, the optimal $(j^*, \Delta t_k^*)$ is selected by

$$(j^*, \Delta t_k^*) = \arg\min_{j \subset A^*, \Phi(j,k) \leq \Phi_0} \left\{ \frac{E(i,j)}{\Delta t_k} \right\}, \tag{24}$$

where A^* is the set of sensors that can achieve the satisfactory tracking accuracy. Equation (24) utilizes the objective function (22) with $w = 0$. The basic idea of this mode is that when the predicted tracking accuracy is satisfactory, the sensors and the sampling interval are selected according to the energy efficiency.

It is easy to see that information-driven sensor querying (IDSQ) [18] corresponds to the special case of the above adaptive sensor selection approach where the fast tracking approach mode is used in each time step (by set $\Phi_0 = 0$).

For simplification, we suppose the sampling interval is selected from predefined N values $\{T_t\}_1^N$ where $T_1 = T_{\min}$, $T_N = T_{\max}$, and $T_{t_1} < T_{t_2}$ if $t_1 < t_2$. In addition the set $\{T_t\}_1^N$ is selected such that its values can evenly divide the interval $[T_{\min}, T_{\max}]$ into $N - 1$ subintervals.

4. Sensor Node Management Scheme

If the static sensor nodes' location estimation is to be built incrementally as information is gathered from sensors, there is typically a need for a sensor node localization management process in order to prevent the heavy computational burden when the system state matrix is augmented. This process has the function of managing the information present in the knowledge base and possibly aiding the sensing process. Given the fact that computational resources are limited, an information management technique that reduces the stored data without sacrificing much information is required. To improve the applicability of a spatial description to a larger variety of scenarios, it should present the ability to iteratively adapt its geometry to application-specific requirements. The sensor node management process can be divided into three aspects in dynamic environments as follows.

(1) Adding observed sensor nodes: when a sensor node observed in the current scan cannot be matched to the existing sensor node list, a new sensor node is initialized.

(2) Removing redundant sensor nodes: if all static sensor nodes are included for updating the state, the computational requirement will be high. Thus, redundant sensor nodes that have not been observed for a long time interval should be removed.

(3) Removing unstable sensor nodes: sensor nodes become unstable or obsolete if they move or become permanently occluded. For example, sensor nodes might be stationary for a long period of time and can be considered suitable sensor nodes. But if they move, they are unstable sensor nodes and should be removed from the sensor management scheme. Another case is that structural changes may occur in the environment, such as some static sensor nodes removing. In other cases an object might be placed in front of a sensor node, occluding it from view. For whatever reason, some sensor nodes may cease to exist and no longer provide useful information. These unstable sensor nodes should be deleted from the sensor management scheme.

After data association, if a sensor node cannot be matched to any existing sensor node in the map, it is considered as a new sensor node. The sensor node initialization is activated. Otherwise, this observation is used for the system update.

After a specified time interval, we shall check if this sensor node is still matched by any new coming observations during this period. If it is matched by none of the observations sensed from external sensors within the specified interval, this sensor node should be removed from the sensor node listing. Otherwise, this sensor node will still be kept in our system variables.

Finally, the sensing process can be improved if sensors are told where to look at. This directed sensing technique will naturally have benefits, such as to speed up the estimation process or to extract information about the environment in a predefined way.

5. Experimental Results

The human target is assumed to move in the $X - Y$ plane of the Cartesian coordinate frame and the ground truth trajectory consists of the curves and lines. The monitored field is 100 m × 150 m and covered by 25 randomly placed sensors. It is assumed that the sensors can only collect the range measurements from the target. The sensors are placed randomly in the field. We assume the noise covariance $\sigma_j = 0.001$ for any sensor j in the covariance matrix of the process noise. We will apply the adaptive sensor scheduling algorithm presented in Section 3 in tracking a human object. The measurement model for sensor j is assumed as follows:

$$Z_j(k) = \sqrt{\left(x(k) - x_j(k)\right)^2 + \left(y(k) - y_j(k)\right)^2} + v_j(k), \tag{25}$$

where $(x(k), y(k))$ is the location of the human object, $(x_j(k), y_j(k))$ is the known position of sensor j, and $v_j(k)$ is the zero-mean Gaussian measurement noise with variance σ_j. In this simulation, we use the constant velocity model and the constant angular rate (coordinated turn) model explained in Section 2 as the target motion model. IMM filter and sensor selection scheme is applied to predict the trajectory.

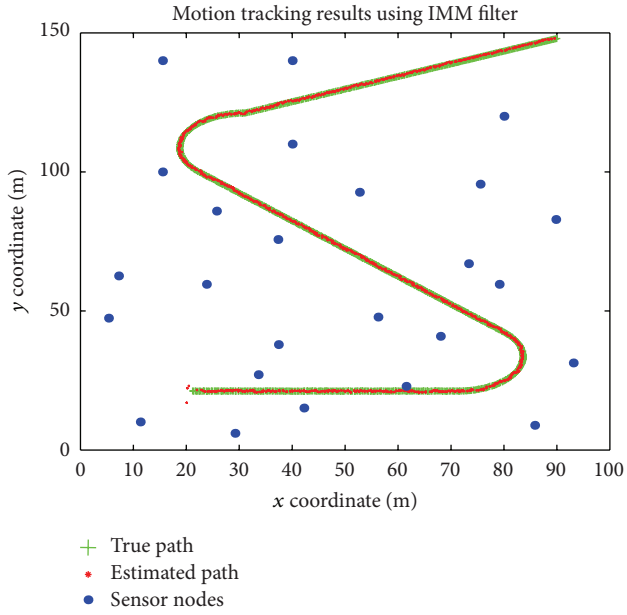

Figure 1: Human Motion Tracking Simulation Results Based on the Proposed Algorithm.

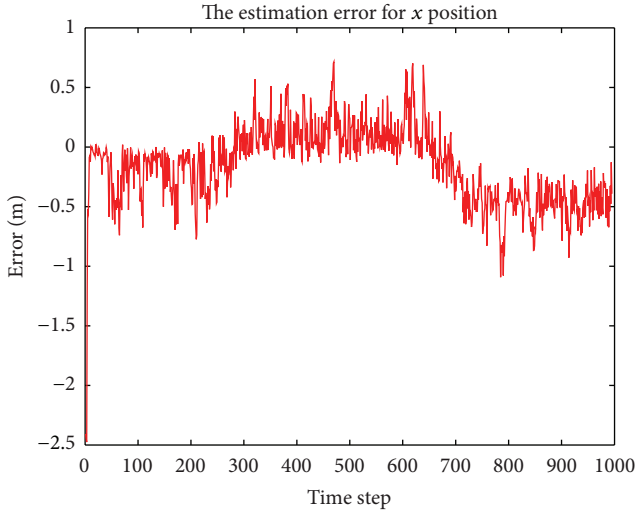

Figure 2: The estimation error between the ground truth of the trajectory and the predicted path.

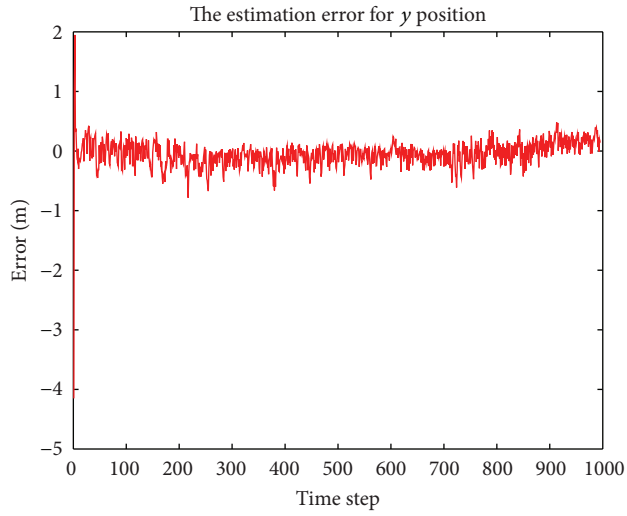

Figure 3: The estimation error between the ground truth of the trajectory and the predicted path.

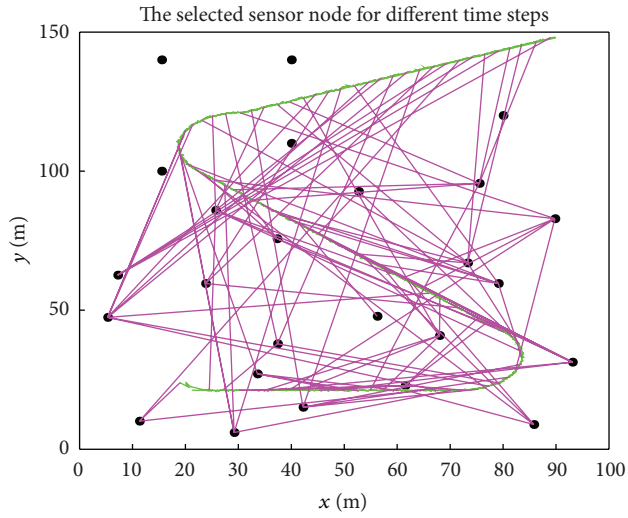

Figure 4: The selected sensor node for different time steps using the proposed sensor selection method.

The following parameter values taken from [20] are used in the energy model: $\alpha = 2$, $e_t = 45 \times 10^{-6}$, $e_r = 135 \times 10^{-6}$, $e_s = 50 \times 10^{-6}$, all in J/bit, and $e_d = 10 \times 10^{-9}$ in mJ/bit·m^2. In addition, b_c and b_s are assumed to be 1024. Thus in (21), $e_0 = 0.23552$ mJ and $e_1 = 1.024 \times 10^{-4}$ mJ/m^2.

For the sampling interval, we suppose $N = 5$, $T_{\min} = 0.1$, and $T_{\max} = 0.5$. We also assume $w = 0.16$ for the objective function (22) and the threshold of the tracking accuracy is set as $\Phi_0 = 2$.

Figure 1 shows the human tracking simulation results by the proposed IMM algorithm and range sensor nodes in the WSN. The green path means the ground truth we assumed and the red path is the estimation of the human trajectory. The blue points are the sensor nodes we randomly placed. Figures 2 and 3 give the estimation errors for Figure 1.

Figure 4 showed the sensor selected every ten steps during the target moving. The pink color line indicated the association of the selected sensor and the human position at that time step. We can see that a sensor can be chosen for several different steps.

We compare the performance of the proposed IMM based adaptive sensor scheduling scheme with the EKF based adaptive sensor scheduling scheme. Figures 5 and 6 showed the tracking accuracy comparison of the x coordinates and y coordinates when we use IMM filter and EKF together with the sensor selection method proposed in this paper. Clearly we can see that more accurate tracking accuracy is obtained when the IMM filter is used.

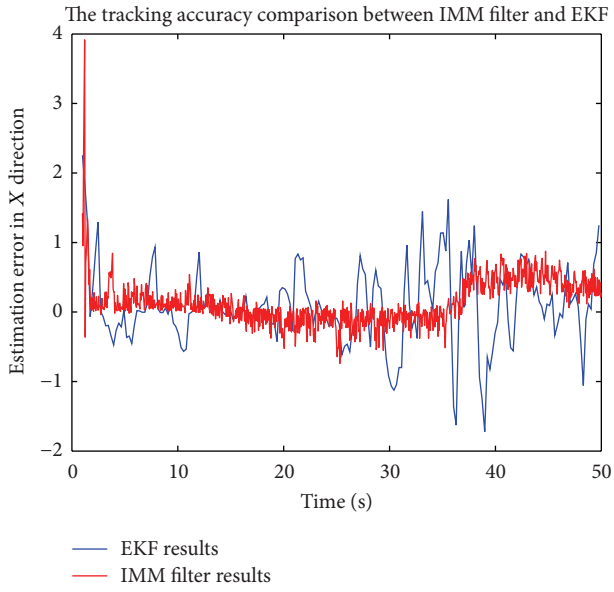

FIGURE 5: The x axis estimation error comparison of IMM filter and EKF.

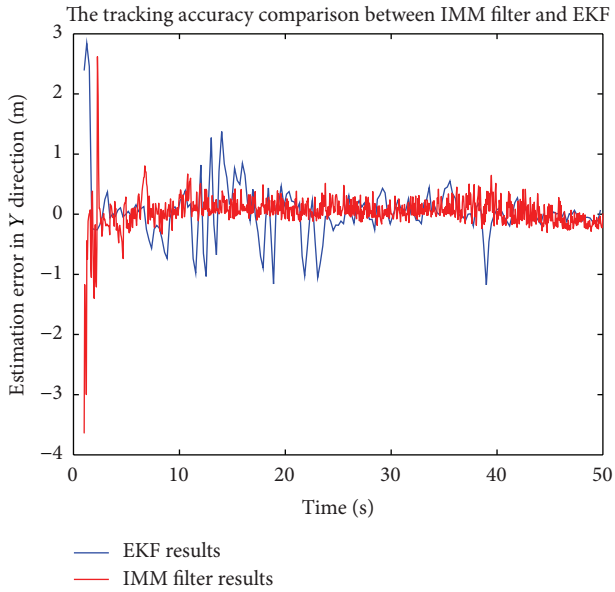

FIGURE 6: The y axis estimation error comparison of IMM filter and EKF.

6. Conclusions

This paper presented an IMM filter based human tracking approach and proposed an adaptive sensor scheduling scheme for the IMM filter based tracking framework in wireless sensor networks. The proposed method uses cheap range sensor nodes in wireless sensor networks by jointly selecting the next tasking sensor and determining the sampling interval based on predicted tracking accuracy and tracking cost under the IMM filter frame. Simulation results show that the new scheme can achieve significant tracking accuracy considering the energy cost at each time step. Real testbed for human motion tracking is built up and the real time data implementation showed that the IMM filter based human motion tracking can give better results compared to the EKF based human motion tracking scheme. There are still many issues remaining for future study. Multistep, multisensor selection based adaptive sensor scheduling and sensor scheduling for multitarget tracking are both challenging problems for further investigations.

Conflict of Interests

The authors declare that there is no conflict of interests regarding the publication of this paper.

References

[1] A. Mittal and L. S. Davis, "M2Tracker: a multi-view approach to segmenting and tracking people in a cluttered scene using region-based stereo," in *Proceedings of the European Conference on Computer Vision*, pp. 18–36, Copenhagen, Denmark, May 2002.

[2] A. Mittal and L. S. Davis, "M2Tracker: a multi-view approach to segmenting and tracking people in a cluttered scene," *International Journal of Computer Vision*, vol. 51, no. 3, pp. 189–203, 2004.

[3] M. Harville, "Stereo person tracking with adaptive plan-view statistical tem-plates," in *Proceedings of European Conference on Computer Vision Workshop on Statistical Methods in Video Processing*, Copenhagen, Denmark, 2002.

[4] Q. Cai and J. K. Aggarwal, "Tracking human motion in structured environments using a distributed-camera system," *IEEE Transactions on Pattern Analysis and Machine Intelligence*, vol. 21, no. 11, pp. 1241–1247, 1999.

[5] T. Darrell, D. Demirdjian, N. Checka, and P. Felzenszwalb, "Plan-View trajectory estimation with dense stereo background models," in *Proceedings of the 8th IEEE International Conference on Computer Vision*, pp. 628–635, Vancouver, Canada, 2001.

[6] W. Hu, T. Tan, L. Wang, and S. Maybank, "A survey on visual surveillance of object motion and behaviors," *IEEE Transactions on Systems, Man and Cybernetics C*, vol. 34, no. 3, pp. 334–352, 2004.

[7] A. La Cour-Harbo, "Geometrical modeling of a two-dimensional sensor array for determining spatial position of a passive object," *IEEE Sensors Journal*, vol. 4, no. 5, pp. 627–642, 2004.

[8] E. Mazor, A. Averbuch, Y. Bar-Shalom, and J. Dayan, "Interacting multiple model methods in target tracking: a survey," *IEEE Transactions on Aerospace and Electronic Systems*, vol. 34, no. 1, pp. 103–123, 1998.

[9] D. Lu, Y. Yao, and F. He, "Sensor management based on cross-entropy in interacting multiple model kalman filter," in *Proceedings of the 2004 American Control Conference (AAC '04)*, pp. 5381–5386, Boston, Mass, USA, July 2004.

[10] Q. Le, L. M. Kaplan, and J. H. McClellan, "Multiple-mode Kalman filtering with node selection using bearings-only measurements," in *Proceedings of the 36th IEEE Southeastern Symposium on System Theory (SSST '04)*, pp. 185–189, Atlanta, Ga, USA, 2004.

[11] M. Mallick and B. F. La Scala, "IMM estimator for ground target tracking with variable measurement sampling intervals," in

Proceedings of the 9th International Conference on Information Fusion (ICIF '06), pp. 1–8, Florence, Italy, July 2006.

[12] P. S. Maybeck and B. D. Smith, "Multiple model tracker based on Gaussian mixture reduction for maneuvering targets in clutter," in *Proceedings of the 8th International Conference on Information Fusion (ICIF '05)*, pp. 2043–2052, Florence, Italy, July 2005.

[13] Q. Hao, D. J. Brady, B. D. Guenther, J. B. Burchett, M. Shankar, and S. Feller, "Human tracking with wireless distributed pyroelectric sensors," *IEEE Sensors Journal*, vol. 6, no. 6, pp. 1683–1695, 2006.

[14] Y. K. Toh, W. Xiao, and L. Xie, "A wireless sensor network target tracking system with distributed competition based sensor scheduling," in *Proceedings of the 2007 International Conference on Intelligent Sensors, Sensor Networks and Information Processing (ISSNIP '07)*, pp. 257–262, Melbourne, Australia, December 2007.

[15] A. Rahimi, B. Dunagan, and T. Darrell, "Tracking people with a sparse network of bearing sensors," in *Proceedings of the 8th European Conference on Computer Vision*, pp. 507–518, Prague, Czech Republic, May 2004.

[16] W. Zajdel, A. T. Cemgil, and B. J. A. Brose, "Dynamic Bayesian networks for visual surveillance with distributed cameras," in *Proceedings of the 1st European Conference on Smart Sensing and Context*, pp. 240–243, Enschede, The Netherlands, 2006.

[17] Y. Bar-Shalom, X. R. Li, and T. Kirubarajan, *Estimation with Applications to Tracking and Navigation*, John Wiley and Sons, 2001.

[18] F. Zhao, J. Liu, L. Guibas, and J. Reich, "Collaborative signal and Information processing: an information directed approach," in *Proceedings of the IEEE Digital Object Identifier*, pp. 1199–1209, New York, NY, USA, 2003.

[19] W. D. Xiao, J. K. Wu, L. H. Xie, and L. Dong, "Sensor scheduling for target tracking in networks of active sensors," *Acta Automatica Sinica*, vol. 32, no. 6, pp. 922–928, 2006.

[20] M. Bhardwaj and A. P. Chandrakasan, "Bounding the lifetime of sensor networks via optimal role assignments," in *Proceedings of the 21st Annual Joint Conference of the IEEE Computer and Communications Societie (INFOCOM '02)*, pp. 1587–1596, New York, NY, USA, 2002.

Hindawi Publishing Corporation
Mathematical Problems in Engineering
Volume 2013, Article ID 505848, 7 pages
http://dx.doi.org/10.1155/2013/505848

Research Article

Average Consensus Analysis of Distributed Inference with Uncertain Markovian Transition Probability

Won Il Kim,[1,2] Rong Xiong,[1] Qiuguo Zhu,[1] and Jun Wu[1]

[1] *State Key Laboratory of Industrial Control Technology, Zhejiang University, Hangzhou 310027, China*
[2] *Kimchaek Industry University, Pyongyang 999093, Democratic People's Republic of Korea*

Correspondence should be addressed to Rong Xiong; rxiong@iipc.zju.edu.cn

Received 18 June 2013; Revised 9 October 2013; Accepted 29 October 2013

Academic Editor: Shuli Sun

The average consensus problem of distributed inference in a wireless sensor network under Markovian communication topology of uncertain transition probability is studied. A sufficient condition for average consensus of linear distributed inference algorithm is presented. Based on linear matrix inequalities and numerical optimization, a design method of fast distributed inference is provided.

1. Introduction

During the past few decades, consensus problems of multiagent systems by information exchange have been extensively studied by many researchers, due to their widespread applications in autonomous spacecraft, unmanned air vehicles, mobile robots, and distributed sensor networks. Olfati-Saber and Murray introduced in [1, 2] a theoretical framework for solving consensus problems. In [3, 4], consensus problems of first-order integrator systems were proposed based on algebra graph theory. In [5, 6], consensus problems of directed second-order systems were presented. In [5], the authors provided necessary and sufficient condition for reaching mean square consensus of discrete-time second order systems. Consensus conditions were studied in [6] of continuous-time second order systems by Linear Matrix Inequality (LMI) approach.

Among consensus problems, the average consensus problem is challenging which requires distributed computation of the average of the initial state of a network [1, 2]. For a strongly connected network, [1] proved that the average consensus problem is solvable if and only if the network is balanced. The discrete-time average consensus plays a key role in distributed inference in sensor networks. In networks of fixed topology, [7] gave necessary and sufficient conditions for linear distributed inference to achieve average consensus. A design method was presented in [7] to implement linear distributed inference of fastest consensus. Because of noisy communication channels, link failures often occur in a real network. Therefore, it is meaningful to study distributed inference in networks of swing topology. Through a common Lyapunov function, a result of [1] stated that distributed inference reaches average consensus in a network of swing topology if the network holds strongly connected and balanced topology. Reference [8] modeled a network of swing topology using a Bernoulli process and established a necessary and sufficient condition for average consensus of distributed inference. The condition is related to a mean Laplacian matrix.

The Bernoulli process in [8] means that the network link failure events are temporally independent. From the viewpoint of engineering, it is more reasonable to consider network link failures of temporal independence. The most famous and most tractable stochastic process of temporal independence is Markovian chain in which any future event is independent of the past events and depends only on the present event. This motivates us to model a network of swing topology using a Markovian chain and hence to study distributed inference using Markovian jump linear system method [9–12]. In practice, transition probabilities of a Markovian chain are not known precisely a priori, and only estimated values of transition probabilities are available. Hence, this paper thinks of networks with Markovian communication of uncertain transition probability.

In fact, in the research on networked control systems, Markovian chain has been used by several authors to describe random communication in networks. Reference [13] provided packet-loss model by Markovian chain in H_∞ networked control. Under network communication of update times driven by Markovian chain, [14] gave stability conditions of model-based networked control systems. Networked control systems with bounded packet losses and transmission delays are modeled through Markovian chain in [15]. The networked predictive control system in [16] adopted 2 Markovian chains to express date transmission in both the controller-actuator channel and the sensor-controller channel.

In this paper, $\mathbb{Z}$ is used to denote the set of all nonnegative integers. The real identity matrix of $n\times n$ is denoted by I_n. Let $\mathbf{1}$ be the vector whose elements are all equal to 1. The Euclidean norm is denoted by $\|\bullet\|$. If a matrix P is positive (negative) definite, it is denoted by $P > 0(<0)$. The notation $*$ within a matrix represents the symmetric term of the matrix. The expected value is represented by $E[\bullet]$.

The paper is organized as follows. Section 2 contains a description of the network and linear distributed inference. Section 3 presents average consensus conditions and a design method. Numerical simulation results are in Section 4. Finally, Section 5 draws conclusions.

2. Network Description

Consider distributed inference in a wireless sensor network consisting of n sensor. Each sensor $i \in N \triangleq \{1, 2, \ldots, n\}$ collects a local measurement $y_i \in \mathbb{R}$ about the situation of environment. It is assumed that these local measurements $y_1, y_2, \ldots, y_n$ are independent and identically distributed random variables. The goal of inference is for all sensors to reach the global measurement

$$\overline{y} = \frac{1}{n}\sum_{i=1}^{n} y_i \tag{1}$$

such that the true situation of environment can be monitored convincingly.

This paper studies iterative distributed inference. Define

$$U = \{(s,t) \mid s < t, s \in N, t \in N\} \tag{2}$$

which includes all realizable undirected links in the wireless sensor network. At the kth iteration $k \in \mathbb{Z}$, the successful communication links in the wireless sensor network are described by the set

$$E(k) \subset U. \tag{3}$$

A pair $(s_1, t_1) \in E(k)$ means that the sensors s_1 and t_1 communicate with each other at k. A pair $(s_2, t_2) \in U$ but $(s_2, t_2) \notin E(k)$ means that there is no communication link between the sensors s_2 and t_2 at k. Due to noisy communication channels and limited network power budget, $E(k)$ is assumed to be random and to be modeled as follows. Given m distinct subsets $F_1, F_2, \ldots, F_m \subset U$. Let θ_k be a stochastic process taking values in $M = \{1, 2, \ldots, m\}$ and driven by a Markov chain with a transition probability matrix $\Gamma = [\gamma_{hl}] \in \mathbb{R}^{m\times m}$, where $\gamma_{hl} = \Pr(\theta_{k+1} = l \mid \theta_k = h)$, for all $h \in M$, for all $l \in M$. However, these γ_{hl}s are not known precisely. Each γ_{hl} is expressed as

$$\gamma_{hl} = \overline{\gamma}_{hl} + \Delta\gamma_{hl}, \tag{4}$$

with a known $\overline{\gamma}_{hl}$ and a unknown $\Delta\gamma_{hl}$ whose absolute value is less than a given positive constant $2\pi_{hl}$. For any for all $h \in M$, $\sum_{l=1}^{m} \overline{\gamma}_{hl} = 1$ and $\sum_{l=1}^{m} \Delta\gamma_{hl} = 0$. This paper models

$$E(k) = F_{\theta_k}. \tag{5}$$

The neighborhood of sensor i at k is denoted by

$$\Omega_i(k) = \left\{ j \in N \mid (i,j) \in F_{\theta_k} \text{ or } (j,i) \in F_{\theta_k} \right\}, \tag{6}$$

and the element number of set $\Omega_i(k)$ is denoted by $d_i(k)$.

For sensor i, set its initial state $x_i(0) = y_i$. At the kth iteration, each sensor i obtains its neighbors' states and updates its state using the following linear iteration law:

$$x_i(k+1) = x_i(k) + \alpha \sum_{j\in\Omega_i(k)} \left(x_j(k) - x_i(k) \right), \quad i \in N, \tag{7}$$

where $\alpha > 0$ is the weight parameter which is assigned by designers. Our study on the above distributed inference has two objectives: one is to derive a condition on the convergence of $x_i(k)$ to $\overline{y}$ in the sense of mean square; the other is how to find α such that a fast convergence is achieved.

3. Average Consensus Analysis

3.1. Convergence Condition. Denote

$$x(k) = \begin{bmatrix} x_1(k) \\ x_2(k) \\ \vdots \\ x_n(k) \end{bmatrix} \in \mathbb{R}^n. \tag{8}$$

The system in Section 2 can be described as

$$x(k+1) = W(\alpha, \theta_k)\, x(k), \quad k \in \mathbb{Z}, \qquad x(0) = \begin{bmatrix} y_1 & y_2 & \cdots & y_n \end{bmatrix}^T, \tag{9}$$

where $W(\alpha, \theta_k)$ is a $n \times n$ matrix with entries $w_{ij}(\alpha, \theta_k)$. For $i \neq j$,

$$w_{ij}(\alpha, \theta_k) = \begin{cases} \alpha, & \text{when } j \in \Omega_i(k) \\ 0, & \text{when } j \notin \Omega_i(k) \end{cases}. \tag{10}$$

For $i = j$,

$$w_{ii}(\alpha, \theta_k) = 1 - \alpha d_i(k). \tag{11}$$

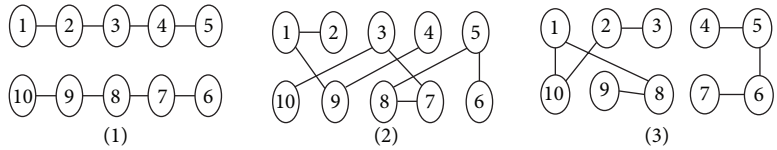

Figure 1: Three communication situations.

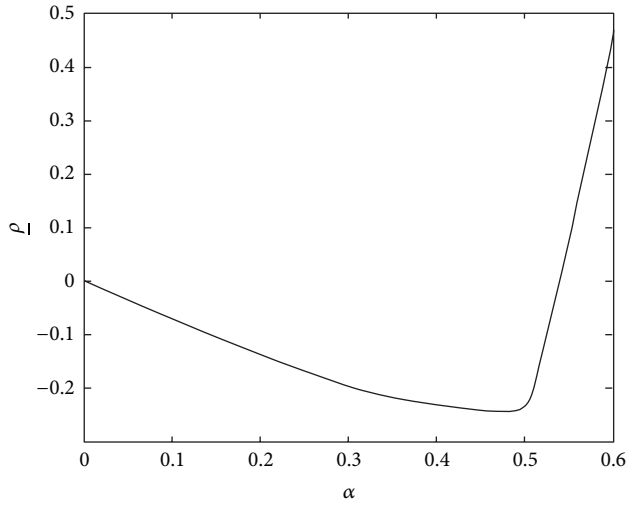

Figure 2: Graph of $\underline{\rho}(\alpha)$.

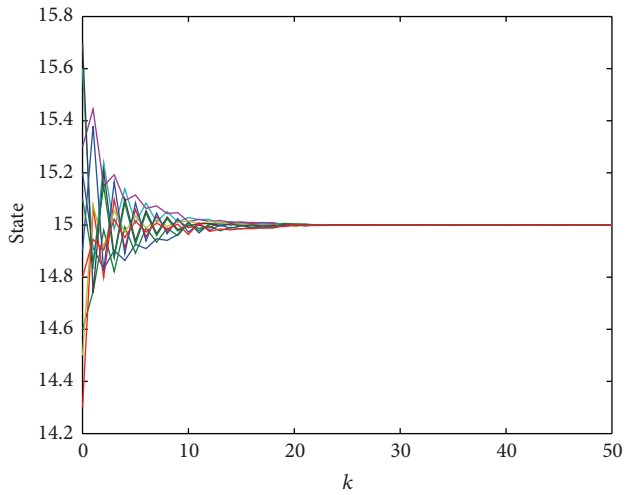

Figure 3: State curve when $\alpha_{\text{opt}} = 0.4812$.

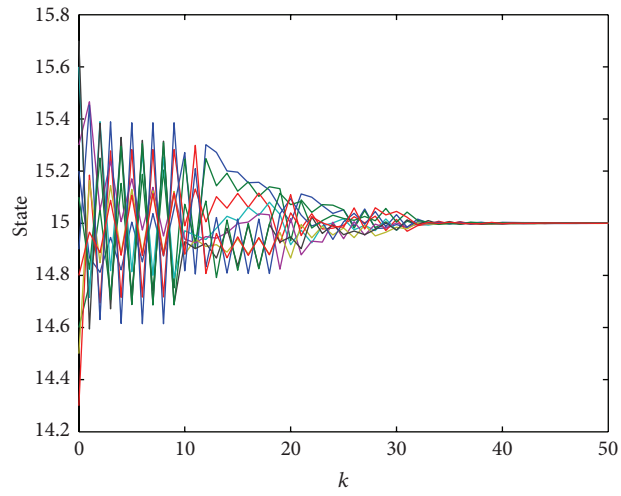

Figure 4: State curve when $\alpha_1 = 0.5528$.

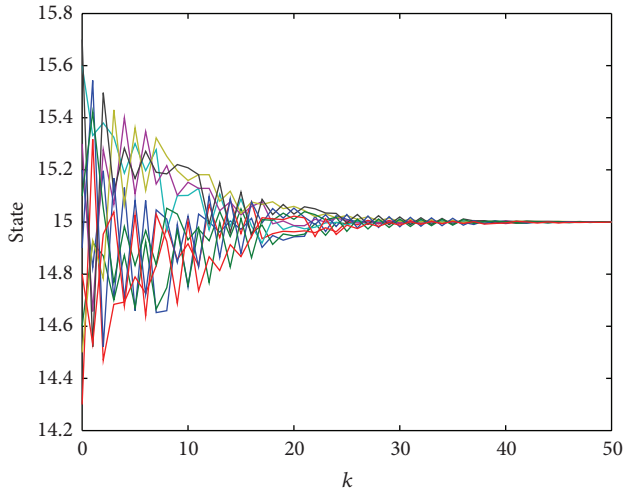

Figure 5: State curve when $\alpha_2 = 0.5359$.

From (2)~(6), it is seen that $i \in \Omega_j(k)$ if and only if $j \in \Omega_i(k)$, and hence

$$W(\alpha, \theta_k) = W^T(\alpha, \theta_k). \tag{12}$$

Furthermore, (10)~(12) imply that for all $k \in \mathbb{Z}$

$$\begin{aligned} \mathbf{1}^T W(\alpha, \theta_k) &= \mathbf{1}^T, \\ W(\alpha, \theta_k)\,\mathbf{1} &= \mathbf{1}. \end{aligned} \tag{13}$$

Then, we have

$$W(\alpha, \theta_k)\,\overline{y}\mathbf{1} = \overline{y}W(\alpha, \theta_k)\,\mathbf{1} = \overline{y}\mathbf{1}, \tag{14}$$

$$\frac{1}{n}\mathbf{1}\mathbf{1}^T x(k+1) = \frac{1}{n}\mathbf{1}\mathbf{1}^T W(\alpha, \theta_k)\,x(k) = \frac{1}{n}\mathbf{1}\mathbf{1}^T x(k), \tag{15}$$

which means that for all $k \in \mathbb{Z}$

$$\frac{1}{n}\mathbf{1}\mathbf{1}^T x(k) = \frac{1}{n}\mathbf{1}\mathbf{1}^T x(k-1) = \cdots = \frac{1}{n}\mathbf{1}\mathbf{1}^T x(0) = \overline{y}\mathbf{1}. \tag{16}$$

Denote $e(k) = x(k) - \overline{y}\mathbf{1}$. The iterative distributed inference is said to be average consensus in mean square sense if $\lim_{k\to\infty} E[\|e(k)\|^2] = 0$ for any initial condition $x(0) \in \mathbb{R}^n$ and $\theta_0 \in M$.

Theorem 1. *The linear distributed inference* (7) *reaches average consensus by choice of* α*, if there exist* m *positive definite matrices* $P_1, P_2, \ldots, P_m \in \mathbb{R}^{n\times n}$ *such that for all* $h \in M$

$$Q^T(\alpha,h)\left(\sum_{l=1}^{m}\overline{\gamma}_{hl}P_l + \sum_{l=1,l\neq h}^{m}\pi_{hl}^2 I_n\right)Q(\alpha,h) + Q^T(\alpha,h) \times \sum_{l=1}^{m}(P_h - P_l)^2 Q(\alpha,h) - P_h < 0 \tag{17}$$

with $Q(\alpha,h) = W(\alpha,h) - 1/n\mathbf{1}\mathbf{1}^T$.

Proof. Assume $\theta_k = h \in M$ at time step k. From (9), (14), and (16), one has

$$\begin{aligned} e(k+1) &= x(k+1) - \overline{y}\mathbf{1} \\ &= W(\alpha,h)x(k) - W(\alpha,h)\overline{y}\mathbf{1} - \frac{1}{n}\mathbf{1}\mathbf{1}^T x(k) + \overline{y}\mathbf{1} \\ &= W(\alpha,h)x(k) - W(\alpha,h)\overline{y}\mathbf{1} - \frac{1}{n}\mathbf{1}\mathbf{1}^T x(k) \\ &\quad + \frac{1}{n}\mathbf{1}\mathbf{1}^T\overline{y}\mathbf{1} \\ &= \left(W(\alpha,h) - \frac{1}{n}\mathbf{1}\mathbf{1}^T\right)(x(k) - \overline{y}\mathbf{1}) \\ &= Q(\alpha,h)e(k). \end{aligned} \tag{18}$$

We now consider the stochastic Lyapunov function

$$V(e(k),\theta_k) = e^T(k)P_{\theta_k}e(k). \tag{19}$$

Then for all $\theta_k = h \in M$, we have

$$\begin{aligned} &E\left[V(e(k+1),\theta_{k+1} \mid e(k),\theta_k)\right] - V(e(k),\theta_k) \\ &= e^T(k)\left(Q^T(\alpha,h)\sum_{l=1}^{m}\gamma_{hl}P_l Q(\alpha,h) - P_h\right)e(k) \\ &= e^T(k)\left(Q^T(\alpha,h)\sum_{l=1}^{m}(\overline{\gamma}_{hl}+\Delta\gamma_{hl})P_l Q(\alpha,h) - P_h\right)e(k) \\ &= e^T(k)\left(Q^T(\alpha,h)\sum_{l=1}^{m}\overline{\gamma}_{hl}P_l Q(\alpha,h) + Q^T(\alpha,h) \times \left(\sum_{l=1,l\neq h}^{m}\Delta\gamma_{hl}P_l + \Delta\gamma_{hh}P_h\right) \times Q(\alpha,h) - P_h\right)e(k) \\ &= e^T(k)\left(Q^T(\alpha,h)\sum_{l=1}^{m}\overline{\gamma}_{hl}P_l Q(\alpha,h) + Q^T(\alpha,h)\left(\sum_{l=1,l\neq h}^{m}\Delta\gamma_{hl}P_l - \sum_{l=1,l\neq h}^{m}\Delta\gamma_{hl}P_h\right) \times Q(\alpha,h) - P_h\right)e(k) \\ &= e^T(k)\left(Q^T(\alpha,h)\sum_{l=1}^{m}\overline{\gamma}_{hl}P_l Q(\alpha,h) + Q^T(\alpha,h)\left(\sum_{l=1,l\neq h}^{m}\Delta\gamma_{hl}(P_l - P_h)\right) \times Q(\alpha,h) - P_h\right)e(k) \\ &\le e^T(k)\left(Q^T(\alpha,h)\sum_{l=1}^{m}\overline{\gamma}_{hl}P_l Q(\alpha,h) + Q^T(\alpha,h)\sum_{l=1,l\neq h}^{m}\left(\frac{1}{4}\Delta\gamma_{hl}^2 I_n + (P_l - P_h)^2\right) \times Q(\alpha,h) - P_h\right)e(k) \\ &\le e^T(k)\left(Q^T(\alpha,h)\sum_{l=1}^{m}\overline{\gamma}_{hl}P_l Q(\alpha,h) + Q^T(\alpha,h)\sum_{l=1,l\neq h}^{m}\left(\pi_{hl}^2 I_n + (P_l - P_h)^2\right) \times Q(\alpha,h) - P_h\right)e(k) \\ &\le e^T(k)\left(Q^T(\alpha,h)\left(\sum_{l=1}^{m}\overline{\gamma}_{hl}P_l + \sum_{l=1,l\neq h}^{m}\pi_{hl}^2 I_n\right)Q(\alpha,h) + Q^T(\alpha,h)\sum_{l=1}^{m}(P_l - P_h)^2 Q(\alpha,h) - P_h\right)e(k). \end{aligned} \tag{20}$$

Denote

$$\Theta_h = Q^T(\alpha,h)\left(\sum_{l=1}^{m}\overline{\gamma}_{hl}P_l + \sum_{l=1,l\neq h}^{m}\pi_{hl}^2 I_n\right)Q(\alpha,h) + Q^T(\alpha,h)\sum_{l=1}^{m}(P_h - P_l)^2 Q(\alpha,h) - P_h. \tag{21}$$

When the conditions in Theorem 1 are satisfied, we have

$$\begin{aligned} &E\left[V(e(k+1),\theta_{k+1} \mid e(k),\theta_k)\right] - V(e(k),\theta_k) \\ &\le -\lambda_{\min}(-\Theta_h)\|e(k)\|^2 \\ &\le -\eta\|e(k)\|^2, \end{aligned} \tag{22}$$

where $\lambda_{\min}(-\Theta_h)$ denotes the minimal eigenvalue of $-\Theta_h$ and

$$\eta = \inf\{\lambda_{\min}(-\Theta_h), h \in M\}. \tag{23}$$

Therefore, for all $e(0) \in \mathbb{R}^n$, for all $\theta_0 \in M$, for all $T \in \mathbb{Z}$,

$$\begin{aligned}\sum_{k=0}^{T} E\left[\|e(k)\|^2\right] &\le \frac{1}{\eta}\sum_{k=0}^{T}\left(E\left[V\left(e(k),\theta_k\right)\right]\right.\\ &\qquad \left.-E\left[V\left(e(k+1),\theta_{k+1}\right)\right]\right)\\ &\le \frac{1}{\eta}\left(V\left(e(0),\theta_0\right)-E\left[V\left(e(T+1),\theta_{T+1}\right)\right]\right)\\ &\le \frac{1}{\eta}V\left(e(0),\theta_0\right).\end{aligned} \tag{24}$$

This means $\lim_{k\to\infty} E[\|e(k)\|^2] = 0$. □

3.2. Optimal Design. From the above proof, it is seen that the conditions in Theorem 1 result in not only $\lim_{k\to\infty} E[\|e(k)\|^2] = 0$ but also decreasing $E[V(e(k),\theta_k)]$. Moreover, $\lim_{k\to\infty} E[\|e(k)\|^2] = 0$ implies $\lim_{k\to\infty} E[V(e(k),\theta_k)] = 0$; that is, $E[V(e(k),\theta_k)]$ also converges to zero. Therefore, the decrease rate of $E[V(e(k),\theta_k)]$ can express the convergence speed of distributed inference. The following theorem is about the decrease rate of $E[V(e(k),\theta_k)]$.

Theorem 2. *Given $\alpha > 0$ and $\rho \in \mathbb{R}$, if there exist m positive definite matrices $P_1, P_2, \ldots, P_m \in \mathbb{R}^{n\times n}$ such that for all $h \in M$,*

$$\begin{bmatrix} Q^T(\alpha,h)\left(\sum_{l=1}^{m}\overline{\gamma}_{hl}P_l + \sum_{l=1,l\neq h}^{m}\pi_{hl}^2 I_n\right)Q(\alpha,h) - (1+\rho)P_h & * \\ \left(P_h - P_1\right)Q(\alpha,h) & \\ \vdots & -I_{mn} \\ \left(P_h - P_m\right)Q(\alpha,h) & \end{bmatrix} < 0, \tag{25}$$

then in linear distributed inference (7)*, for any nonzero $e(k) \in \mathbb{R}^n$,*

$$\frac{E\left[V\left(e(k+1),\theta_{k+1}\right)\right] - E\left[V\left(e(k),\theta_k\right)\right]}{E\left[V\left(e(k),\theta_k\right)\right]} < \rho. \tag{26}$$

Proof. According to Schur complement [17], condition (25) can be rewritten as

$$\begin{aligned}Q^T(\alpha,h)&\left(\sum_{l=1}^{m}\overline{\gamma}_{hl}P_l + \sum_{l=1,l\neq h}^{m}\pi_{hl}^2 I_n\right.\\ &\left.+\sum_{l=1}^{m}\left(P_h - P_l\right)^2\right)Q(\alpha,h) - (1+\rho)P_h < 0.\end{aligned} \tag{27}$$

From (27), for any nonzero $e(k) \in \mathbb{R}^n$, one has

$$\begin{aligned}e^T(k)&\left(Q^T(\alpha,h)\left(\sum_{l=1}^{m}\overline{\gamma}_{hl}P_l + \sum_{l=1,l\neq h}^{m}\pi_{hl}^2 I_n\right.\right.\\ &\left.\left.+\sum_{l=1}^{m}\left(P_h - P_l\right)^2\right)\right.\\ &\left.\times Q(\alpha,h) - P_h\right)e(k)\\ &< \rho e^T(k)P_h e(k),\end{aligned} \tag{28}$$

for all $\theta_k = h \in M$ and for all $\theta_{k+1} = l \in M$. From (28), (19), and (20), it is known that

$$\begin{aligned}&E\left[V\left(e(k+1),\theta_{k+1} \mid e(k),\theta_k\right)\right]\\ &\quad - V\left(e(k),\theta_k\right) < \rho V\left(e(k),\theta_k\right),\end{aligned} \tag{29}$$

and hence

$$\frac{E\left[V\left(e(k+1),\theta_{k+1}\right)\right] - E\left[V\left(e(k),\theta_k\right)\right]}{E\left[V\left(e(k),\theta_k\right)\right]} < \rho. \tag{30}$$

□

Condition (25) in Theorem 2 is a LMI. We denote condition (25) as $\Xi(\alpha,\rho) < 0$ and for any $\alpha > 0$ define

$$\underline{\rho}(\alpha) = \inf\left\{\rho \mid \rho \in \mathbb{R}, \Xi(\alpha,\rho) < 0 \text{ has solutions}\right\}. \tag{31}$$

Using the LMI toolbox of MATLAB, $\underline{\rho}(\alpha)$ can be computed by Algorithm 1.

For a $\alpha > 0$ with $\underline{\rho} < 0$, it is known from Theorems 1 and 2 that linear distributed inference (7) is average consensus and that $\underline{\rho}$ is a bound of convergence speed. Since a less value of $\underline{\rho} < 0$ gives a faster convergence speed, the fast distributed inference problem is addressed as

$$\mu = \inf_{\alpha>0}\underline{\rho}(\alpha) \tag{32}$$

which is an unconstrainted optimization problem of only one variable. Many existing numerical optimization methods [18] can be utilized to solve this problem efficiently. When $\mu < 0$, the optimal parameter

$$\alpha_{\text{opt}} = \operatorname*{arginf}_{\alpha>0}\underline{\rho}(\alpha) \tag{33}$$

provides a fast linear distributed inference which reaches average consensus.

Choose TOL > 0;
Choose enough large $\rho_1 \in \mathbb{R}$ such that $\Xi(\alpha, \rho_1)$ has solutions;
Choose enough small $\rho_2 \in \mathbb{R}$ such that $\Xi(\alpha, \rho_2)$ has no solution;
repeat until $\rho_1 - \rho_2 < \text{TOL}$
  $\rho_0 \leftarrow (\rho_1 + \rho_2)/2$;
  Solve $\Xi(\alpha, \rho_0) < 0$
  if $\Xi(\alpha, \rho_0) < 0$ has solutions
    $\rho_1 \leftarrow \rho_0$;
  else
    $\rho_2 \leftarrow \rho_0$;
end (repeat)
Set $\underline{\rho}(\alpha) \leftarrow \rho_1$.

Algorithm 1

4. Numerical Example

In this section, we present simulation results for average consensus of distributed inference in a simple sensor network. The network has 10 sensor nodes and switched in three possible communication situations. Figure 1 illustrates 3 communication situations. The estimated transition probabilities of θ_k is

$$\overline{\Gamma} = [\overline{\gamma}_{hl}] = \begin{bmatrix} 0.7 & 0.2 & 0.1 \\ 0.45 & 0.3 & 0.25 \\ 0.5 & 0.1 & 0.4 \end{bmatrix}. \tag{34}$$

The estimate error $\Delta\gamma_{hl}$ satisfies

$$\left|\Delta\gamma_{hl}\right| \le 2\pi_{hl} = 0.1, \quad \forall h \in \{1, 2, 3\}, \forall l \in \{1, 2, 3\}. \tag{35}$$

Using the computation procedure in Section 3, the optimization problem (32) is solved. Graph of $\underline{\rho}(\alpha)$ is displayed in Figure 2. The result is $\mu = -0.2407 < 0$ and $\alpha_{\text{opt}} = 0.4812$. For the communication situation in Figure 1(1), we use the design method in [7] of minimizing asymptotic convergence factor and obtain $\alpha_1 = 0.5528$. The design method in [7] is also applied to the other 2 situations in Figure 1 and get $\alpha_2 = \alpha_3 = 0.5359$.

In order to compare our method with that in [7], the initial states of each sensor node is selected as

$$\begin{aligned} x(0) &= \begin{bmatrix} y_1 & y_2 & y_3 & y_4 & y_5 & y_6 & y_7 & y_8 & y_9 & y_{10} \end{bmatrix}^T \\ &= \begin{bmatrix} 15.2 & 14.6 & 14.3 & 15.6 & 15.3 & 14.5 & 15.7 & 14.9 & 15.1 & 14.8 \end{bmatrix}^T. \end{aligned} \tag{36}$$

Thus from (1), we have $\overline{y} = 15$. The real transition probability matrix is set as

$$\Gamma = [\gamma_{hl}] = \begin{bmatrix} 0.68 & 0.24 & 0.08 \\ 0.4 & 0.27 & 0.33 \\ 0.53 & 0.11 & 0.36 \end{bmatrix}. \tag{37}$$

Figures 3, 4, and 5 show state curves of all sensor nodes under α_{opt}, α_1, and α_2, respectively. It can be seen that all sensor states convergence to $\overline{y} = 15$ and that our α_{opt} has faster convergence rate than α_1 or α_2 has. Achieving faster convergence is because our method considers the random switching among the 3 communication situations while [7]'s method considers only 1 communication situation.

5. Conclusion

The distributed average consensus problem in sensor networks has been studied under a Markovian switching communication topology of uncertain transition probabilities. Stochastic Lyapunov functions have been employed to investigate average consensus of linear distributed inference. A sufficient condition of average consensus has been proposed based on feasibility of a set of coupled LMIs. The design problem of fast distributed inference has been solved by numerical optimization techniques.

Acknowledgment

This work was supported by 973 Program of China (Grant 2009CB320603).

References

[1] R. Olfati-Saber and R. M. Murray, "Consensus problems in networks of agents with switching topology and time-delays," *IEEE Transactions on Automatic Control*, vol. 49, no. 9, pp. 1520–1533, 2004.

[2] R. Olfati-Saber and R. M. Murray, "Consensus protocols for networks of dynamic agents," in *Proceedings of the American Control Conference*, pp. 951–956, June 2003.

[3] L. Moreau, "Stability of multiagent systems with time-dependent communication links," *IEEE Transactions on Automatic Control*, vol. 50, no. 2, pp. 169–182, 2005.

[4] A. Jadbabaie, J. Lin, and A. S. Morse, "Coordination of groups of mobile autonomous agents using nearest neighbor rules," *IEEE Transactions on Automatic Control*, vol. 48, no. 6, pp. 988–1001, 2003.

[5] W. Ren and R. W. Beard, "Consensus seeking in multiagent systems under dynamically changing interaction topologies," *IEEE Transactions on Automatic Control*, vol. 50, no. 5, pp. 655–661, 2005.

[6] Y. Hatano and M. Mesbahi, "Agreement over random networks," *IEEE Transactions on Automatic Control*, vol. 50, no. 11, pp. 1867–1872, 2005.

[7] L. Xiao and S. Boyd, "Fast linear iterations for distributed averaging," *Systems & Control Letters*, vol. 53, no. 1, pp. 65–78, 2004.

[8] S. Kar and J. M. F. Moura, "Sensor networks with random links: topology design for distributed consensus," *IEEE Transactions on Signal Processing*, vol. 56, no. 7, part 2, pp. 3315–3326, 2008.

[9] Y. Ji, H. J. Chizeck, X. Feng, and K. A. Loparo, "Stability and control of discrete-time jump linear systems," *Control Theory and Advanced Technology*, vol. 7, no. 2, pp. 247–270, 1991.

[10] O. L. V. Costa and M. D. Fragoso, "Stability results for discrete-time linear systems with Markovian jumping parameters," *Journal of Mathematical Analysis and Applications*, vol. 179, no. 1, pp. 154–178, 1993.

[11] J. Xiong, J. Lam, H. Gao, and D. W. C. Ho, "On robust stabilization of Markovian jump systems with uncertain switching probabilities," *Automatica*, vol. 41, no. 5, pp. 897–903, 2005.

[12] L. Zhang and E.-K. Boukas, "H_∞ control for discrete-time Markovian jump linear systems with partly unknown transition probabilities," *International Journal of Robust and Nonlinear Control*, vol. 19, no. 8, pp. 868–883, 2009.

[13] P. Seiler and R. Sengupta, "An H_∞ approach to networked control," *IEEE Transactions on Automatic Control*, vol. 50, no. 3, pp. 356–364, 2005.

[14] L. A. Montestruque and P. Antsaklis, "Stability of model-based networked control systems with time-varying transmission times," *IEEE Transactions on Automatic Control*, vol. 49, no. 9, pp. 1562–1572, 2004.

[15] J. Yu, L. Wang, and M. Yu, "Switched system approach to stabilization of networked control systems," *International Journal of Robust and Nonlinear Control*, vol. 21, no. 17, pp. 1925–1946, 2011.

[16] Y. Xia, G.-P. Liu, M. Fu, and D. Rees, "Predictive control of networked systems with random delay and data dropout," *IET Control Theory and Applications*, vol. 3, no. 11, pp. 1476–1486, 2009.

[17] S. Boyd, L. El Ghaoui, E. Feron, and V. Balakrishnan, *Linear Matrix Inequalities in System and Control Theory*, vol. 15 of *SIAM Studies in Applied Mathematics*, SIAM, Philadelphia, Pa, USA, 1994.

[18] J. Nocedal and S. J. Wright, *Numerical Optimization*, Springer Series in Operations Research, Springer, New York, NY, USA, 1999.